

CR-185173

# SOLAR CONCENTRATOR ADVANCED DEVELOPMENT PROGRAM

FINAL REPORT  
October 1989

NASA Lewis Research Center

Contract NAS3-24670

N90-22834

(NASA-CR-185173) SOLAR CONCENTRATOR  
ADVANCED DEVELOPMENT PROGRAM Final Report  
(Harris Corp.) 333 p

CSC 10A

Unclass

63/44 0270170



HARRIS CORPORATION GOVERNMENT AEROSPACE SYSTEMS DIVISION  
P.O. BOX 94000 MELBOURNE, FLORIDA 32909 (407) 327-5115

ORIGINAL CONTAINS  
COLOR ILLUSTRATIONS

NASA CR-185173  
SOLAR CONCENTRATOR  
ADVANCED DEVELOPMENT PROGRAM  
FINAL REPORT

FOR:  
NASA LEWIS RESEARCH CENTER  
CONTRACT NAS3-24670

From:  
Harris Corporation  
Government Aerospace Systems Division  
P. O. Box 94000  
Melbourne, FL 32902

Written By:  
Don Knasel  
Senior Engineer  
and

Derik J. Ehresman  
Derik Ehresman  
Project Manager



### Summary

The Solar Concentrator Advanced Development Project has successfully designed, fabricated and tested a full scale prototypical solar dynamic concentrator.

A Truss Hexagonal Panel reflector was selected as a viable solar concentrator concept to be used for space station applications. This concentrator utilizes a modular design approach and is flexible in attainable flux profiles and assembly techniques. The detailed design of the concentrator, which included structural, thermal and optical analysis, identified the feasibility of the design and specific technologies that were required to fabricate it. The needed surface accuracy of the reflectors surface was found to be very tight, within 5 mrad RMS slope error, and results in very close tolerances for fabrication. To meet the design requirements a modular structure composed of hexagonal panels was used. The panels, made up of graphite epoxy box beams provided the strength, stiffness and dimensional stability needed. All initial project requirements were met or exceeded by hardware demonstration. Initial testing of structural repeatability of a seven panel portion of the concentrator was followed by assembly and testing of the full nineteen panel structure. The testing, which consisted of theodolite and optical measurements over an assembly-disassembly-reassembly cycle, demonstrated that the concentrator maintained the as-built contour and optical characteristics. The facet development effort within the project, which included developing the vapor deposited reflective facet, produced a viable design with demonstrated optical characteristics that are within the project goals.

## Table Of Contents

<u>Section</u>	<u>Title</u>	<u>Page</u>
1.0	INTRODUCTION.....	1
1.1	SUMMARY of Task I.....	1
1.2	SUMMARY of Task II.....	10
1.3	SUMMARY of Task III.....	12
2.0	MECHANICAL DESIGN.....	15
2.1	SCAD Prototype Concentrator.....	20
2.2	Detailed Design Description.....	36
2.3	Box Beam Development and Testing.....	44
2.4	Corner Fitting Assembly.....	55
2.5	Hub and Corner Shear Plates.....	61
2.6	Composite Mirror Facet Development and Design.....	61
2.7	Mirror Facet To Hexagonal Panel Interface.....	70
2.8	Latch History and Design.....	81
3.0	MANUFACTURING.....	97
3.1	Hexagonal Panel Fabrication.....	97
3.2	Establishing Hexagonal Panel Loads and Panel Proofloading....	107
3.3	Flexure and Standoff Installation and Adjustment.....	124
3.4	Latch and Striker and Assembly.....	124
3.5	Latch and Striker Installation/Alignment On The Hexagonal Panel.....	133
3.6	Concentrator Weight Summary.....	139
4.0	ASSEMBLY AND ALIGNMENT OF THE COUNTERBALANCE AND OPTICAL SCANNING EQUIPMENT.....	141
4.1	Counterbalance Description and Assembly.....	143
4.2	Laser Scanner.....	164
4.3	Concentrator Assembly.....	179
5.0	TESTING.....	188
5.1	Seven Panel 1-G Structural Repeatability Test.....	188
5.2	Nineteen Panel Counterbalanced/Structural Repeatability Testing.....	196
6.0	REFERENCES.....	218

## List Of Appendices

<u>Appendix</u>	<u>Title</u>
A	SCAD Mirror Facet Final Report (Hercules Corporation)
B	Hex Panel Repair Outline
C	Panel Proofload Procedure
D	Latch and Striker Installation Procedure
E	Theodolite Measurement System Description
F	Laser Scanner



## List Of Illustrations

<u>Figure #</u>	<u>Title</u>	<u>Page</u>
1.0-1	The Completed Solar Dynamic Concentrator Advanced Development Reflector Shown In The Power Systems Facility (PSF) At NASA Lewis Research Center In Cleveland, Ohio.....	2
1.1-1	Offset Optics Truss Hex Concentrator Consisting Of 19 Hexagonal Panels Mapped Onto A Sphere Of 877 Inches. The 456 Triangular Facets Are Adjusted To Approximate The Parabolic Optics.....	4
1.1-2	Splined Radial Panel Concentrator Is Self-Deploying, Light Weight and Efficiently Packaged.....	6
1.1-3	The Domed Fresnel Concentrator Combines Harris Deployable Precision Space Structure and ENTECH Fresnel Optic Technologies.....	7
1.1-4	Preliminary Optical Test Plan Meets Concentrator Demonstration Test Objectives.....	9
1.1-5	Master Tool List That Was Generated and Presented In The SCAD Critical Design Review.....	13
2.0-1	SCAD System Sizing Requirements Used To Design The Truss Hex Solar Concentrator. Presented In The Critical Design Review.....	16
2.0-2	Harris Generated Design Constraints That Were Used In The Design Of The SCAD Concentrator.....	17
2.0-3	System Level Requirements That Would Be Used For A Flight Concentrator But Used As Guidelines For The Prototype Model.....	18
2.0-4	A List Of Design Drivers That Are Used For Design Of Lightweight High Stiffness Space Structures.....	19
2.0-5	Performance Error Budget.....	21
2.1-1	Basic Dimensions Of The Truss Hex Concentrator As Well As The Deployed and Stowed Dimensions Of The Concentrator...	23
2.1-2	Deployed Geometry Of The SCAD Prototype Concentrator As Seen From A Side View.....	24

## List Of Illustrations

<u>Figure #</u>	<u>Title</u>	<u>Page</u>
2.1-3	Shows A Front View Of The SCAD Concentrator Looking Down The Z Axis. This Is A Projected View Looking From The Sun..	25
2.1-4	Stowed Envelope Of The Nineteen Hexagonal Panels Of The SCAD Concentrator.....	28
2.1-5	Shows The Number Of Different Facet Radii Versus The Resulting Slope Error In Milliradians.....	31
2.1-6	Illustrates The Radius and Location Of The Four Facets Selected For The SCAD Concentrator.....	32
2.1-7	The Results Of The Thermal Distortion Sensitivity Analysis. It Shows A Hot, Cold and Intermediate Distortion As Well As A 10X Change In Coefficient Of Thermal Expansion.....	35
2.2-1	Description Of The Basic Components Of The SCAD Concentrator and The Panel Designation.....	38
2.2-2	The Basic Building Block Of The Truss Hex Concentrator Hexagonal Panel.....	39
2.2-3	Completed Hexagonal Panel Showing The Basic Graphite Box Beams And Corner Fittings.....	40
2.2-4	A Typical Corner Fitting.....	41
2.2-5	Ball and Socket Latch Provides Three Degree Of Freedom In Rotation While It Has Zero Degrees Of Freedom In Translation. This Allows The Ball To Rotate and The Hexagonal Panel To Seek Its True Geometric Location.....	42
2.2-6	Composite Mirror Facet Is Attached To The Box Beams Using One Flexure At Each Corner. This Isolates The Facet Thermally and Structurally From The Box Beams.....	43
2.3-1	Graphite Epoxy Box Beam.....	45
2.3-2	Beam Cross Section Composed Of Eleven Plys Of Ultra High Modulus (UHM) Prepreg Material.....	46
2.2-3	The Zero Degree Plies Are Placed On The Mandrel In The Longitudinal Direction Of The Aluminum Mandrel .....	48

## List Of Illustrations

<u>Figure #</u>	<u>Title</u>	<u>Page</u>
2.3-4	The 45 Degree Plies Are Wrapped Around The Mandrel Like Stripes On A Barber Shop Pole. Three Wide Strips Are Needed To Complete One Layer.....	49
2.3-5	The Final Step Of The Top Wrap Process Is Completed By Adding The Consolidated Strip, .033 Inches Thick, To The Caps Of The Beam.....	50
2.3-6	The Two Consolidated Sheets Of Prepreg Material Are Placed On The Mandrel In The Overlap Configuration Shown Above To Form The Co-Cured C-Channel Box Beam.....	52
2.3-7	Strain Gauge Location and Orientation For The Four Point Bend Test Performed By Hercules Corporation In Salt Lake City, Utah.....	53
2.3-8	Four Point Bend Test Fixture Used To Determine Load Versus Deflection Data For The Graphite Epoxy Box Beam.....	54
2.4-1	Hex Panel Corner Fitting Detail That Shows Box Beams Bonded To The Corner Fittings; And The Shear Plates Bonded To The Top And Bottom.....	56
2.4-2	Actual Corner Fitting With Short Sections Of Box Beam In Place. The Shear Plate Is Removed To Allow Viewing Of The Fitting.....	57
2.4-3	Corner Fitting Assembly Components. Two Identical Corner Fitting Interfaces and A Round Spacer Rod.....	58
2.4-4	The Corner Fitting Bond Jig Holds The Top And Bottom Corner Fitting Pieces Co-planer On The Top and Side Surfaces.....	59
2.4-5	Completed Corner Fitting Assembly With .007 Inch Thick Bond Wire.....	60
2.5-1	The Hub and Corner Shear Plates. The Ply Orientation Corresponds To The Angle The Beams Meet At The Corner (Zero, +60 and -60).....	62
2.6-1	Typical Composite Mirror Facet Cross Section.....	67
2.6-2	Typical Assembly Features.....	68



# List Of Illustrations

<u>Figure #</u>	<u>Title</u>	<u>Page</u>
2.6-3	The Four Facet Radii and Their Location Within The Assembled Solar Concentrator.....	69
2.6-4	Completed Composite Mirror Facet Produced By Hercules Corporation.....	71
2.6-5	Vapor Deposited Aluminum Facet With Picture And The Clear Reflected Image Of Space Station Freedom.....	72
2.7-1	Standoff Interface Between The Hexagonal Panel And The Composite Mirror Facet. The Flexure Bracket Interfaces To The Box Beam.....	73
2.7-2	Flexure Assembly On An Internal Hex Panel Beam. The Spacer Is Shown In A Cutaway View In The Upper Left Corner.....	74
2.7-3	Cross Section Of A Typical Flexure.....	75
2.7-4	Type I Flexure Mounted To the Box Beams.....	76
2.7-5	Flexure Shown At The Middle Of A Typical Box Beam. The Wide Flexures Are Type II While The Smaller Cross Section Is The Type I.....	78
2.7-6	Typical Standoff Assembly Used To Support The Composite Mirror Facets.....	79
2.7-7	Facet To Standoff Interfaces.....	80
2.8-1	Truss Hex Concentrator Single Fold Deployment Method.....	82
2.8-2	Truss Hex Concentrator Unfolding Deployment.....	83
2.8-3	Latching Sequence For The All-Latch Design. Panels Are Latched Together Using A Single Radial Motion, As Indicated By Arrows.....	84
2.8-4	Typical Latch/Striker Assembly For The Harris Designed Zero Translation, Regenerative Latch System.....	86
2.8-5	Latch Kinematics.....	87
2.8-6	Isometric View Of The Type I Latch In Locked Position.....	89

## List Of Illustrations

<u>Figure #</u>	<u>Title</u>	<u>Page</u>
3.2-4	Nineteen Panel FEM With The Counterbalance Lines At A 25 Degree Angle To Simulate The Optical Scanning Position...	111
3.2-5	Description Of The FEM Showing How The Box Beams and Latches Were Modeled To Represent The Structure.....	113
3.2-6	Describes The Element Properties Used To Model The Hexagonal Panel Box Beams and Latches.....	114
3.2-7	Maximum Box Beam Loads Obtained From The Three FEM's Developed On SCAD.....	115
3.2-8	Maximum Latch Loads Obtained From The Three FEM's Developed On SCAD.....	116
3.2-9	Locations For Application Of Proofload Weights On The Radial Beams Of The Hexagonal Panel.....	117
3.2-10	Locations For Application Of The Proofload Weights On the Circumferential Beams Of The Hexagonal Panel.....	118
3.2-11	Application Points and Angles For Proofloading The Corner Fitting Assemblies. The Angles Apply The Proper Tensile and Moment Loads In The Corner Fitting That Are Transmitted From The Latch.....	119
3.2-12	Proofloading Of A Radial Beam On The SCAD Program. Turnbuckles and Loadcells Would Be used On The Actual Flight Program.....	120
3.2-13	Proofloading Of Two Circumferential Beams On The SCAD Program. Turnbuckles and Load Cells Would Be Used On The Actual Flight Equipment.....	122
3.2-14	Proofloading Of The Hexagonal Panel Corner Fitting. The Angle Of Load Application Generates The Proper Tensile and Moment Loads In The Corner Fitting.....	123
3.3-1	The Flexures and Standoffs Are Installed Using The Hex Panel Assembly Fixture To Hold The Panel Vertical.....	125
3.3-2	Threaded Beam Spacers Are Bonded Inside Of The Box Beams To Attach The Flexures. Spacer Is Shown In A Cutaway View In Upper Left Corner.....	126

## List Of Illustrations

<u>Figure #</u>	<u>Title</u>	<u>Page</u>
2.8-7	Type II Latch Between Panel Number 2 And Panel Number 7.....	90
2.8-8	Isometric View Of The Type II Latch And Striker.....	91
2.8-9	Typical Type III Latch Interfaces Panel 8 to Panel 7.....	93
2.8-10	Isometric View Of The Type III Latch and Striker.....	94
2.8-11	Type IV Latch That Is Used Between Panel 9 and Panel 10.....	95
2.8-12	Isometric View Of A Type IV Latch.....	96
3.1-1	Hexagonal Panel Bonding Fixture Insures Accurate Geometry For The Corner Fittings That Interface With The Latches.....	99
3.1-2	Precision Tooling Jig Plates Hold The Corner Fittings In Place During The Bonding Operation. The Cutout In The Plate Allows For Epoxy To Be Removed From The Underside Of The Box Beam During Bonding.....	100
3.1-3	The First Step Of The Hexagonal Panel Bonding Process Is Shown Above. Group 1 and Group 2 Are Bonded On Day One Of The Three Day Process.....	102
3.1-4	Two Box Beams Numbered Six (Horizontal Top and Bottom) Are Placed On Corner Fittings B and C Respectively To Complete The Hex Panel. The Shear Plates Are Bonded On The Six Corners And The Hub Also During Day Two.....	104
3.1-5	Completed Shear Plate Bond With Tooling Plate In Place. The Tooling Plate Applies A Uniform Force Over The Shear Plate And Pushed It Down To The .010 Inch Bond Beads For A Uniform Bondline Thickness.....	106
3.2-1	Two Finite Element Models (FEM's) Were Constructed For The SCAD Program. A Seven and Nineteen Panel Configuration Were Built.....	108
3.2-2	Seven Panel FEM That Was Used To Determine The Loads For The Seven Panel Non-counterbalanced Structural Repeatability Test.....	109
3.2-3	Nineteen Panel FEM Of The Concentrator In The Assembly Position. The Center Panel Is Restrained To Simulate The Central Panel Support.....	110



## List Of Illustrations

<u>Figure #</u>	<u>Title</u>	<u>Page</u>
3.3-3	Modified Dial Calipers Are Used To Set The Standoffs To Their Proper Height With Respect To The Bottom Of The Box Beam. They Are Set Per The Panel Assembly Drawing 500010...	127
3.3-4	A Type II Flexure Is Set and Bonded On The Bench Using A Modified Micrometer To Contact The Sphere.....	128
3.4-1	The Latch Striker Plates Are Set Using A Cylindrical Rod That Matches The Striker Sphere Diameter. The Tooling Rod Is Keyed To The Latch Pawl Shaft Hole and The Delatch Pin Hole.....	129
3.4-2	EA 934 Epoxy Is Placed Around The Bolts That Hold On The Striker Plates To Prevent Slippage Of The Plates By Taking Away The Clearance Between The Bolt and The Clearance Hole..	131
3.4-3	Striker Sphere Is Set Using A Modified Height Gauge Shown Above. The Height Is Set Per The Striker Assembly Drawing 500065.....	132
3.5-1	Concept For Latch Alignment Table Presented In The Harris Critical Design Review.....	134
3.5-2	The Striker Alignment Tooling Captures The Sphere Using A V-Block And Vertical Pin. A Gauge Block With The Proper Length Insert Places The Sphere The Correct Distance From The Corner Fitting.....	136
3.5-3	The Striker Assembly Is Placed In The V-Block and Mounted To the Hexagonal Panel And The Vernier Is Pushed Up Against The Sphere. The Difference Between The First Reading In Figure 3.5-2 and This Reading Determines The Shim Thickness.....	137
3.5-4	A Striker Sphere Is Mounted On The Vernier To Mount The Latches In Their Proper Location. The First Reading Is The Proper Location Of The Latch Sphere.....	138
3.5-5	The Latch Is Attached To The Tooling Sphere Then It Is Mounted To The Hexagonal Panel. A Vernier Reading Is Taken To Establish the Proper Shim Thickness To Place Behind The Latch Housing.....	140
4.0-1	Schematic Of The Counterbalance System Showing The Concentrator In The Assembly and Optical Scanning Positions.....	142

## List Of Illustrations

<u>Figure #</u>	<u>Title</u>	<u>Page</u>
4.0-2	Schematic Of The Entire Laser Scanner System That Was Presented In The SCAD Critical Design Review.....	144
4.1-1	Schematic Of The Counterbalance Structure Comprised Of Four Standard Roof Trusses That Are Supported By Eight 10 Inch Diameter Columns.....	146
4.1-2	Nomenclature For The Columns C1 Through C8 and Trusses T1 Through T4. The Structural Stiffeners (Cross-Braces) Are Represented As ST1 Through ST6 and The Outriggers For The Optical Scanner Are OR1 Through OR4.....	147
4.1-3	Erection Of The First Counterbalance Column At The Power System Facility (PSF) At NASA LeRC In Cleveland, Ohio.....	148
4.1-4	Completion Of The First Bay Of The Counterbalance System With Columns C1 and C2 and Truss T1.....	149
4.1-5	Completed Counterbalance Mainframe Structure. The Outriggers and Stiffening Cross Members Can Be Seen In The Upper Left Portion Of The Photograph.....	151
4.1-6	Centerline Of The Truss Must Be Located To Within 0.5 Inches Of The Column Centerline. The Scanner Rails Have Only Plus Or Minus 0.5 Inches Of Adjustment To Compensate For Truss Bow.....	153
4.1-7	The Linear Bearing Shaft Is Mounted Loosely To The Top Of Truss 2 and The Shimming and Alignment Process Has Started.....	154
4.1-8	Linear Bearing Shaft Alignment Tool Was Combined With A Theodolite Mounted To The Columns To Set The Rails. The Pillow Block Holds The Tool Along The Rail Axis And The Bubble Level On The Front Is Used To Keep The Tooling Ball Vertical.....	156
4.1-9	The Shimming Operation Is Completed For The First Rail On Truss 2 and Was Then Performed On The Remaining Three Trusses.....	157
4.1-10	Large Rubber Stops Are Mounted To The Ends Of The Trusses To Prevent The Scanner From Running Off The End Of The Rail. Motor Control Software Also Prevents The Scanner From Hitting The Stops.....	158

## List Of Illustrations

<u>Figure #</u>	<u>Title</u>	<u>Page</u>
4.1-11	Panel Support System Used To Counterbalance Nineteen Individual Hexagonal Panels During Assembly and Test.....	160
4.1-12	The Aluminum I-Beams Are Mounted To The Bottom Of The Counterbalance Trusses. They Support The Pulley Trolley System That Is Used To Offload The Panels In The Assembly and Scan Position.....	162
4.1-13	Pulley Control Blocks Are Attached to The Ends Of The Aluminum I-Beams. The Small Pulley and Cable Are Used To Pull The Trolley Against The Stops From The Ground To Place The Concentrator In The Assembly and Scan Position....	163
4.1-14	The Target Support Structure and Viewing Camera Are Mounted To The Counterbalance Structure At A Precise Location On Truss 4.....	165
4.1-15	The Scanning Towers Are Used To Support The Concentrator In The Optical Scan Position and To Simulate The Three Point Mount Of The Delta Frame Structure On The Flight Design.....	166
4.1-16	Short Support Stand Used At The Point Closest To The Floor. There Are Two Tall Towers, Figure 4.1-15 and One Short Support To Make Up The Three Point Mount.....	167
4.2-1	Laser Scanner Assembly Is Comprised Of The Main Beam With Two Synchronized Drive Motors That Travels In The Y-Direction and The Carriage With A Single Motor That Travels Across The Beam In the X-Direction.....	168
4.2-2	The Main Gantry (Beam) Travels Across The Counterbalance Structure In The Y Direction (Along The Trusses) and The Carriage Travels Perpendicular To The Trusses In The X-Direction.....	170
4.2-3	Shows The Actual Laser Scanner System In PSF At NASA LeRC In Cleveland. The Foreground Shows The Rack and Gear Drive System. The Laser Carriage Is Shown On the Far Side Of The Structure.....	171
4.2-4	Functional Mechanical Diagram Of The Laser Scanner System...	172
4.2-5	A Functional Electrical Diagram Of The Laser Scanner Motor Control Circuit. This Circuit Is Used To Keep The Two Motors On The Main Gantry Synchronized.....	173



## List Of Illustrations

<u>Figure #</u>	<u>Title</u>	<u>Page</u>
4.2-6	The Neutral Density Filter Was Placed On The Laser To Result In A Class I System That Is Safe For Operation In The PSF Building.....	175
4.2-7	The Two Tilt Sensors Are Mounted Orthogonal To Each Other To Maintain Laser Verticality For the Optical Repeatability Testing.....	177
4.2-8	An Actual Photograph Of The Laser Scanner Carriage System The Sperry Tilt Sensors Can Be Seen On The Two Vertical Faces and The Laser Is Pointed Over The Side Of The Gantry. The Vertical Card Is The Harris "Top Gun" Feed Back and Control Loop Between The Motor Micrometers and The Tilt Sensors.....	178
4.2-9	Cable Festoon That Allows The Electrical and Feedback Wiring To Follow The Gantry As It Travels In The Y-Direction.....	180
4.2-10	Wiring Is Routed From The Cable Festoon To The Back Of The Control Console In The PSF Highbay Area.....	181
4.2-11	Laser Scanner Control Console Contains The PC Used To Control The Scanner Location. The System Kill Switch Is Seen On The Far Left Of The Console and The Motor Control Circuit Boards and Power Supply Appear In The Center Of The Photograph.....	182
4.3-1	The Hexagonal Panel Interfaces With The Counterbalance Cable Through A Pseudo Three Degree Of Freedom Rotational Device Figure 4.3-2. The Cable Is Tensioned After Being Attached To The Hexagonal Panel. The Arch Of The Slot Forces The Line Of Action Of The Cable Through The Center Of Gravity Of The Panel.....	183
4.3-2	Cable Is Tensioned After Being Attached To The Hexagonal Panel. The Arch Of The Slot Forces The Line Of Action Of The Cable Through The Center Of Gravity Of The Panel.....	185
4.3-3	The Slotted Metallic Part Shown In The Picture Is Mounted To A Bearing Which Allows The Part To Rotate For Compound Angles As Seen Above.....	186
5.1-1	The Seven Panel Structural Repeatability Target Locations, Panel Numbers and Theodolite Locations Are Shown Above.....	189

# List Of Illustrations

<u>Figure #</u>	<u>Title</u>	<u>Page</u>
5.1-2	Tooling Target Used To Define The Location Of The Hexagonal Panel. Three Targets Were Placed On Each Panel To Define A Plane And Measure Rotational Variations...	190
5.1-3	Regressed Theodolite Data From 7-Panel Test.....	193
5.1-4	Comparison Of The Original Data Set For A Panel (P) To The Second Data Set (P Prime) To Obtain The Rotational Change Of The Hexagonal Panel.....	194
5.1-5	Hexagonal Panel Error For The Three Measurement Sets Taken In the Seven Panel Structural Repeatability Test.....	195
5.1-6	Seven Panel Structural Repeatability Test Performed At Harris Corporation In Palm Bay, Florida.....	197
5.2-1	Optical Test Schematic For The Full Up Nineteen Panel Optical Repeatability Test.....	198
5.2-2	Solar Concentrator Advanced Development Concentrator Rotated Up To The Optical Scan Position. Harris Engineers and Technicians Are Measuring The Concentrator Using The Theodolite System As Part Of The Structural Repeatability Test.....	200
5.2-3	The Facet Is Adjusted Until The Reflected Image Of The Laser Beam Intersects The Center Of The Receiver Aperture Target Located At The Focal Point Of The Concentrator.....	201
5.2-4	Picture Of The Television Monitor Which Receives The Signal From The Camera Behind The Aperture Target. This Is The Image Seen On The Ground From Figure 5.2-3.....	202
5.2-5	Shows The Theodolite Placement For The Measurement Of The Concentrator During The Optical/Structural Repeatability Test. The T-Numbers Correspond To The Three Targets Per Hexagonal Panel Used To Define The Plane and Location Of That Panel.....	203
5.2-6	Regressed Theodolite Data From The 19 Panel Test.....	205
5.2-7	Rotational Change Of The Hexagonal Panels Following Disassembly and Re-assembly As Measured With The Theodolite System.....	206

# List Of Illustrations

<u>Figure #</u>	<u>Title</u>	<u>Page</u>
5.2-8	The Concept Of Specularity Is Shown Above. An Ideal Ray Would Reflect At N Prime If The Surface Was Flat and Specular. The Reflected Ray Has A Distribution Of Light That Is Not Perfect and Causes A Spreading Of The Image.....	208
5.2-9	In Order To Obtain More Accurate Data For The Optical Repeatability Test Optical Mirrors Were Placed On The Facets To Reduce The Beam Spreading Seen Above. Figure 5.2-4 Shows The Image With The Mirrors.....	209
5.2-10	The Angular Change Of The Image On The Focal Plane Is Calculated By Knowing The Distance From The Facet To The Focal Plane and The Distance The Image Moves In The Focal Plane.....	210
5.2-11	Resulting Optical Repeatability Data From The SCAD Testing..	211
5.2-12	Results Of Optical Repeatability Data From The SCAD Prototype Testing.....	212
5.2-13	Map Showing The Location Of The 48 Facets In The Concentrator. The Central Panel Denotes The Facet Numbers and Are The Same For The Remaining 18 Hexagonal Panels.....	213
5.2-14	The Small Squares Are The Theoretical Circumferential Flux Distribution If All Facets Are Pointed Toward The Focal Point. The Small Circles Are The Comparison With The Hex Error Measured During The Optical Repeatability Test Applied To the Model. The Difference Is Negligible....	214

## 1.0 INTRODUCTION

The Solar Concentrator Advanced Development (SCAD) Program was awarded to Harris Corporation in September 1985, to develop a solar dynamic power system for space applications, in particular the NASA Space Station Freedom. Solar dynamic systems have been developed for terrestrial applications, but have not been developed for space applications. The Harris SCAD contract (NAS3-24670) was for development of a prototype solar collector for space applications.

The contract was broken into three tasks:

- Task 1    Conceptual Design Trade Studies, Materials, Special Tooling and Testing
- Task 2    Mechanical Design of Prototype Concentrator and Associated Tooling
- Task 3    Fabrication and Testing of the Prototype Concentrator and Tooling

A final report was previously written for Task 1. This report focuses on Tasks 2 and 3 and marks the completion of the Solar Concentrator Advanced Development Program. The end product achieved during the SCAD contract, a prototype solar concentrator, can be seen in Figure 1.0-1.

### 1.1 Summary of Task 1

Task I was divided into the following subtasks: Conceptual Designs and Trade Studies, Material Selection, and Identification of Tooling and Test Requirements. The objective of these tasks were: 1) to develop conceptual



ORIGINAL PAGE  
BLACK AND WHITE PHOTOGRAPH

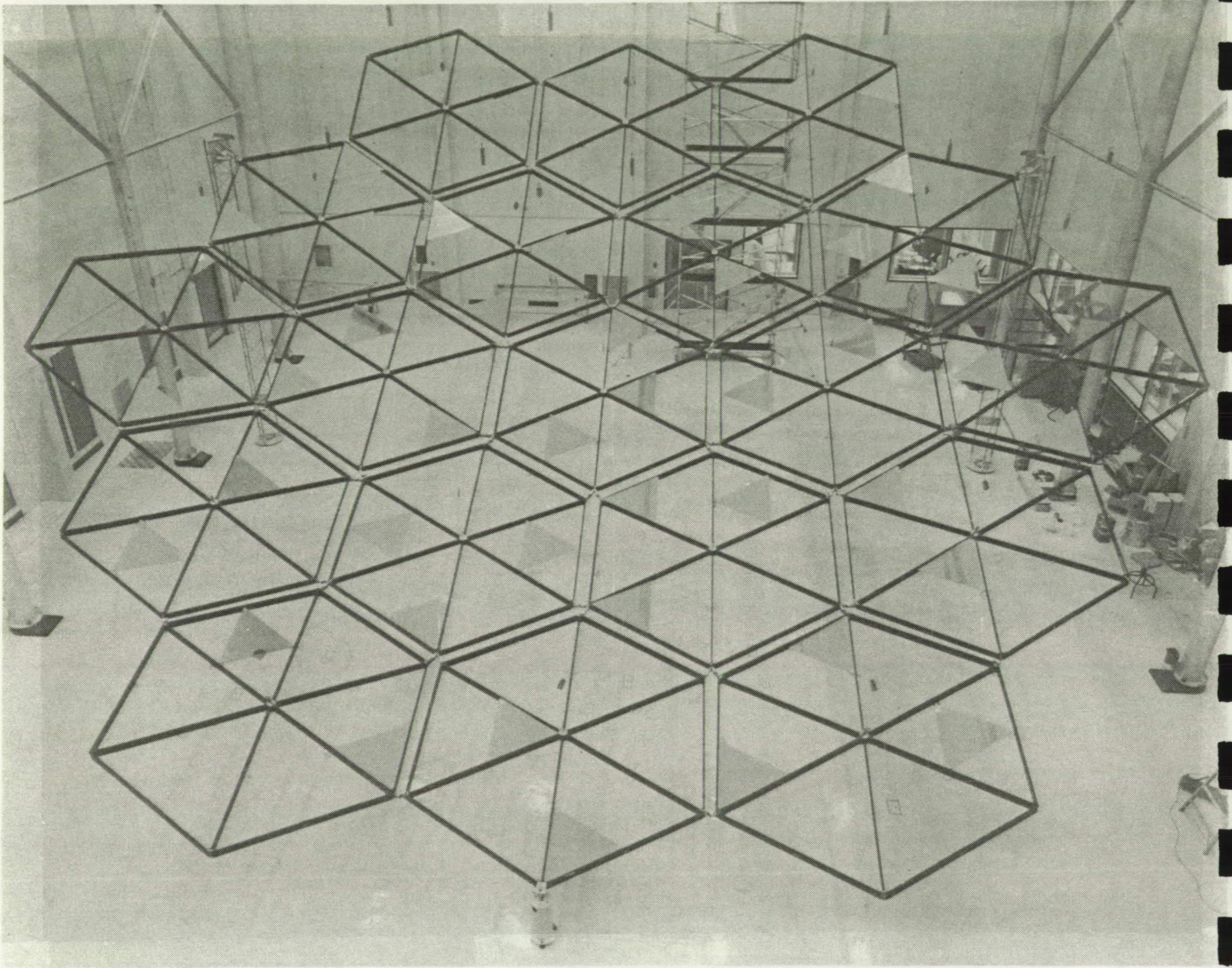


Figure 1.0-1. The Completed Solar Dynamic Concentrator Advanced Development Reflector Shown In The Power Systems Facility (PSF) At NASA Lewis Research Center In Cleveland, Ohio

designs for concentrators with application for the Space Station Freedom, 2) to select and recommend a concept based on a trade comparison, 3) to perform materials testing to provide a data base for concept selection and subsequent design, and 4) to identify the special tooling and testing requirements of the recommended concept.

#### Subtask 1 - Conceptual designs and Trade Studies

Three conceptual designs of a solar concentrator were generated during Task 1: Truss Hex, Splined Radial Panel (SRP), and Domed Fresnel. These designs were compared using trade studies that addressed complexity, reliability, cost, deployment method, on-orbit maintainability, and other similar parameters which affect the overall performance of a space system. A brief description of each concept and trade study results follows.

#### Truss Hex

The Truss Hex concentrator in Figure 1.1-1 is an offset parabolic configuration consisting of 19 hexagonal panels. The reflective surface consists of 456 adjustable spherical mirror facets of only 4 radii of curvature. The adjustable facet concept provides an excellent approximation of the parent paraboloids surface by dividing it into 456 smaller pieces and allows for tailoring the flux profiles to meet receiver requirements. The hex panels are interconnected with a series of "ball and socket" latches and are Astronaut (EVA) or Teleroboticly assembled.

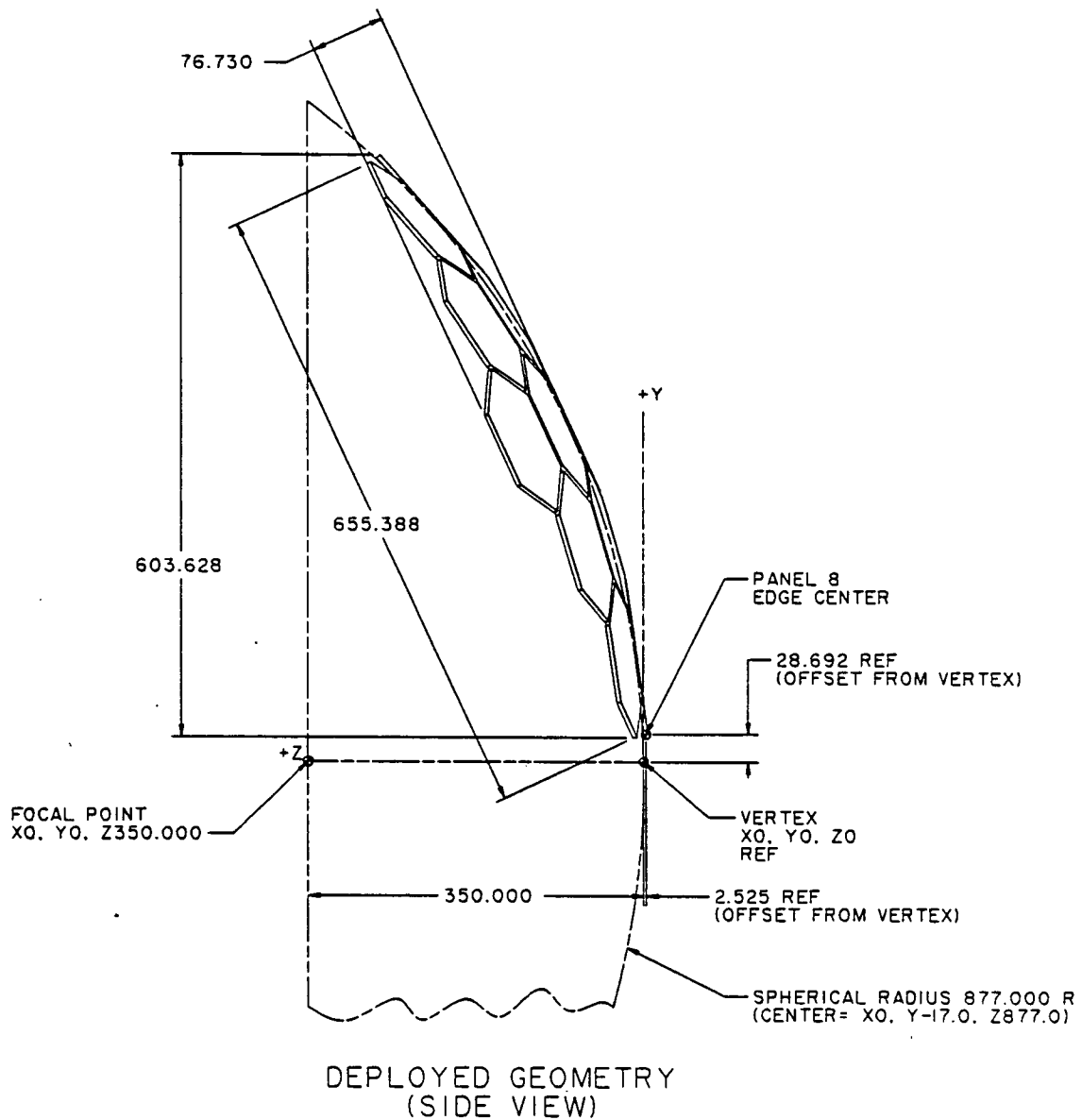


Figure 1.1-1. Offset Optics Truss Hex Concentrator Consisting Of 19 Hexagonal Panels Mapped Onto A Sphere Of 877 Inches. The 456 Triangular Facets Are Adjusted To Approximate The Parabolic Optics.



### Splined Radial Panel

The Splined Radial Panel (SRP) concentrator in Figure 1.1-2 is a parabolic structure consisting of a semi-rigid reflective surface supported by a Harris Deployable Truss Structure (DTS). The reflective surface is composed of thin graphite epoxy panels which are drawn into a splined parabolic curve using a flexible cord and tie shaping technique. The SRP is lightweight and self deploying.

### Domed Fresnel

The Domed Fresnel concentrator in Figure 1.1-3 consists of a transparent lens populated with Fresnel prisms. This concentrator refracts the solar rays rather than reflecting them into the receiver. The domed surface is approximated with flat prismatic panels shaped by using the cord and tie technology which Harris used on the Tracking and Data Relay Satellite System's deployable RF antennas. The Domed Fresnel is also a lightweight, self deploying DTS structure.

### Trade Study Result

The trade comparison evaluated the three concentrator concepts; truss hex, splined radial panel and domed fresnel; against 16 weighted criteria. These criteria included: optical performance, packaging efficiency, maintainability, design complexity, development risk and other criteria. The Truss Hex concept was ranked highest by the trade comparison and was recommended as the concept which best supported the Space Station Freedom mission.



## SPLINED RADIAL PANEL CONCENTRATOR

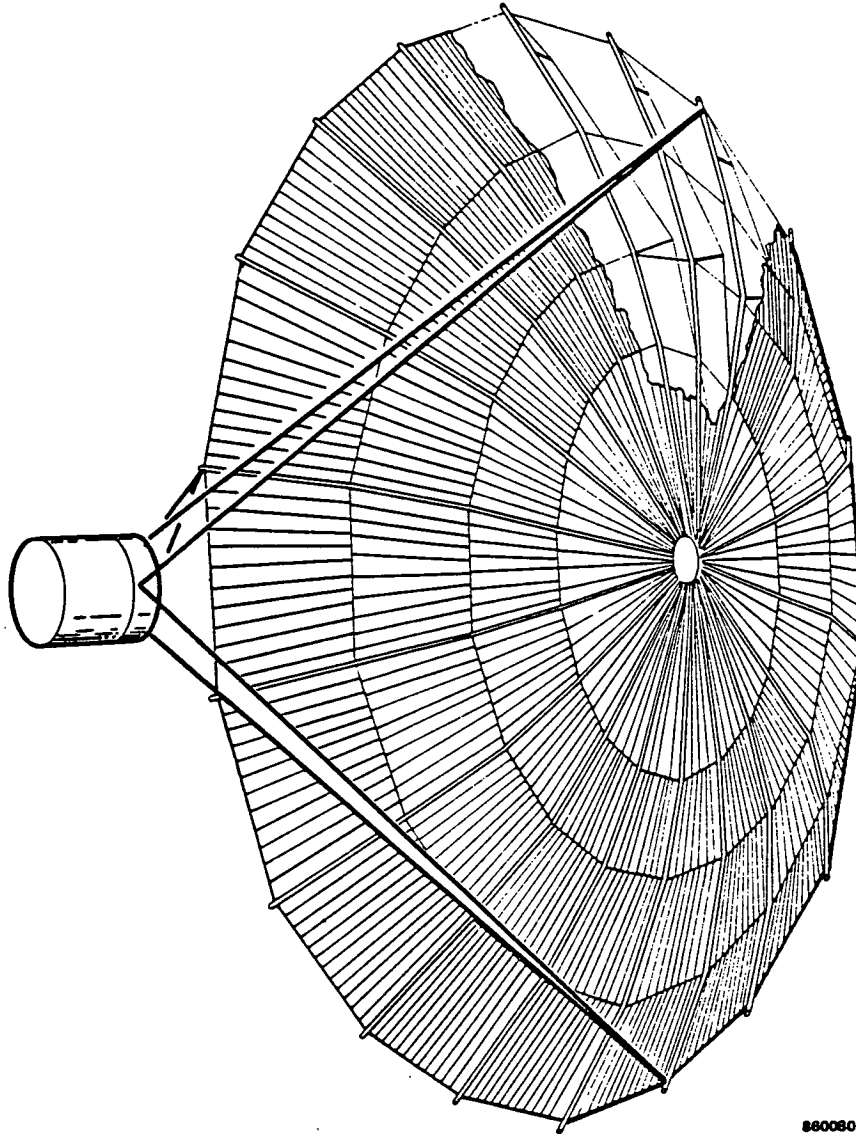
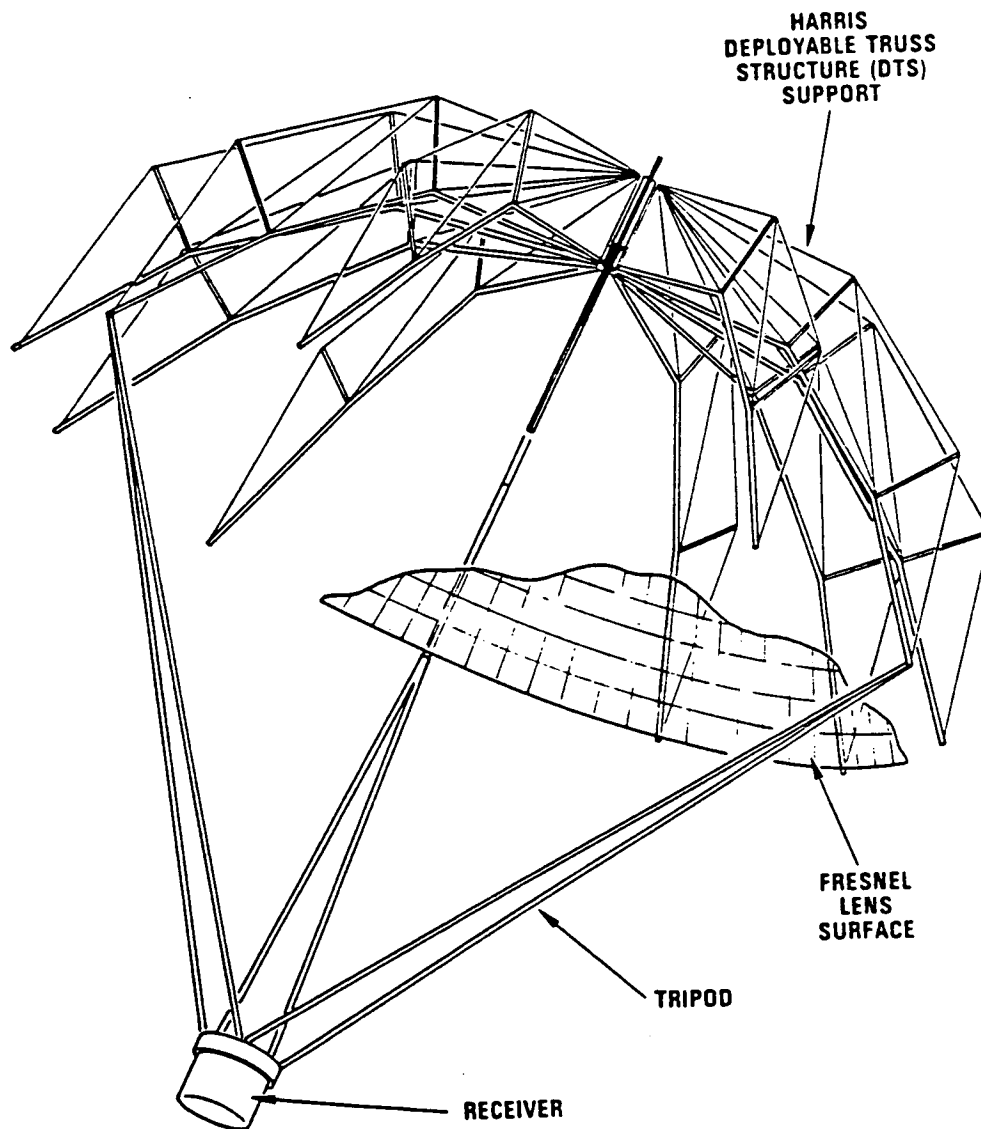


Figure 1.1-2. Splined Radial Panel Concentrator Is Self-Deploying, Light Weight and Efficiently Packaged

## DOMED FRESNEL CONCENTRATOR



14215-1

Figure 1.1-3. The Domed Fresnel Concentrator Combines Harris Deployable Precision Space Structure and ENTECH Fresnel Optic Technologies

The Splined Radial Panel and the Domed Fresnel concepts were ranked nearly equal and were judged to be sound concepts with unique features better suited for other applications, but which required significant technology development effort. Risks in the area of maintainability, produceability, and materials were deemed too large for these two concepts, for use on the space station, in view of the goal of the program to use current technology.

#### Subtask 2 - Material Selection

A preliminary evaluation of materials was made to establish their mechanical and optical property suitability for the environment (low earth orbit) and their resulting degradation over a 10 year (15 years Flight System) life. The primary thrust of the material selection effort was to demonstrate the ability of selected reflective mirror and refractive lens materials to withstand degradation due to atomic oxygen impingement.

Materials tested for Fresnel lens applications showed severe degradation at lower exposure times than did the reflective samples for the Truss Hex and Splined Radial Panel concepts. The decrease in specular transmittance and mass loss associated with lens materials made the Fresnel lens concept a risk at this time. Simulated oxygen exposure testing indicates that aluminum and silver reflective mirror materials can be adequately protected with several materials including silica ( $\text{SiO}_x$ ), magnesium fluoride ( $\text{MgF}_2$ ) and indium tin oxide (ITO). Additional testing was performed to document the effects of micrometeoroid impacts and thermal cycling on sample integrity. Based on NASA micrometeoroid fluence models

and debris data, conservative estimates show that less than .002 percent of the concentrator surface would be damaged as a result of high velocity impacts. Thermal cycling tests indicated that composite substrate materials suffer adverse effects as a result of thermal cycling. However, no specular readings were taken at elevated temperatures at this time. This issue will be addressed in the Phase C/D (Flight Program) portion of the concentrator program.

### Subtask 3 - Identification of Tooling and Test Requirements

During this phase of Task 1 a plan was formulated for testing the selected solar concentrator to demonstrate or verify on-orbit performance. Also, any special tooling or facilities needed to fabricate, assemble and test the concentrator were identified. The test plan shown in Figure 1.1-4 was developed.

## 1.2 Summary of Task 2 - Mechanical Design of Prototype Concentrator and Associated Tooling

The overall objective of Task II was to complete the design of the selected concept from Task I. That is, the baseline Offset Truss Hex Parabolic Concentrator which would deliver 185 KW of thermal flux to the receiver aperture and use the Closed Brayton Cycle for energy conversion. All tooling needed for in-house fabrication and testing was also designed. Task II was comprised of the following subtasks: Preliminary Design, Preliminary Design Review, Concentrator Detail Design, Critical Design Review and Detailed Tooling Design. A summary of each subtask follows.

#### PRELIMINARY OPTICAL TEST PLAN

##### OBJECTIVE

- DETERMINE SPECULAR REFLECTANCE OF COATINGS
- PERFORM DETAILED FIRST ARTICLE FACET CHARACTERIZATION (EACH MOLD)
- PROVIDE LOW COST ACCEPTANCE TEST FOR EACH FACET
- PERFORM OPTICAL FACET ALIGNMENT AT ASSEMBLY LEVEL
- DETERMINE GLOBAL CHARACTERISTICS
  - OPTICAL BORESIGHT
  - EFFECTIVE SLOPE ERROR
  - FOCAL LENGTH
- ASSESS EFFECTS OF 1 g DISTORTIONS
- DEMONSTRATE DEPLOYMENT REPEATABILITY
- CHARACTERIZE RECEIVER OPTICS

##### DEMONSTRATE BY

- REFLECTANCE TESTS PERFORMED BY DEPOSITION VENDOR
- LASER SCAN
- GO-NO/GO AUTOFOCUS TEST
- USE TRANSLATING VERTICAL LASER BEAM TO AIM FACETS AT PRE-DETERMINED CYLINDRICAL GRID POINTS
- TRANSLATING VERTICAL LASER BEAM WITH DIGITIZED PHOTOSENSING SCAN IN THE APERTURE PLANE
- PERFORM ABOVE WITH & WITHOUT COUNTER WEIGHTS
- APERTURE PLANE SCANS WITH INTERVENING STOW/DEPLOY
- MAINTAIN CORRESPONDENCE DATA FOR LASER BEAM LOCATION & INTERCEPT LOCATION AT APERTURE PLANE. DEFINE VECTOR INPUTS FOR OPTICAL ANALYSIS TO PREDICT FLUX

Figure 1.1-4. Preliminary Optical Test Plan Meets  
Concentrator Demonstration Test Objectives

#### Subtask I - Preliminary Design

A preliminary drawing package was generated of the concentrator that defined overall aspects of the design such as stowed and deployed geometry, truss/hex structure and latch configurations. The configuration sizing and material selections were based on structural and optical analysis that were performed in the program. The detailed results of this task were presented in the Preliminary Design Review.

#### Subtask II - Preliminary Design Review (PDR)

A PDR was held at NASA Lewis Research Center in Cleveland, Ohio on 16 September 1986. The results of Subtask I were presented in viewgraph format to NASA technical personnel. A list of action items were generated and sent to Robert Hyland (NASA Project Manager) on 24 September 1986. All action items were addressed and completed before starting Subtask III.

#### Subtask III - Concentrator Detailed Design

A detailed drawing package was generated of the concentrator which described it in enough detail that procurement and subsequent fabrication of the concentrator were possible. The drawings were completed to DOD-D-1000B Level 2 which is used for production prototype and limited production projects.

#### Subtask IV - Critical Design Review (CDR)

A CDR was held at Harris Corporation in Melbourne, Florida on 27 and 28 January 1987. The results of Subtask III were presented in viewgraph form to NASA Lewis technical personnel. A list of action items was generated and all technical issues were addressed before the start of the assembly and test effort for Task 3 of the program. A detailed description of the resulting design is provided in section 2.0 of this document.

#### Subtask V - Detailed Tooling Design

A detailed drawing package which describes the tools necessary for in-house fabrication and testing of the concentrator was generated during this task. A master tool list was generated and can be seen in Figure 1.1-5. Each tool and how it was used are explained in the manufacturing and test sections of this report.

Following completion of Task 2 (Mechanical Design of Prototype Concentrator and Associated Tooling) Harris started Task 3.

### 1.3 Summary of Task 3 - Fabrication and Testing of the Prototype Concentrator

The objective of Task 3 was to fabricate the selected concentrator from Task 1 which was designed and analyzed during Task 2. Task 3 was divided into three subtasks; Fabrication, Testing, and Delivery and on site support. The following is a summary of those subtasks.

# MASTER TOOL LIST

<u>TOOL NAME</u>	<u>DETAILS</u>	<u>TOOL NO.</u>
* HEX FRAME BONDING JIG	16	1232-B-0100
* FACET RETAINER BOND JIG	5	1232-B-0200
CORNER FITTING BOND JIG	3	1232-B-0300
* LATCH & STRIKER POSITIONER	15	1232-A-0200
* STANDOFF SETTING TOOL	4	1232-A-0400
FRAME POSITIONER	17	1232-A-0500
FACET INSTALLATION HANDLE	6	1232-A-0600
CENTRAL SUPPORT	12	1232-C-0100
COUNTERBALANCE FRAME	60	1232-C-0200
LASER SCANNER	35	1232-C-0400
SCAFFOLDING	10	1232-C-0300
* HEX FRAME STORAGE RACK	3	1232-D-0500
HEX SHIPPING CONTAINER	2	1232-D-0200
	188	

## LEGEND:

A = ASSEMBLY TOOLS

B = BONDING TOOLS

C = COUNTERBALANCE SYSTEM

D = STORAGE EQUIPMENT

\* = DESIGN COMPLETE

Figure 1.1-5. Master Tool List That Was Generated and Presented  
In The SCAD Critical Design Review



#### Subtask I - Fabrication

All necessary materials and equipment were procured and then fabricated into the concentrator and associated hardware. This included the concentrator assembly, assembly tooling, support structure, and counterbalance and laser scanner systems all of which were shown in Figure 1.0-1. The details of fabricating the nineteen hexagonal panels, proofloading the panels, and installation of the latches and associated tooling are described in Section 3.0.

#### Subtask II - Testing

Test plans and detailed test procedures were developed for verification of the concentrator design. The tests were conducted to verify the optical and structural characteristics of the concentrator and to demonstrate possible assembly techniques to be used on the Space Station Freedom. The original program plan had this activity taking place at Harris Corporation but, due to the cancellation of the Mast Program and its production facility, it was moved to NASA LeRC. This joint effort allowed NASA and Harris to gain valuable experience and data on structural and optical performance. Results of the Test effort, demonstrating the design met program objectives, are described in Section 5.0 of this document.

#### Subtask III - Delivery and On-Site Support

The concentrator and its associated equipment were delivered to NASA LeRC prior to the testing of the concentrator. NASA personnel were trained in the operation and setup of the concentrator and associated tooling during

the actual testing of the concentrator. An operational manual for the laser scanner was produced and NASA technicians were trained in proper techniques used to assemble and disassemble the concentrator.

## 2.0 MECHANICAL DESIGN

The mechanical design of the Solar Concentrator Advanced Development (SCAD) prototype Truss Hex concentrator was driven by a Task Authorization NAS3-24670-2 from NASA LeRC. Harris Corporation was directed to develop the Truss Hex Concentrator selected during Task 1 to a Production Prototype level and produce Limited Production Drawings (Level II) of the design. The system sizing requirements were generated from the NASA Task 2 Task Order (Figure 2.0-1). These are parameters that the system must meet to provide the desired power for the Space Station Freedom. Using the system requirements, a list of design constraints were determined and are shown in Figure 2.0-2. Constraints are subsets of the system sizing requirements which may be varied without impacting satisfaction of the program system requirements. For example the unblocked projected area could be larger if the slope error were larger and more spillover of energy occurs. The projected area could be smaller if the slope error were much smaller and less spillover of energy occurs. The guidelines in Figure 2.0-3 are specifications applied to a flight concentrator system. A production prototype (ground test model) should be designed with adaptability to these specifications when the program develops to a flight status. Harris complied with the guidelines for the prototype design whenever possible within program scope and funding constraints.

## SCAD System Sizing Requirements

<u>Parameter</u>	<u>Requirements</u>
o Thermal Flux To The Receiver	o 185 KW SCAD
o Solar Constant	o 1323 W/M <sup>2</sup> (For Sizing Concentrator)
o Intercept Factor	o 95% Minimum (97% Design Goal) (At Worst Case Operational TE, MFG Uncertainties)
o Specular Reflectance	o .90 Or Greater (EOL 10 Years)
o Configuration	o Offset Optics
o Weight and Moment Of Inertia	o Minimize
o Deployed Stiffness	o Maximize ( $\geq 1$ HZ)
o Stowed Volume	o Reflector and Cradle Cylinder 4.58 MDIA x 2.63M (180 inch Diameter x 104 inch)
o Design Life	o 10 Years
o Heat Cycle	o Closed Brayton (Operating At 700-760° C)

Figure 2.0-1. SCAD System Sizing Requirements Used To Design The Truss Hex Solar Concentrator. Presented In The Critical Design Review

### Harris Generated Design Constraints

<u>Parameter</u>	<u>Constraint</u>
o Concentrator Surface Area	o 168.86M <sup>2</sup> (Unblocked Projected Area)
o Slope Error	o 3 MRAD
o Receiver Aperture Diameter	o .43M (17 Inches)
o Environmental	
- Temperature	o -20°F To + 120°F
- Temperature Gradient	o Minimize During Measurement
- Humidity	o Maintain Facility Between 40-60%
- Loads (Handling)	o Size For 1.5 G's
	- 7 Panels With Center Support
	- 19 Panels With Counterbalance

Figure 2.0-2. Harris Generated Design Constraints That Were Used  
In The Design Of The SCAD Concentrator

Figure 2.0-4 provides a list of design drivers that were generated by NASA LeRC and Harris Corporation. The design drivers are standard rules for light weight and high stiffness space structures and were used during the design process.

### System Design Guidelines

<u>Parameter</u>	<u>Guidelines</u>
Environments:	
o Launch Loads	o JSC007700 (STS Loads and I/FS)
o Acoustics	o JSC07700, ISD 2-19001
o Fracture Control	o JSC19659
o Stress Corrosion	o MSFC-522
o Outgassing	o NASA-SPR-022A
o Thermal	o JSC07700, Vol XIV, Rev H
o Vibration	o JSC07700, ICD-2-19001

Figure 2.0-3. System Level Requirements That Would Be Used For A Flight Concentrator But Used As Guidelines For The Prototype Model

### Design Drivers From Task Letter

- o Have A High Stiffness To Weight Ratio
- o Have A High Strength-To-Weight Ratio For Structural Material
- o Have Sufficient Planar Isotropic Thermal Properties To Prevent Warping Due To Thermal Excursions
- o Have A Predictable Thermal Cycling Behavior To Ensure Long-Term Dimensional Stability
- o Have A Low CTE-To-Thermal Conductivity Ratio To Minimize Thermal Gradients and Distortion
- o Have Good Resistance To Corrosion To Survive Earth Bound Uses Of Concentrator During Several Years Of Testing
- o Have Low Moisture Absorbance To Minimize Effects Of Distortions Due To Dryout (For Epoxy Based Composites).

Figure 2.0-4. A List Of Design Drivers That Are Used For Design Of Lightweight High Stiffness Space Structures

An optical performance error budget was established for the Truss Hex design and is presented in Figure 2.0-5. The budget was established by allocating the total error budget to identify error sources. Nominal worst-case deviations are estimated from known data, past experience or perceived relative difficulty. Uncertainty errors are estimated from past program experience. Nominal worst-case deviations are summed because they are known errors while the uncertainty errors are root sum squared (RSS'd) due to the randomness of their occurrence. The total budget is the RSS of the nominal and uncertainty errors. The total error budget reflects specification compliance.

## 2.1 SCAD Prototype Concentrator

By applying the SCAD system sizing requirements, constraints, guidelines and design drivers summarized in Section 2.0, the following offset Truss Hex concentrator design was generated.

The Truss Hex concentrator is an offset parabolic configuration that employs a faceted reflective surface. The selection of the offset configuration was based on the results of a Space Station Freedom Phase B study (Reference 1). To accommodate the unsymmetrical flux distribution of the offset configuration, the receiver is tilted  $50^{\circ}$  to  $54^{\circ}$  with respect to the vertex to circumferentially distribute the flux on the receiver cavity wall. The concentrator is a self-supporting structure consisting of an array of 19 flat hexagonal panels mapped onto a contoured surface. The reflective surface is composed of spherically contoured, equilateral

<u>Error Source</u>	<u>Worst Case Nominal Diviation From Bias Milliradians</u>	<u>One Sigma Uncertainty Milliradians</u>
Alignment (Face-up face-down average)	.50	0
Target location		.20
Measurement		.50
Non-repeatability (Hexagon location)		1.25
Facet manufacturing		
Macroscopic error (slope error)		1.50
Microscopic error (specular reflectance)		1.00
Receiver to reflector alignment	.70	.70
Environmental, life aging, etc.	.50	1.55
Temperature		
Microcracking		
Moisture dryout		
RSS error	.995	2.830
RSS Total Error		3.0 Milliradians

Figure 2.0-5. Performance Error Budget



triangle facets mounted within the panels. There are 24 facets per panel; each facet individually focusable and aligned such that it approximates paraboloidal optics. The concept of individually focusable facets allows tailoring the flux pattern in order to meet receiver requirements. The hexagonal panels can be interconnected with either latches and hinges or all latches. This provides the options of automated deployment by the use of motorized hinges or robotic/manual assembly of the concentrator. The projected reflective surface area required by the Truss Hex concentrator is  $160\text{m}^2$ .

The Truss Hex concentrator concept affords a readily producible and design flexible concentrator. It utilizes several levels of modularity and commonality between parts. The technology required to fabricate the concentrator is available, and reflective surface materials have been identified that are potentially durable in the LEO environment.

Figure 2.1-1 gives the basic dimensions of the concentrator when it is stowed in the shuttle bay and when it is deployed on orbit. Figure 2.1-2 illustrates the deployed concentrator from a side view and Figure 2.1-3 shows a view from the sun toward the concentrator. The concentrator hexagonal panels are mapped onto a sphere with a radius of 877 inches. This radius was selected because it closely approximated the parent parabola. By mapping the panels onto a sphere the geometry of the resulting concentrator becomes symmetric about the central panel of the nineteen panel assembly.

## SCAD Model Description Summary

- o Basic Model Parameters
  - 350 Inch Focal Length
  - Hex Dimensions
    - Point To Point 4.10 Meters  
(13.46 Ft.)
    - Flat To Flat 3.55 Meters  
(11.66 Ft.)
- o Deployed Envelope
  - Overall Diameter 16.75 Meters  
(54.83 Ft.)
  - Overall Depth 1.95 Meters  
(6.39 Ft.)
- o Stowed Envelope (SCAD)
  - Overall Diameter 4.41 Meters  
(Outside Of Latches) (14.46 Ft.)
  - Overall Length 2.17 Meters  
(Stack Height) (7.13 Ft.)

Figure 2.1-1. Basic Dimensions Of The Truss Hex Concentrator As Well As The Deployed and Stowed Dimensions Of The Concentrator

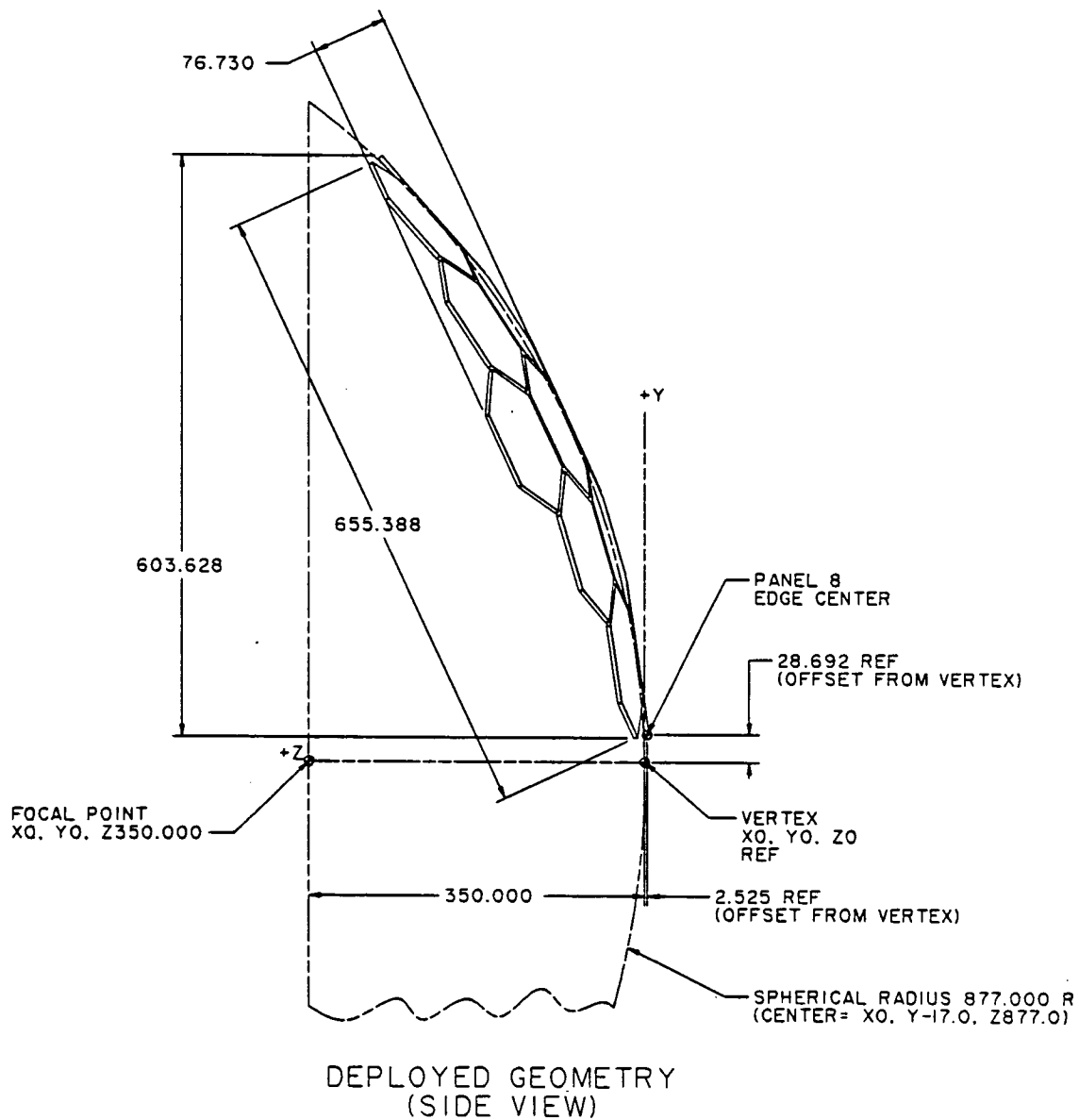


Figure 2.1-2. Deployed Geometry Of The SCAD Prototype Concentrator As Seen From A Side View

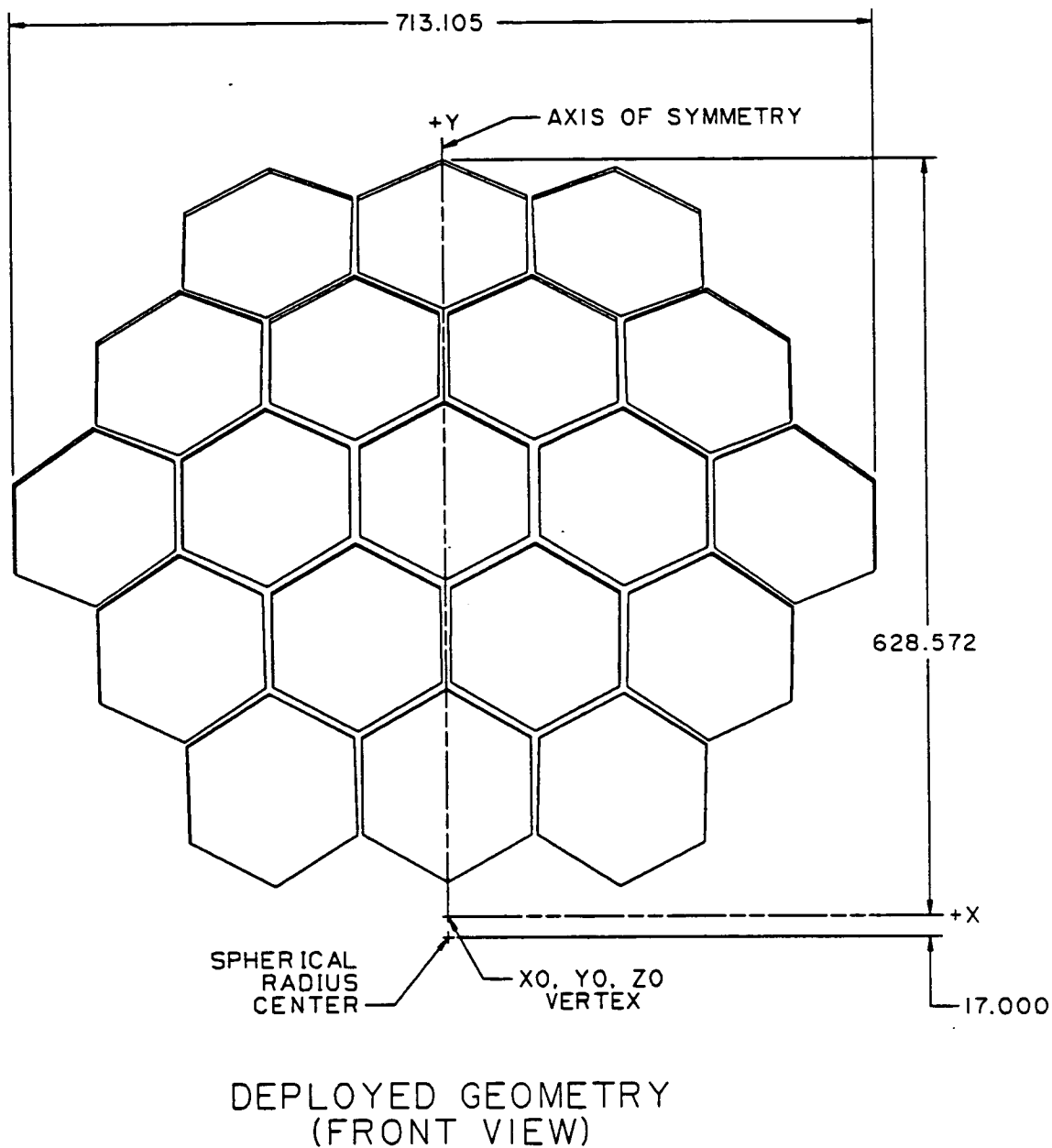


Figure 2.1-3. Shows A Front View Of The SCAD Concentrator Looking Down The Z Axis. This Is A Projected View Looking From The Sun.

This significantly increased the commonality of components. The individually adjustable mirror facets, mounted within the panels, are then pointed to simulate the parabolic optics of the reflective surface. This allows the hex panels to be mapped on a sphere with no degradation in optical performance. A study performed early in the program comparing the flux distributions obtained by mapping the hexagonal panels onto a parabola and onto a sphere showed negligible differences. Due to the reduced complexity, cost savings incurred from fewer parts and reduced design time, the spherical map was selected.

An edge offset of 28.692 inches away from the vertex of the parent parabola in the positive Y direction was selected for the concentrator. This offset reduced the blockage of the incoming rays by the receiver aperture plate which would be located at the focal point of the concentrator. The 2.525 inch offset of the concentrator edge from the vertex of the parabola in the negative Z direction was selected to minimize the mirror facet rotations within the hexagonal panels. A parametric study was performed using an optical analysis program and determined this offset to be optimum.

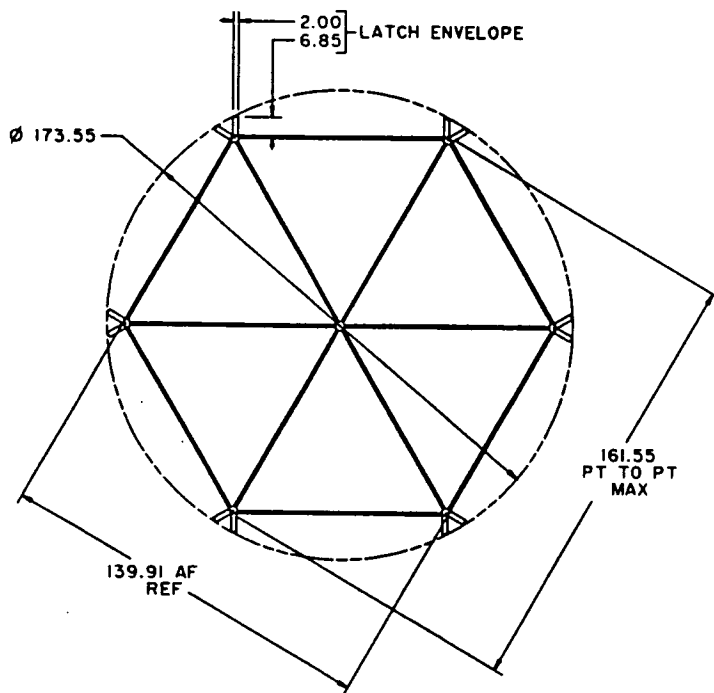
#### Optical Analysis

An optical analysis program developed at Harris Corporation, by Dr. J. D. Sturgis, defined the reflector geometry, determined the mirror facet spherical radii, calculated the thermal flux delivered to the receiver and mapped the flux distribution within the receiver canister. The following

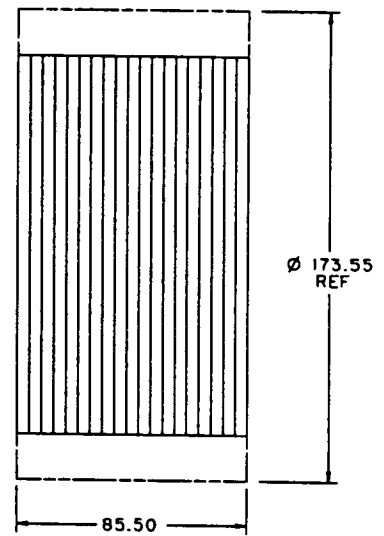
paragraphs provide a brief description of how the program works, the inputs required for the program, and the output which is received.

The first portion of the program is called the hex and facet mapping (Hexmap). The program places seven normal vectors on each of the nineteen hexagonal panels. One at the center of each hexagonal panel and one at each of six corners. The vectors are perpendicular to the plane of the hex panels and point toward the focal point of the reflector (Figure 2.1-2). A spherical radius is then defined at a distance greater than the focal point and the hex panels are then best fit to the spherical contour. Each reflective mirror facet contains a series of normal vectors on the reflective surface side, which are pointed to the focus of the reflector. The number of normal vectors on the facet can be varied from three to fifteen depending on the accuracy required. By changing the contour of the mirror facet from flat to spherical the normal vectors begin to converge onto the reflector focal point. A random error is assigned to the normal vectors on the mirror facets which is a combination of manufacturing tolerances, optical surface errors, and measurement/setting capabilities. The spherical shape and angle of tilt of the mirrors is then iterated until the maximum number of normal vectors pass through the focal point.

After the facet radii and angle of tilt have been calculated the program determines the maximum hex panel depth allowed. The depth corresponds to the hex panel thickness which currently cannot exceed 4.5 inches if two 19 panel solar dynamic modules are to fit in the shuttle. The stowed envelope for the SCAD program can be seen in Figure 2.1-4. If the



(END VIEW)



(EDGE VIEW)

## STOWED ENVELOPE

Figure 2.1-4. Stowed Envelope Of The Nineteen Hexagonal Panels Of The SCAD Concentrator

facet rotation exceeds the 4.5 inch envelope then the program will select another spherical radius on which to best fit the hex panels of the concentrator.

The current reflector spherical mapping radius is 877 inches, with a 350 inch focal length. Parabolic mapping of the hexagonal panels is currently available in the software. The parabolic mapping of the hex panels results in smaller facet tilt angles but results in a non-symmetric reflector structure. The parabolic concentrator mapping is more costly in terms of drawings, latch configurations and production time but results in a slightly smaller stowed package volume for Shuttle launch. Design trade studies determined that the spherical mapping technique would be the most cost effective for the SCAD program.

Determination of the number of different spherical facet radii can also be a program input variable. For a nineteen hexagon concentrator reflector the program can determine 456 optimum mirror facet radii or one optimum mirror facet radius. A parametric trade study was performed by Dr. Sturgis and presented during the Solar Concentrator Advanced Development program preliminary design review. If 456 facets with 456 different spherical facet radii are used the RMS slope error is 1.97 milliradians, with 10 different spherical radii groups the RMS slope error is 1.98 milliradians and with 4 different spherical radii groups the RMS slope error is 2.04 milliradians (Figure 2.1-5). The slope error then begins to rapidly increase to  $\approx 3$  milliradians for 1 radius of curvature. Four radii groups were chosen based on a slight increase in slope error, but a large decrease in facet manufacturing costs as well as overall concentrator cost. The location and



radius of the selected facets within the concentrator can be seen in Figure 2.1-6.

Once the geometry of the reflector is established and the facet radii determined, the ray tracing portion of the program is started. The ray tracing program uses the same node locations which were generated on the facets used in the mapping portion of the program. Ten nodes per facet are converted from normal vector nodes into reflector nodes. With 24 facets per hexagon and 19 hexagons per concentrator, a total of 4560 reflector nodes are generated. The rays are generated from far field source points which are arranged in a disk consisting of eight rings, whose width is based on their area weighting. Each ring contains 10 source points for a total of eighty sources to simulate the sun. Limb darkening is used to account for the spherical shape of the sun and the intensity loss which occurs as one moves from the center of the sun to the outer edge. A ray is then traced from each source to each reflector for a total of 364,800 rays. The rays will then be reflected by the reflector nodes on the mirror facets back toward the receiver aperture. By modeling the support struts as a collection of surfaces of revolution as defined by line segments, the rays leaving the source will contact the support struts and not continue to the receiver canister. The receiver is modeled in a manner similar to the support struts. The front surfaces within the receiver canister are divided into segmented ring cells extending circumferentially around the receiver wall. The number of rays and their intensity contacting each cell can be summed to obtain the total relative power in the receiver canister. A ray

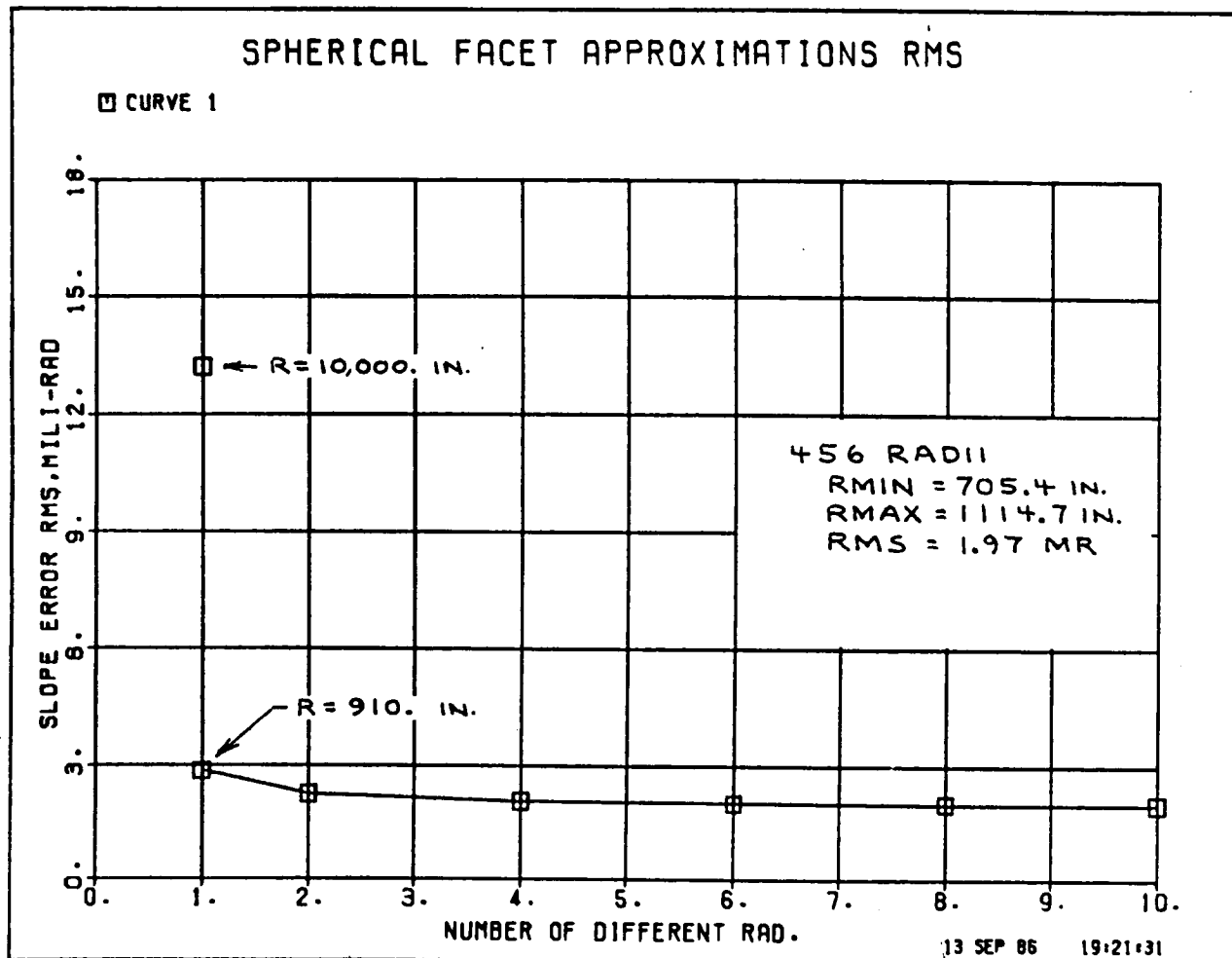


Figure 2.1-5. Shows The Number Of Different Facet Radii Versus The Resulting Slope Error In Milliradians

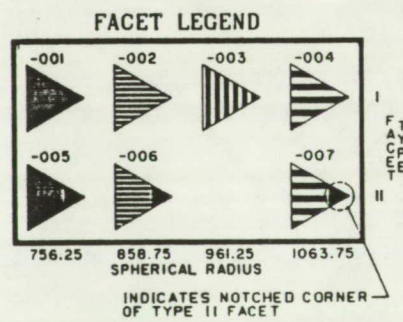
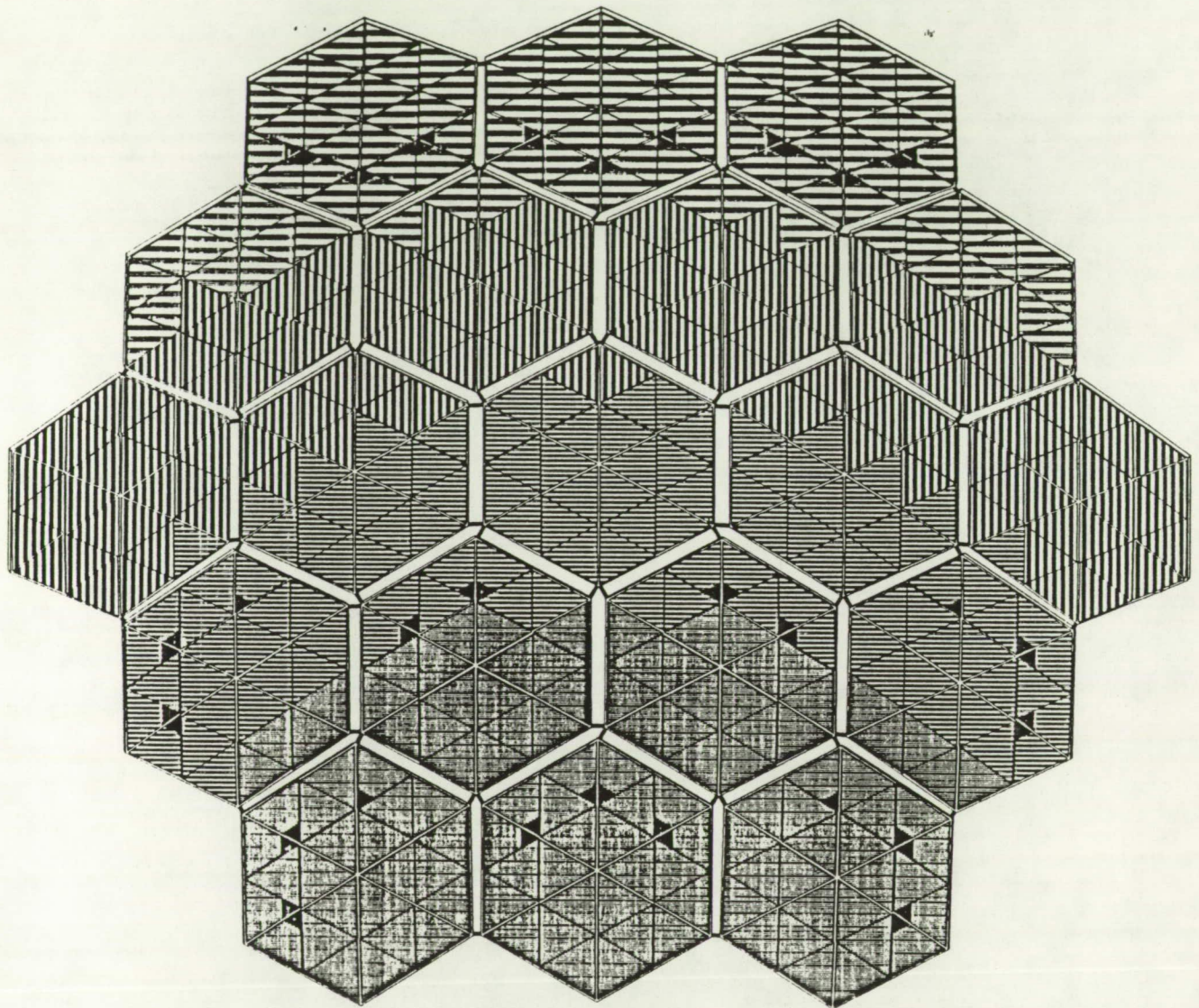


Figure 2.1-6. Illustrates The Radius and Location Of The Four Facets Selected For The SCAD Concentrator

which contacts a solid surface before contacting the reflective mirror facet surface or exiting the reflective surface will stop tracing, be summed, and not be traced into the receiver aperture. Knowing the total number of rays leaving the source and subtracting the number of rays which contact the struts or structure and do not enter the receiver aperture, the total number of rays can be counted. Using the total number of rays entering the aperture, the total flux into the receiver can be calculated.

#### Thermal Analysis

To determine the thermal stability of the concentrator, a thermal analysis was performed to establish operational temperatures of the concentrator. Preliminary thermal analysis results show the thermal environment in the reflector structure is fairly benign. This is accomplished through extensive thermal design and analysis iterations. To achieve the benign temperature throughout the reflector and support struts, a combination of first surface mirror (FSM) and second surface mirror (SSM) reflective thermal blankets or coatings must be used on the structure. The box beams, struts, and back side of the mirror facet are covered with a FSM or SSM blanket or coating, while the latches are aluminum with a gold iridite finish. The maximum temperature change in a component occurs at the mirror facets with a swing of  $125^{\circ}\text{ F}$  (+ 110 to -15) with only a  $6^{\circ}\text{ F}$  gradient through the thickness of the facet.

Temperatures for other major components are as follows:

Latches             $100^{\circ}$  --  $70^{\circ}$  F Non shaded

Box Beams             $75^{\circ}$  --  $40^{\circ}$  F

Struts             $30^{\circ}$  --  $-23^{\circ}$  F

Cross Struts         $7^{\circ}$  --  $-50^{\circ}$  F

In the analysis, the maximum hot temperature and the minimum cold temperature were then applied to the box beams in the hexagonal panels and the latches on the reflector to obtain two thermal cases to be compared to an intermediate case which occurs midway between the two temperature cases. By varying the box beam coefficient of thermal expansion (CTE) the sensitivity of the structure to CTE can be assessed. The resulting structural distortion caused by the application of the two thermal cases to the reflective surface can be seen in Figure 2.1-7.

The thermal distortion FEM models were then inserted into the optical analysis ray tracing program to evaluate the effect of the thermal cases on the optical performance of the concentrator reflector. Distortions of the concentrator were modeled as rigid body displacements of the mirror facets. Thermal analysis of individual facets showed local facet deflections were only .0008 inches at worst case hot temperatures, and .0012 inches at worst case cold temperature. Since individual facet distortions proved to be insignificant they were not applied to the FEM while running the ray tracking program. Using the RMS, defocus, and mispointing results from the thermal distortion analysis, an equivalent facet displacement of .023 inches at any given facet corner was determined and used as input to the optical

analysis program. The final optical analysis results showed less than .08% change in total flux delivered to the receiver over the thermal range expected for the concentrator. Thus the current thermal environment was determined to have little or no effect on the concentrator performance.

#### Thermal Distortion Sensitivity Analysis

$$\text{Graphite CTE} = -0.1 \times 10^{-6} \text{ In/In } ^\circ \text{F}$$

	RMS	Defocus	Mispointing
	(In)	(In)	(Deg)
Hot Case	0.00607	-0.105	0.00564
Cold Case	0.00839	+0.021	0.00157
Intermediate	0.00762	-0.014	0.00043

$$\text{Graphite CTE} = -1.0 \times 10^{-6} \text{ In/In } ^\circ \text{F}$$

Hot Case	0.00748	-0.099	0.00526
Cold Case	0.00616	+0.029	0.00146
Intermediate	0.00414	-0.006	0.00038

Figure 2.1-7. The Results Of The Thermal Distortion Sensitivity Analysis. It Shows A Hot, Cold and Intermediate Distortion As Well As A 10X Change In Coefficient Of Thermal Expansion.

### Structural

Structural and dynamic analyses was conducted for both the concentrator structure and facet assemblies. Finite element models were generated using a Harris Corporation Code. Structural analysis was done to predict the worst case loads that occur during the assembly and handling of the concentrator for both the 7 panel and 19 panel configurations; and the facet for launch and thermal load conditions. The worst load case for the structure was the 7 panel configuration, simply supported, with the high contact stress/subsurface shear occurring at the latching sphere and latch housing/pawl contact points. The worst load case for the facet was during assembly at the facet to standoff interface, where preloading the retainer plates resulted in high contact stress on it and the standoff spherical ball. Dynamic analysis was done to assess the assembled concentrator's first mode natural frequency. The analysis results indicated a first mode natural frequency of 1.652 Hz.

### 2.2 Detailed Design Description

The structure of the solar concentrator is comprised of nineteen hexagonal panels which are latched together to form the reflector (Figure 2.2-1). The basic building block is the hex panel structure. The hex panel structure is comprised of twelve graphite epoxy box beams which are joined together at the corners by shear plates and metallic fittings to form the basic hexagon (Figures 2.2-2 - 2.2-4). The panels are held together using metallic latches that are mounted onto the panels at the corner fittings shown in the previous figure. The "ball and socket" latches provide



translational restraint in three axis but are free to rotate about the ball (Figure 2.2-5). System geometry is determined by the latch location on the panel and the location of the latching sphere in the latch housing. A small error in the latch placement is multiplied twelve times when the outer ring of the concentrator is assembled. This means that very precise location of each latch is needed to ensure proper deployed geometry. The "ball and socket" latch allows the panels to settle into an equilibrium geometry without applying moments to the panel corners that would result in structural distortion and mispointing of the mirror facets mounted in the structure. The composite reflective mirror facets are mounted to the hexagonal panels using three standoff/flexure assemblies, one flexure at each corner of the triangular facet (Figure 2.2-6). By isolating the mirror facets from the hexagonal panel, thermal distortions are greatly reduced. The weak axis of the flexure is placed perpendicular to the radial direction of thermal expansion of the mirror facet. As the facet expands and contracts, due to temperature variations, the flexures deflect rather than constrains the facet thus causing no distortion of its curvature. The strong direction of the flexure prevents the facet from hitting the box beams under launch loads. A more detailed description of the concentrator components is provided in the following sections.



## SOLAR CONCENTRATOR MODEL NOMENCLATURE

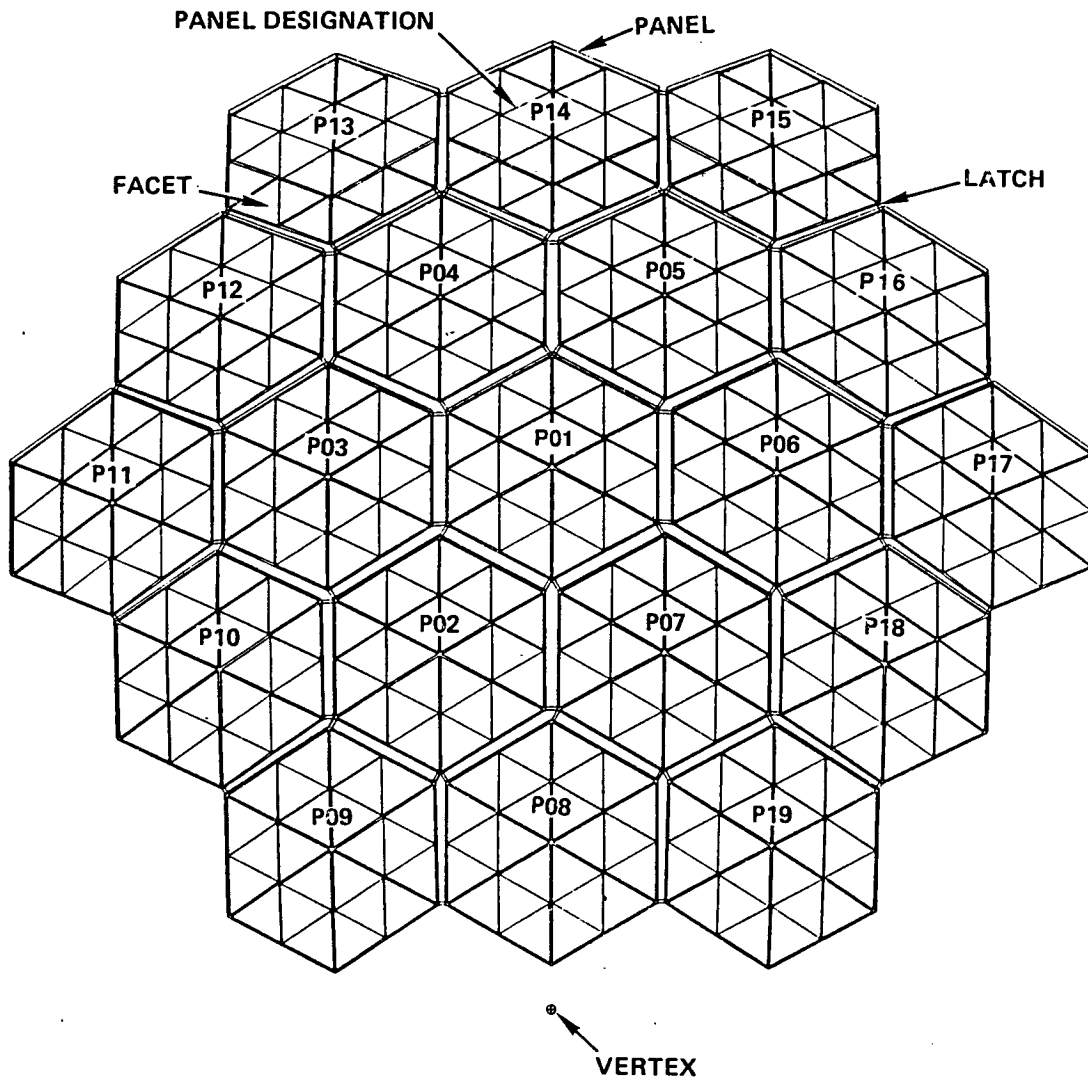
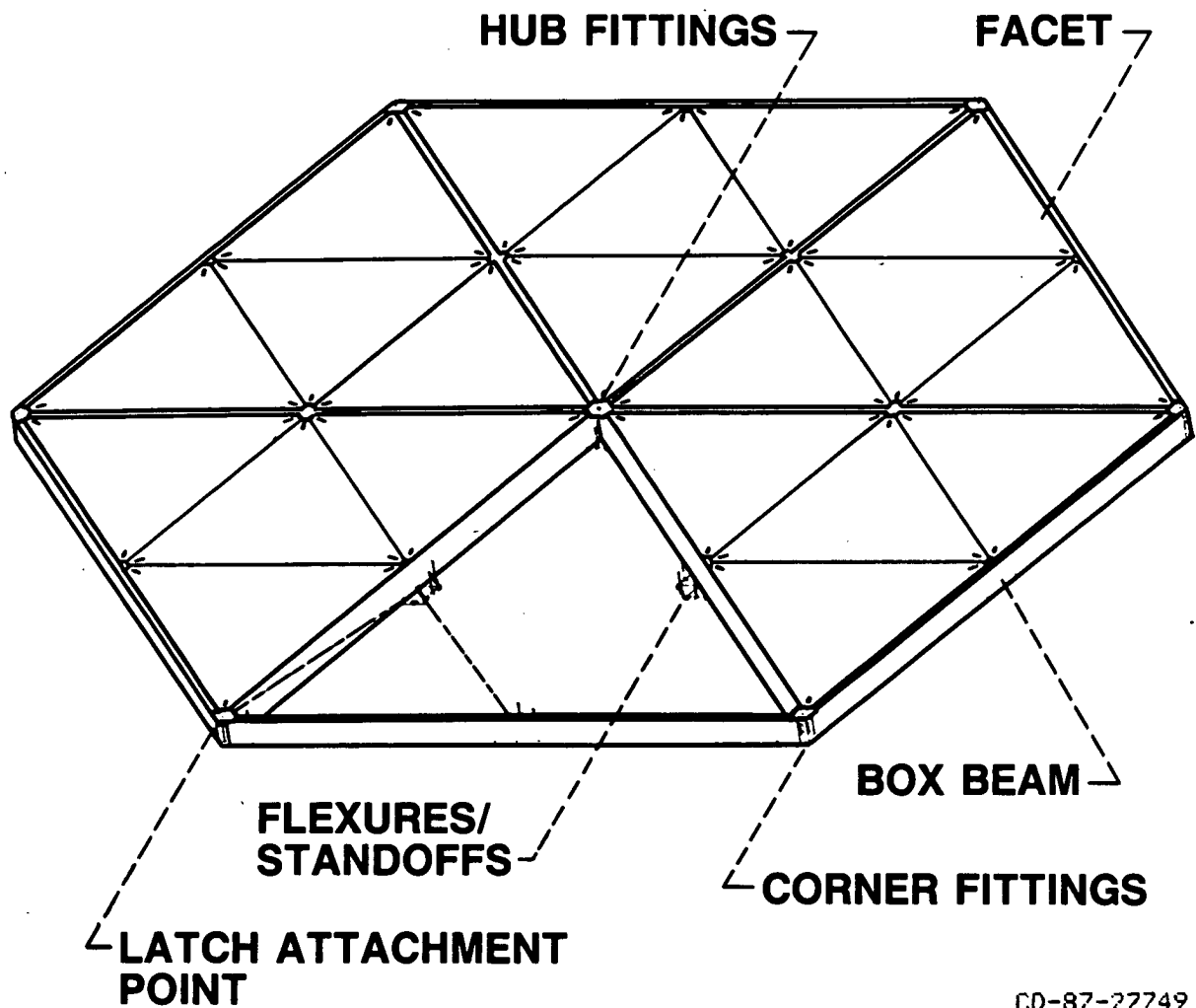


Figure 2.2-1. Description Of The Basic Components Of The SCAD Concentrator and The Panel Designation

# HEXAGONAL PANEL NOMENCLATURE



CD-87-27749

Figure 2.2-2. The Basic Building Block Of The Truss Hex Concentrator Hexagonal Panel

ORIGINAL PAGE  
BLACK AND WHITE PHOTOGRAPH

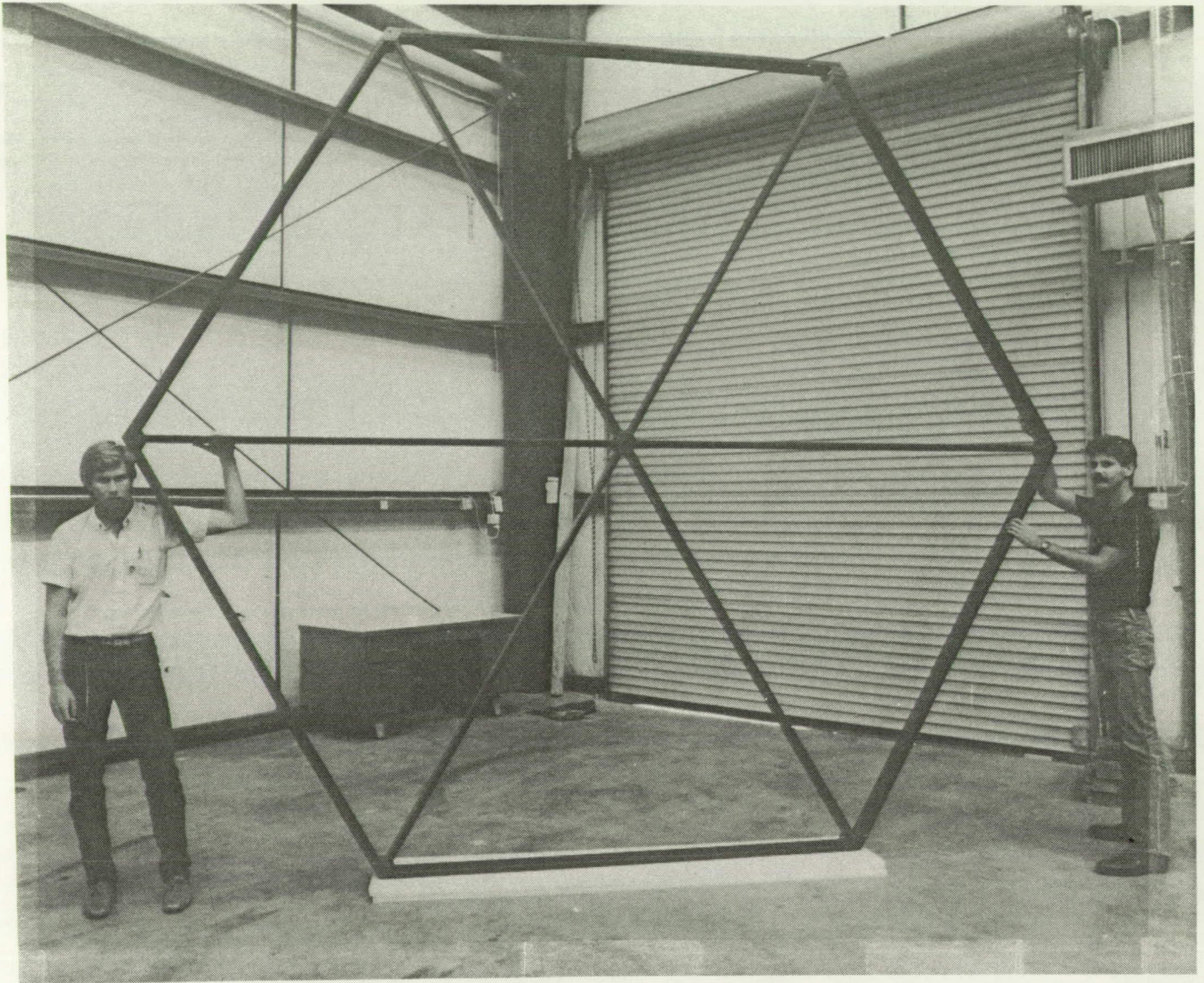


Figure 2.2-3. Completed Hexagonal Panel Showing The Basic Graphite Box Beams And Corner Fittings

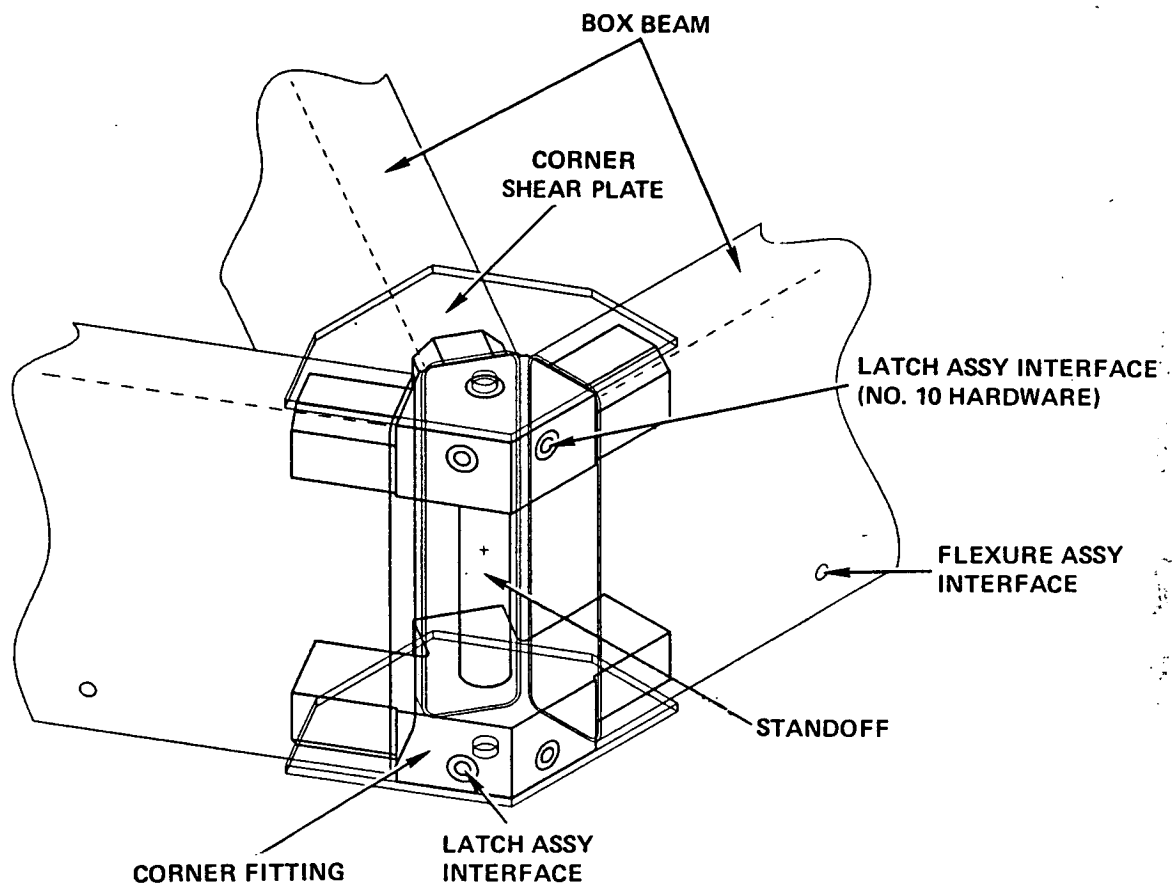
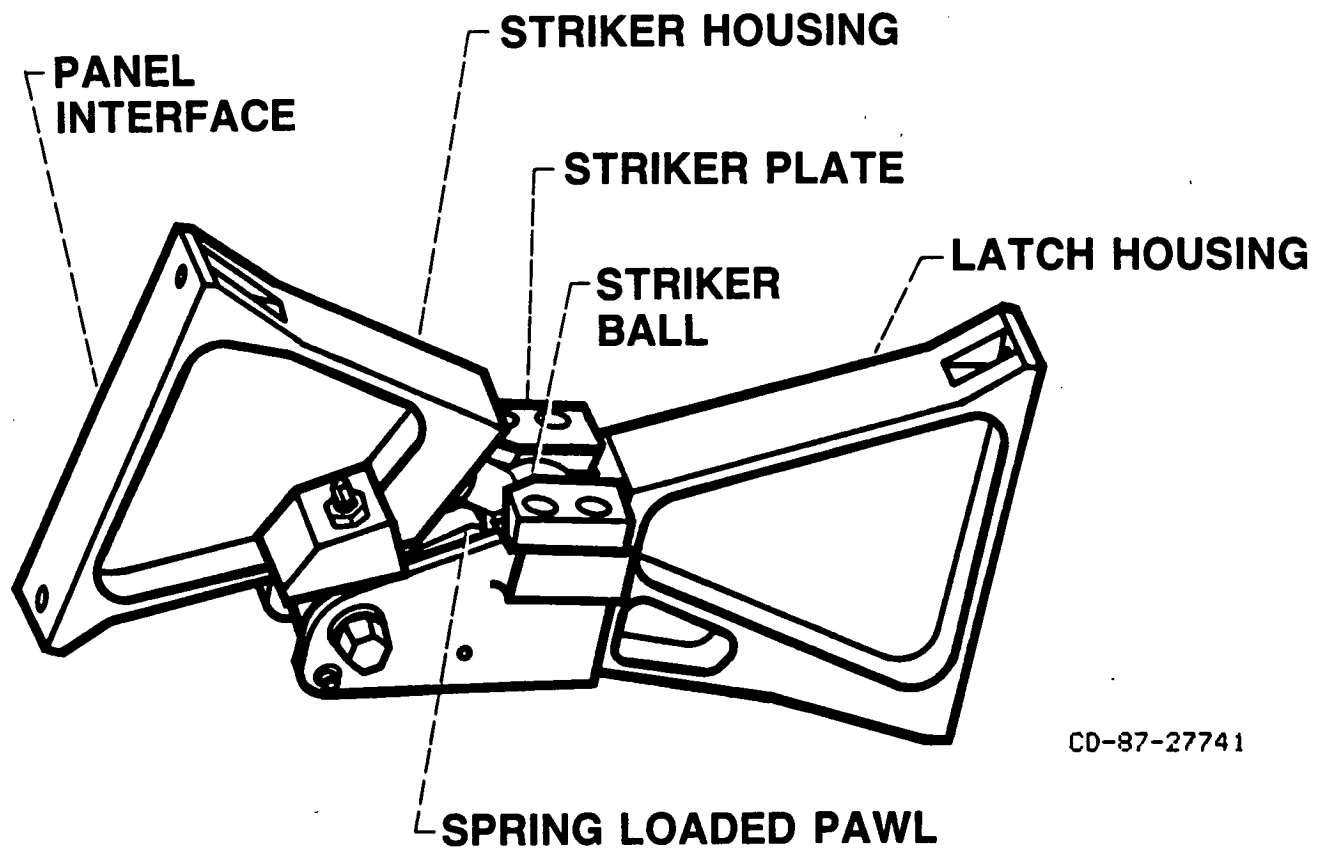


Figure 2.2-4. A Typical Corner Fitting

## TYPICAL LATCH ASSEMBLY



CD-87-27741

Figure 2.2-5. Ball and Socket Latch Provides Three Degree Of Freedom In Rotation While It Has Zero Degrees Of Freedom In Translation. This Allows The Ball To Rotate and The Hexagonal Panel To Seek Its True Geometric Location

## FACET TO PANEL INTERFACE ASSEMBLY DETAILS

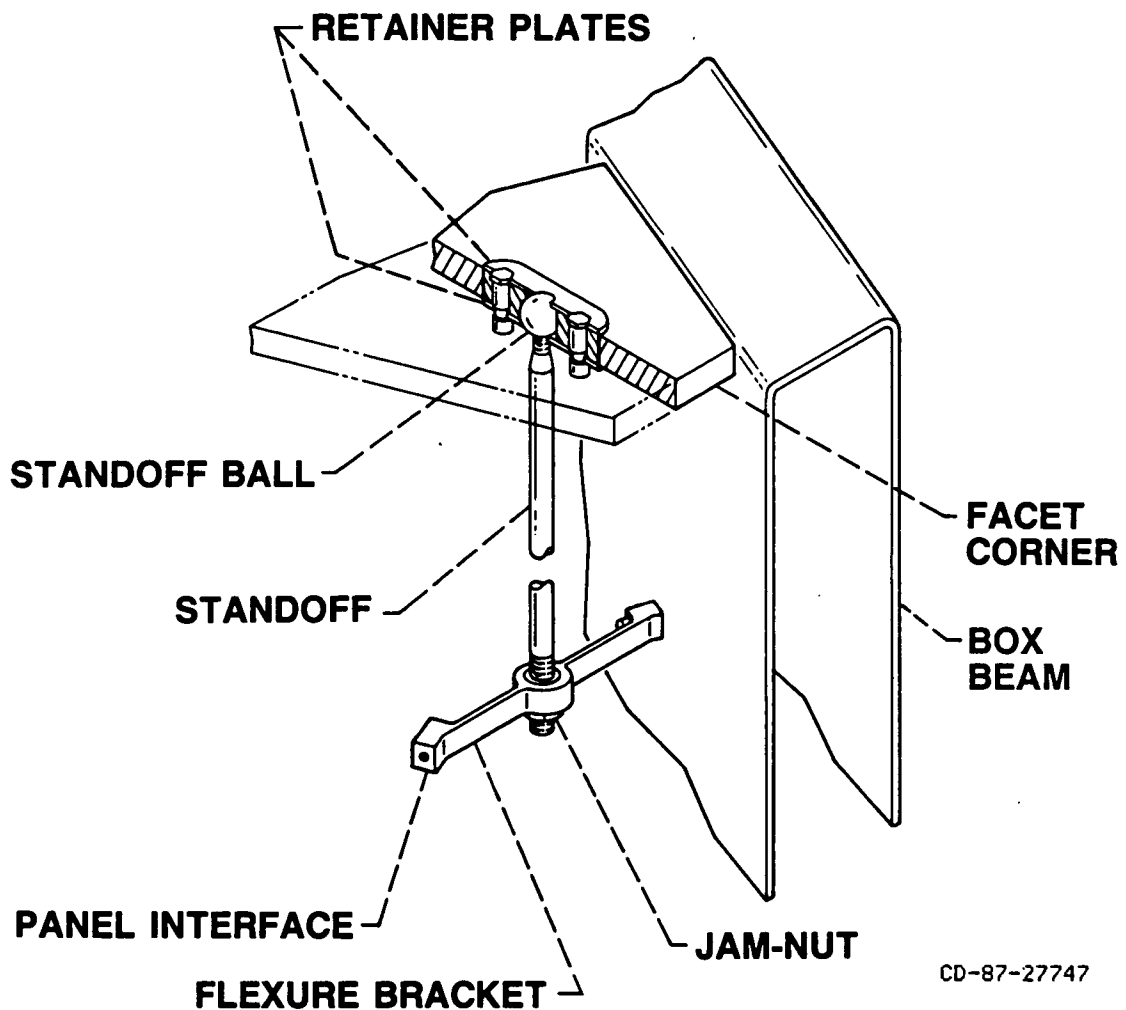


Figure 2.2-6. Composite Mirror Facet Is Attached To The Box Beams Using One Flexure At Each Corner. This Isolates The Facet Thermally and Structurally From The Box Beams.



### 2.3 Box Beams Development and Testing

The box beam, shown in Figures 2.3-1 and 2.3-2, is the main structural element of a panel. The material, cross section, and ply layup were chosen to achieve the desired dimensions, stiffness, and thermal properties as determined by the thermal and structural analysis. Hercules Corporation supplied the beams as well as all other graphite components used on the program.

The box beam was constructed of ultra high modulus (UHM) prepreg graphite.

Two different manufacturing processes were used in the SCAD program. The first method is a tape wrapping process. An aluminum mandrel sprayed with mold release is wrapped with the first -45 degree angular ply of graphite prepreg and is then consolidated to remove wrinkles and ensure contact between layers. A die cut  $0^{\circ}$  ply is applied and consolidated. This process is repeated for the first seven layers -45, 00, + 45, 000. The mandrel is then placed in a vacuum bag and heated to consolidate the first seven layers. This process allows the layers to flow together and remove air voids between the layers of prepreg and remove excess epoxy that may exist. When the initial consolidation is complete the remaining four plies of prepreg are applied and then consolidated. The box beams have a top and bottom section that is twice as thick as the sides. To achieve the double thickness, two caps are die cut from consolidated sheets of prepreg with the correct layup -45, 0<sub>2</sub>, +45, 0<sub>3</sub>, +45, 0<sub>2</sub> -45 and installed on the top and bottom

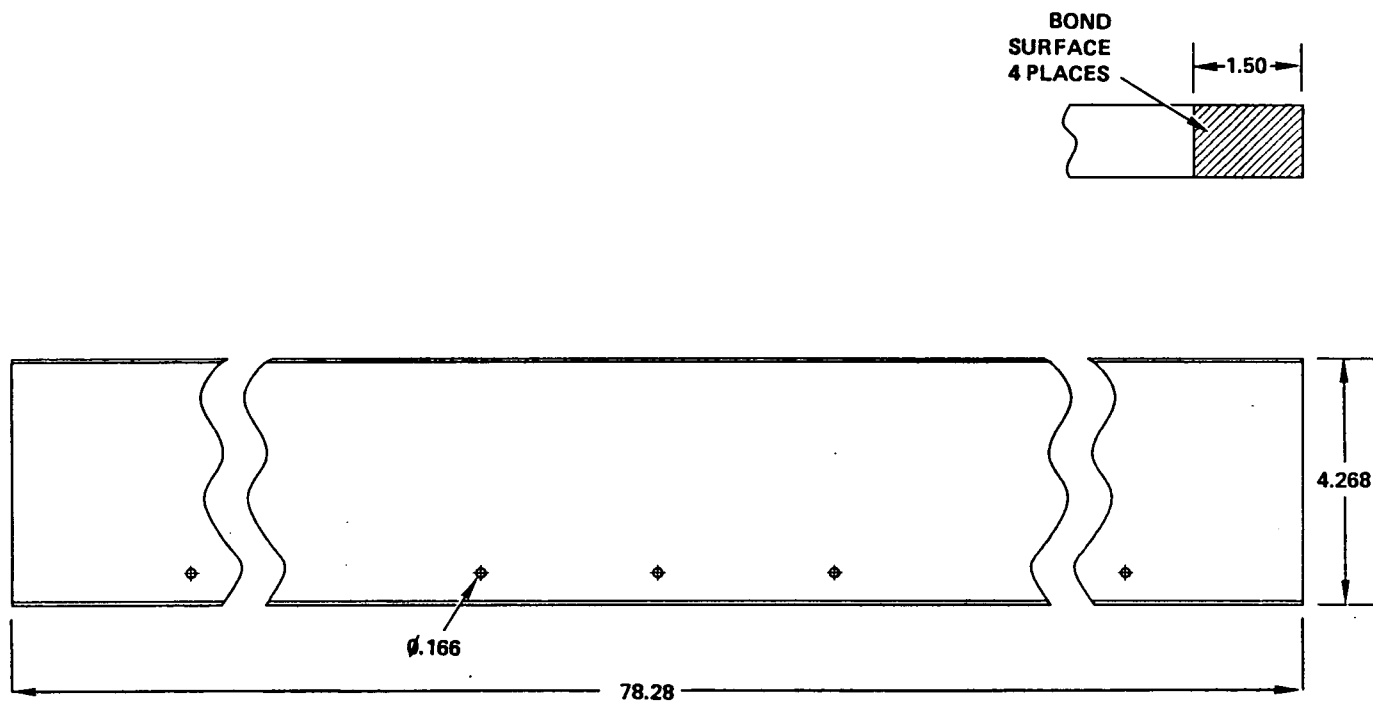
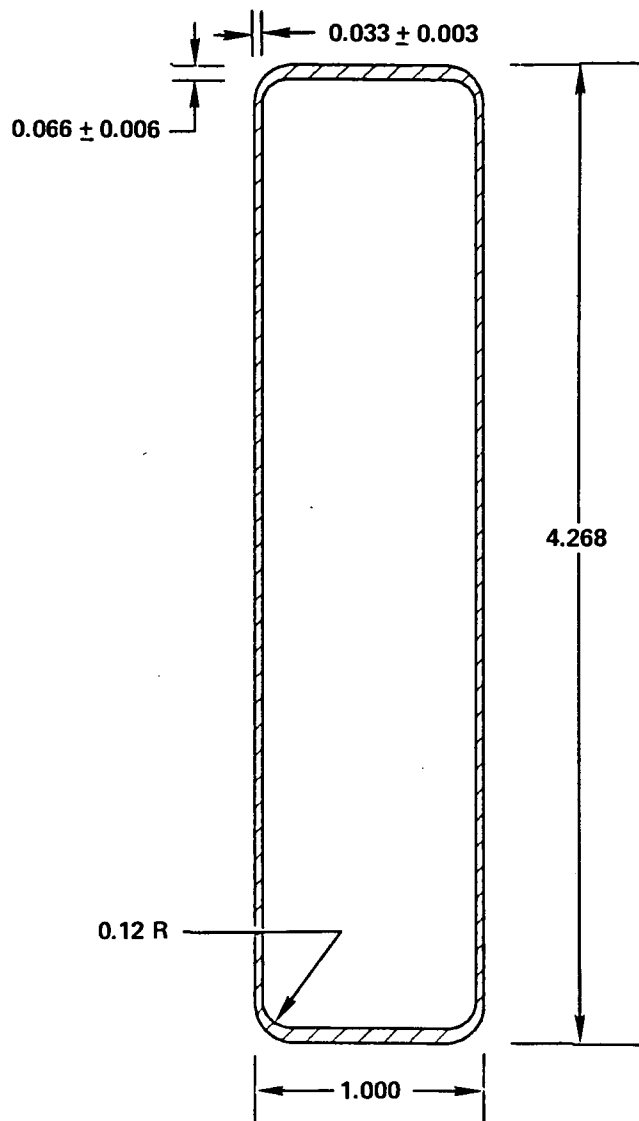


Figure 2.3-1. Graphite Epoxy Box Beam





PLY LAY-UP: -45; 0<sub>2</sub>; +45; 0<sub>3</sub>; +45; 0<sub>2</sub>; -45

PLY THICKNESS: 0.003

Figure 2.3-2. Beam Cross Section Composed Of Eleven Plies  
Of Ultra High Modulus (UHM) Prepreg Material

of the wrapped beam. The final process involves consolidation of the assembly by wrapping it with heat shrink tape and conducting a final cure in the autoclave. The autoclave is operated at 100 PSI and 350 degrees Fahrenheit for two hours. After the cure is complete and the assembly has cooled, the aluminum mandrel is removed. Due to the high coefficient of thermal expansion (CTE) of the aluminum and the low CTE of the graphite epoxy layup, the mandrel shrinks more during the cooling process and can be slipped out of the box beam. The finished beams were machined using a diamond saw and diamond drill bit to achieve the proper length and hole pattern. The process is shown in Figures 2.3-3 to 2.3-5.

BEAM MANUFACTURING  
ZERO DEGREE PREPREG TAPE APPLICATION

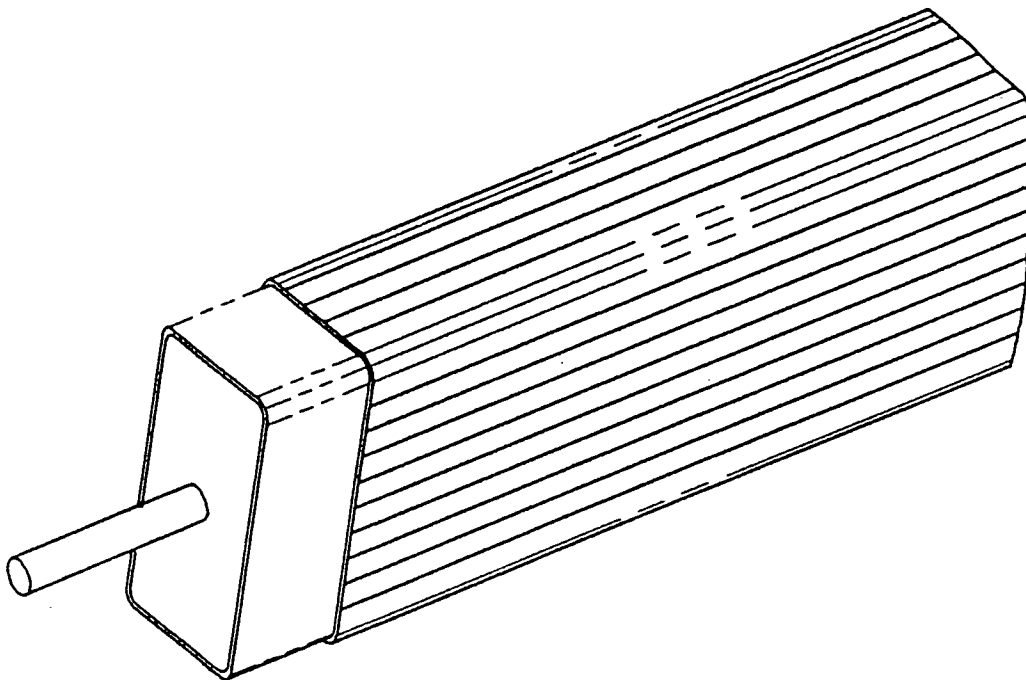


Figure 2.2-3. The Zero Degree Plies Are Placed On The Mandrel In The Longitudinal Direction Of The Aluminum Mandrel

## ANGLE PLY PREPREG TAPE APPLICATION

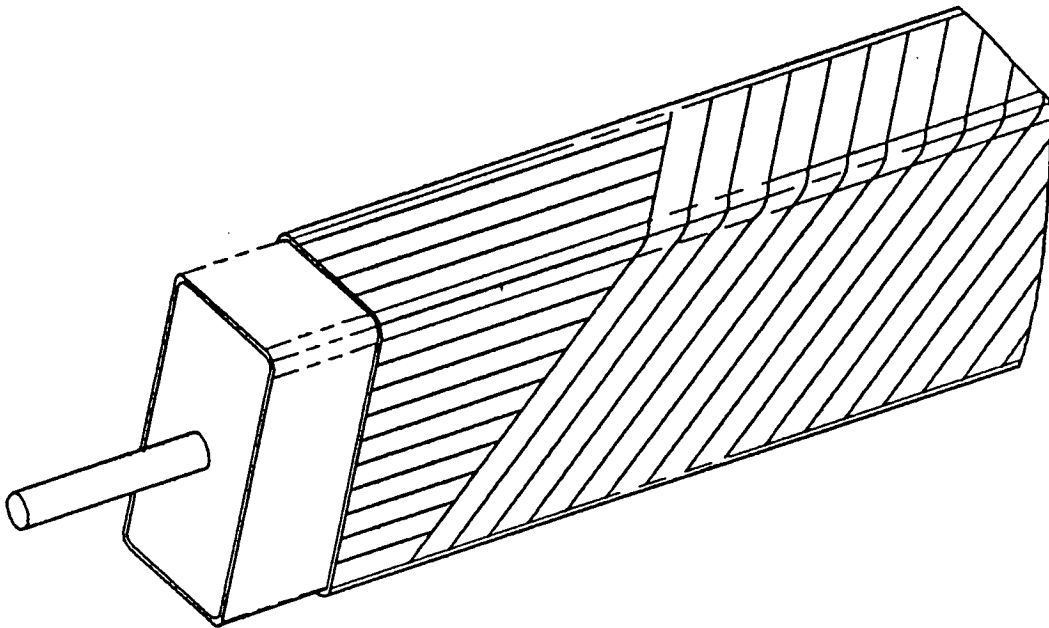
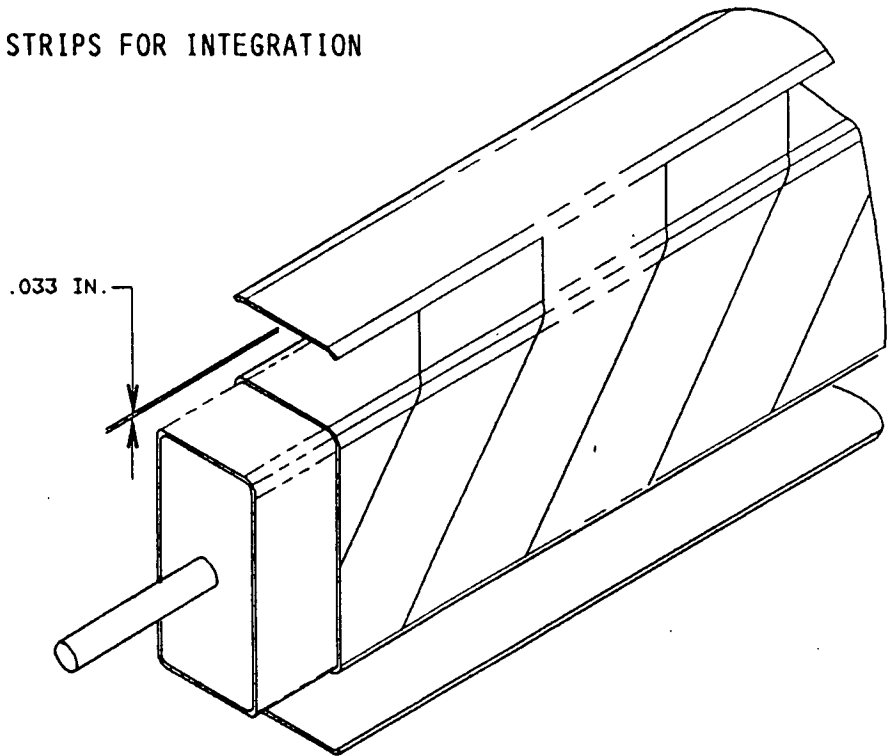


Figure 2.3-4. The 45 Degree Plies Are Wrapped Around The Mandrel Like Stripes On A Barber Shop Pole. Three Wide Strips Are Needed To Complete One Layer

- LAYUP ELEVEN PLY PREPREG PANEL AND  
DIE CUT SHORT SIDE STRIPS FOR INTEGRATION  
INTO BEAM LAYUP



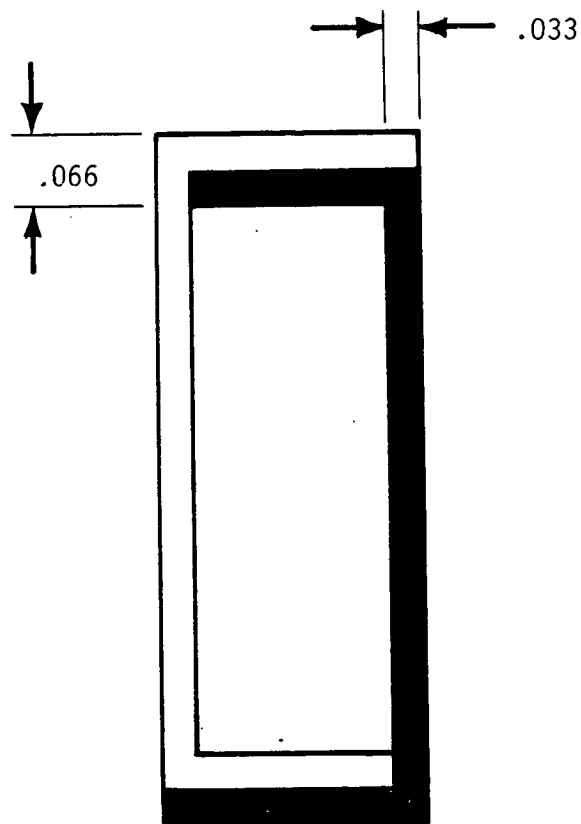
NOTE: STRIP LAYUP AND BEAM TUBE LAYUP ARE COMMON  
ORIENTATIONS AND THICKNESS FOR UNIFORM CTE.

Figure 2.3-5. The Final Step Of The Top Wrap Process Is Completed By Adding The Consolidated Strip, .033 Inches Thick, To The Caps Of The Beam

The second box beam manufacturing method is called the Co-cured C-channel design. This method was used to help eliminate the twist experienced in some of the wrapped beams. In addition, the new process allowed a production rate increase of 50%. The C-channel process involves die cutting two pieces of flat vacuum bagged and consolidated prepreg material from the -45,0,0 +45,0,0,0, +45,0,0, -45 layup which is .033 inches thick or the same as the side walls. The two pieces are placed on the same aluminum mandrel as the tape wrap beams shown in Figure 2.3-6. The assembly is then wrapped with heat shrink tape which contracts as the part is heated. The assembly is co-cured in an autoclave similar to the tape wrapping process and finished machined in the same manner.

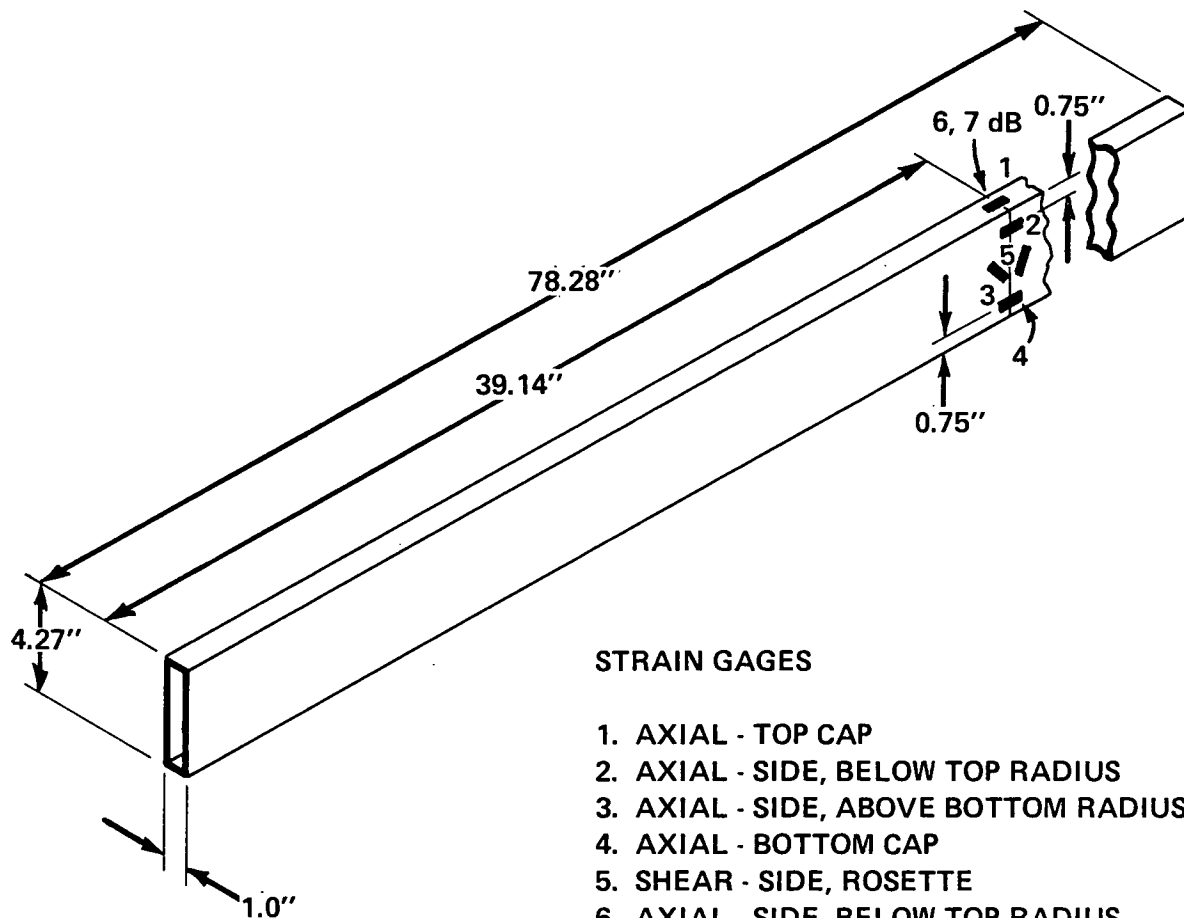
The finished beams were qualified by Hercules using a 4 point bend test. The 4-point bend test was performed on the box beams with Strain Gauges mounted as shown in Figure 2.3-7. The tests were conducted at room temperature and the loads applied at a rate of 500 +/- 100 pounds per minute until failure. The test fixture is depicted in Figure 2.3-8. The failure strength of the two beams was 2013 lbs (Tape Wrap Process) and 2020 lbs (Co-cured C-Channel Process). The resulting stiffnesses from proofload tests were virtually identical at  $24.2 \times 10^6$  lbs-in<sup>2</sup> (EI).

This data suggested that the beams had identical structural properties and the Co-cured C-channel process was chosen for the remaining box beams to be manufactured.



890300

Figure 2.3-6. The Two Consolidated Sheets Of Prepreg Material Are Placed On The Mandrel In The Overlap Configuration Shown Above To Form The Co-Cured C-Channel Box Beam



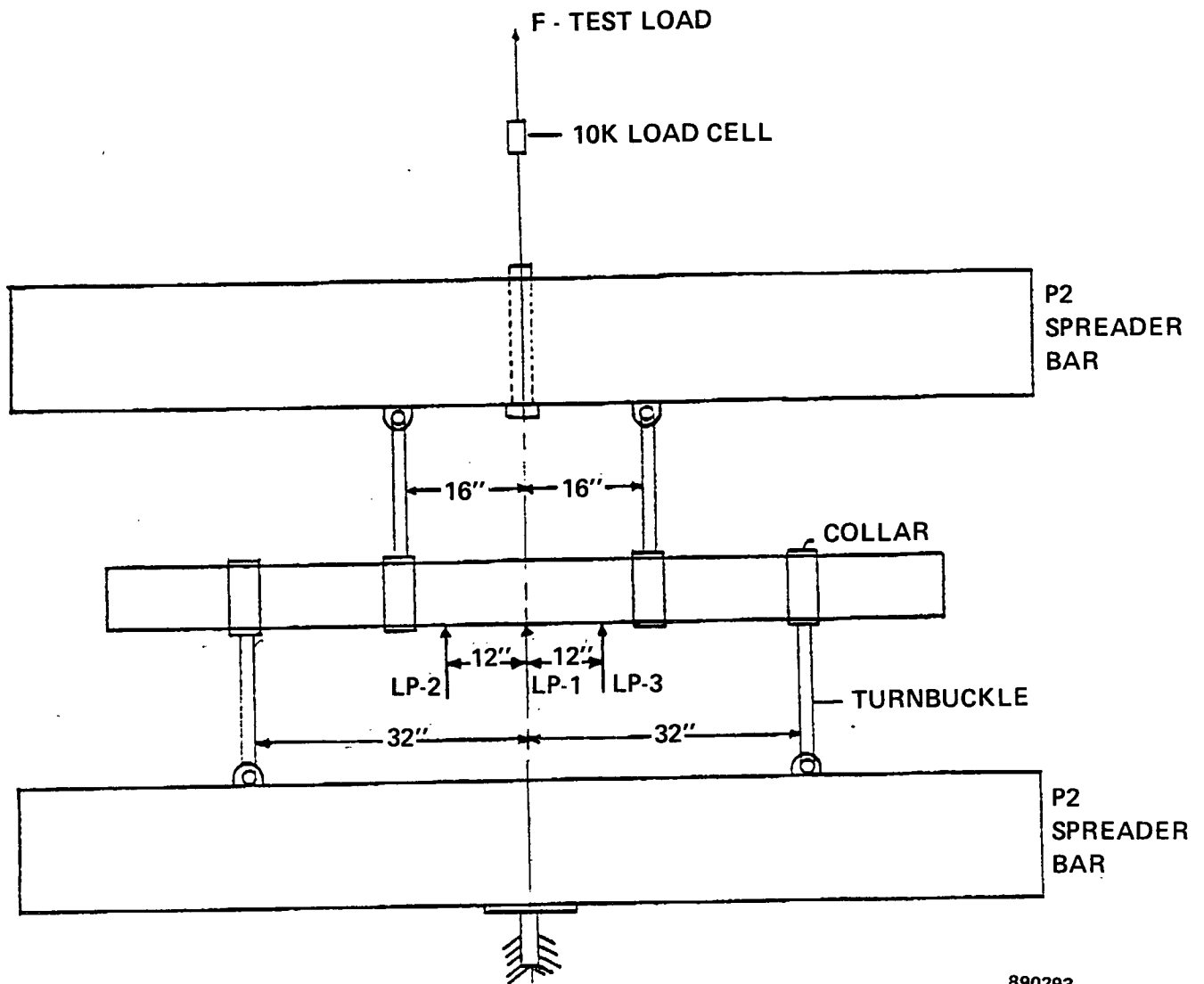
#### STRAIN GAGES

1. AXIAL - TOP CAP
2. AXIAL - SIDE, BELOW TOP RADIUS
3. AXIAL - SIDE, ABOVE BOTTOM RADIUS
4. AXIAL - BOTTOM CAP
5. SHEAR - SIDE, ROSETTE
6. AXIAL - SIDE, BELOW TOP RADIUS
7. AXIAL - SIDE, ABOVE BOTTOM RADIUS
8. SHEAR - SIDE, ROSETTE

890301

Figure 2.3-7. Strain Gauge Location and Orientation For The Four Point Bend Test Performed By Hercules Corporation In Salt Lake City, Utah





890293

Figure 2.3-8. Four Point Bend Test Fixture Used To Determine Load Versus Deflection Data For The Graphite Epoxy Box Beam.

## 2.4 Corner Fitting Assembly

The graphite beams are joined at the six exterior corners by a metallic corner fitting, shown in Figures 2.4-1 and 2.4-2. Although the panel does not require the corner fitting to achieve its overall structural integrity, the corner fitting is used as a geometric locational device during panel manufacturing. The corner fitting defines the location of all box beam centerlines and the six points of the hexagon. The corner fitting also provides the structural attachment and geometric location for the panel latches, which define the overall concentrator geometry.

The corner fitting is constructed from three aluminum piece parts shown in Figure 2.4-3. The two identical corner fitting interface pieces are acid etched to provide a porous surface for structural bonding to the box beams. They are then sprayed with primer to prevent further oxidation and to protect the bonding surface until the bonding operation takes place. The corner fitting interface pieces are aligned and bonded to the spacer rod in the corner fitting bond fixture as shown in Figure 2.4-4. This method of bonding piece parts together to form the corner fitting produces a part with the precision tolerances required for overall structural performance. After the corner fitting has cured, bond wires are attached to the bond surfaces that contact the box beam. The bond wires are used to maintain a normal bond line thickness between the fitting and the graphite beams. The completed corner fitting is shown in Figure 2.4-5. A bond thickness of .005 to .010 inches has proven to provide the highest strength in destructive bond testing.

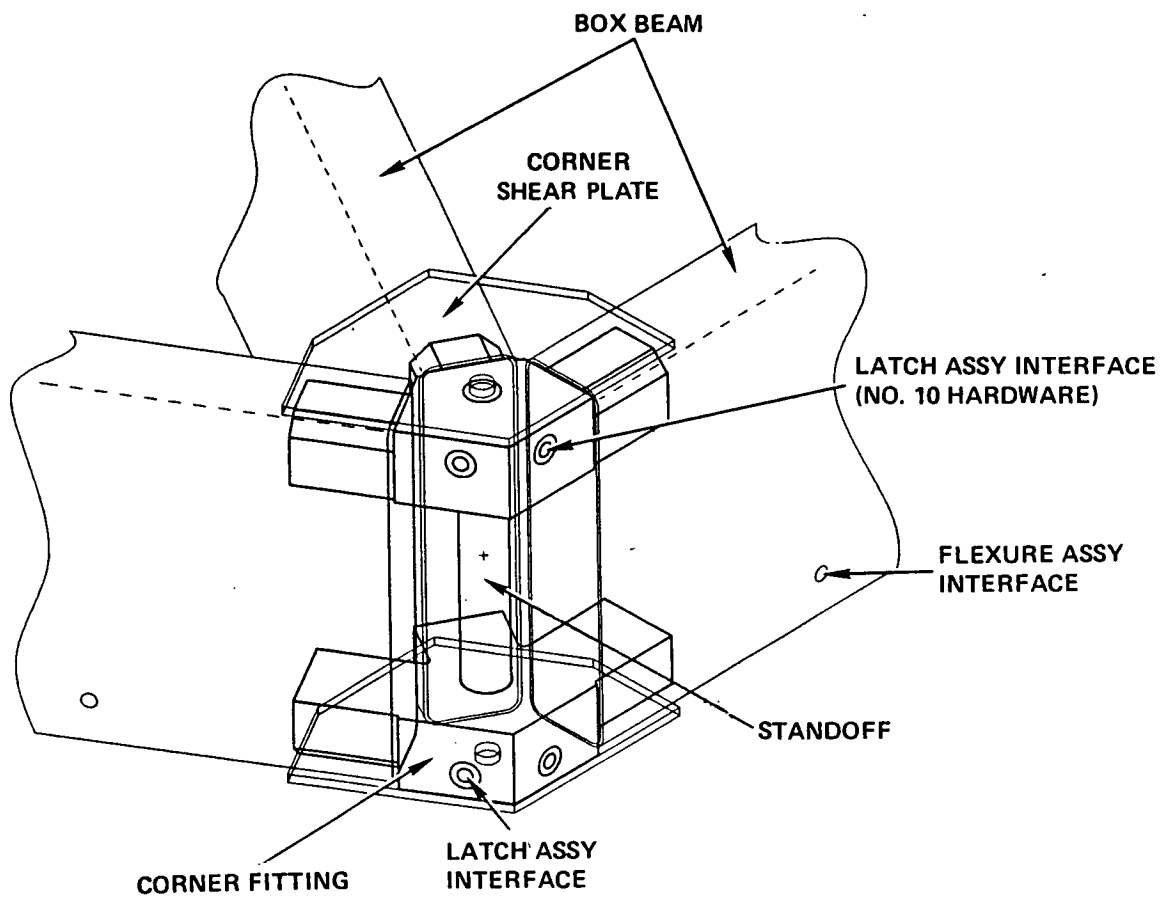


Figure 2.4-1. Hex Panel Corner Detail That Shows Box Beams Bonded To The Corner Fittings; and The Shear Plates Bonded To The Top And Bottom

ORIGINAL PAGE  
BLACK AND WHITE PHOTOGRAPH

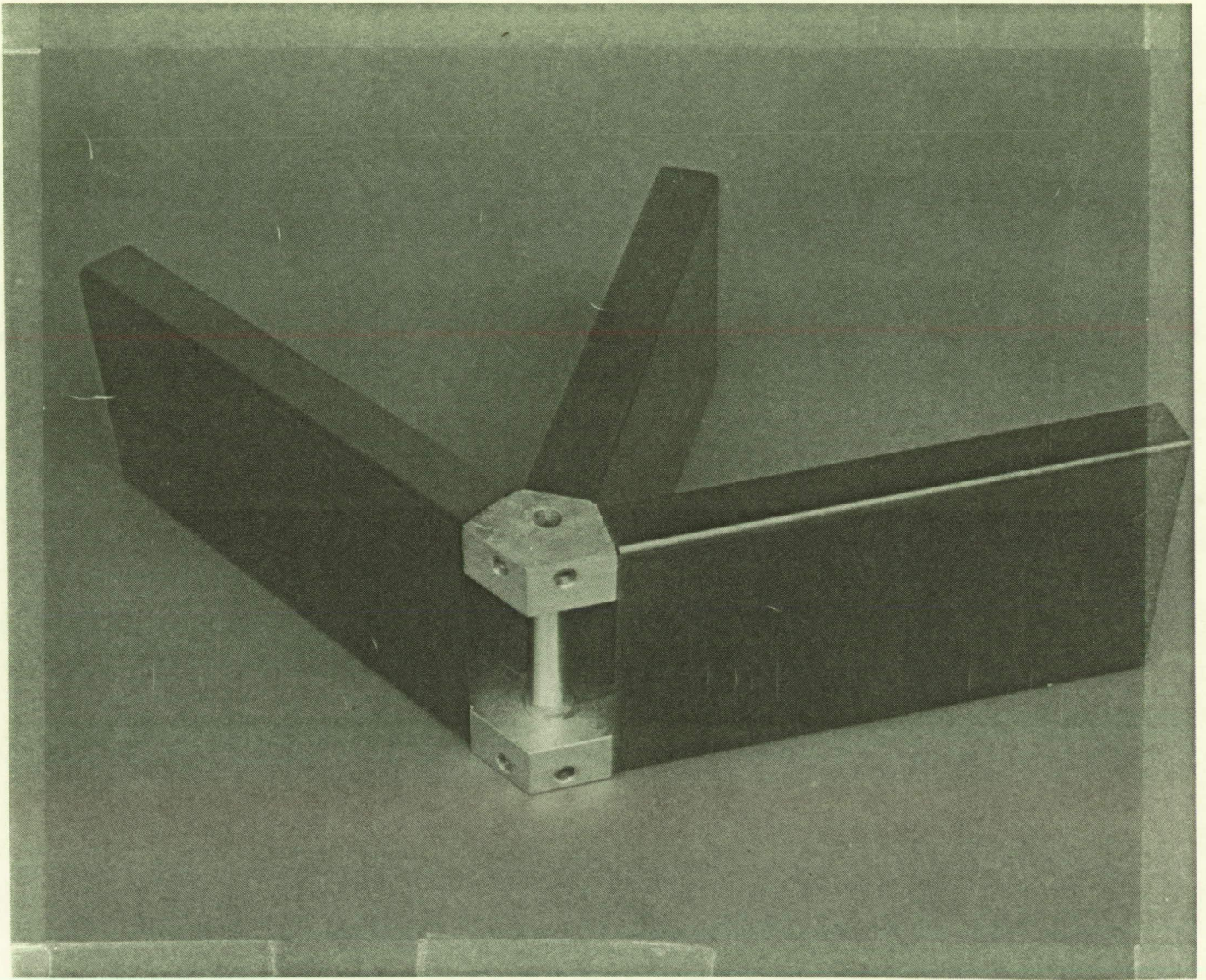


Figure 2.4-2. Actual Corner Fitting With Short Sections Of Box Beam In Place. The Shear Plate Is Removed To Allow Viewing Of The Fitting.



ORIGINAL PAGE  
BLACK AND WHITE PHOTOGRAPH

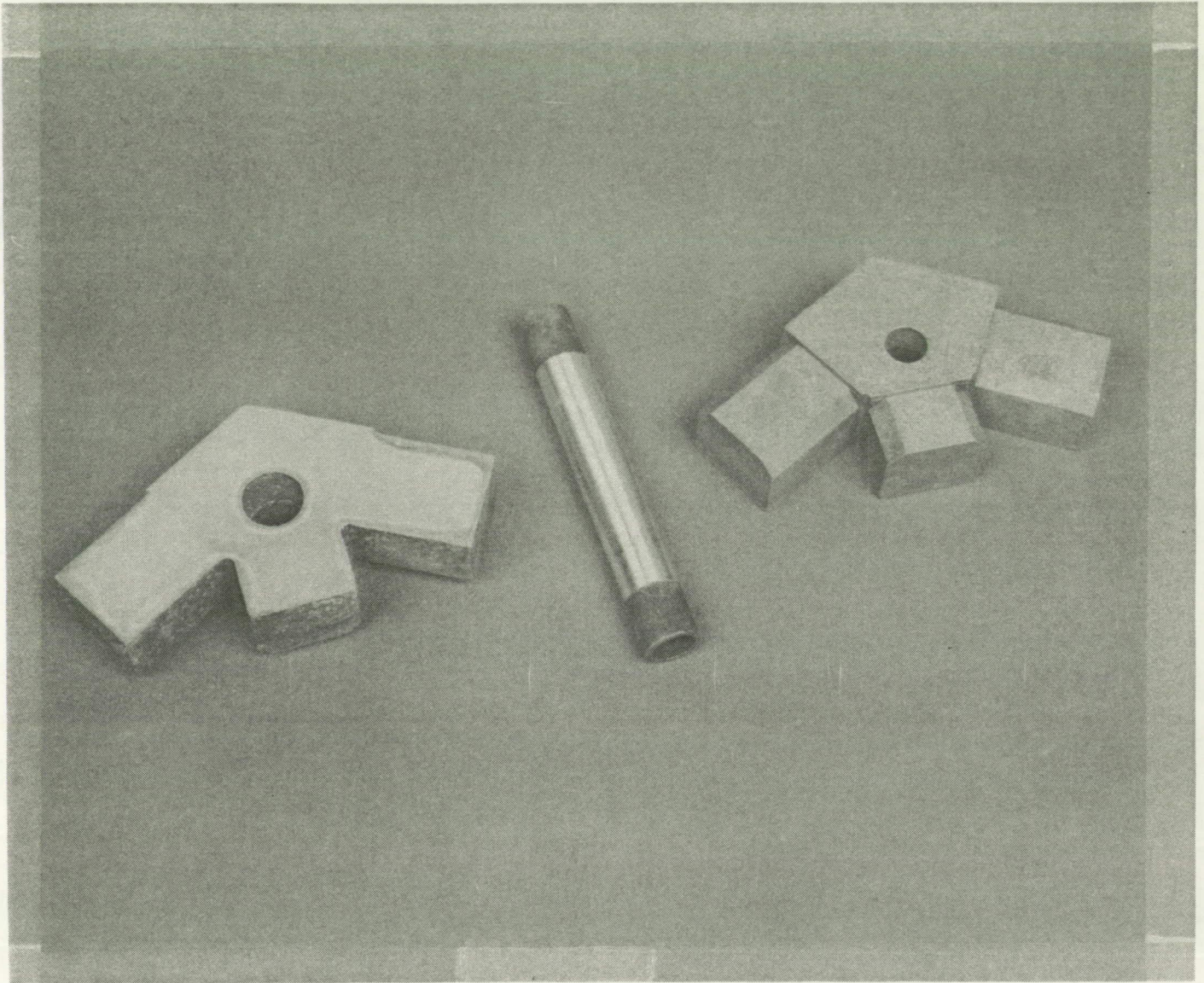


Figure 2.4-3. Corner Fitting Assembly Components.  
Two Identical Corner Fitting Interfaces and A Round Spacer Rod.



ORIGINAL PAGE  
BLACK AND WHITE PHOTOGRAPH

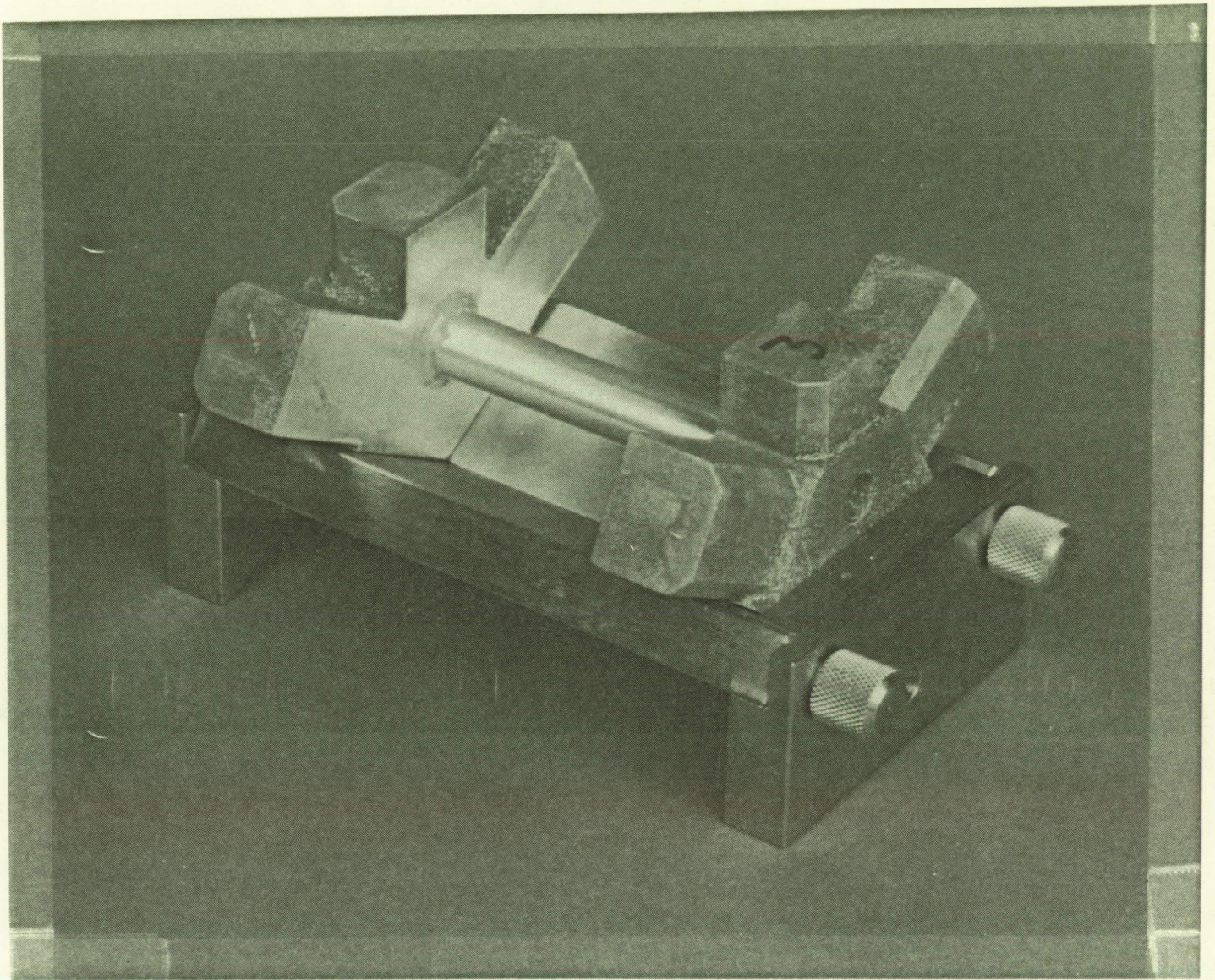


Figure 2.4-4. The Corner Fitting Bond Jig Holds The Top and Bottom Corner Fitting Interface Pieces Co-planar On The Top and Side Surfaces.



ORIGINAL PAGE  
BLACK AND WHITE PHOTOGRAPH

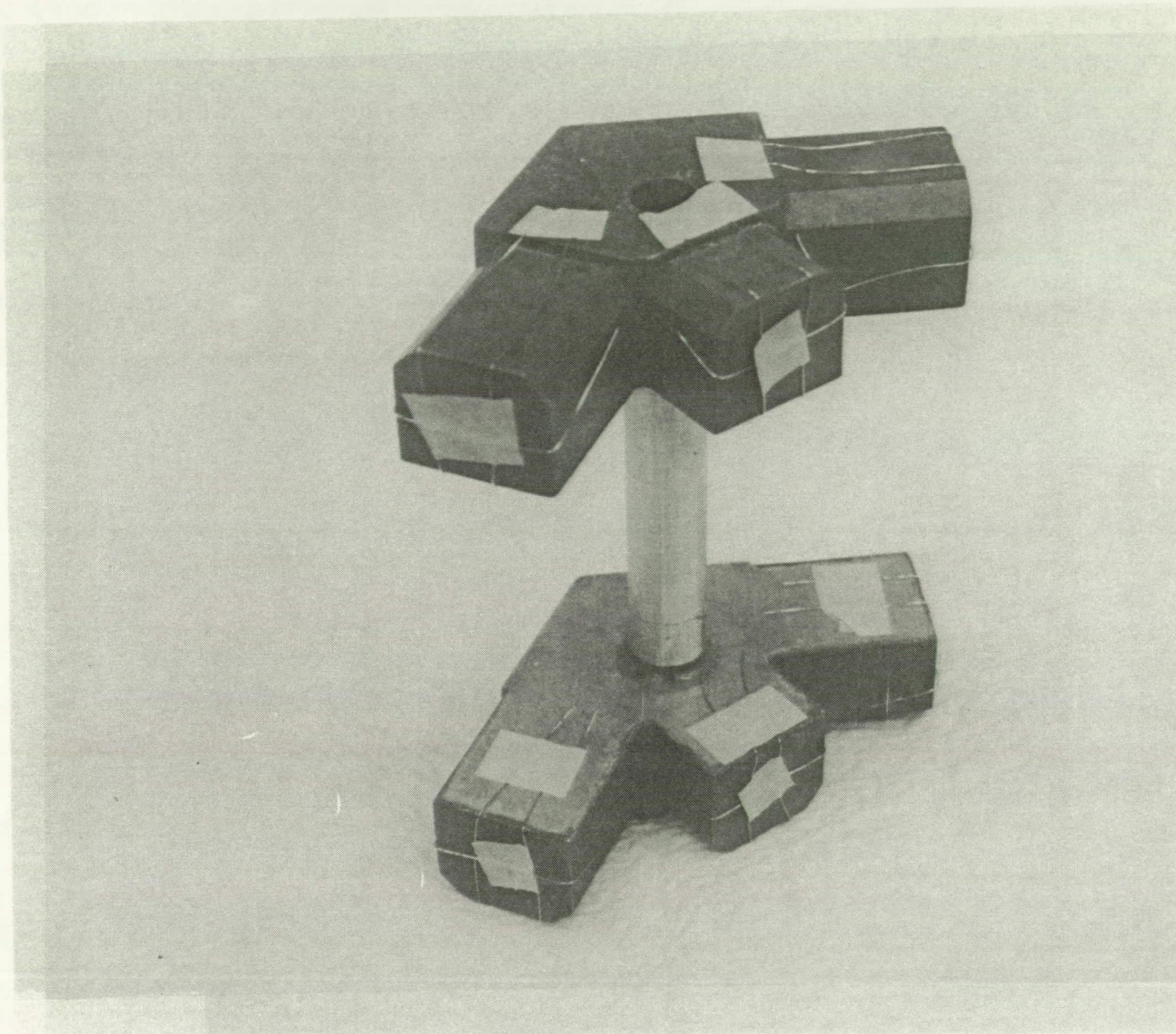


Figure 2.4-5. Completed Corner Fitting Assembly With  
.007 Inch Thick Bond Wire.

## 2.5 Hub and Corner Shear Plates

The in plane stiffness of the panel is provided by graphite shear plates. Each panel has 14 shear plates; two hub shear plates at the panel center and two corner shear plates at each corner. The shear plates, shown in Figure 2.5-1, are manufactured in a manner similar to the caps and C-channel pieces used on the box beams. A bleeder cloth is placed on the prepreg layup under the vacuum bag and is used to pull the excess resin out of the laminate. The table with the graphite layup is then placed in an autoclave and fully cured. The finished parts are die cut and machined from these sheets.

## 2.6 Composite Mirror Facet Development and Design

During Task 1 of the SCAD program, candidate materials for reflective mirror facets were evaluated to determine their susceptibility to low earth orbit (LEO) degradation and are shown in Table 1. Reflective surface studies focused on a variety of substrates, reflective coatings and protective coatings in an effort to maximize the end of life (EOL) specular reflectance. Substrates were tested for mechanical and thermal properties, surface quality and outgassing behavior. Coatings were evaluated for reflectivity, adhesion and resistance to both LEO and terrestrial environmental degradation.

Glass reflective substrates yielded the highest specularity and exhibited strong resistance to atomic oxygen bombardment. However, glass is relatively heavy and would increase the weight of the concentrator by more than 30% over graphite epoxy substrates. Reflective samples which meet the



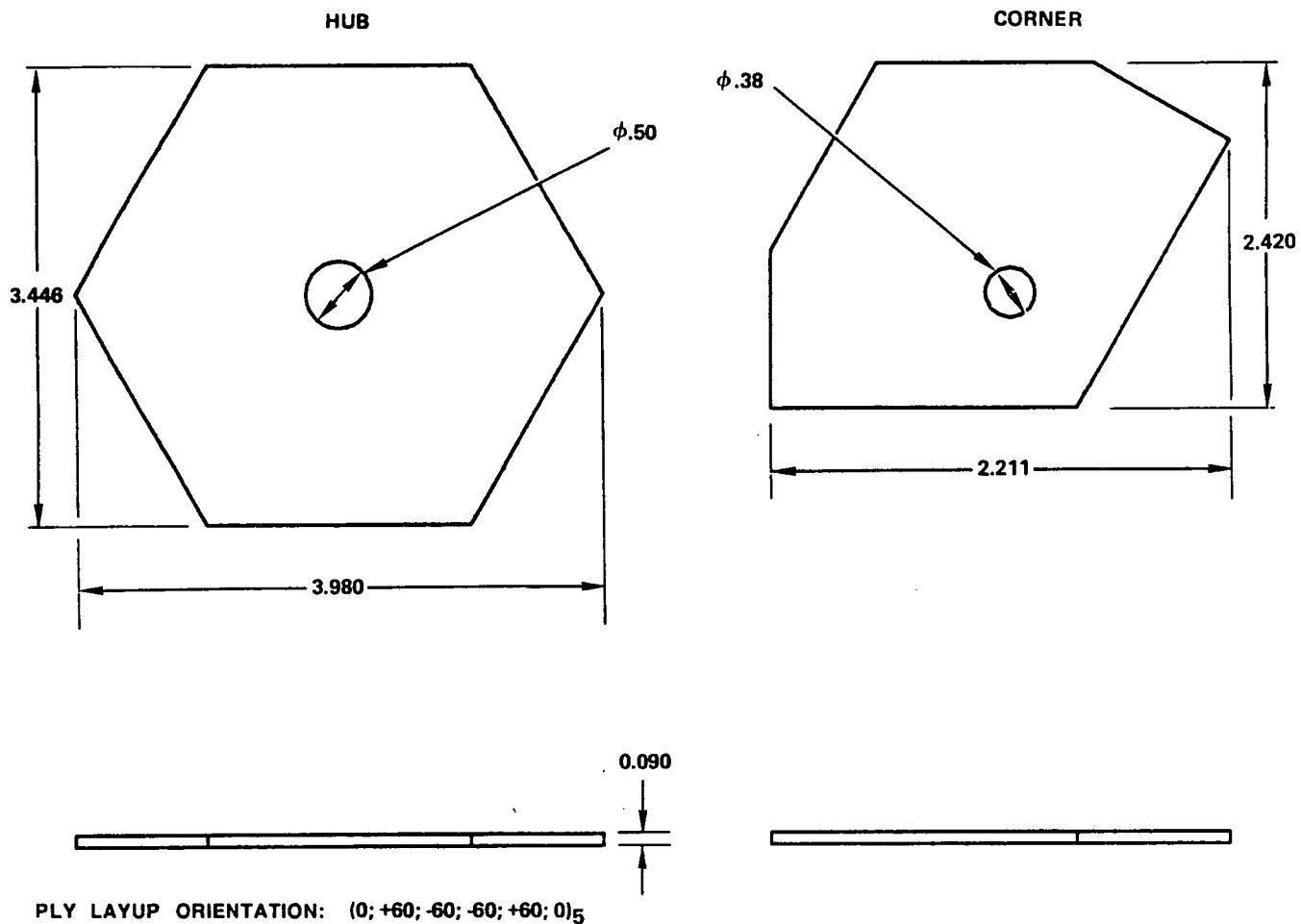


Figure 2.5-1. The Hub and Corner Shear Plates. The Ply Orientation Corresponds To The Angle The Beams Meet At The Corner (Zero, +60 and -60).

Table 1. Candidate Substrates and Coatings Evaluated  
For LEO Environmental Degradation

<u>Reflective Substrates</u>	<u>Reflective Coatings</u>	<u>Protective Coatings</u>
ULE Glass	Silver	RTV Silicones
Graphite/Epoxy	Aluminum	MgF <sub>2</sub>
PEEK	Aluminum/Silver	SiO <sub>2</sub>
Zerodur	Gold	ITO
Aluminum	Copper	Si <sub>3</sub> N <sub>4</sub>
Graphite/Glass	Nickel	Al <sub>2</sub> O <sub>3</sub>
Graphite/Polymer	Chromium	SiO <sub>2</sub> /PTFE
Graphite/Aluminum	Platinum	MgF <sub>2</sub> /PTFE

optical requirements of the SCAD program have been produced with graphite fiber reinforced plastic (GFRP) substrates. GFRP substrates substantially increase thermal and structural performance while considerably reducing weight. The other substrates have lower performance in the areas of specularly, weight or manufacturability.

Silver has the greatest solar averaged hemispherical reflectance of all the tested reflective coatings, followed by aluminum. Silver does not adhere well to untreated GFRP material; but, the application of an adhesion promoter can eliminate this problem. Copper, aluminum,  $\text{SiO}_2$  and  $\text{Al}_2\text{O}_3$  provide good adhesion between both silver and GFRP. Of the protective coatings,  $\text{MgF}_2$ ,  $\text{SiO}_2$  and  $\text{Al}_2\text{O}_3$  provide the greatest protection against atomic oxygen degradation. Limited experimental testing and analytical modeling by Harris and Sandia National Laboratories suggest that the overcoat protection and surface reflectivity can be optimized by varying the thickness and combination of protective coatings.

Based upon the SCAD materials evaluation, the baseline design for the mirror facet reflective surface for a flight design is a graphite epoxy substrate coated with 3000 A of silver, 1000 A of  $\text{SiO}_2$ , and 750 A of  $\text{MgF}_2$ . Initial reflective and atomic oxygen environment durability tests have been performed on subscale coupons. Combined and sequential environmental exposure to acoustics, thermal cycling, atomic oxygen, and high intensity UV will be performed on full size mirror facets during the Phase C/D program.

Vapor deposited silver was selected as the flight material because it yields the highest hemispherical reflectance. The SCAD prototype had additional requirements because it will be used for terrestrial application, and tested for ten to fifteen years. A material that would survive the salt air environment at Harris Corporation for several years and then the subsequent testing at NASA Lewis was needed. Harris Corporation began research to select a reflective material that could be used in the earth environment and then adapted for space applications.

3M Corporation in St. Paul, Minnesota, produces a polyester (mylar) film coated on the front surface with silver followed by an acrylic to protect the silver from oxidation and allow cleaning of the facets. The product is called Silverlux and it met the optical requirements of the SCAD program. The film proved to be a cost effective method for achieving a reflective surface on the facets that was similar to the vapor deposited silver selected as the flight baseline. ECP 300, a silver coated acrylic film, was also considered. It also met the program requirements but was manufactured only in twenty four inch widths, which would require a seam to complete a mirror facet. The silverlux material was selected as the baseline for the SCAD prototype concentrator reflective material.

In late 1987, a meeting was held at NASA Lewis Research Center, with Harris and Hercules present, in which the scope of the SCAD program was changed. Although facets using Silverlux film met SCAD optical requirements, they were not candidates for the Spaceborne Solar Concentrator because the adhesive backing used to bond the Silverlux film to the GFRP facet was not space qualified. Thus, it was decided that the SCAD funding

would be better used by fabricating a limited number of Silverlux facets and further developing a more space-like vapor deposited facet. The development facet was to have a graphite face sheet with a surface finish smooth enough and clean enough to accept a vapor deposited coating of aluminum or silver and meet the SCAD optical requirements.

The rescoped SCAD program consisted of (a) production of 48 Silverlux mirror facets (determined to be the minimum number of facets needed to selectively populate the prototype solar concentrator and still permit optical characterization), and (b) a development program aimed at improving the reflective surface of the facets. To meet these two objectives, it was necessary to define and further understand mirror facet reflectance requirements and then to identify, perform, and interpret tests to confirm facet optical properties.

A composite mirror facet is comprised of graphite epoxy face and back sheets with an aluminum honey comb core using the sandwich structure shown in cross section in Figure 2.6-1. The dimensions and radii of curvature of a typical SCAD facet appear in Figure 2.6-2. The SCAD model used 4 different radii of curvature that were located in the concentrator as shown in Figure 2.6-3. The facet approach is perhaps the largest advantage of the Truss Hex concentrator over the other concepts considered. The small removable facets can be replaced if damaged by debris and the small mirrors can be adjusted to simulate parabolic optics without the stringent requirements of the parabolic geometry for the backup structure.

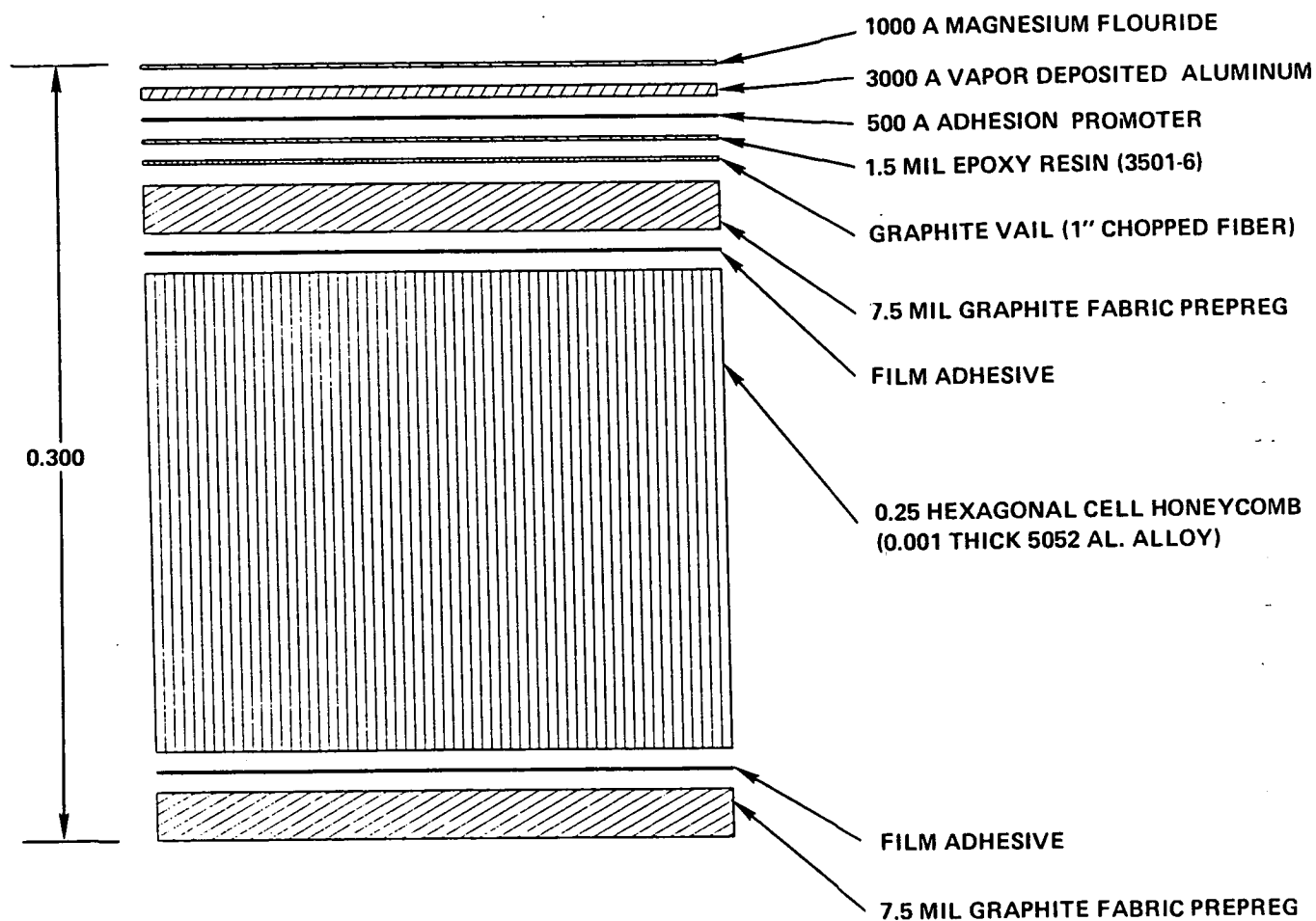


Figure 2.6-1. Typical Composite Mirror Facet Cross Section

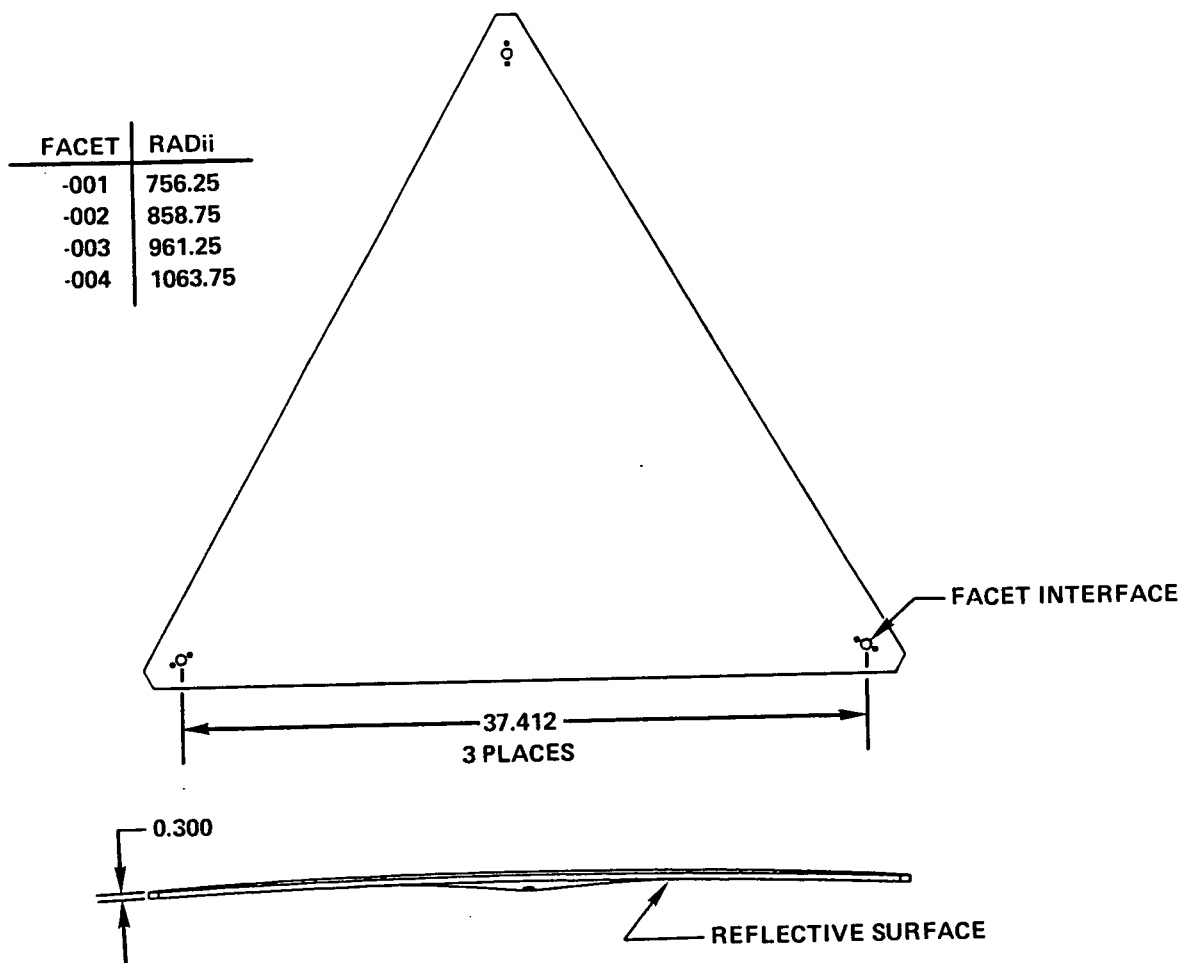


Figure 2.6-2. Typical Facet Assembly Features

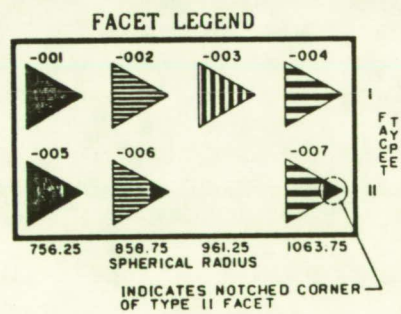
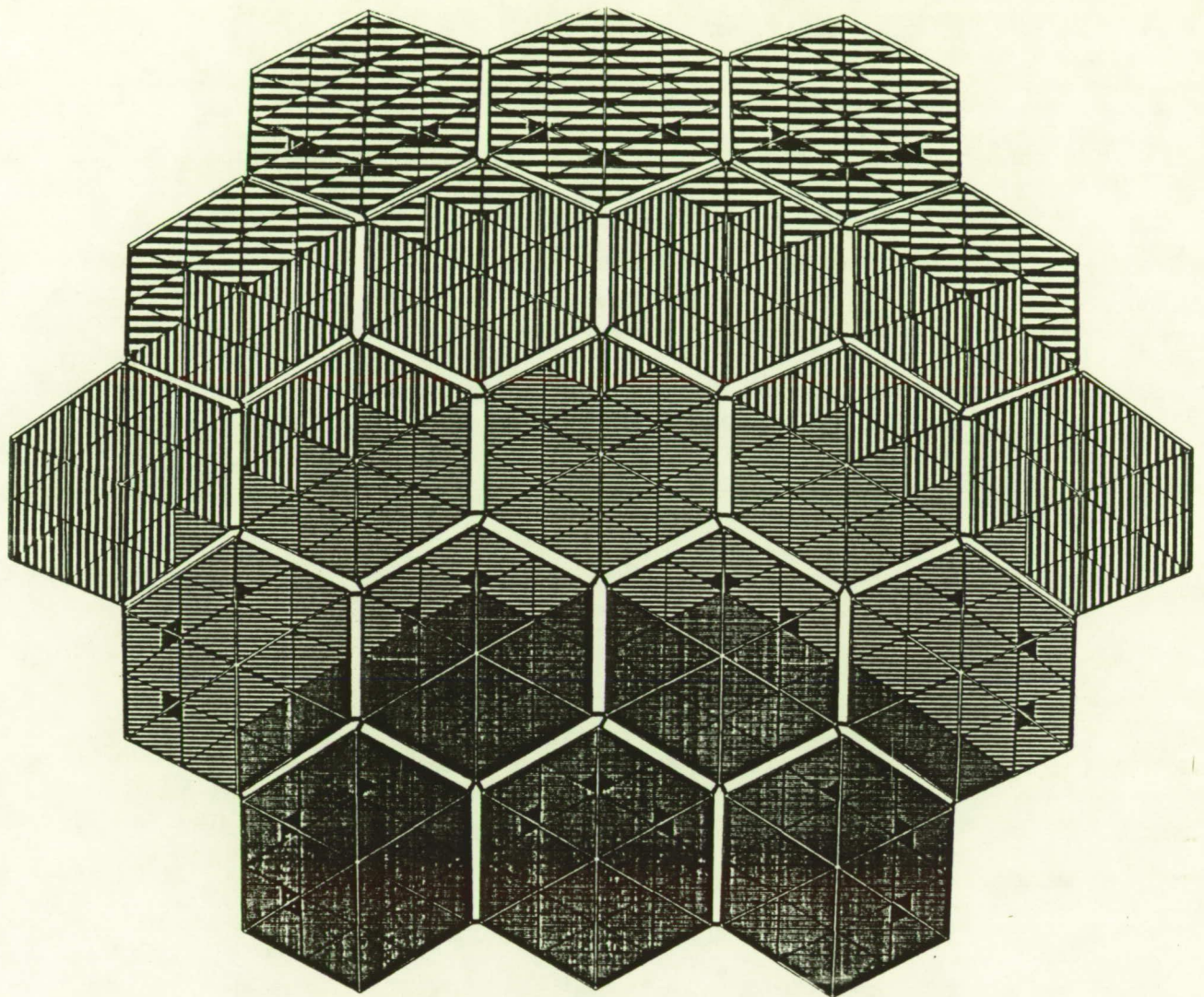


Figure 2.6-3. The Four Facet Radii And Their Location Within The Assembled Solar Concentrator.



Three VDA composite mirror facets were fabricated on the SCAD program at the completion of the development effort. A photograph of one facet can be seen in Figure 2.6-4. A photograph showing a reflected image of a poster can be seen in Figure 2.6-5. As can be seen the reflected image was very good and actually exceeded the SCAD optical requirements for a mirror facet. A detailed description of the facet development effort and the fabrication process can be seen in the Hercules final report in Appendix A. The Hercules report gives a detailed description of all subcontract development work performed on the facets.

## 2.7 Mirror Facet To Hexagonal Panel Interface

The facet to panel interface is shown in Figure 2.7-1. The panel interface is provided by a threaded aluminum beam spacer that is bonded into machined through holes of the graphite box beams (Figure 2.7-2). The metallic beam spacers are used to attach the flexures to the beams, and prevent the beam sidewalls from being damaged during launch dynamics. The pad prevents crushing of the graphite in the local area due to compressive loads. The flexure ("Flex" Bracket) is fastened to the panel at these threaded spacers. Two types of flexures were incorporated into the design. The Type 1 flexure has the cross section shown in Figure 2.7-3. This cross section allows for torsional bending about the normal axis to compensate for thermal growth in the facets. The Type 1 flexure is shown in Figure 2.7-4.

ORIGINAL PAGE  
BLACK AND WHITE PHOTOGRAPH

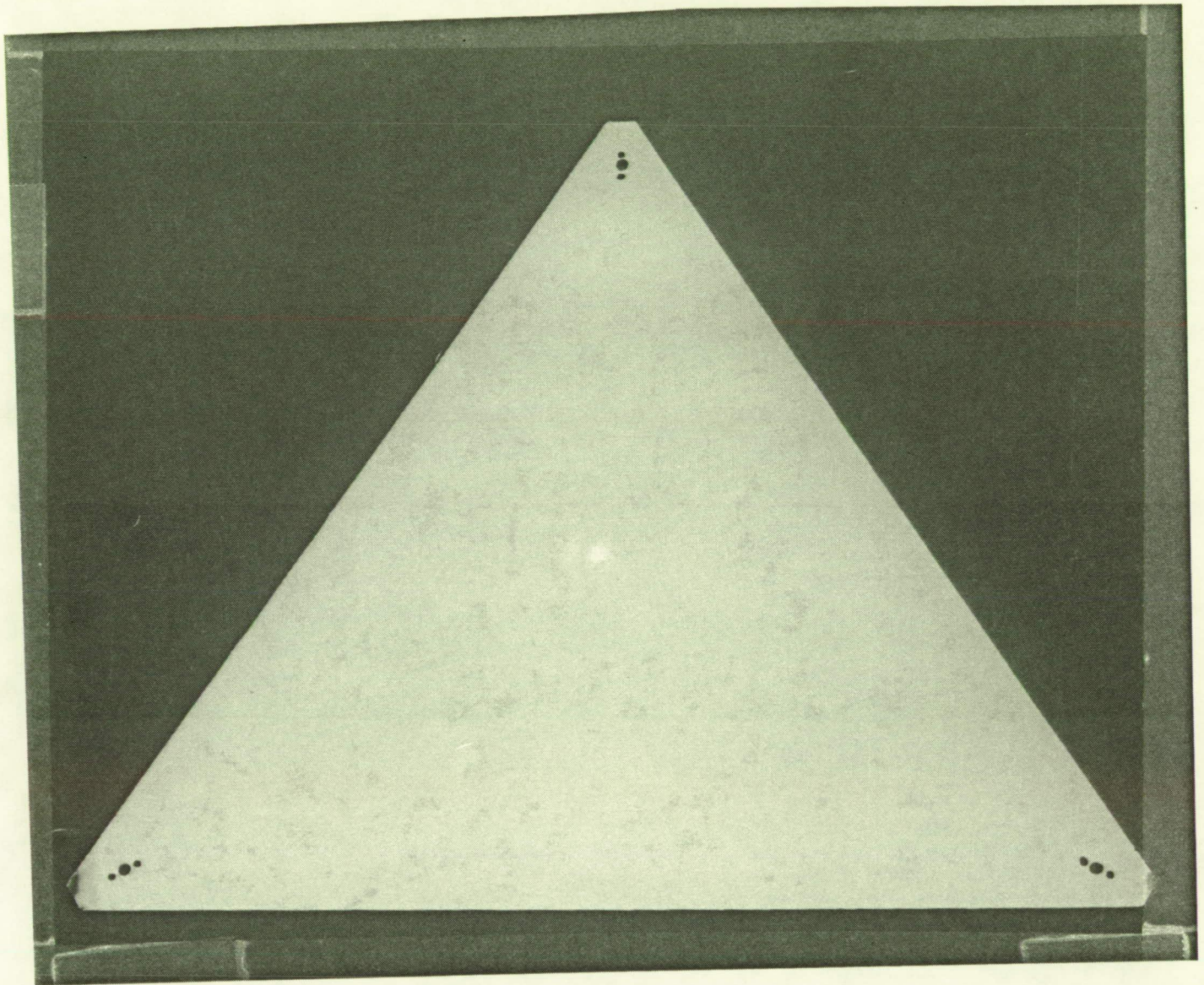


Figure 2.6-4. Completed Composite Mirror Facet  
Produced By Hercules Corporation.



ORIGINAL PAGE  
BLACK AND WHITE PHOTOGRAPH

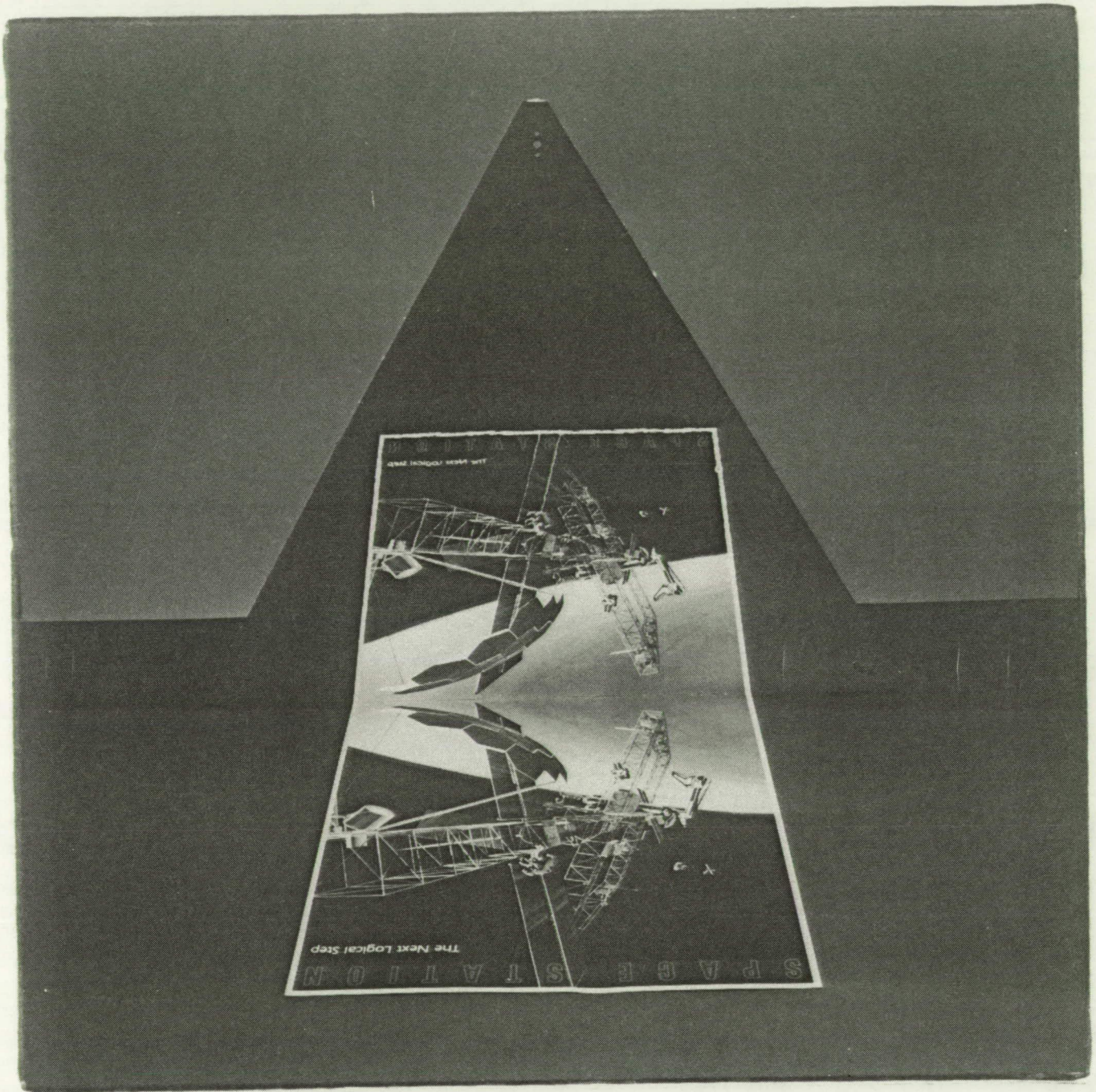


Figure 2.6-5. Vapor Deposited Aluminum Facet With Picture and  
The Clear Reflected Image Of Space Station Freedom

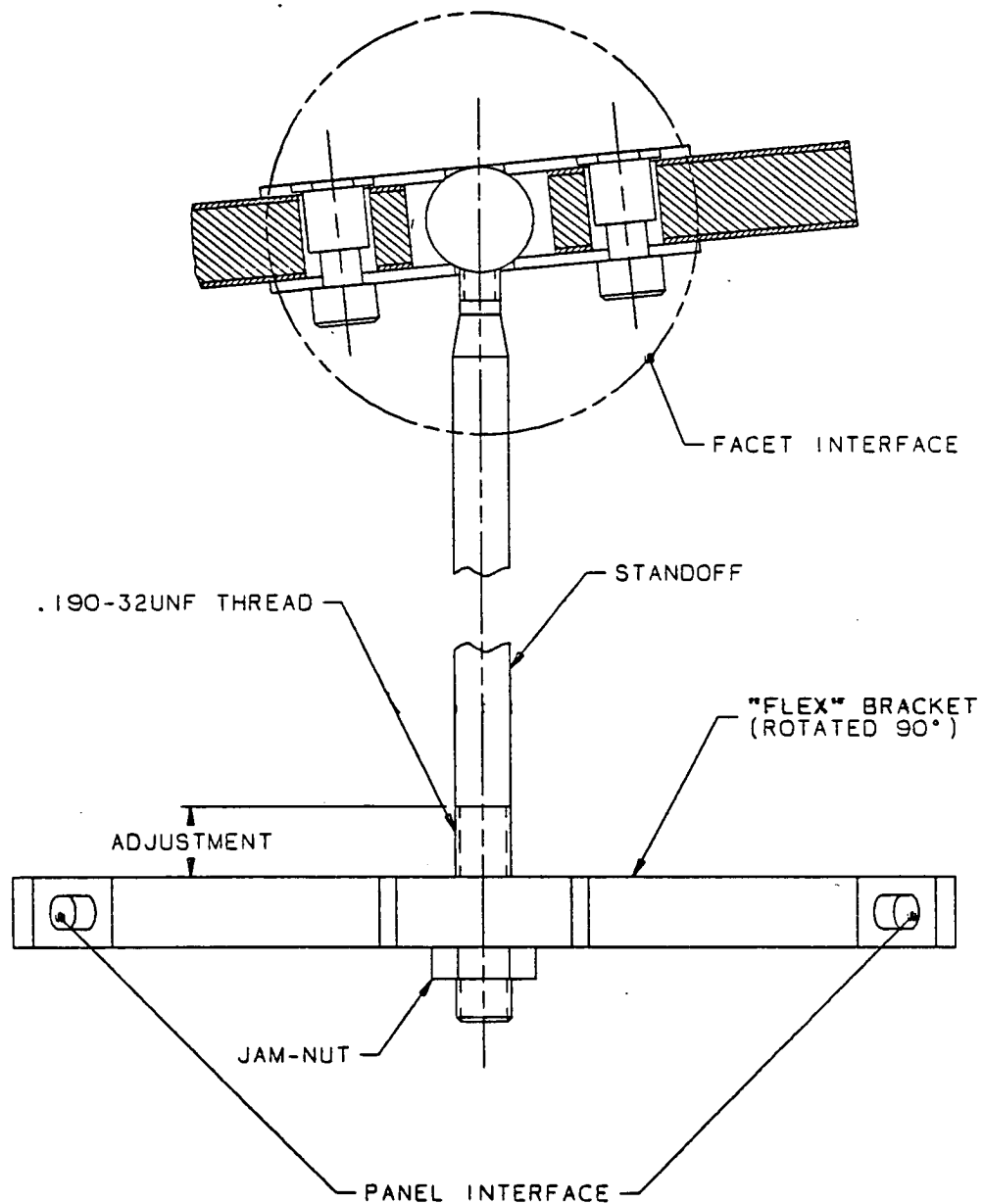


Figure 2.7-1. Standoff Interface Between The Hexagonal Panel And The Composite Mirror Facet. The Flexure Bracket Interfaces To The Box Beam.

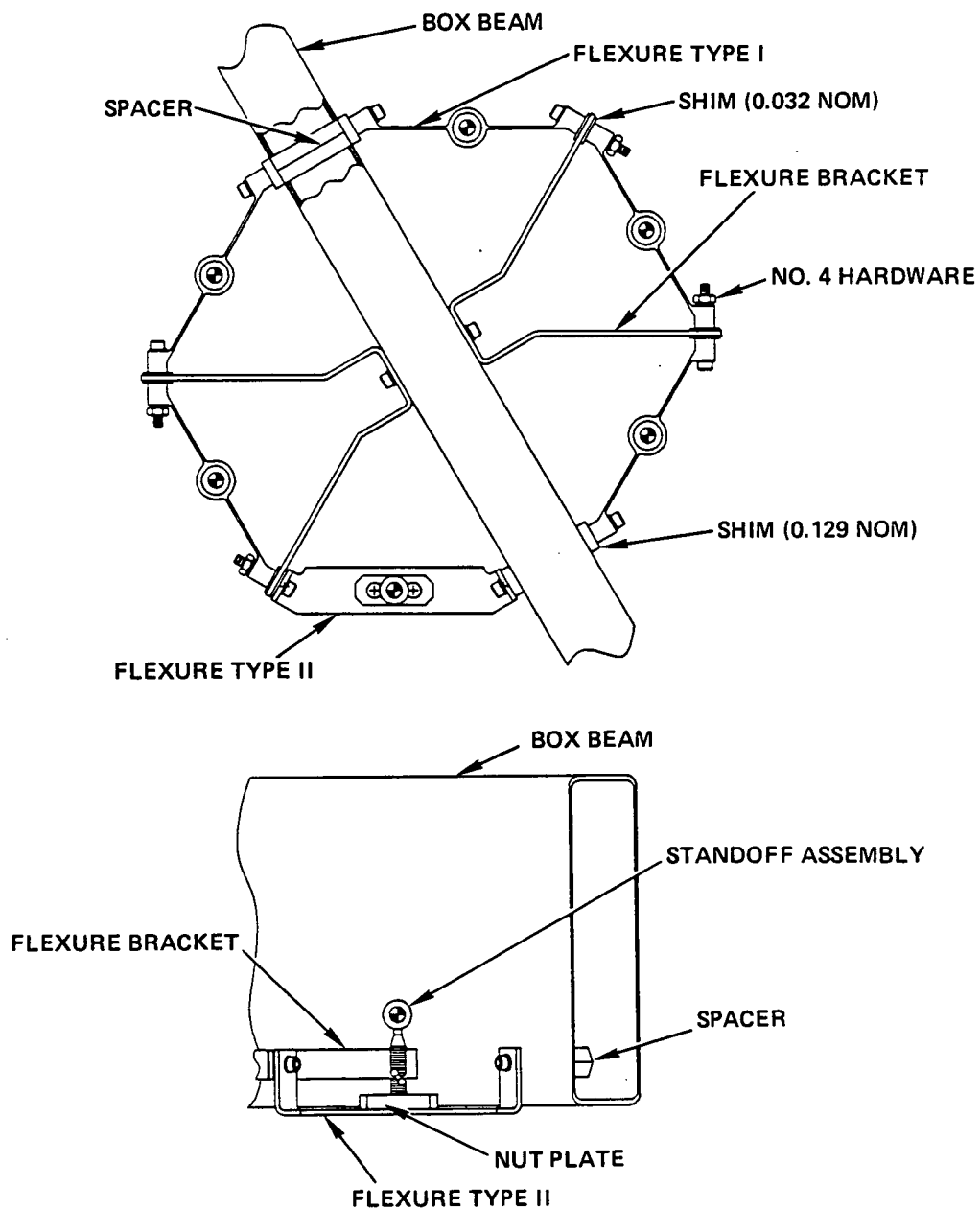
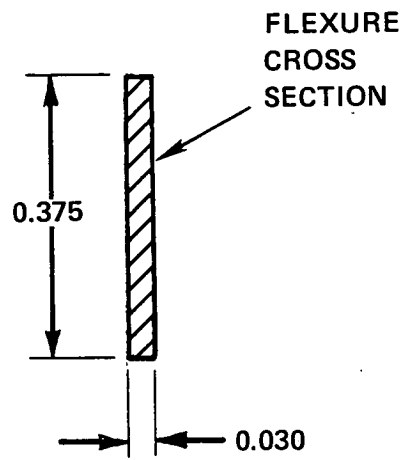


Figure 2.7-2. Flexure Assembly On An Internal Hex Panel Beam. The Spacer Is Shown In A Cutaway View In The Upper Left Corner.





890303

Figure 2.7-3. Cross Section Of A Typical Flexure

ORIGINAL PAGE  
BLACK AND WHITE PHOTOGRAPH

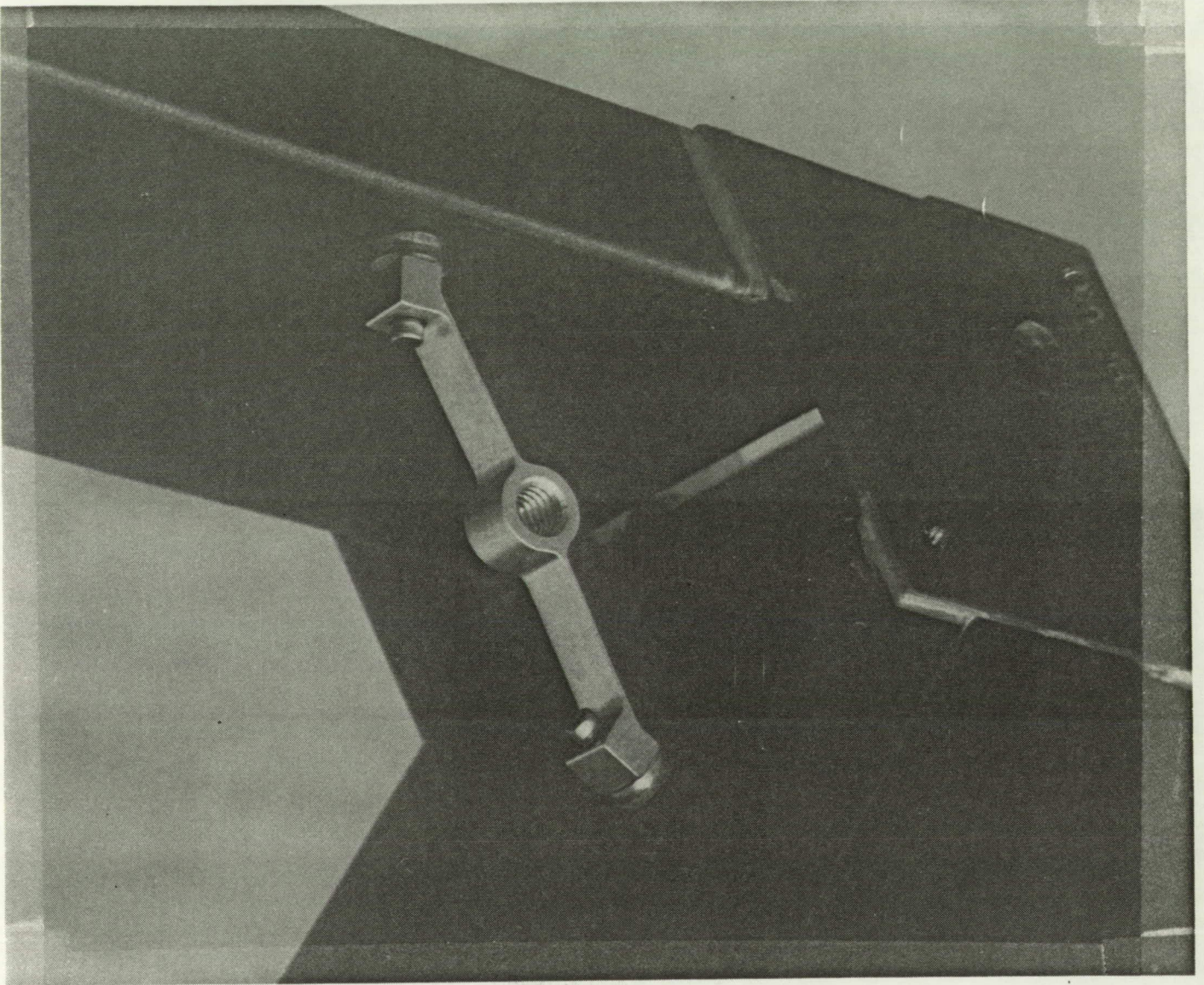


Figure 2.7-4. Type I Flexure Mounted To the Box Beams

The Type 2 flexure was required to allow for maximum facet rotation within a panel. The location of the Type 2 flexures on the concentrator can be seen in Figure 2.6-3 (previous section) and are indicated by the black triangle in the corner of the mirror facet. The type two flexure was located slightly below the box beam, but flush with the shear plates at the corner fitting. A Type 2 flexure is not adjustable, thus, the setting of the mirror is accomplished by moving the other two standoffs. Thermal growth is then taken up in the adjustable standoffs with their associated flexure bracket. A picture of a Type 2 flexure can be seen in Figure 2.7-5.

The facet to flexure interface is accomplished with a standoff. A typical threaded standoff, shown in Figure 2.7-6, provides the adjustment mechanism to move the facet and position the reflected solar flux. This feature allows for tailoring the solar flux profile in the receiver cavity.

The Facet-to-Standoff interface, shown in Figure 2.7-7, consists of an aluminum spacer block in each corner of a mirror facet. The spherical ball on the standoff recedes into the spacer block and is held in place by a top retainer plate that is bonded to the facet and a bottom retainer plate that fastens to the top plate. The bottom retainer plate is actually a spring clip that tightens up against the standoff ball to lock the facet securely into place. The spring clip flexes to allow for a variance in facet thickness due to manufacturing tolerances.



ORIGINAL PAGE  
BLACK AND WHITE PHOTOGRAPH

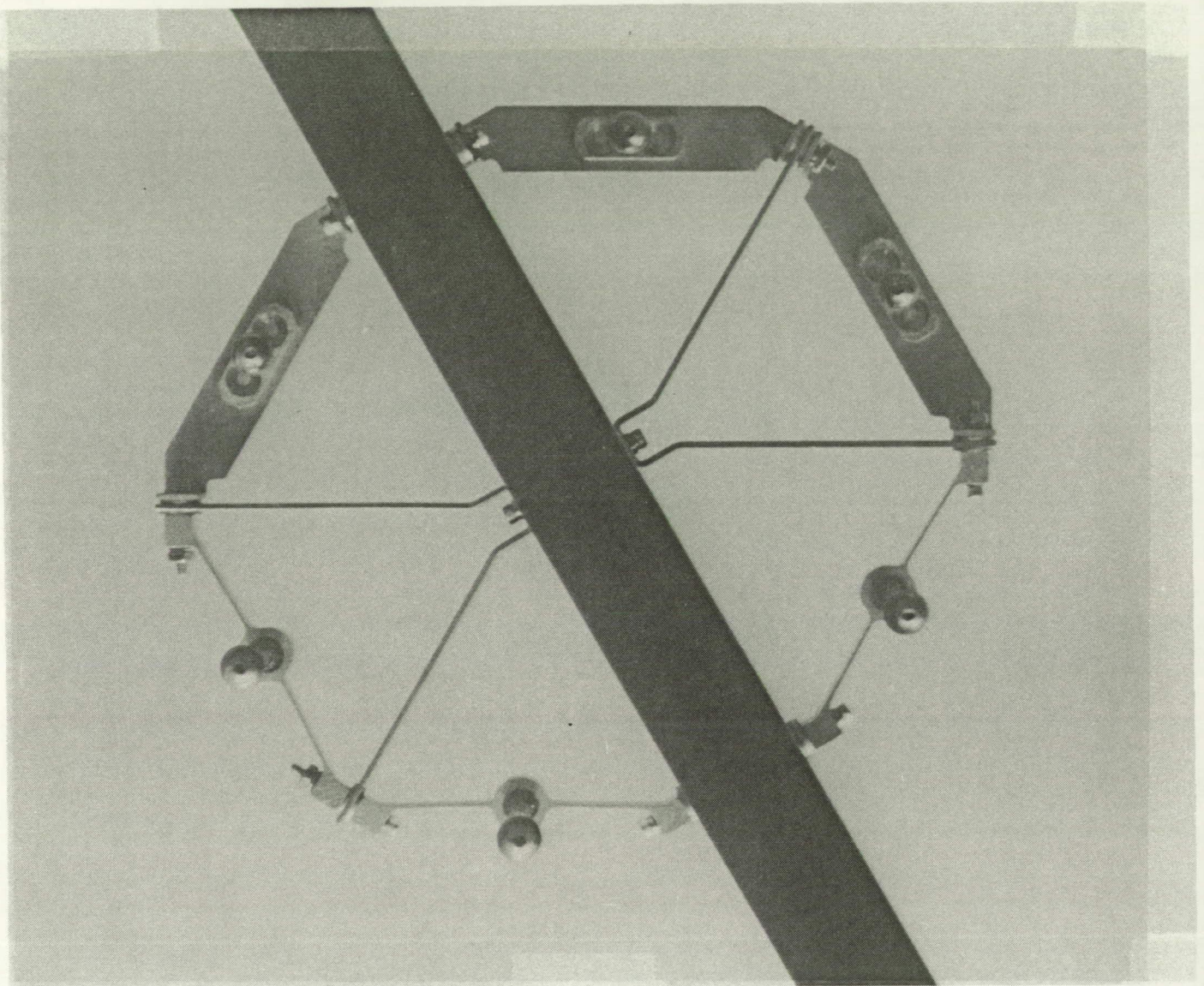
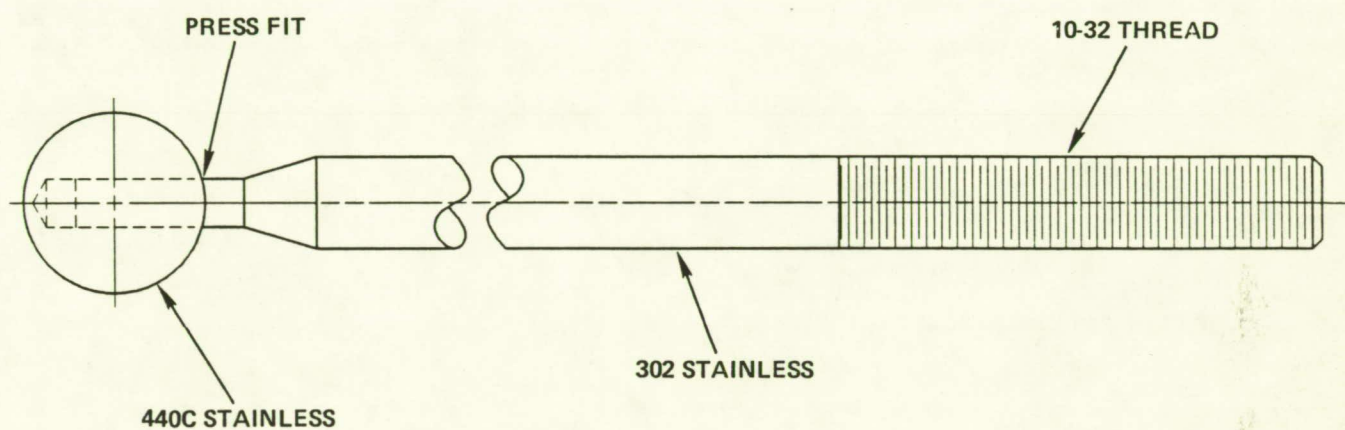


Figure 2.7-5. Flexures Shown At The Middle Of A Typical Box Beam. The Wide Flexures Are Type II While The Smaller Cross Section Is The Type I.



44	DIFFERENT ASSEMBLIES
	IN
0.10	INCREMENTAL LENGTHS (APPROX.)
	WITH
+0.10	ADJUSTMENT

Figure 2.7-6. Typical Standoff Assembly Used To Support The Composite Mirror Facets



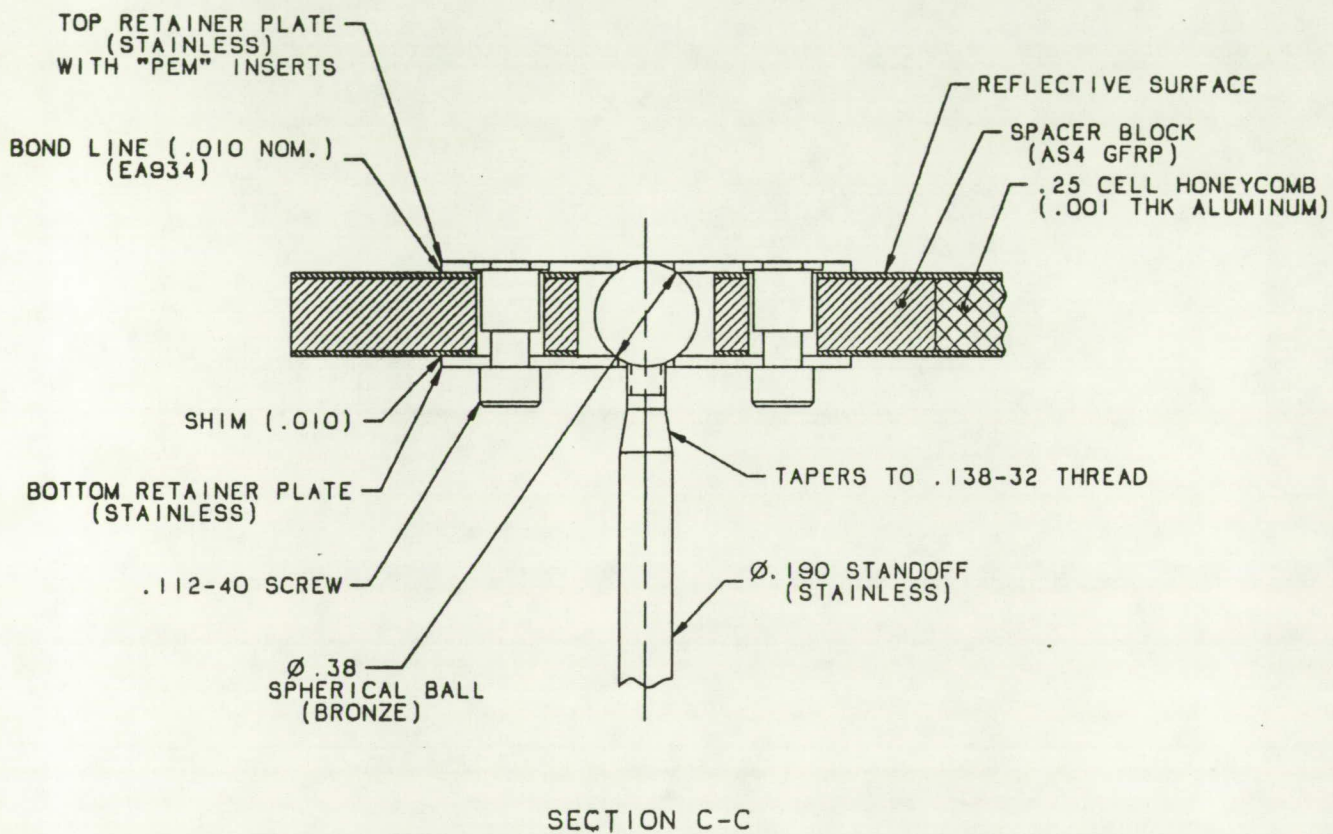
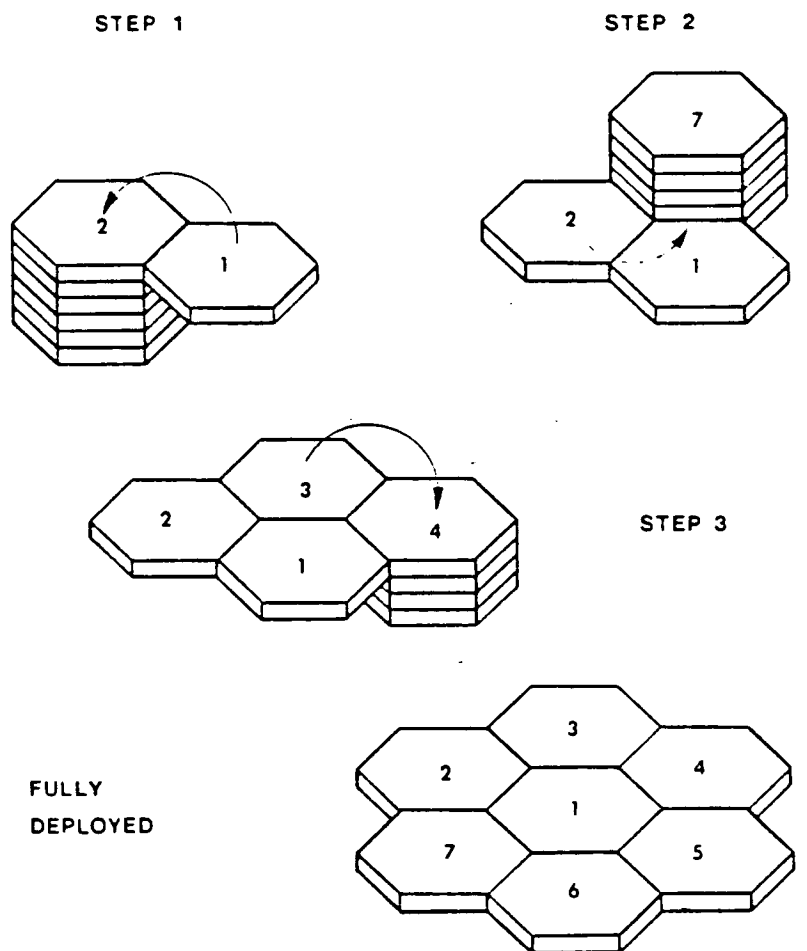


Figure 2.7-7. Facet To Standoff Interface

## 2.8 Latch History and Design

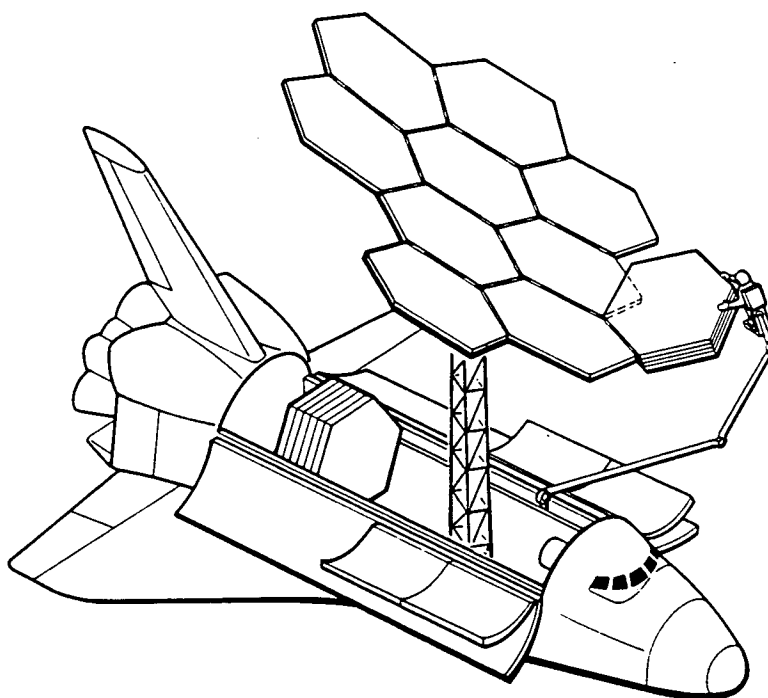
The Truss Hex concentrator developed during Task I of the SCAD program was deployable using a series of hinges and latches. The deployment could be done manually by astronauts or could be fully automated for remote deployment. In either case, the full stack of panels (19 total) was deployable with the appropriate design consideration for hinge and latch interferences where the stack of panels passes by the adjoining panel edge. Another option was to join no more than seven panels by folding hinges, completing a ring of six panels around a central panel. Additional "partial system modules" of six hinged panels are later attached to the inner ring with latches, and then sequentially unfolded, forming the second ring. This method is demonstrated in Figure 2.8-1 and 2.8-2. Figure 2.8-2 shows an artists concept of a set of six panels being attached to the inner seven and deployed manually. The remainder of the 19 panel concentrator panels are shown still stowed in the payload bay.

A trade study was performed early in Task 2 of the program to develop the best assembly technique for the concentrator based on complexity, implementation, EVA requirements, cost and other variables. The number of viable techniques was reduced to five during the preliminary design phase of the program. Four of the candidates used the hinge and latch design or some variation of the design explained above. The fifth candidate was the all-latch design. The all latch design was selected for the following reasons; it was the most flexible with respect to assembly location and method, it contained the lowest technical risk, it had the lowest overall program cost,



860125

Figure 2.8-1. Truss Hex Concentrator Single Fold Deployment Method



14201-13A

Figure 2.8-2. Truss Hex Concentrator Unfolding Deployment

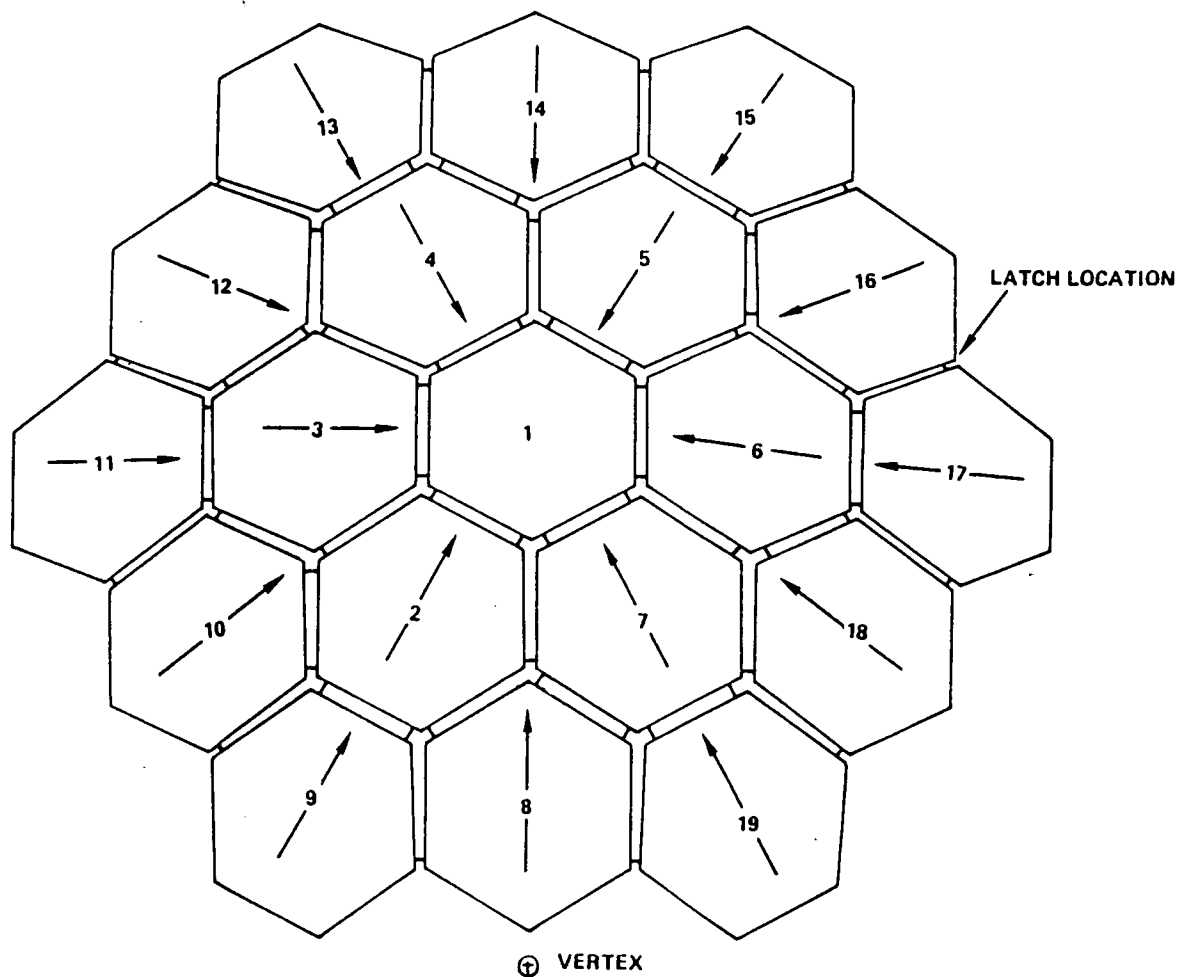


Figure 2.8-3. Latching Sequence For The All-Latch Design. Panels Are Latched Together Using A Single Radial Motion, As Indicated By Arrows.

and the EVA time required for assembly was within the 4 hours program requirement. The all latch design also met the primary NASA objectives of demonstrating the optical performance with analysis correlation, demonstrating the basic structural properties with analysis correlation and providing a first cut evaluation of the assembly method. The trade study was performed as part of the Phase B program (concentrator study funded by Rocketdyne) and the results are provided in the Phase B final report.

The all-latch design is assembled using the latching sequence shown in Figure 2.8-3. Panel number one would be supported by the Mobile Service Center Remote Manipulator System (SSRMS). Two astronauts, one on each side of the remaining panel stack, latch panel number two to panel number one in a single radial motion. Panel number one is then rotated using the SSRMS so that the astronauts do not change their position and panel three is latched in place. This operation is repeated until the first seven panels are latched together. The seven panel assembly is then translated away from the astronauts and the outer ring of twelve panels is attached in the same manner as the inner ring of six.

Four basic latch types are needed to accomplish the concentrator assembly using the latching sequence shown previously in Figure 2.8-3. Each latch consists of two mating parts; a striker assembly and a latch assembly. The latch assembly provides a spring driven pawl that seats against the striker assembly sphere the two are assembled together. A typical latch and striker assembly can be seen in Figure 2.8-4. The kinematics of the latch are shown in Figure 2.8-5. As the striker assembly is moved toward the latch, the striker sphere makes initial contact on the latch pawl detent.



## LATCH ASSEMBLY TYPE I

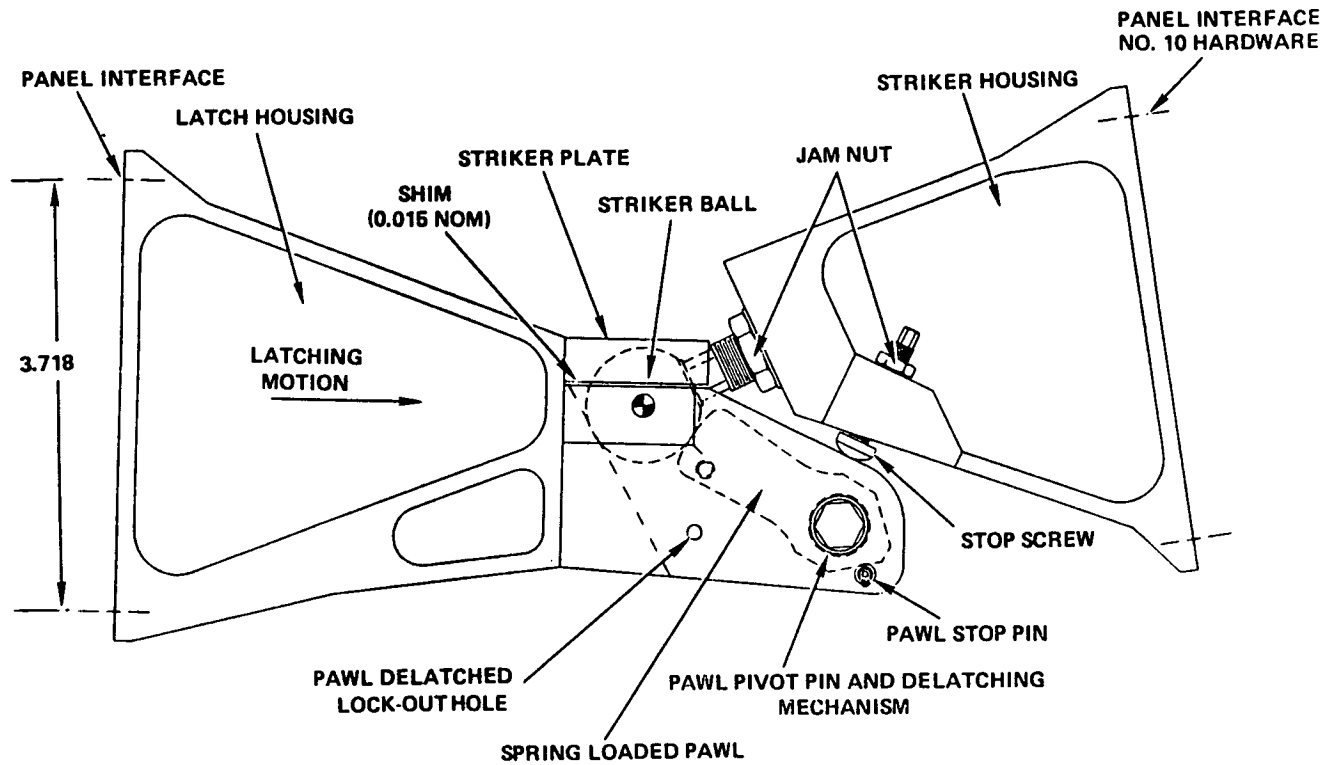


Figure 2.8-4. Typical Latch/Striker Assembly For The Harris Designed Zero Translation, Regenerative Latch System

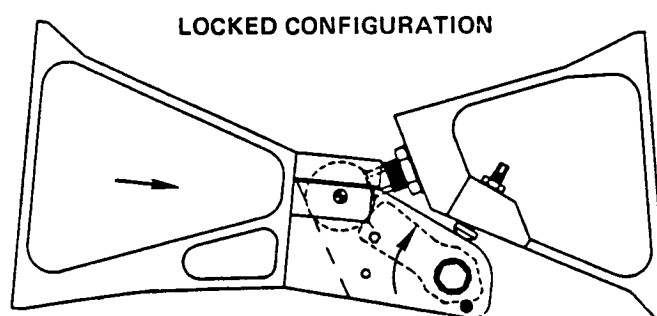
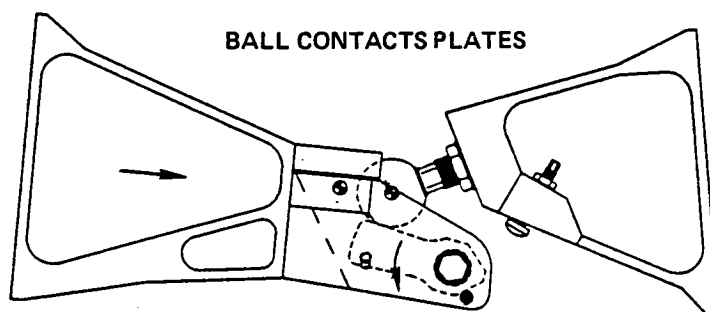
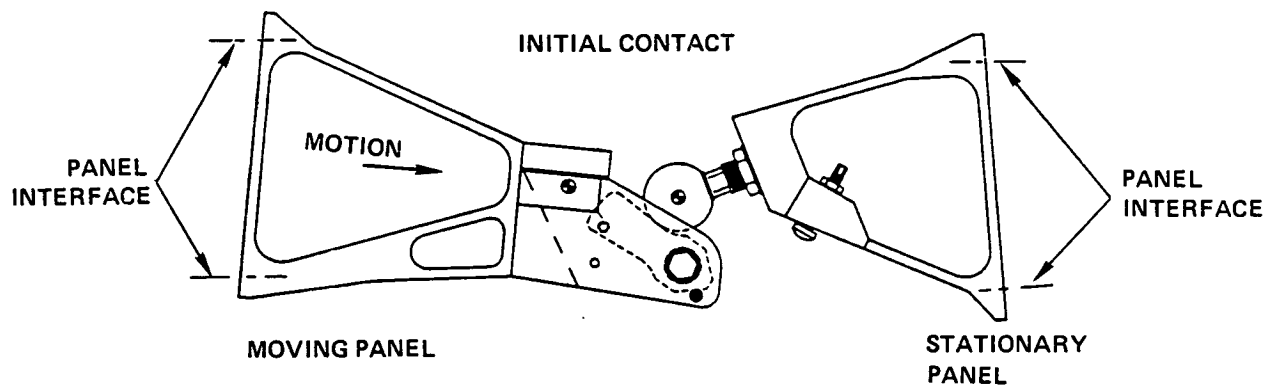


Figure 2.8-5. Latch Kinematics

The latch pawl then rotates back and the sphere is guided into the latch by the pawl and the two striker plates. The latch provides four discrete points of contact; the back surface (latch housing), the top in two places on the striker plates and the latch pawl. The latch concept provides three degrees of translational restraint but no rotational restraint. This is required to assure that misadjustments and thermal warping distortions do not accumulate during successive panel latching. By not having moment fixity in the latch, the hexagonal panel is allowed to seek an equilibrium position that is determined by the geometric dimensions of the latch rather than a forced rotational position. This makes the overall design more forgiving and less alignment critical during assembly. The latch is considered to be regenerative because the latch pawl is actually cam shaped so that it wedges itself against the striker sphere. As the latch is shaken or moved dynamically the spring loaded pawl wedges itself tighter against the sphere to make the latch more secure. The Type I latch shown in Figure 2.8-4 has a 180 degree angle between the latch housing and the striker plates. A Type I latch is used for the radial connection of panels such as the panel 1 to panel 2 interface (Isometric Figure 2.8-6). A Type II latch would be used in a circumferential area, such as, the panel 2 to panel 3 interface. The latch shown in Figure 2.8-7 represents the interface between panel 2 and panel 7. An isometric view of that latch can be seen in Figure 2.8-8. On the Type III latch, the latch housing to striker plate interface is at a 150 degree angle (Figure 2.8-9 and 10). This latch is used for the panel 8 to panel 7 interface connection. The angle is needed to allow panel

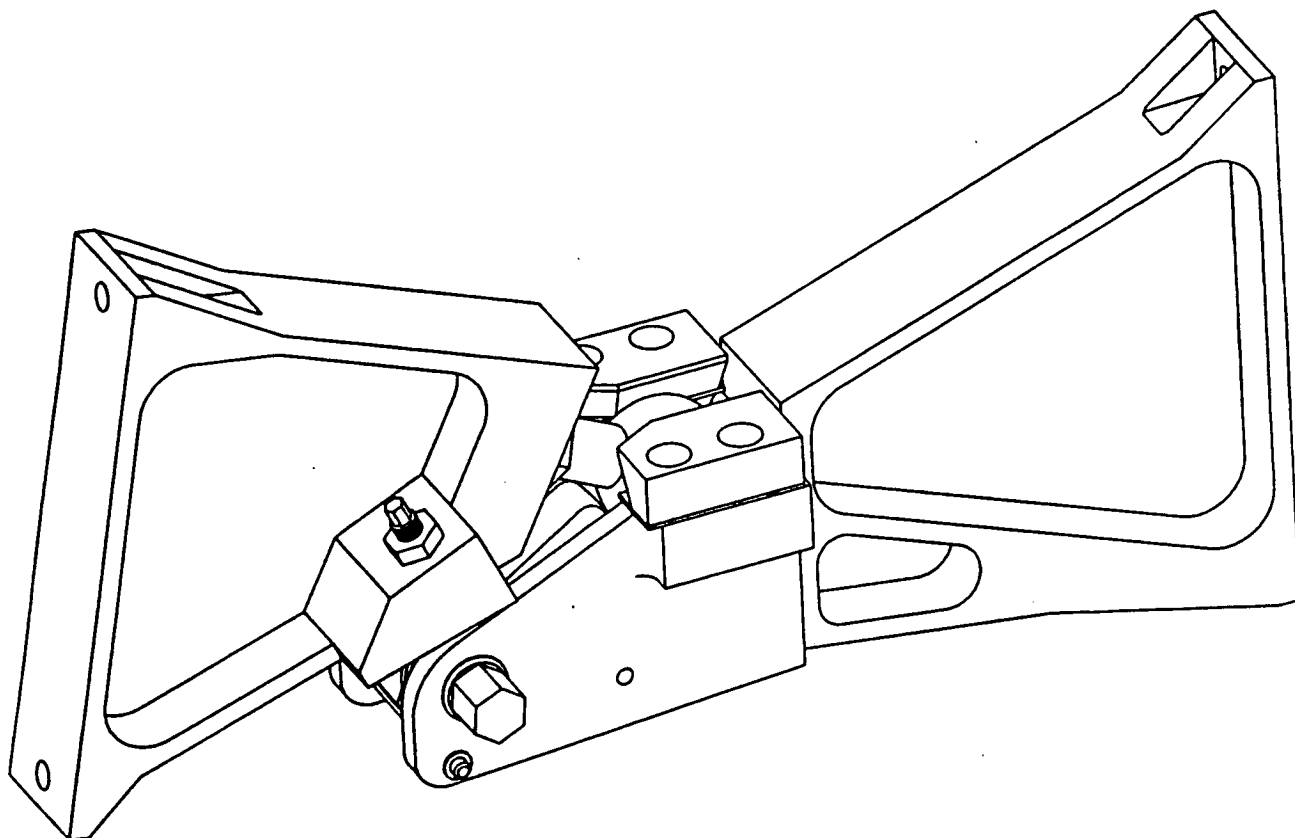


Figure 2.8-6. Isometric View Of The Type 1 Latch In Locked Position

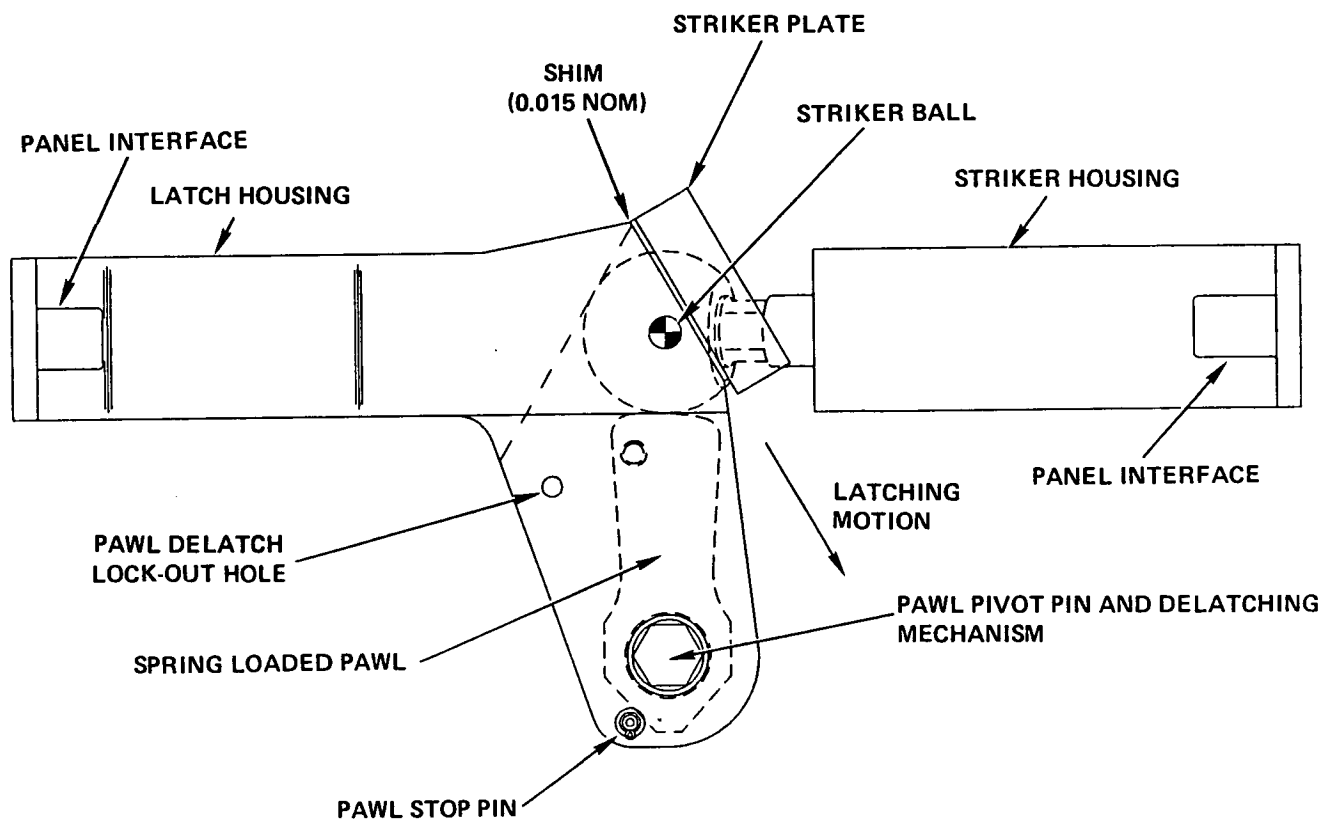


Figure 2.8-7. Type II Latch Between Panel Number 2 and Panel Number 7

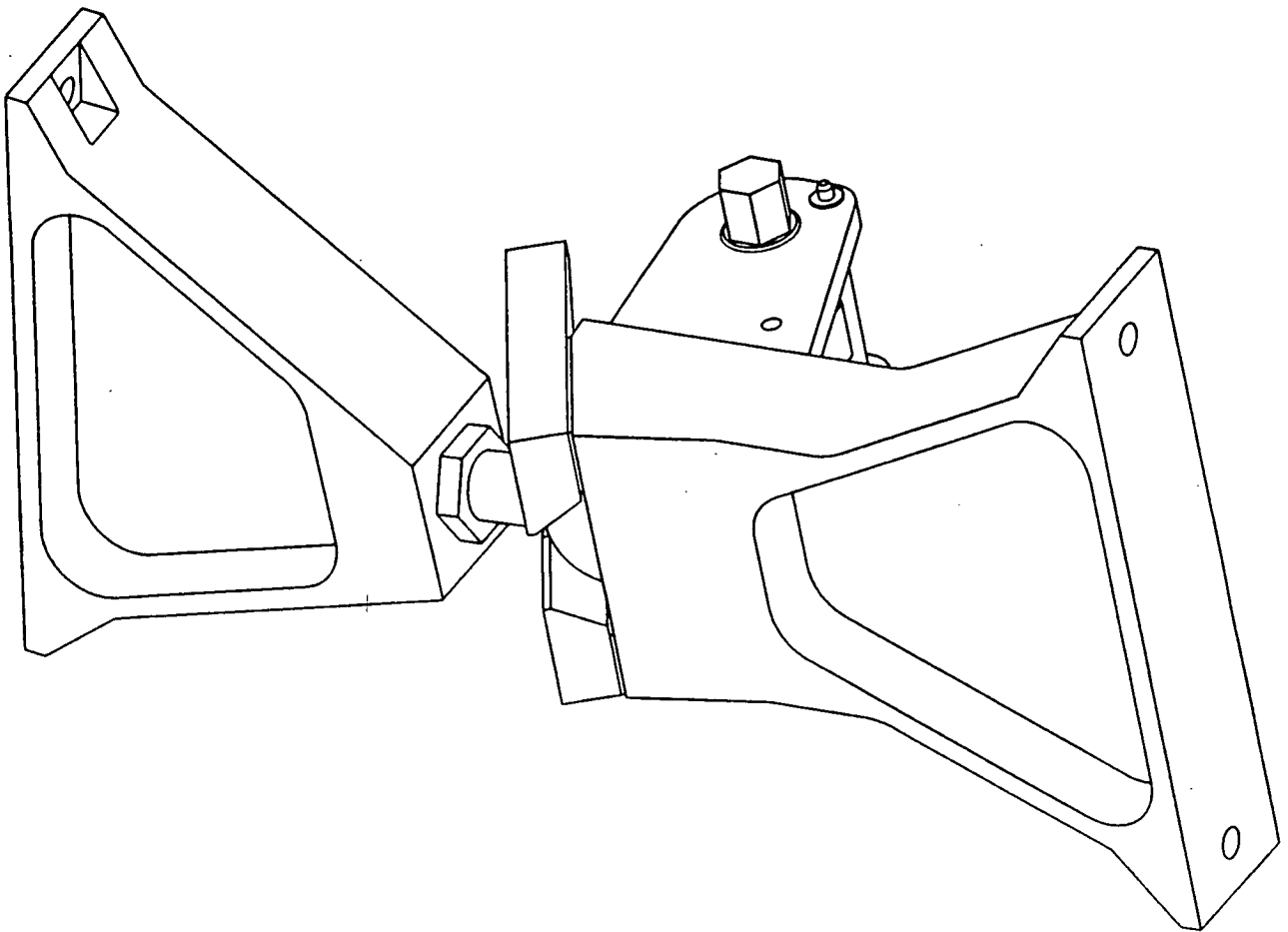


Figure 2.8-8. Isometric View Of The Type II Latch and Striker

8 to be installed using a single radial motion toward the center of the concentrator. The final latch type (Type IV) would be used for a 90 degree interface between panels. A Type IV latch would be located between panel 9 and panel 10. The latch and its associated isometric view can be seen in Figure 2.8-11 and 2.8-12. The all latch design is engaged using a single radial motion of each panel toward panel number one. This was a design constraint that will facilitate an option for robotic assembly of the concentrator. The kinematics of such an operation would be much easier than a two motion deployment scenario.

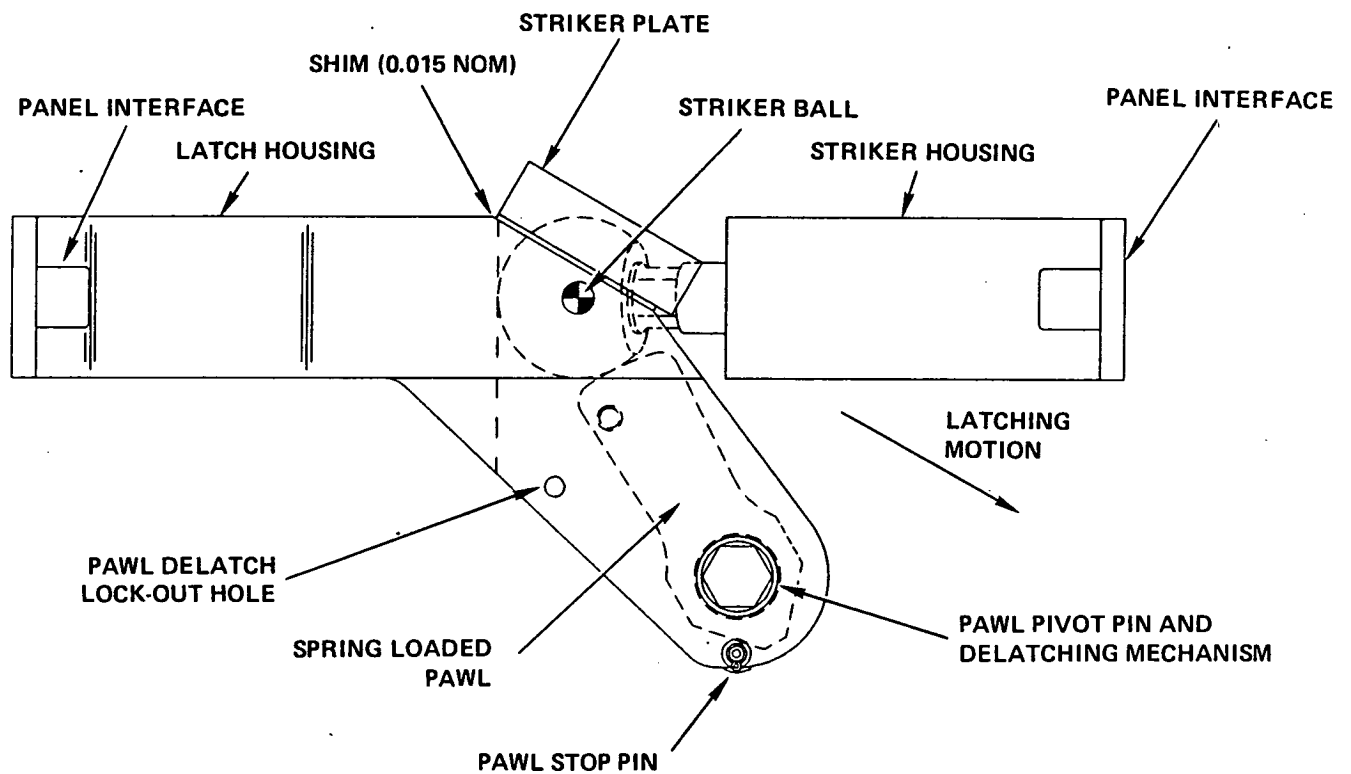


Figure 2.8-9. Typical Type III Latch Interfaces Panel 8 to Panel 7



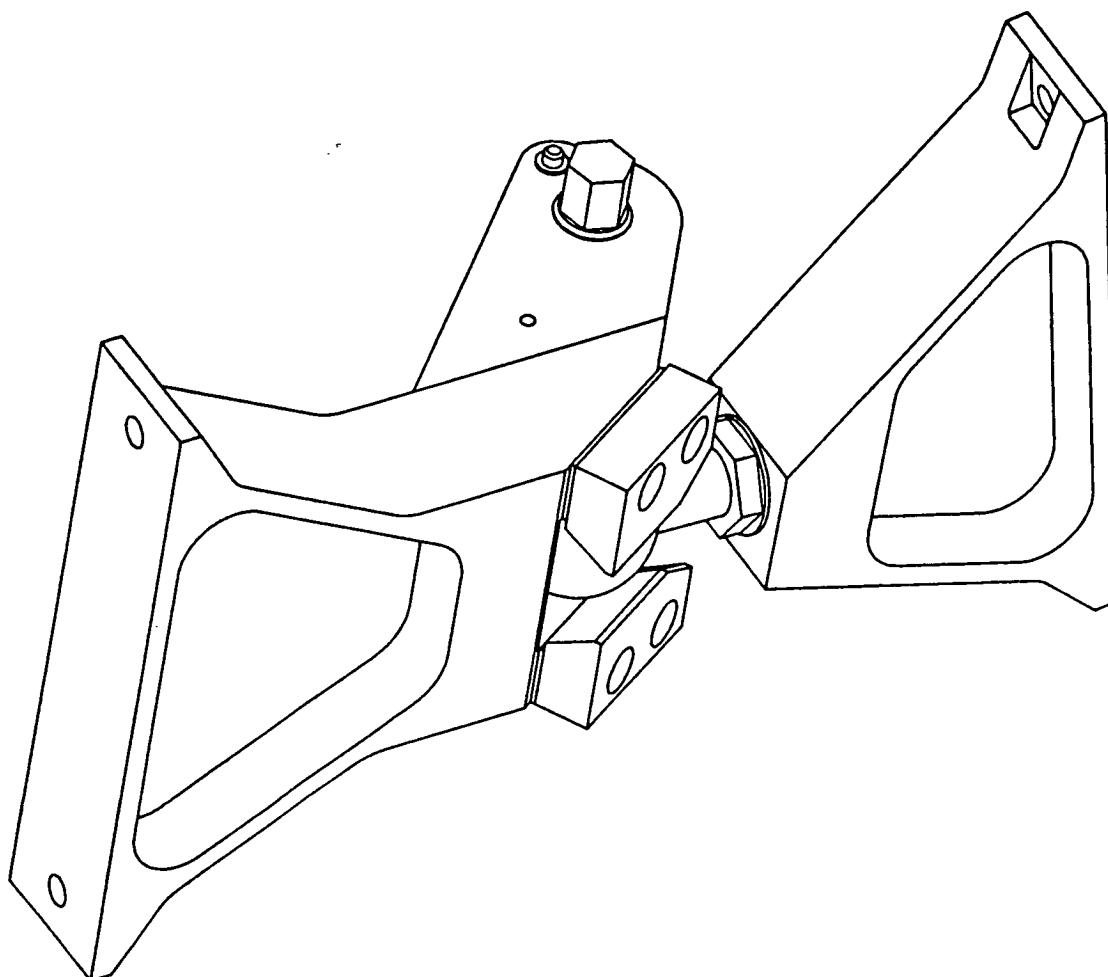


Figure 2.8-10. Isometric View Of The Type III Latch and Striker

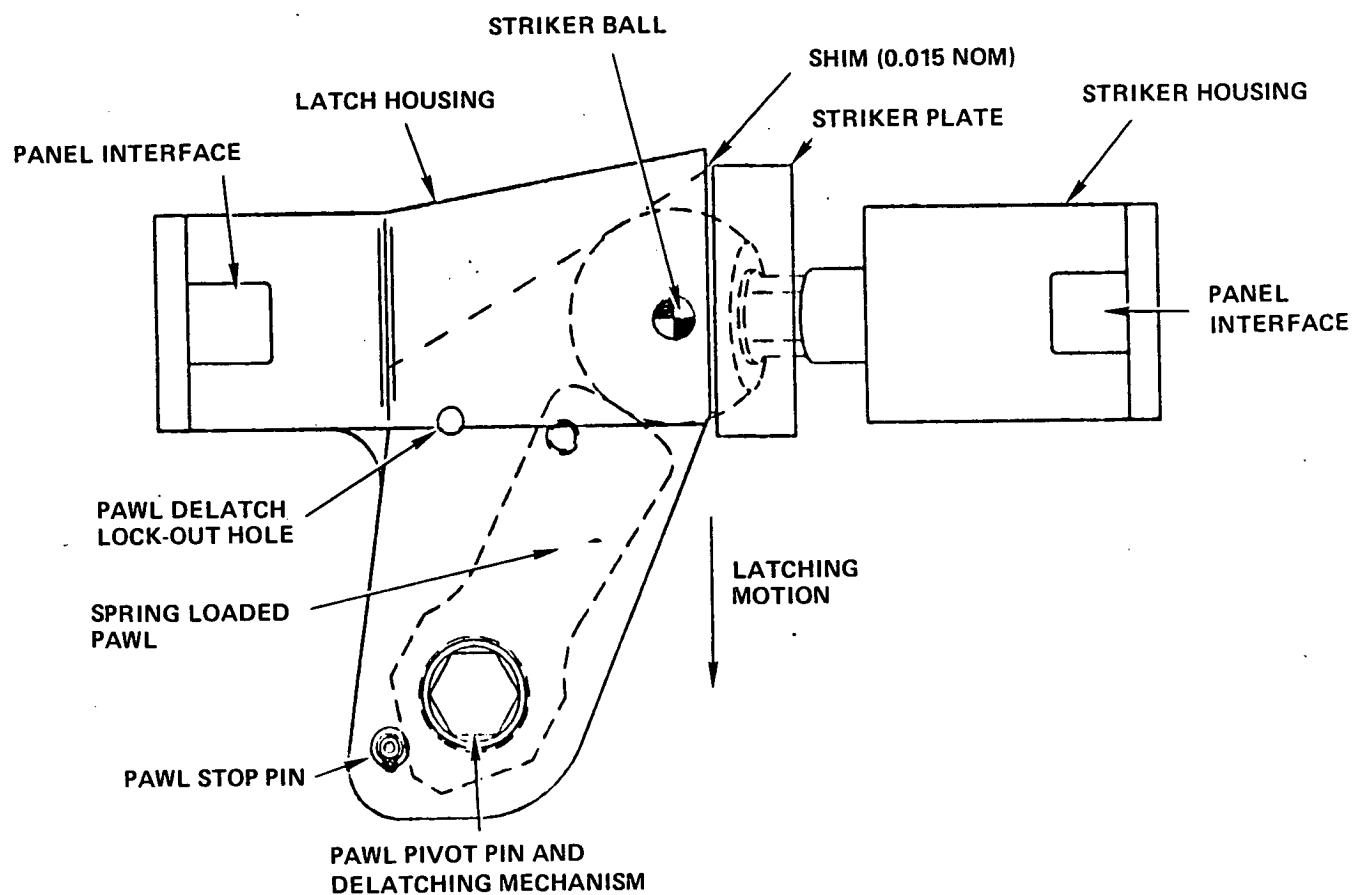


Figure 2.8-11. Type IV Latch That Is Used Between Panel 9 and Panel 10

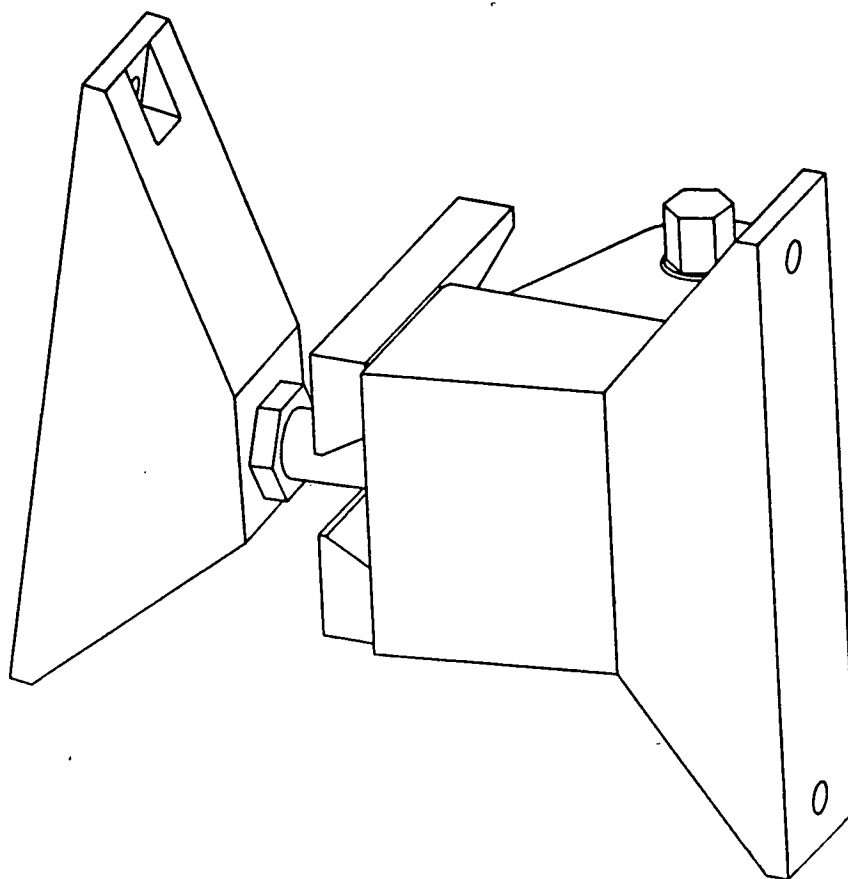


Figure 2.8-12. Isometric View Of A Type IV Latch

### 3.0 MANUFACTURING

Section 2.0 described the design and development of the Solar Dynamic Concentrator model to be tested on the SCAD program. Section 3.0 describes the steps involved in fabricating a hexagonal panel and installing all associated hardware to complete a hex panel assembly. This section provides a historical record for completing a hexagonal panel assembly and when combined with the procedures in the appendix will allow NASA LeRC to fabricate new hexagonal panels and install latches.

The following areas will be covered in this section; Hexagonal Panel Fabrication, Hexagonal Panel Proofloading, Flexure and Standoff Installation, Latch and Striker Assembly and Latch and Striker Installation/Alignment on the Hexagonal Panels. All piece parts used in the assembly process were produced by Harris approved vendors under the supervision of the SCAD Production Engineer.

#### 3.1 Hex Panel Fabrication

There are three major components used to fabricate the hexagonal panel structure. It is comprised of twelve graphite epoxy box beams, six aluminum corner fittings and fourteen shear plates (twelve corner and two hub plates). These items were described in detail in Section 2.0 and the fabrication methods used on these individual parts were instrumental in achieving the desired functionality and structural requirements of the panel.

The structural integrity of the truss hex solar concentrator design starts at the panel level. Thus, extreme care must be taken to ensure that

the hexagonal panel meets the dimensional requirements that are needed. The dimensional hard points of the hex panel are the metallic corner fittings. To ensure that the concentrator will latch together and not have a large tolerance buildup, the corner fittings must be within their true position tolerance of .005 inches. This is accomplished by using a very accurate tooling fixture shown in Figure 3.1-1. The corner fitting is held between two gauge blocks which are machined to very tight tolerance and attached to the corner pad as shown in Figure 3.1-2.

The required panel point to point dimensions were obtained by placing the metallic corner fitting in the tooling and measuring the distance between fittings. That distance was accurate to .010 inches. The perpendicularity of the corner fitting was obtained by locating the corner pads and the central pad to the same vertical height with respect to gravity. This was accomplished using a bubble leveled theodolite (surveyors telescope) and a scale. Once the pads were at the same height they were leveled and then checked to assure they were at the same height. The tooling was now set to guarantee that the panel would meet the requirements on the panel structure drawing (Structure Assembly 500020).

ORIGINAL PAGE  
BLACK AND WHITE PHOTOGRAPH

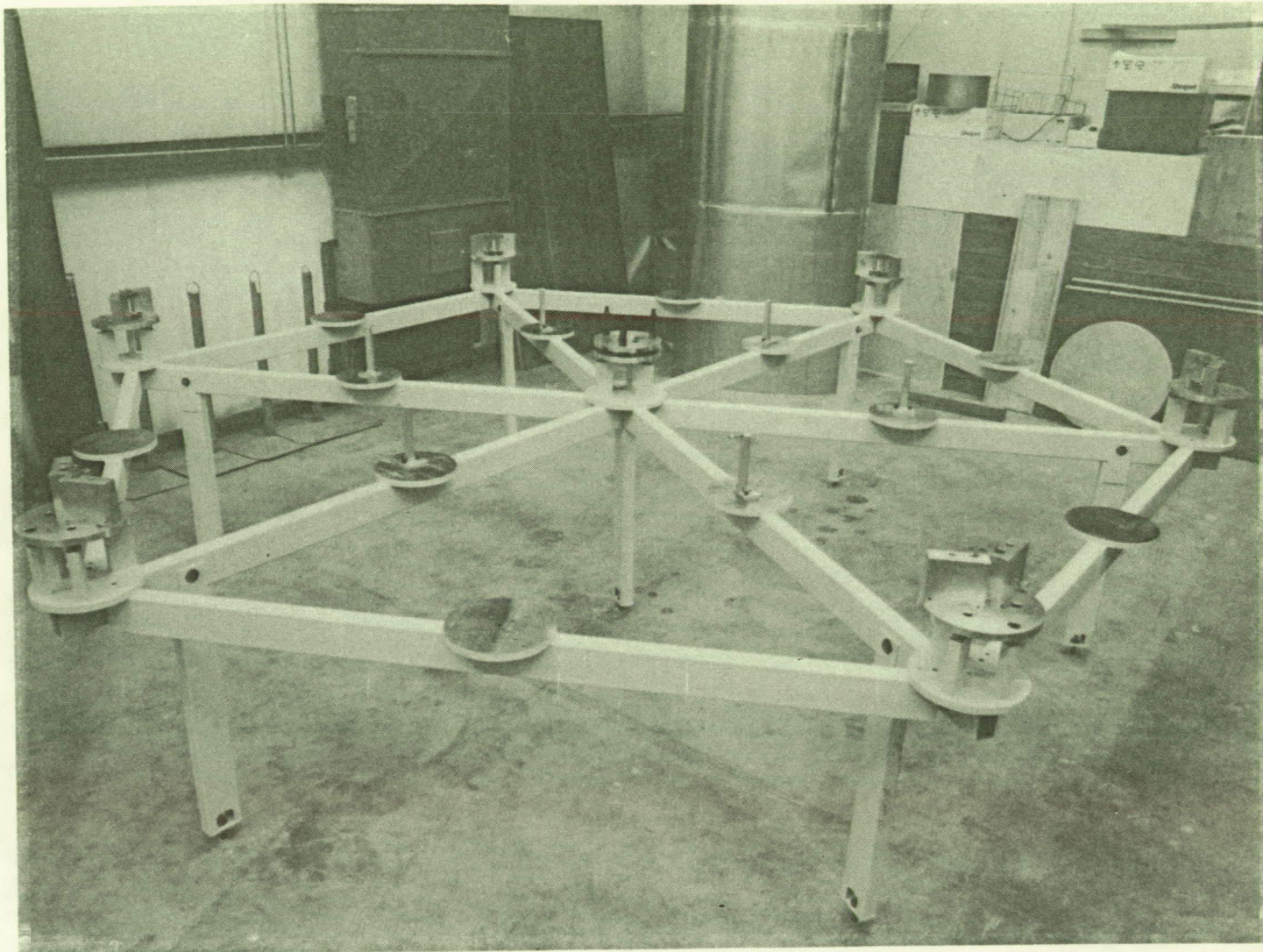


Figure 3.1-1. Hexagonal Panel Bonding Fixture Insures Accurate Geometry For The Corner Fittings That Interface With The Latches



ORIGINAL PAGE  
BLACK AND WHITE PHOTOGRAPH

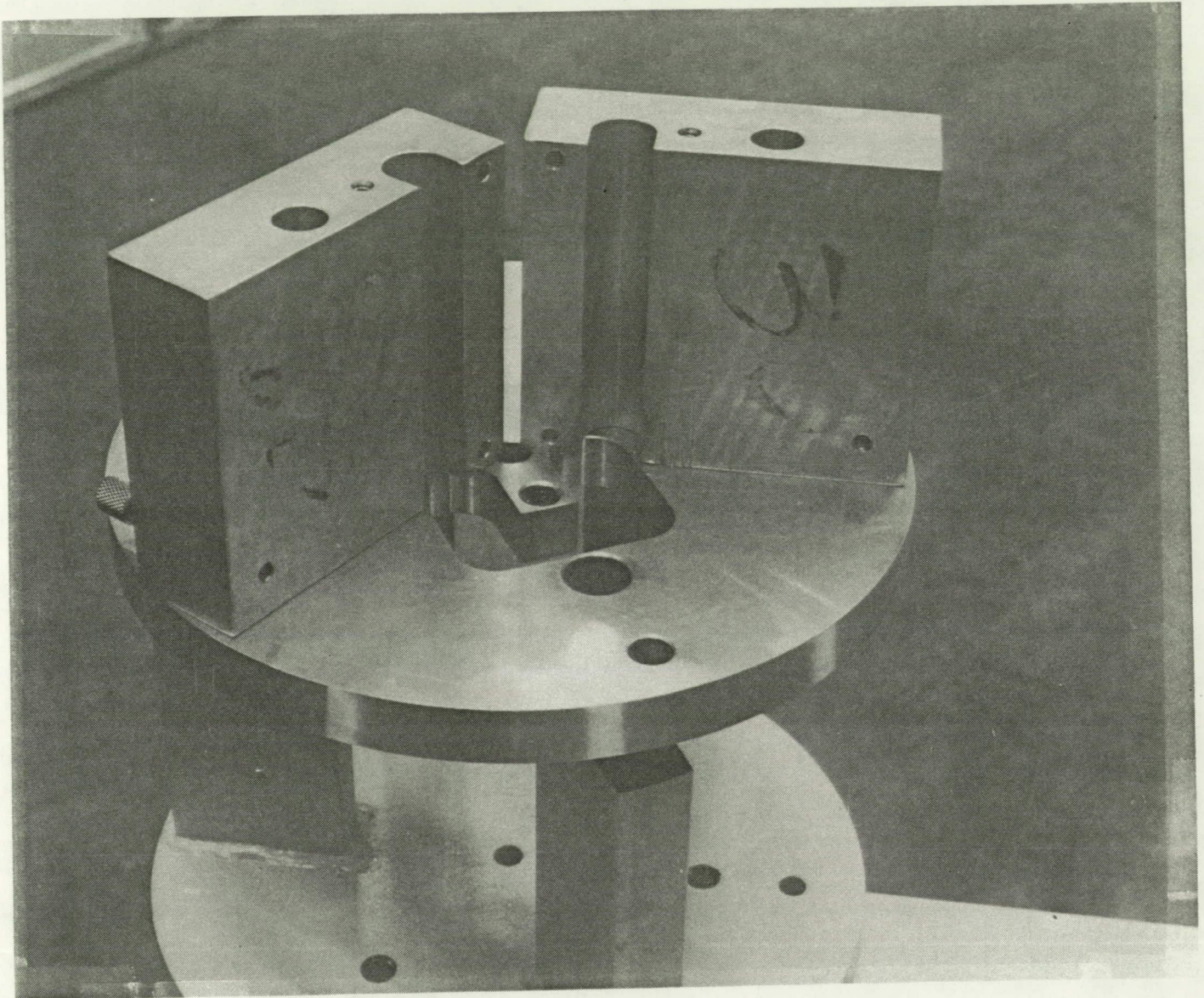


Figure 3.1-2. Precision Tooling Plates Hold The Corner Fittings In Place During The Bonding Operation. The Cutout In The Plate Allows For Epoxy To Be Removed From The Underside Of The Box Beam During Bonding.

The following pages describe the panel bonding process in sufficient detail to allow the reader to understand the basic steps involved. The bonding procedure is typically a three day process.

Day 1

1. Clean all corner and center pad surfaces on the bonding fixture and treat with a mold release compound to prevent bonding the hex panel to the bond fixture.
2. Prepare the box beam surfaces that will be bonded on the first 10 beams. The surface is prepared by sanding the bonding area to remove films and expose graphite fibers to enhance epoxy wicking and achieve a strong structural bond.
3. Clean the sanded surfaces with alcohol.
4. Clean the corner fittings with alcohol and trim bond wires so they do not protrude past the box beams when they are placed on the fitting.
5. The beams and corner fittings labeled in Figure 3.1-3 are bonded in two groups.
6. Mix 60 grams Hysol EA934 epoxy per Spec 100008 and add 2% by weight cabosil.
7. Apply epoxy to corner fitting stubs that will be used and mount fitting A Group 1 to the table as shown. Also, apply a wetting coat of epoxy to the beam bond areas.



## HEX STRUCTURE ASSEMBLY (CONTINUED)

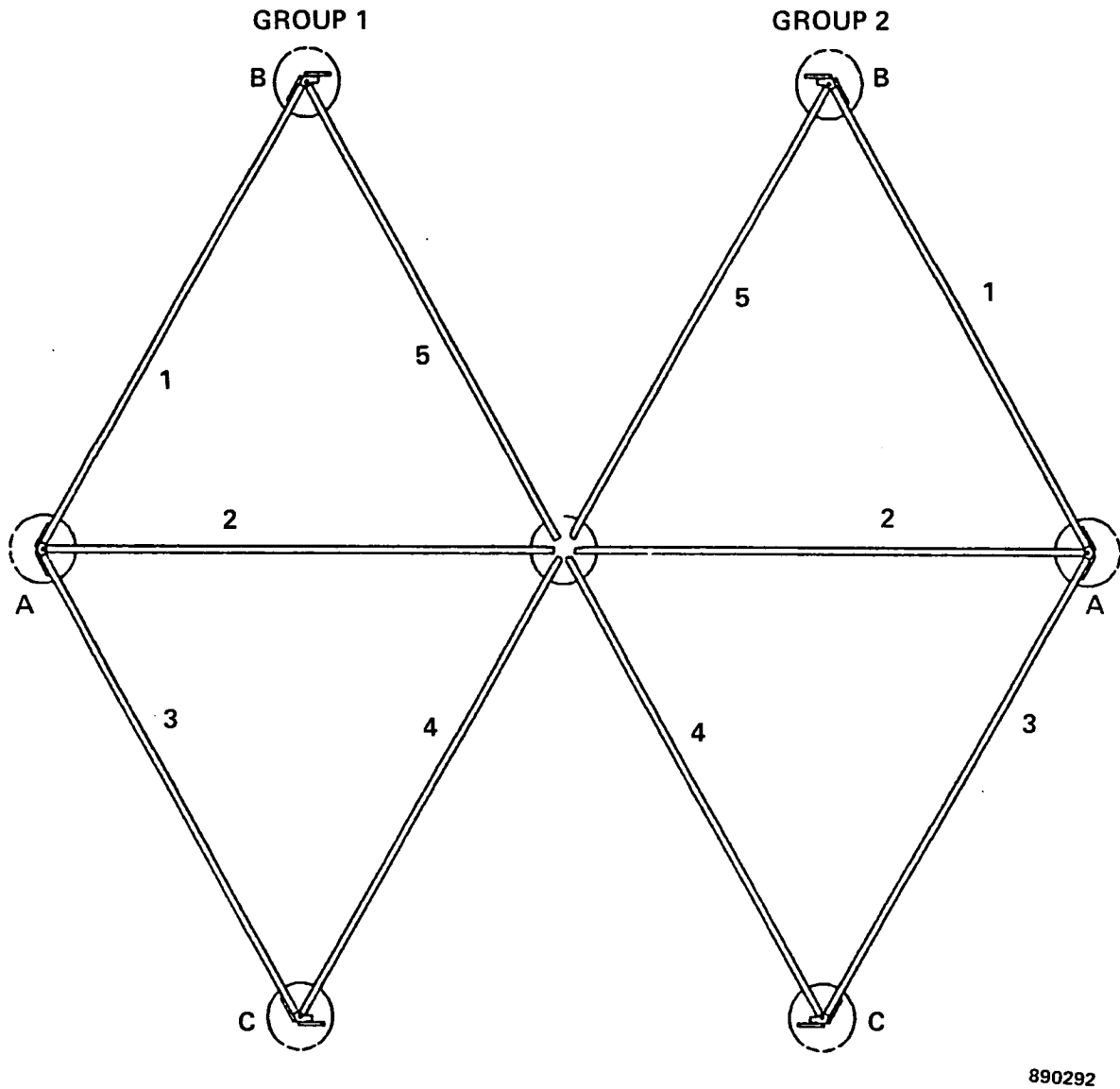


Figure 3.1-3. The First Step Of The Hexagonal Panel Bonding Process Is Shown Above. Group 1 and Group 2 Are Bonded On Day One Of The Three Day Process.

8. Install Beams 1, 2 and 3 then lock in place using the locational devices on the table at corner A.
9. Remove excess epoxy with cotton swabs and alcohol.
10. Install corner fitting B into box beam 1 and C into box beam 2 and mount to corner fitting pads.
11. Install beam 4 on corner fitting C and beam 5 on corner fitting B and lock in place fittings B and C.
12. Remove excess epoxy.
13. Repeat steps 6-12 on the Group 2 hardware.

Day 2 (or 12 hours later)

14. Prepare the two box beams that are needed to complete the hex panel structure shown in Figure 3.1-4 as in step 2.
15. Remove corner holding devices from Group 2 parts.
16. Mix 40 grams of epoxy per Step 6.
17. Apply epoxy to remaining corner stubs at the B and C locations and to the box beams.
18. Slide Group 2 Assembly out such that the two remaining box beams can be installed.
19. Slide Group 2 Assembly in and lock corner fittings A, B and C of Group 2 down in place.
20. Insert beam locational guides into new beams.
21. Remove excess epoxy.

4 hours or more later (to allow the epoxy to partially cure)

### HEX STRUCTURE ASSEMBLY (CONTINUED)

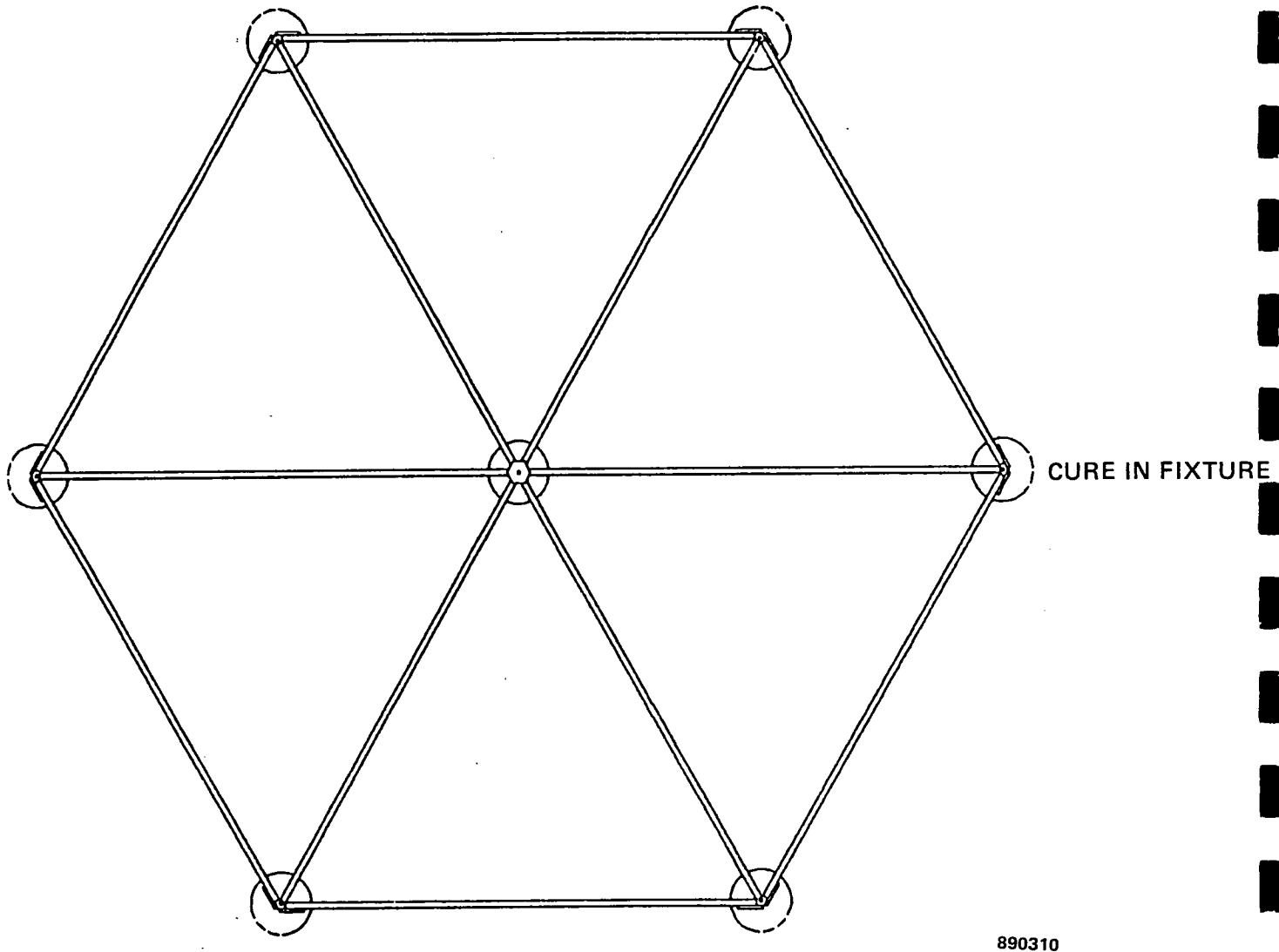


Figure 3.1-4. Two Box Beams Numbered Six (Horizontal Top and Bottom) Are Placed On Corner Fittings B and C Respectively To Complete The Hex Panel. The Shear Plates Are Bonded On The Six Corners And The Hub Also During Day Two.

22. Prepare 1 set of shear plates (6 corner plates and 1 hub plate) by sanding bond surface and cleaning with alcohol.
23. Remove corner fitting holding devices.
24. Clean top of corner fitting and beam area (prepared earlier) where shear plates will be bonded with alcohol.
25. Mix 60 grams of epoxy per Step 6 and add 2% by weight of 10 mil bonding beads (to maintain constant bondline thickness).
26. Apply a thin coat of epoxy to beams and top of corner fittings where shear plates will be bonded.
27. Wet shear plates with epoxy.
28. Insert alignment tool into corner fitting to align shear plate with respect to the corner fitting. The insert also keeps the epoxy from seeping through tooling hole and bonding the hex panel to the tooling.
29. Place shear plate on panel and pull down with tooling plate and bolt.
30. Remove excess epoxy.
31. Reinstall corner fitting holding hardware.
32. Repeat Steps 28-31 5 times.
33. Install hub shear plate with the process in Steps 29 and 30.

A completed shear plate bond and associated tooling can be seen in Figure 3.1-5.

ORIGINAL PAGE  
BLACK AND WHITE PHOTOGRAPH

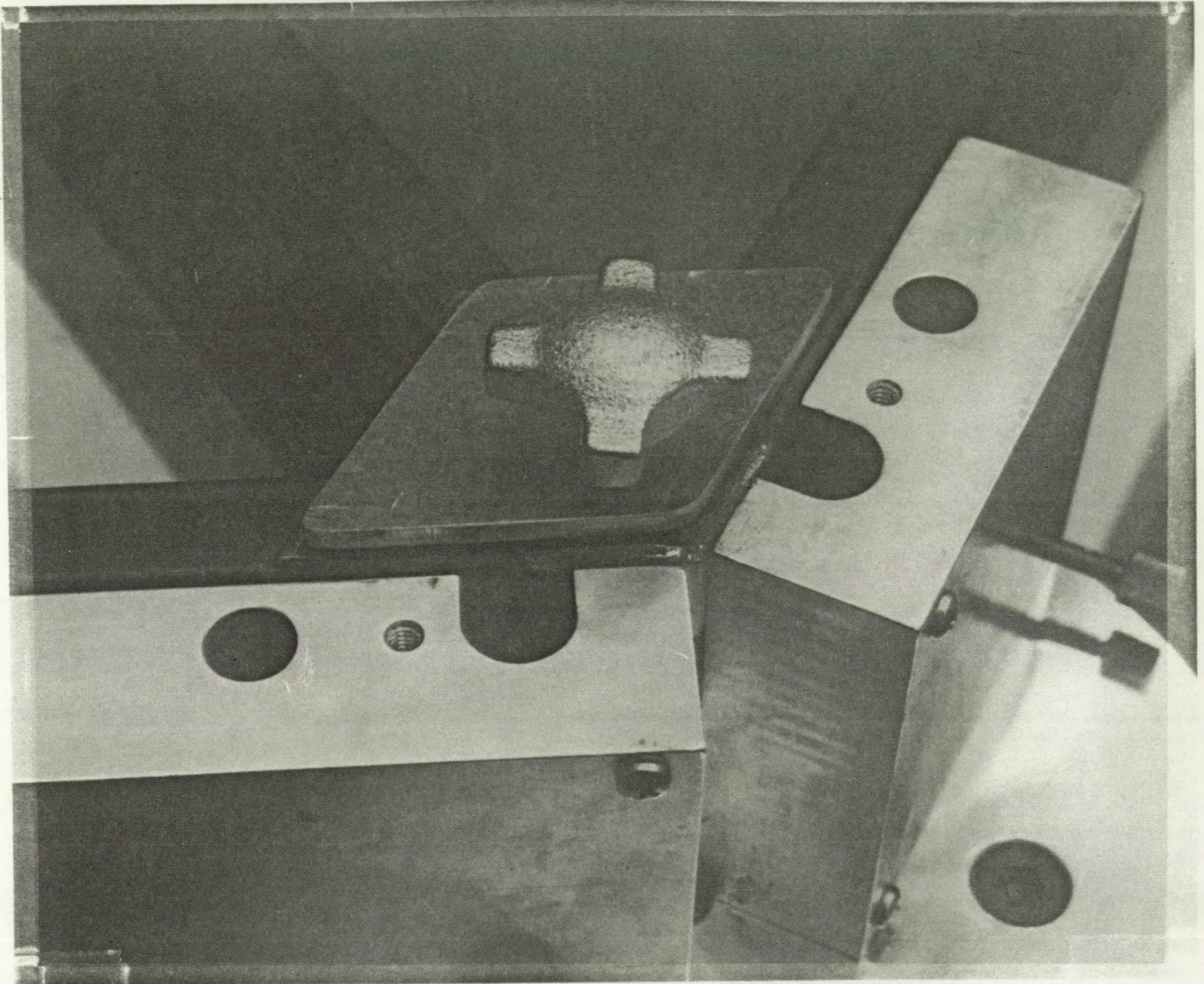


Figure 3.1-5. Completed Shear Plate Bond With Tooling Plate In Place. The Tooling Plate Applies A Uniform Force Over The Shear Plate And Pushed It Down To The .010 Inch Bond Beads For A Uniform Bondline Thickness.



### Day 3

34. Prepare the second set of shear plates (six corner and one hub plate) as in step 22.
35. Turn the panel over and place it back on the tooling fixture.
36. Prepare beam area where shear plate will be bonded, clean with alcohol.
37. Repeat Steps 24-33.

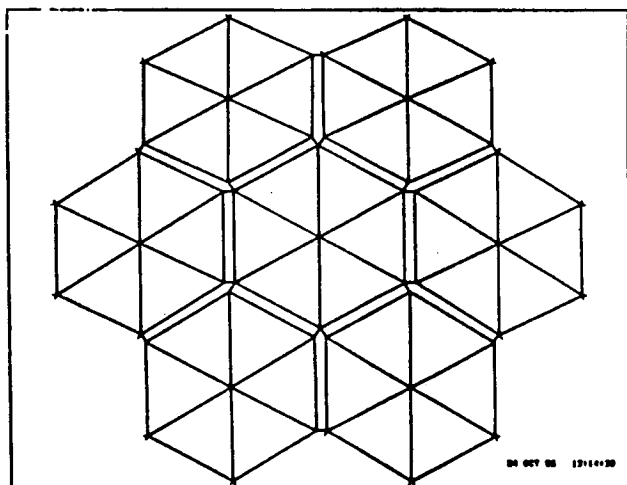
If it is desired to bond another panel starting on Day 3 the panel just finished can be removed 4 hours after completing Step 37 and allowed to final cure sitting flat on the floor. The panels must cure seven days at room temperature before any load is applied.

### 3.2 Establishing Hexagonal Panel Loads and Panel Proofloading

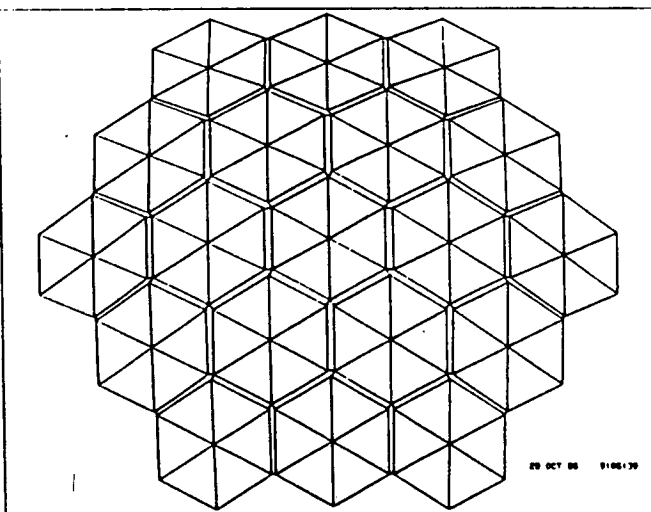
The panels were proofloaded to verify the strength of the bonded joints, validate the structural analysis finite element models and to assure personnel safety at all times during the assembly and testing process. During the SCAD program two finite element models (FEM's) were constructed to determine worst case loads on the hexagonal panel assembly (Figure 3.2-1). These loads were then used to establish the panel proofloading limits. A seven panel FEM model, that represents a seven panel non-counterbalanced configuration (Figure 3.2-2) that would be used for a structural repeatability test prior to availability of the counterbalance. A nineteen panel model with the counterbalance lines attached in the assembly position (Figure 3.2-3) and a nineteen panel configuration in the optical scanning position (Figure 3.2-4) were also developed. A description of the models

CONCENTRATOR F.E.H. MODEL

- o MODEL DESCRIPTION - TWO FINITE ELEMENT MODELS OF THE SCAD UNIT WERE GENERATED USING NLSA IN ORDER TO PREDICT THE WORSE CASE LOADS THAT OCCUR DURING ASSEMBLY/HANDLING.
- 1) 7 HEX PANEL MODEL
  - 2) 19 HEX PANEL MODEL



7 PANEL MODEL



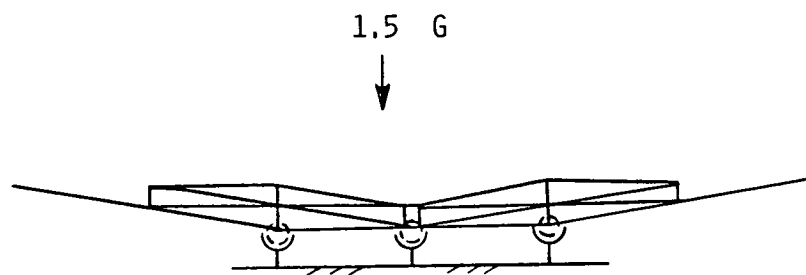
19 PANEL MODEL

Figure 3.2-1. Two Finite Element Models (FEM's) Were Constructed For The SCAD Program. A Seven and Nineteen Panel Configuration Were Built.



o LOADING CONDITIONS AND RESTRAINTS

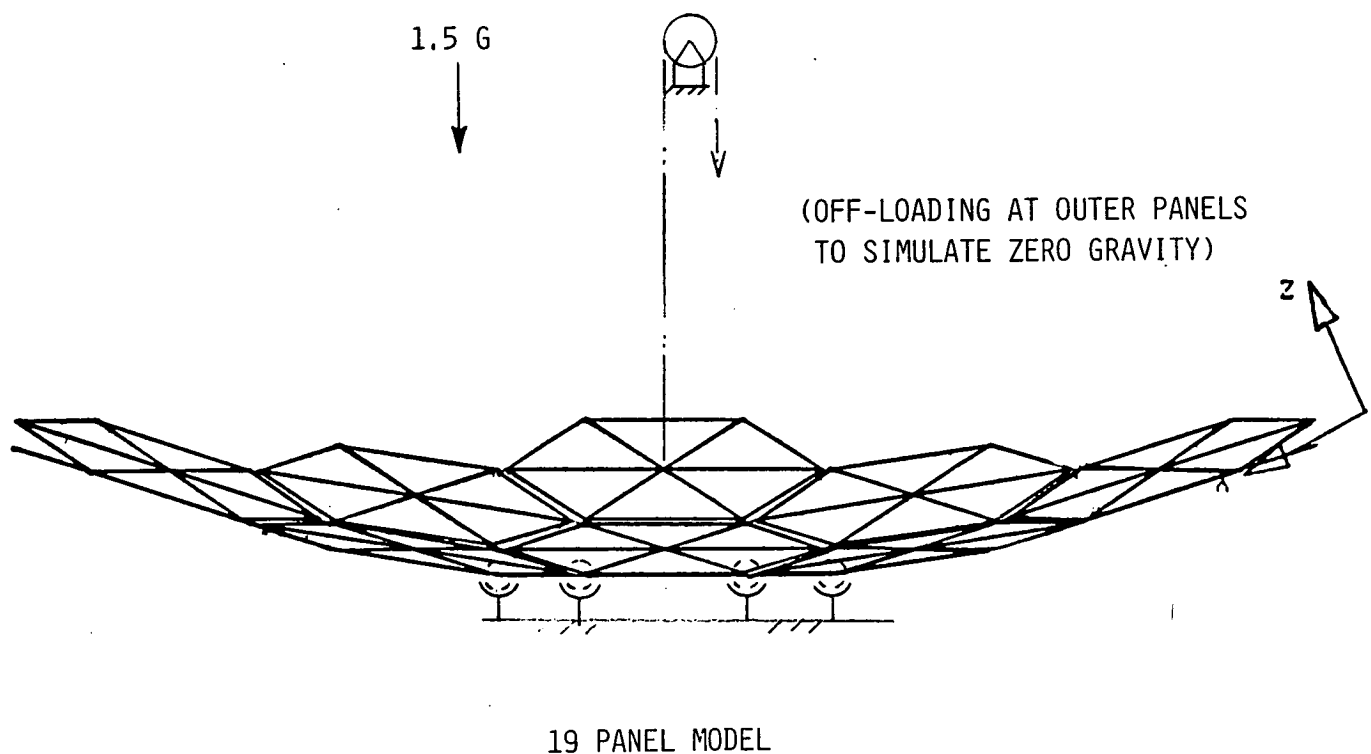
CASE 1 - 7 PANEL MODEL WITH 1.5 G LOADING PERPENDICULAR TO CENTER PANEL.  
CENTER PANEL RESTRAINED FROM TRANSLATION AT 6 VERTICES.



7 PANEL MODEL

Figure 3.2-2. Seven Panel FEM That Was Used To Determine The Loads  
For The Seven Panel Non-counterbalanced Structural Repeatability Test.

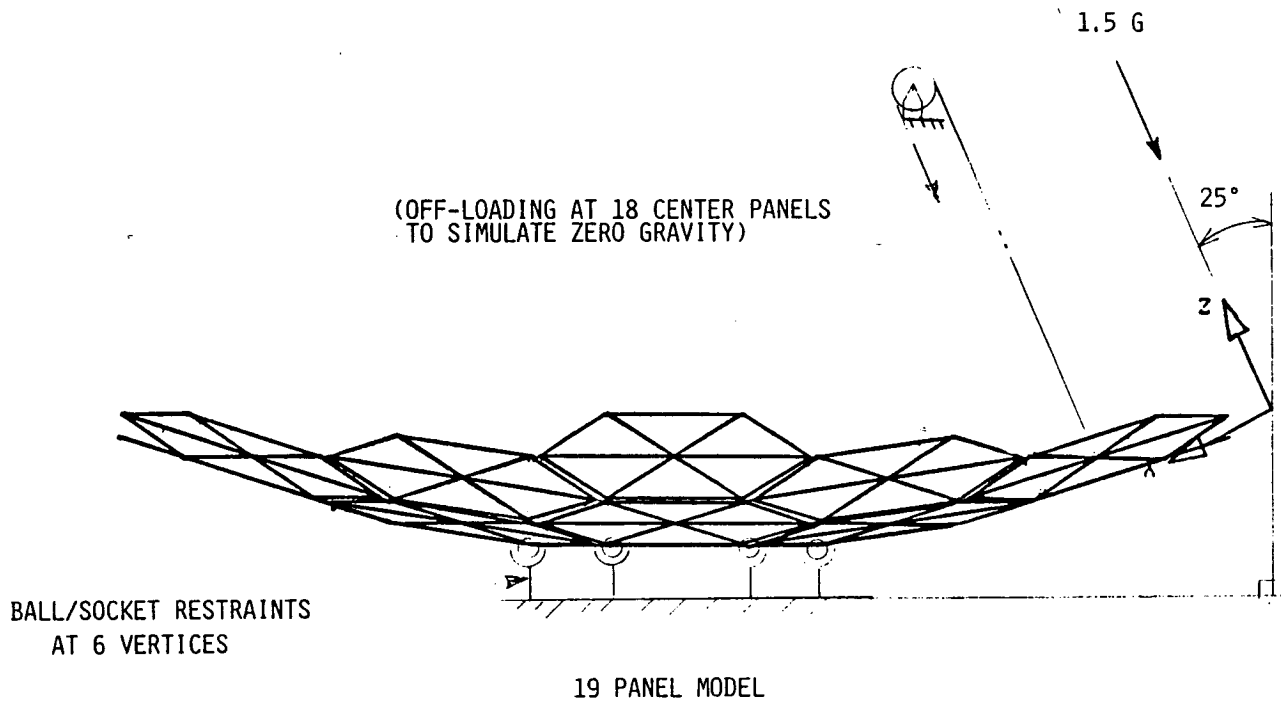
o LOADING CONDITIONS AND RESTRAINTS (CONTINUED)



- CASE 2 - 19 PANEL MODEL WITH 1.5 G LOADING PERPENDICULAR TO CENTER PANEL.  
- RESTRAINED SAME AS CASE 1 PLUS COUNTERBALANCE LINES ON THE 18 OUTER PANELS.

Figure 3.2-3. Nineteen Panel FEM Of The Concentrator In The Assembly Position. The Center Panel Is Restrained To Simulate The Central Panel Support.

o LOADING CONDITIONS AND RESTRAINTS (CONTINUED)



CASE 3 - SAME AS CASE 2, BUT 1.5 G LOADING ALONG Z AXIS  
(BORE SIGHT) OF THE CONCENTRATOR.

Figure 3.2-4. Nineteen Panel FEM With The Counterbalance Lines At A  
25 Degree Angle To Simulate The Optical Scanning Position

and the beam and latch properties used in the model can be seen in Figures 3.2-5 and 3.2-6. The resulting loads for the box beams can be seen in Figure 3.2-7 and the resulting latch loads can be seen in Figure 3.2-8. The seven panel non-counterbalanced model developed the worst case loads. By taking the resulting loads in the box beam and latch areas an equivalent stress can be calculated in the box beams and bond joints. The proofload scenario is based on obtaining the proper stresses plus margin in the beams and bond joints to ensure structural adequacy of the hexagonal panel. Once the stresses were calculated a distributed load was applied to the FEM until the same loads (stresses) were developed in the bond joints, latch interfaces and box beams. Three loading scenarios were used on the panels and can be seen in Figures 3.2-9 through 3.2-11.

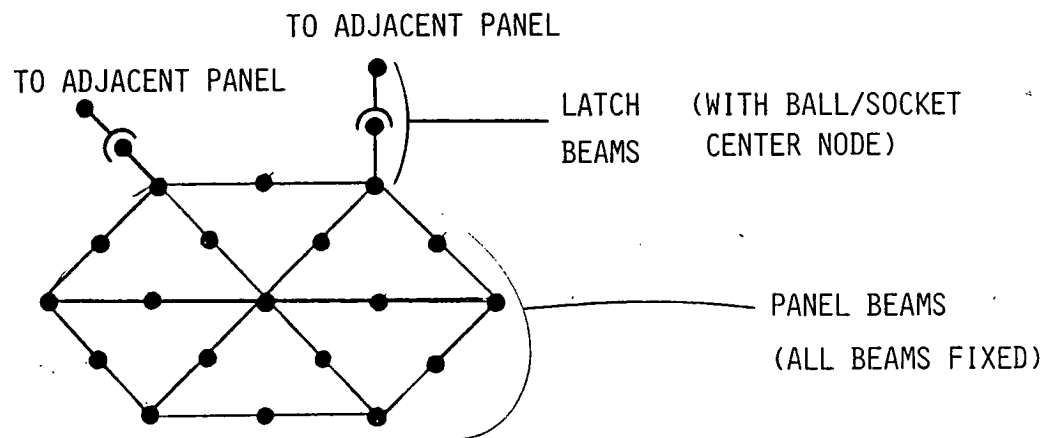
1. Radial Beams
2. Circumferential Beams
3. Corner Fittings

1. The radial beams were loaded in three places as shown in Figure 3.2-9. A picture of the actual operation can be seen in Figure 3.2-12. The loads were applied in four increments of 25 pounds up to a load of 100 pounds in three places on the beam (300 total). Then the loads were decreased incrementally back to the unloaded condition. The radial beam proofloading qualified the radial beams, the hub shear plate, and their bond joints.

o ELEMENT TYPES/CONNECTIVITY

EACH HEX PANEL IN THE MODEL CONSISTS OF:

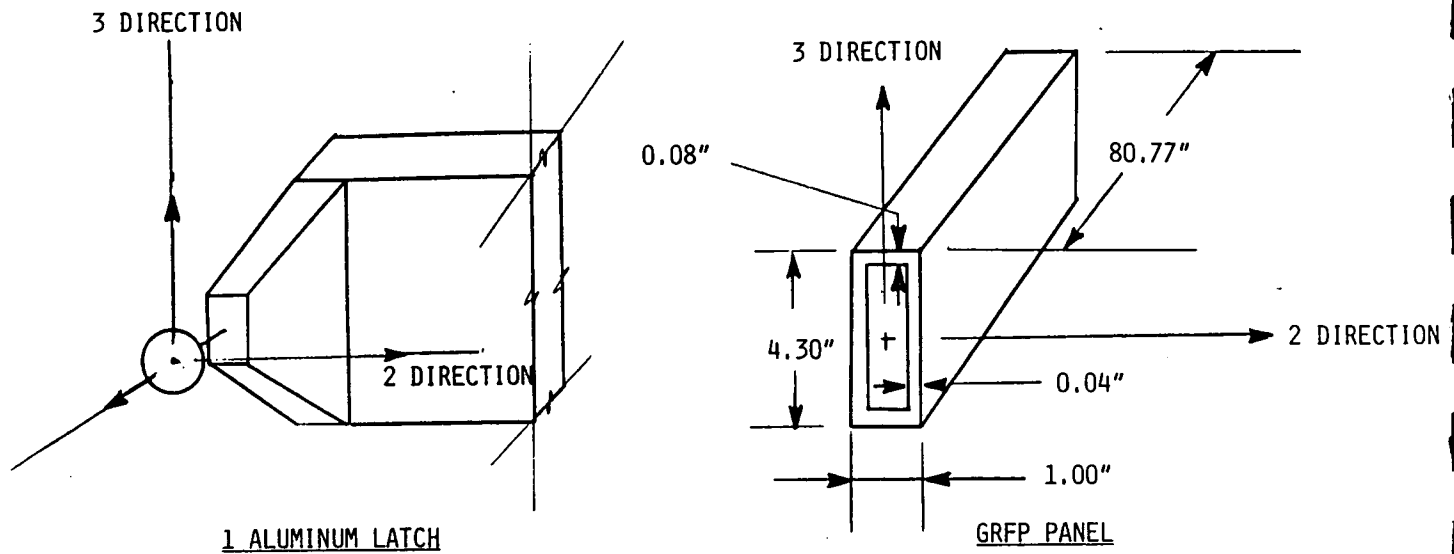
- 1) 3-D ELASTIC BEAMS REPRESENTING THE BOX BEAMS.
- 2) 3-D ELASTIC BEAMS REPRESENTING THE LATCHES.
- 3) NODAL WEIGHTS REPRESENTING THE FACET WEIGHTS.



BEAM CONNECTIVITY FOR A TYPICAL PANEL

Figure 3.2-5. Description Of The FEM Showing How The Box Beams and Latches Were Modeled To Represent The Structure

o ELEMENT PROPERTIES. - ELEMENT COORDINATE DIRECTIONS ARE SHOWN.



BEAM TYPE	AREA (IN <sup>2</sup> )	I <sub>2</sub> (IN <sup>4</sup> )	I <sub>Z</sub> (IN <sup>4</sup> )	J(IN <sup>4</sup> )	SF2 (SHEAR FACTORS)	SF3 (SHEAR FACTORS)	E(PSI)	G (PSI)
LATCH	.293	.377	.01	.351E-3	2/3	2/3	10E6	4E6
PANEL	.491	1.19	.0897	.279	0	0	2.2E7	7.2E6

Figure 3.2-6. Describes The Element Properties Used To Model The Hexagonal Panel Box Beams and Latches

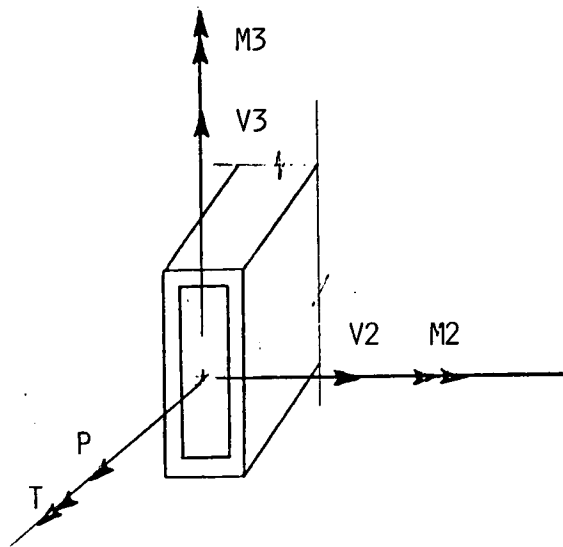


TABLE 1. MAXIMUM LOADS AND MOMENTS FOR THE BOX BEAMS OF THE HEX PANELS.

	LOAD CASE 1 (7 PANEL MODEL)	LOAD CASE 2 (19 PANEL, $G_1$ )	LOAD CASE 3 (19 PANEL, $G$ ALONG $Z$ )
P (LBS)	660.0	131.0	122.0
V2 (LBS)	NIL	NIL	NIL
V3 (LBS)	26.7	14.5	15.0
T (IN-LBS)	100.0	14.8	13.7
M2 (IN-LBS)	1540.0	764.0	778.0
M3 (IN-LBS)	155.0	48.9	59.4

Figure 3.2-7. Maximum Box Beam Loads Obtained From The Three FEM's Developed On SCAD



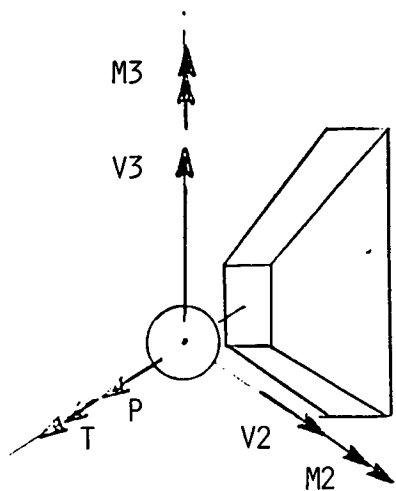
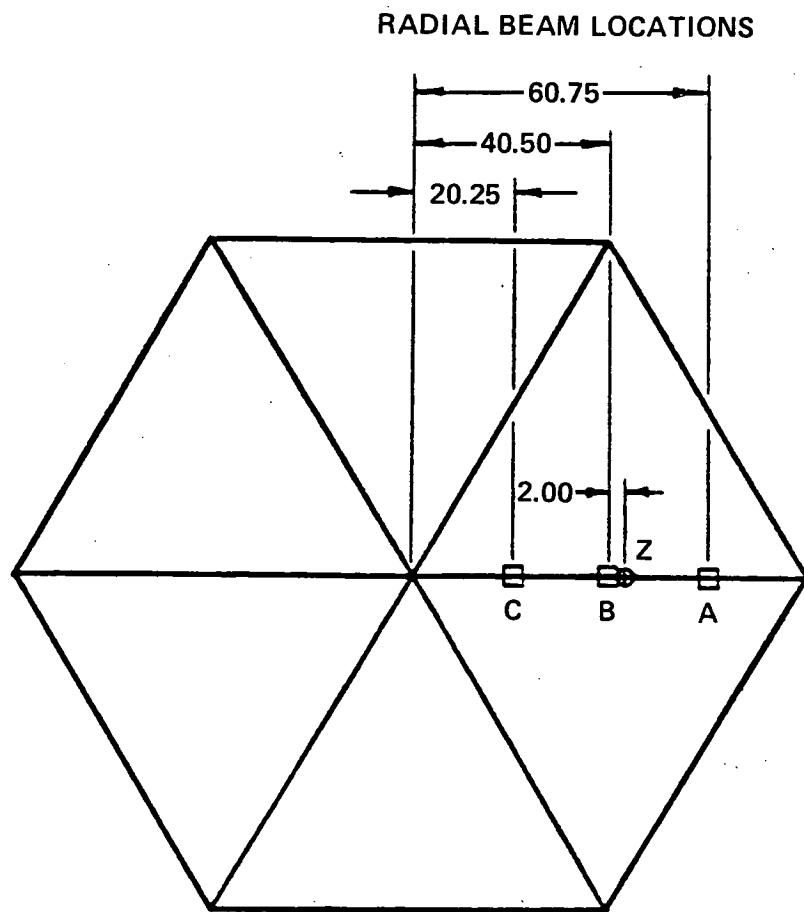


TABLE 2. MAXIMUM LOADS AND MOMENTS FOR THE LATCHES

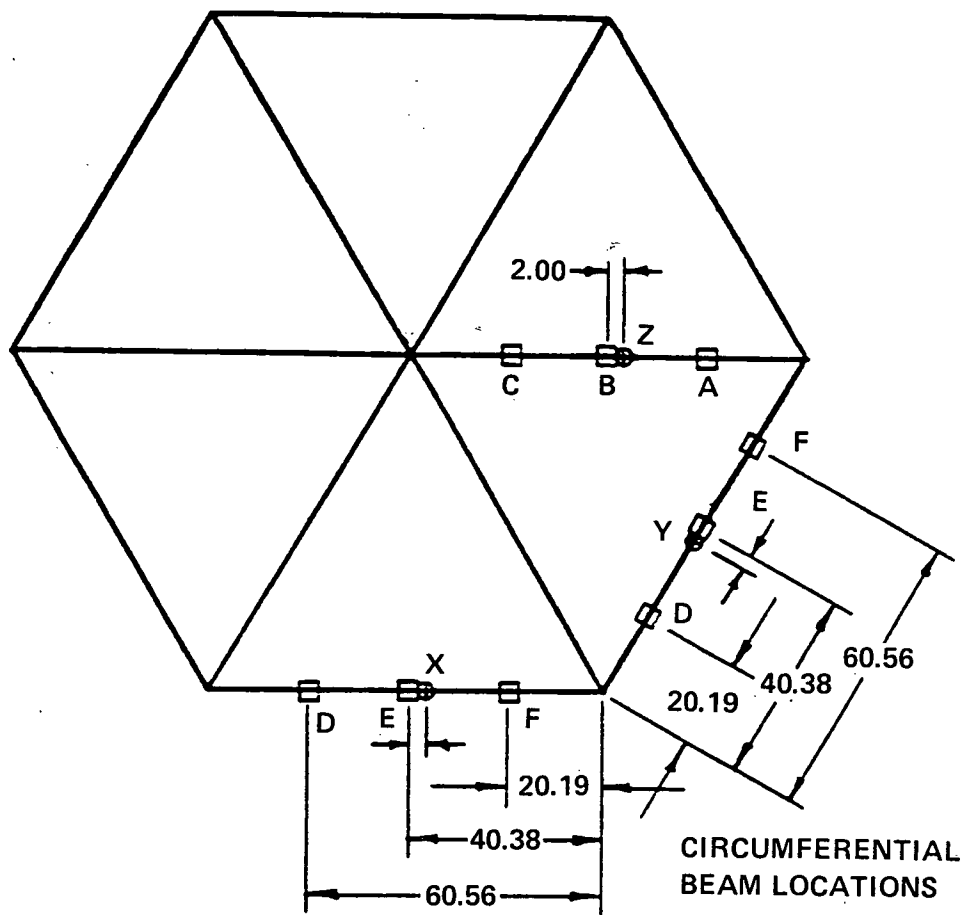
	LOAD CASE 1 (7 PANEL MODEL)	LOAD CASE 2 (19 PANEL, G $\perp$ )	LOAD CASE 3 (19 PANEL ALONG z)
P (LBS)	773.0	155.0	148.0
V2 (LBS)	100.0	24.0	22.0
V3 (LBS)	66.2	27.0	25.8
T (IN-LBS)	0.0	0.0	0.0
M2 (IN-LBS)	282.0	125.0	120.
M3 (IN-LBS)	413.0	98.7	91.1

Figure 3.2-8. Maximum Latch Loads Obtained From The Three FEM's Developed On SCAD



890296

Figure 3.2-9. Locations For Application Of Proofload Weights  
On The Radial Beams Of The Hexagonal Panel



890297

Figure 3.2-10. Locations For Application Of The Proofload Weights  
On the Circumferential Beams Of The Hexagonal Panel

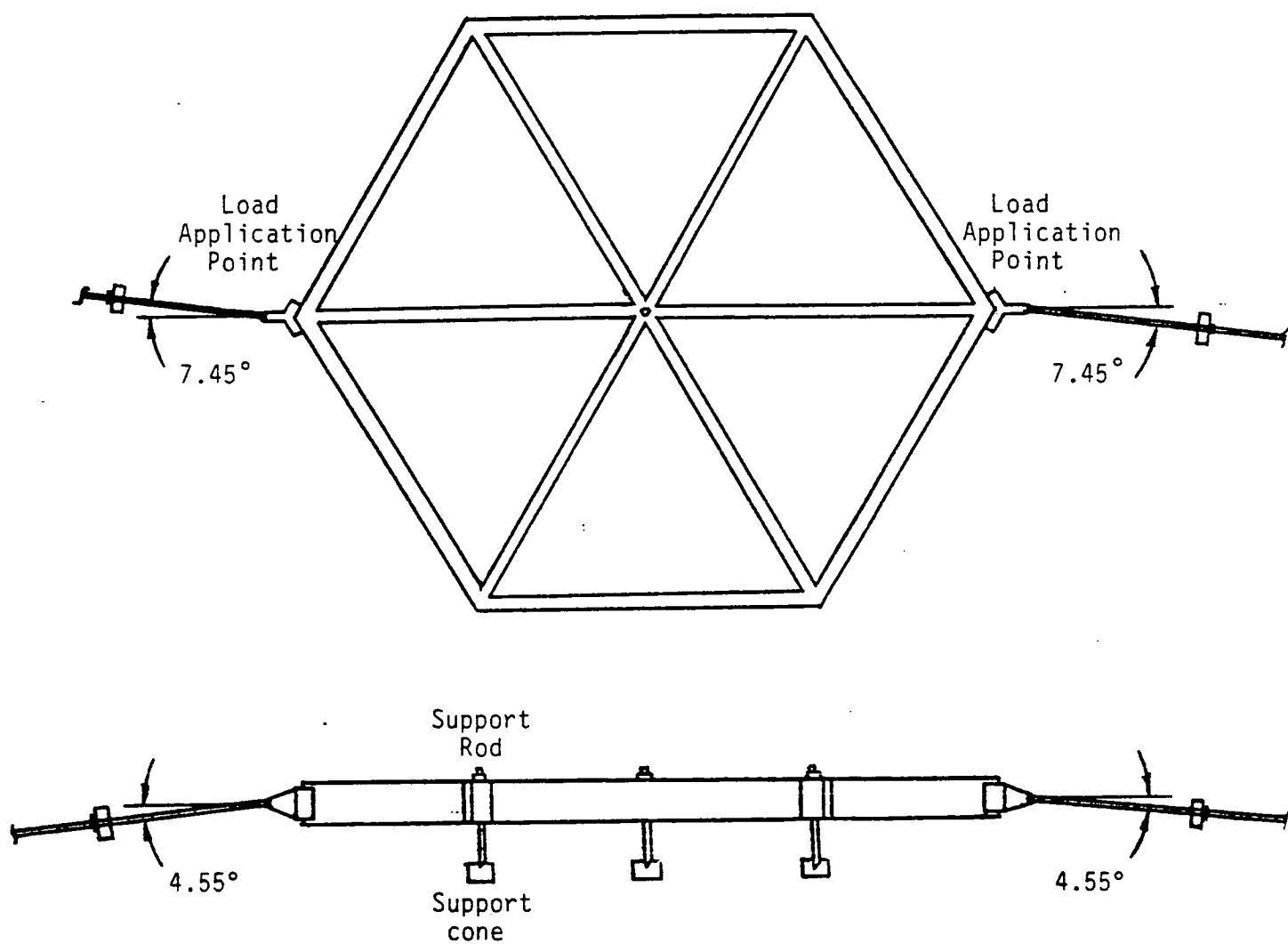


Figure 3.2-11. Application Points and Angles For Proofloading The Corner Fitting Assemblies. The Angles Apply The Proper Tensile and Moment Loads In The Corner Fitting That Are Transmitted From The Latch.

ORIGINAL PAGE  
BLACK AND WHITE PHOTOGRAPH



Figure 3.2-12. Proofloading Of A Radial Beam On The SCAD Program.  
Turnbuckles and Loadcells Would Be Used On The Actual Flight Program.

2. The circumferential beams were loaded on each side of a corner fitting as shown in Figure 3.2-10. An actual picture of the process can be seen in Figure 3.2-13. The loads were applied in two increments of 25 pounds and two increments of 18.5 pounds up to a load of 87 pounds in three places on each beam (261 pounds total). Then the loads were relaxed in reverse order to the unloaded condition. The circumferential beam proofloading loading qualified the circumferential beams and their bond joints.
3. The corner fittings were loaded by applying a load to opposite corner fittings simultaneously (Figure 3.2-11). The apparatus used is shown on one fitting in Figure 3.2-14. The load was applied by tensioning the turnbuckle in increments of 50 pounds to a final load of 781 pounds. The loads were again relaxed in reverse order to the unloaded condition. The corner fitting proofloading qualified the corner fitting, shear plates, and bond joints at the corners.

Deflection data was recorded on the first few panels to provide structural integrity measurements and traceability if any irregularities became apparent in the manufacturing process. In the absence of irregularities, the deflection data was not recorded after the sixth panel in order to save program cost. All panels except one were successfully proofloaded the first time. Panel 10 had a failure in a radial beam that



ORIGINAL PAGE  
BLACK AND WHITE PHOTOGRAPH

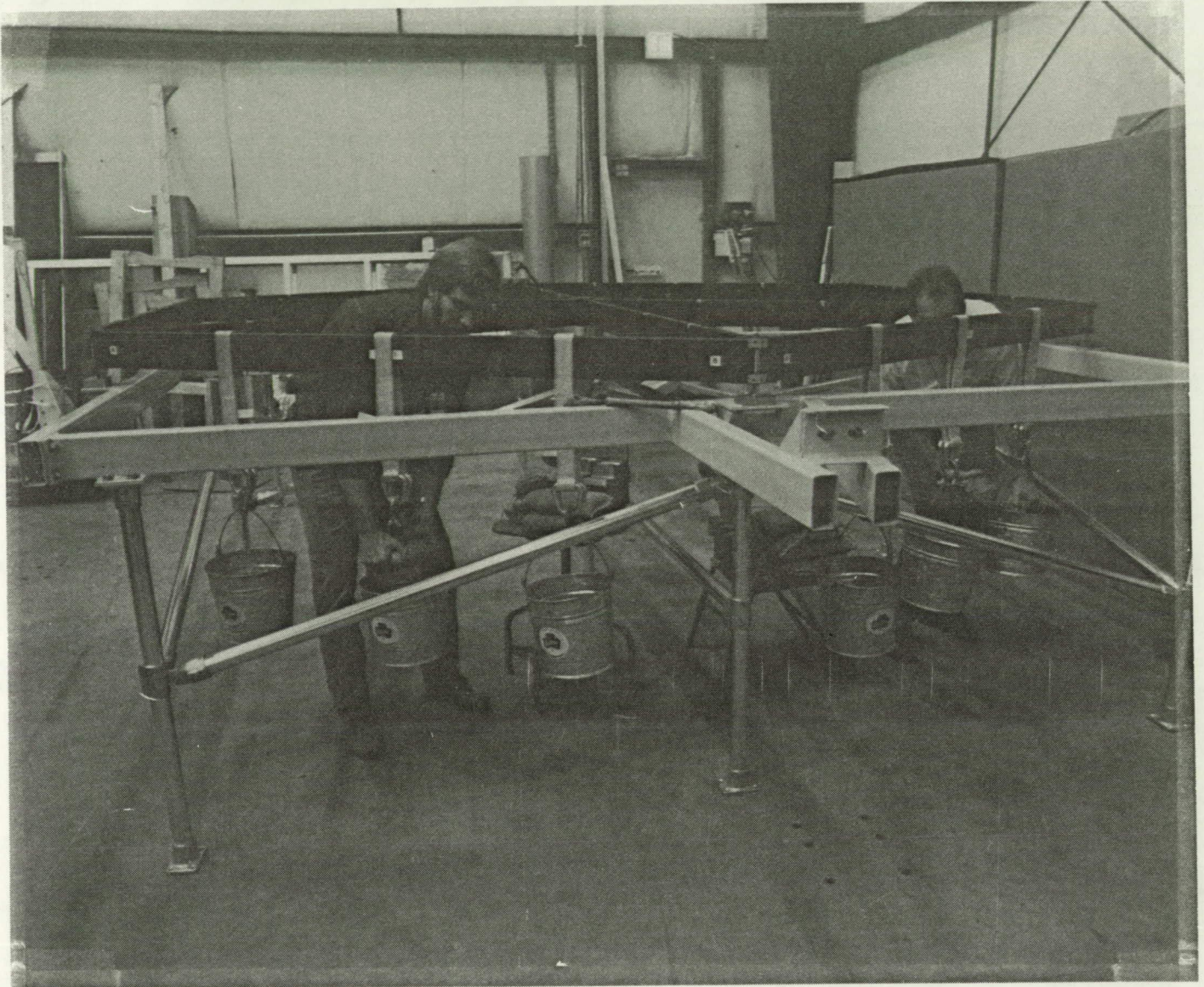


Figure 3.2-13. Proofloading Of Two Circumferential Beams On  
The SCAD Program. Turnbuckles and Load Cells Would Be  
Used On The Actual Flight Equipment.



ORIGINAL PAGE  
BLACK AND WHITE PHOTOGRAPH

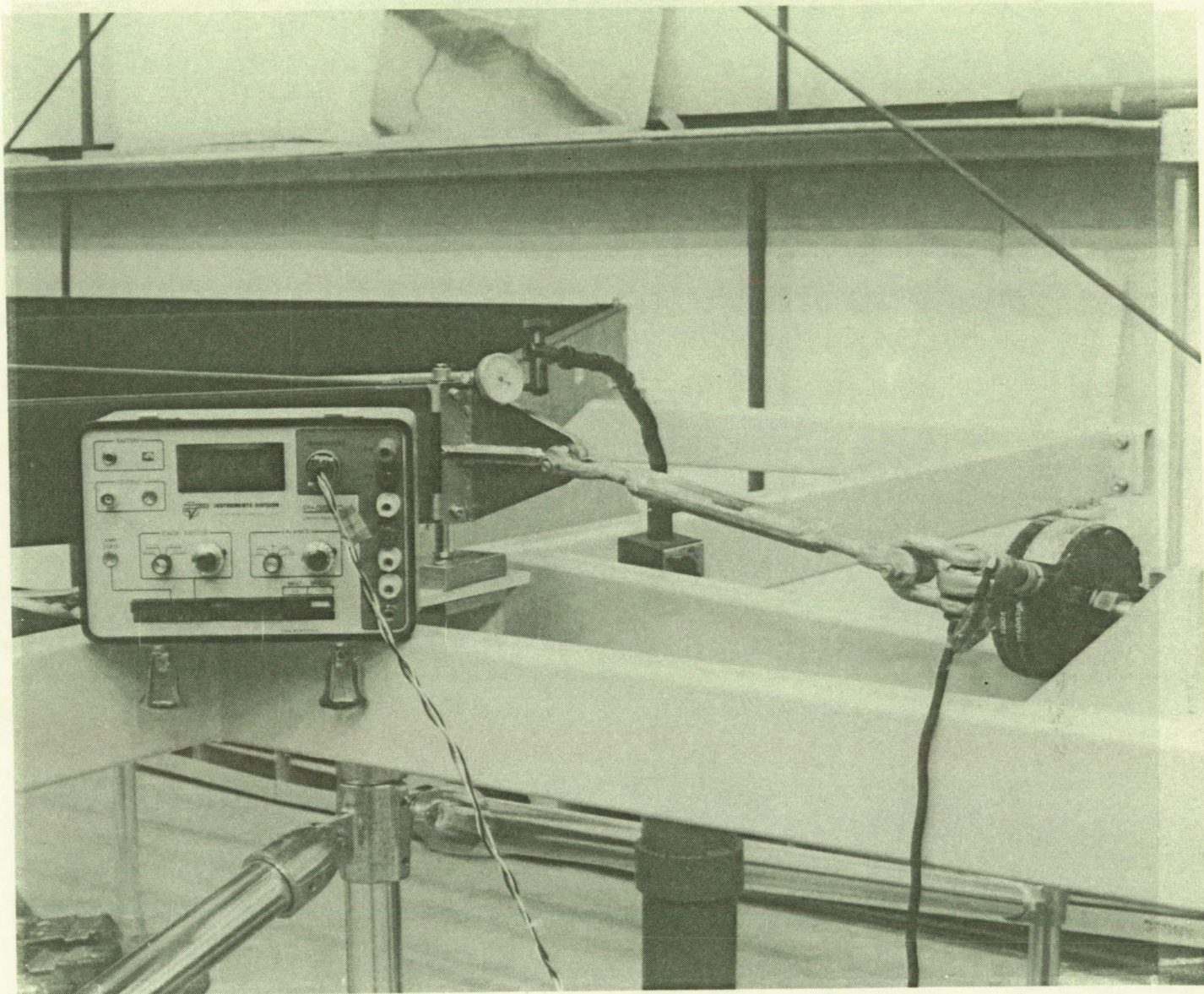


Figure 3.2-14. Proofloading Of The Hexagonal Panel Corner Fitting.  
The Angle Of Load Application Generates The Proper Tensile and  
Moment Loads In The Corner Fitting.

resulted from a defect in the box beam. The beam was replaced and the panel was successfully proofloaded. Panel repairability is outlined in Appendix B and the Proofload procedure is in Appendix C.

### 3.3 Flexures and Standoffs Installation and Adjustment

Assembly of the flexures and standoffs and their associated hardware was accomplished in the holding fixture shown in Figure 3.3-1. The flexure and standoff assemblies were fastened to the panel using a threaded beam spacer that was bonded into the beams (Figure 3.3-2).

The standoff height of the Type 1 flexure was set with a modified dial caliper as shown in Figure 3.3-3. As previously stated, this height is adjusted during testing to fine tune the facet and to offset tolerance buildup. The standoff heights and locations are per the Panel Assembly Drawing 500010.

The Type 2 flexure is pre-set on the bench and bonded to the correct height as shown in Figure 3.3-4 before it is fastened to the panel.

### 3.4 Latch and Striker Assembly

The latch striker plates, two adjustable plates at the top of the latch that contact the striker sphere, are set using the alignment tool shown in Figure 3.4-1. A cylindrical rod that precisely matches the outside diameter of the striker sphere is mounted to a precision V-block and can be shimmed up or down to place the spherical center at the proper height. A precision dowel pin is placed through the latch pawl shaft hole to put the cylinder at the proper Z height and another pin that fits in the cam delatch hole



ORIGINAL PAGE  
BLACK AND WHITE PHOTOGRAPH

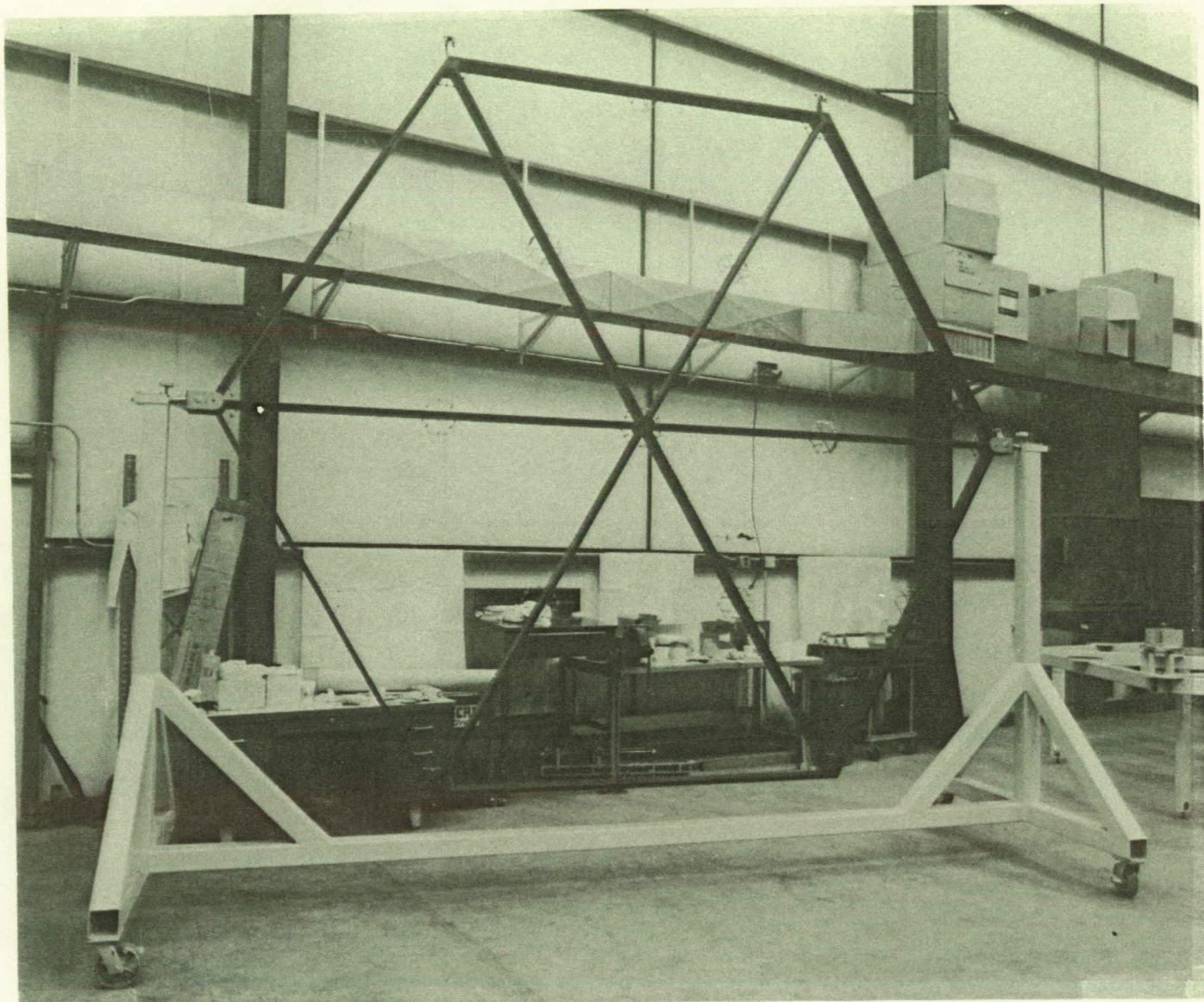


Figure 3.3-1. The Flexures and Standoffs Are Installed Using The Hex Panel Assembly Fixture To Hold The Panel Vertical

## FLEXURE ASSEMBLY (EXTERNAL CORNER)

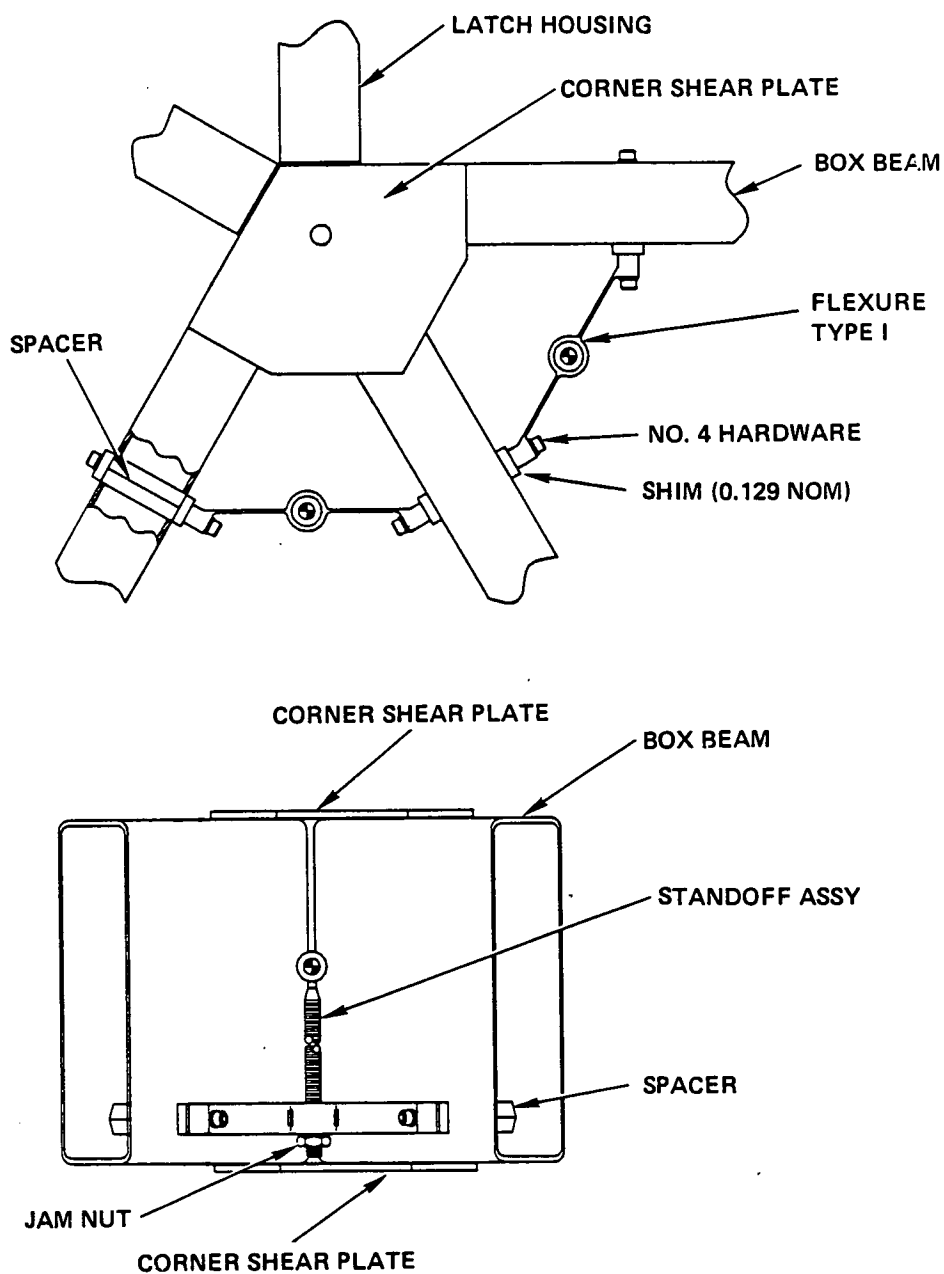


Figure 3.3-2. Threaded Beam Spacers Are Bonded Inside Of The Box Beams To Attach The Flexures. Spacer Is Shown In A Cutaway View In Upper Left Corner.



ORIGINAL PAGE  
BLACK AND WHITE PHOTOGRAPH

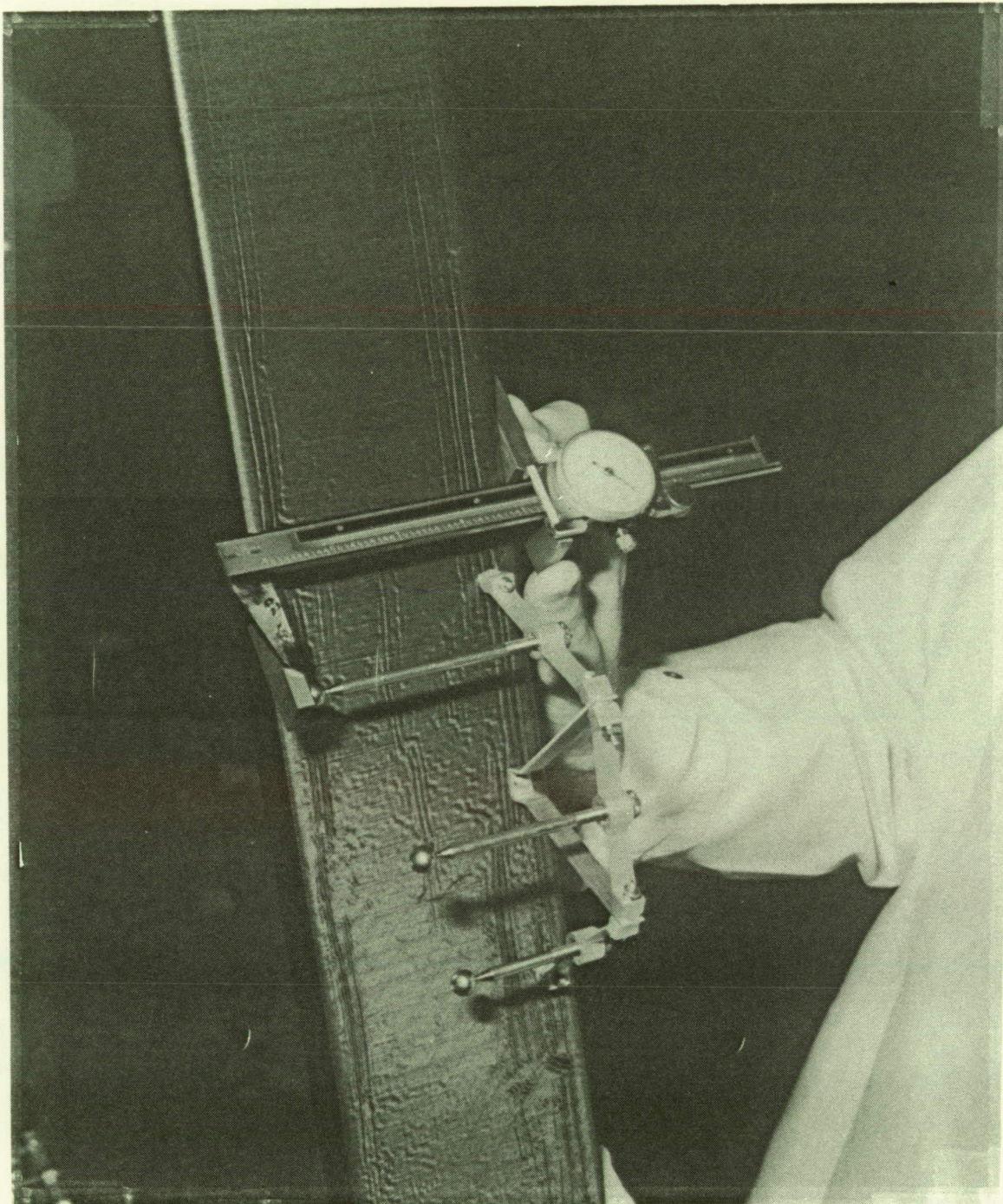


Figure 3.3-3. Modified Dial Calipers Are Used To Set The Standoffs To Their Proper Height With Respect To The Bottom Of The Box Beam. They Are Set Per The Panel Assembly Drawing 500010.



ORIGINAL PAGE  
BLACK AND WHITE PHOTOGRAPH

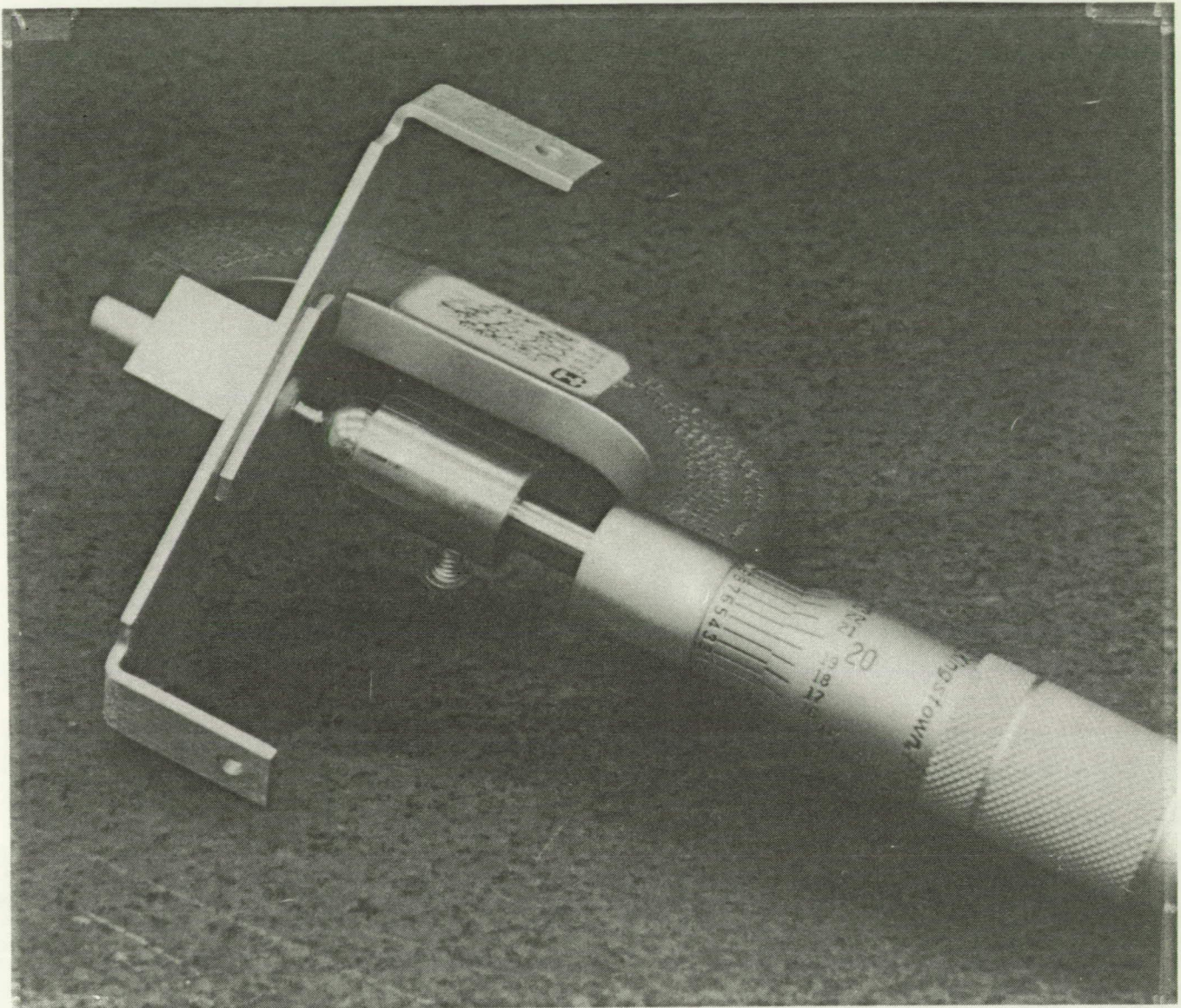


Figure 3.3-4. A Type II Flexure Is Set and Bonded On The Bench  
Using A Modified Micrometer To Contact The Sphere



ORIGINAL PAGE  
BLACK AND WHITE PHOTOGRAPH

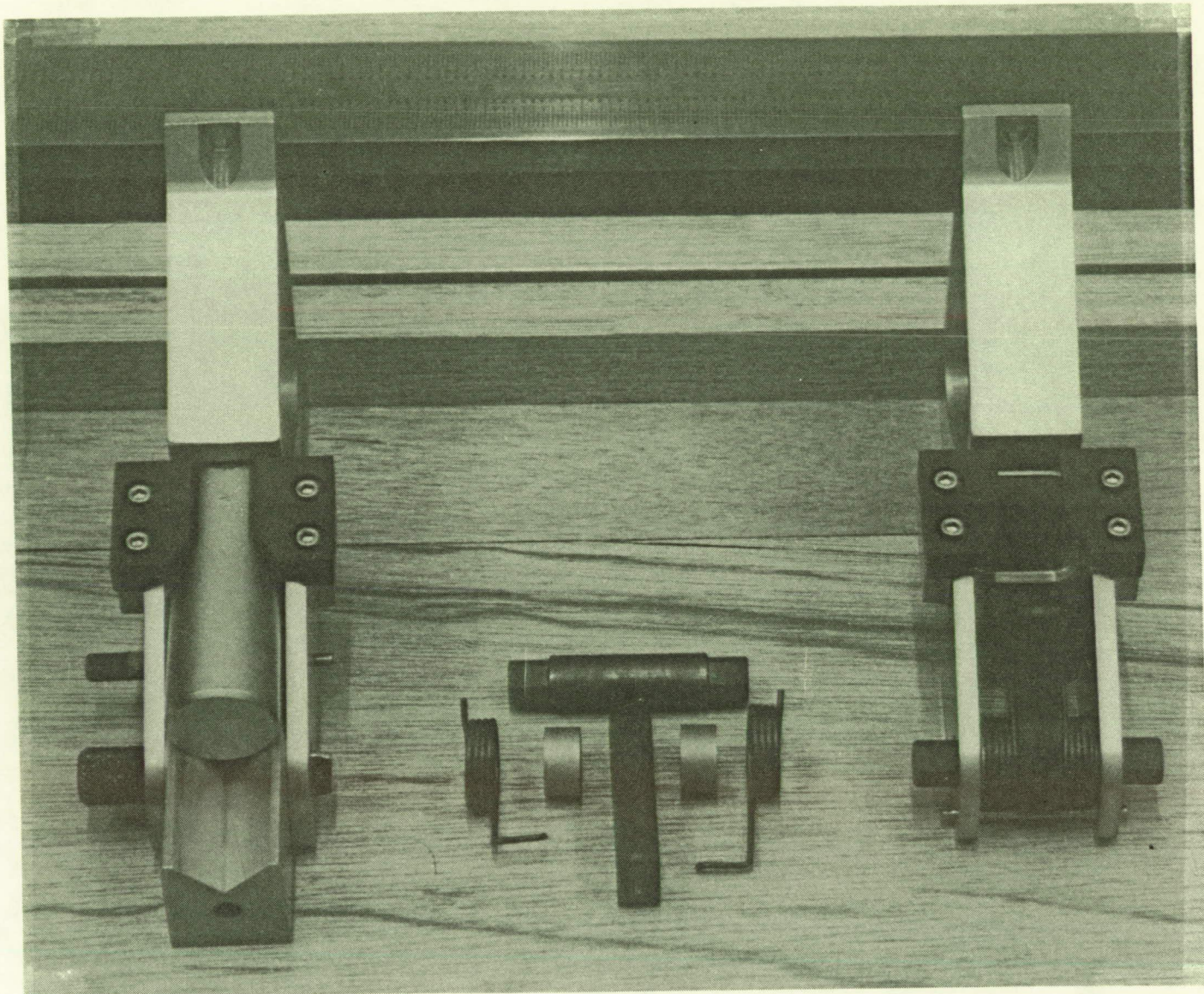


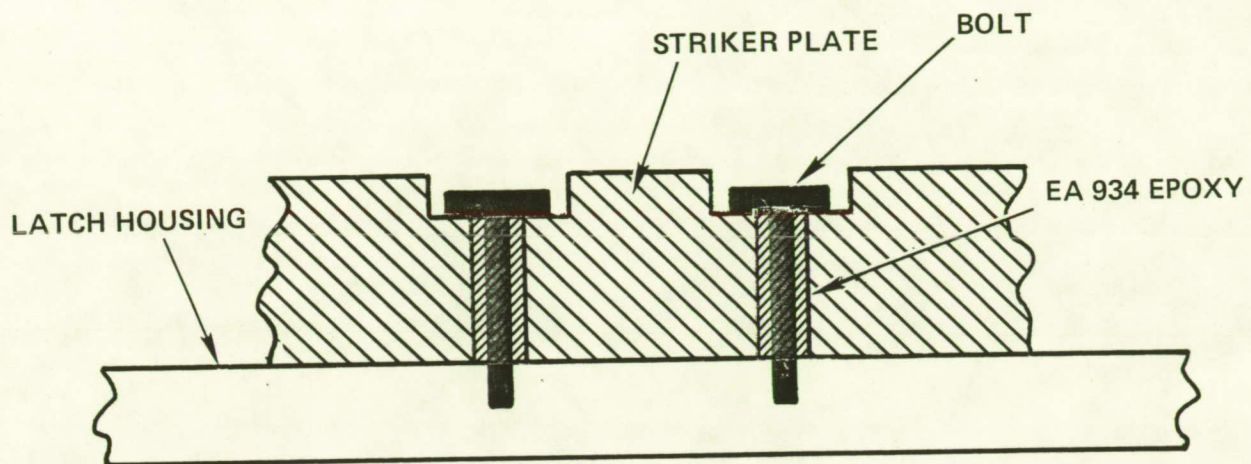
Figure 3.4-1. The Latch Striker Plates Are Set Using A Cylindrical Rod That Matches The Striker Sphere Diameter. The Tooling Rod Is Keyed To The Latch Pawl Shaft Hole and The Delatch Pin Hole.



controls the rotation. The stiker plates are shimmed such that the ball will contact the latch pawl approximately 25% of the way through the total latch pawl travel. Total latch travel is defined by the distance the cam travels while in contact with the sphere, about .5 inches, and is determined by the shape of the cam. Reserving a margin of 75% of the pawl travel allows the regenerative feature of the latch to compensate for assembly loads, tolerance stack ups and wear in the latch.

After the striker plates have been located, they are liquid shimmed into place. Liquid shimming is a process of filling the volume around a fastener with epoxy. This process eliminates all the tolerances between the mating parts and provides a zero tolerance fit. The process is shown in Figure 3.4-2. Liquid shimming prevents the striker plates from sliding during loading which would allow the sphere to move from a pre-determined location which causes a geometrical change in the assembled concentrator.

The striker portion of the latch assembly consists of an aluminum housing and a sphere which is mounted onto a threaded standoff. The sphere center of the latch defines the geometrical location of the hexagonal panel, and thus, the entire geometry of the concentrator. A Striker Assembly Drawing 500065 specifies the height of the striker sphere and the location of the striker on the concentrator can be found in the master geometry drawing 500001. The striker spheres are set to their proper height using the Striker Assembly Drawing 500065 and the height gauge shown in Figure 3.4-3. To prevent the striker from working loose during the many latch and delatch sequences involved in the test program, locktite is applied to the threads of the striker standoff and a jamnut is put in place. This will



890302

Figure 3.4-2. EA 934 Epoxy Is Placed Around The Bolts That Hold On The Striker Plates To Prevent Slippage Of The Plates By Taking Away The Clearance Between The Bolt And The Clearance Hole



ORIGINAL PAGE  
BLACK AND WHITE PHOTOGRAPH

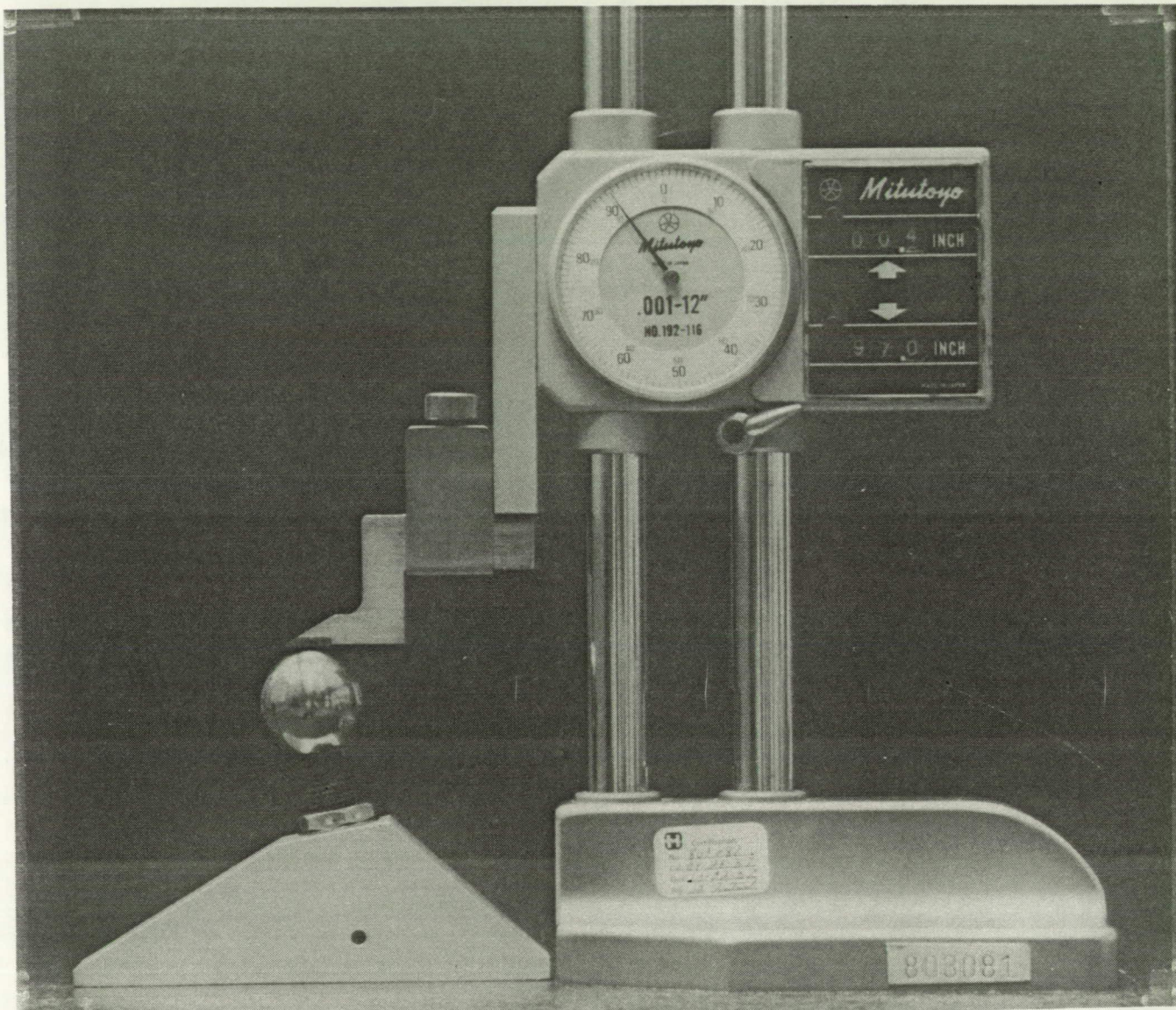


Figure 3.4-3. Striker Sphere Is Set Using A Modified Height Gauge Shown Above. The Height Is Set Per The Striker Assembly Drawing 500065.

give a redundant lock to hold the sphere at its proper position.

### 3.5 Latch and Striker Installation/Alignment On The Hexagonal Panel

The next step in manufacturing the concentrator is the installation of the latches and strikers to the completed hexagonal panel structure. Very precise tooling is needed to locate the latches and strikers in their proper geometric location. A small error in the striker or latch placement would be multiplied twelve times in the assembly of the reflectors outer ring. The latch assembly locates the hexagonal panel within the reflector geometry and must locate the mirror facets within the allowable standoff adjustment capability. If this does not happen, the mirrors cannot be properly pointed or aligned during concentrator testing.

The hexagonal panel is held in the proper location on the latch alignment fixture by two precision pins that go through the corner fitting and into a machined stainless steel plate. The fixture will allow alignment of a latch or striker on either of the two faces of the hexagonal panel corner fitting. A top view of the alignment table concept is shown in Figure 3.5-1.

By design, all striker spheres were located at the same height with respect to the bottom of the hexagonal panel (when the panel is on the fixture). This allows for the same tooling equipment to be used on all striker installation operations. A V-block with a vertical pin was installed on a x-y machine positioner to supply a pocket for the sphere to rest. The two sides of the V-block and the vertical pin provide three

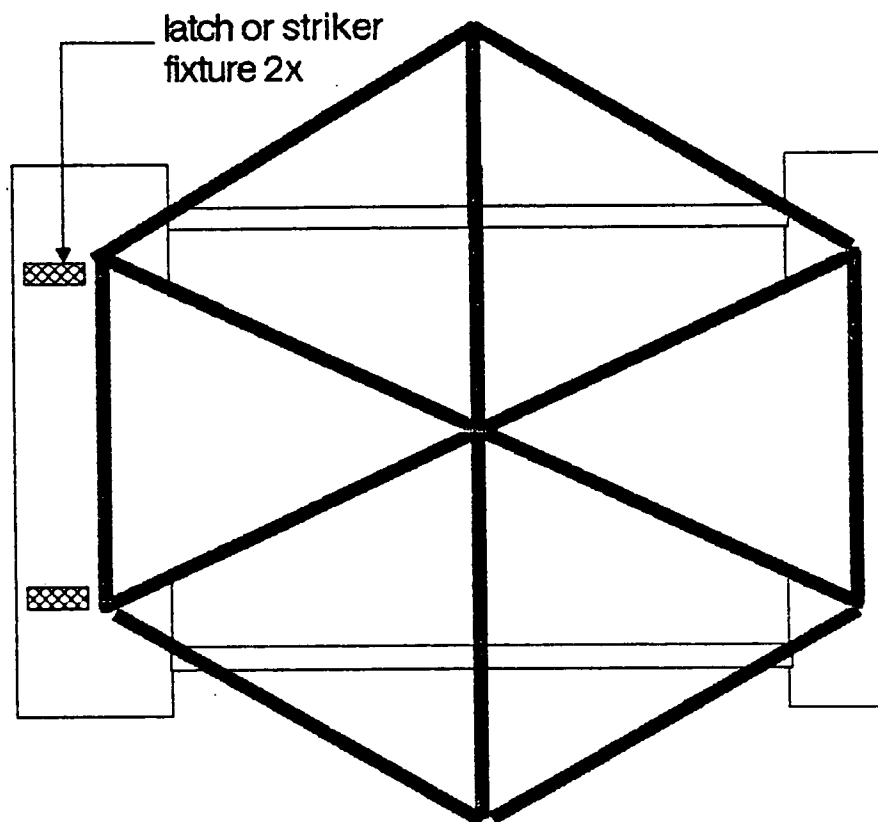


Figure 3.5-1. Concept For Latch Alignment Table Presented In The Harris Critical Design Review

points of contact to hold the sphere in place. This can be seen in Figure 3.5-2. A gauge block of the proper length is placed flush against the corner fitting. A tooling sphere is placed into the v-block to represent the striker and the x-y positioner is pushed toward the panel until contact is made between the sphere and the gauge block. The vernier reading is recorded and represents the ideal location of the striker sphere. A nominal shim of .060 inches was designed to be placed between the hexagonal panel corner fitting and the striker housing. The striker is then bolted loosely (without shims) to the panel and the x-y positioner is moved into place as seen in Figure 3.5-3. The new vernier reading is recorded for this position. The two positions are subtracted and the resulting number establishes the proper shim thickness. Theoretically the number should be .060 inches, but due to manufacturing tolerances on the parts it may be slightly higher or lower. The shims are then placed behind the striker housing and the x-y positioner is used as a final check on the striker location. If the reading is within tolerance, the striker is placed on the panel and the fasteners are liquid shimmed into place to ensure slippage does not occur.

The latches are aligned in very much the same manner as the strikers. A x-y machinests positioner with a striker sphere mounted to it is used instead of the V-block and vertical pin. A striker sphere is then pushed up against the gauge block as seen in Figure 3.5-4. The vernier scale is then read and recorded. This reading represents the ideal location of the latch with respect to the hexagonal panel corner fitting. The latch is then placed on the tooling sphere and the housing is pushed up against the corner



ORIGINAL PAGE  
BLACK AND WHITE PHOTOGRAPH

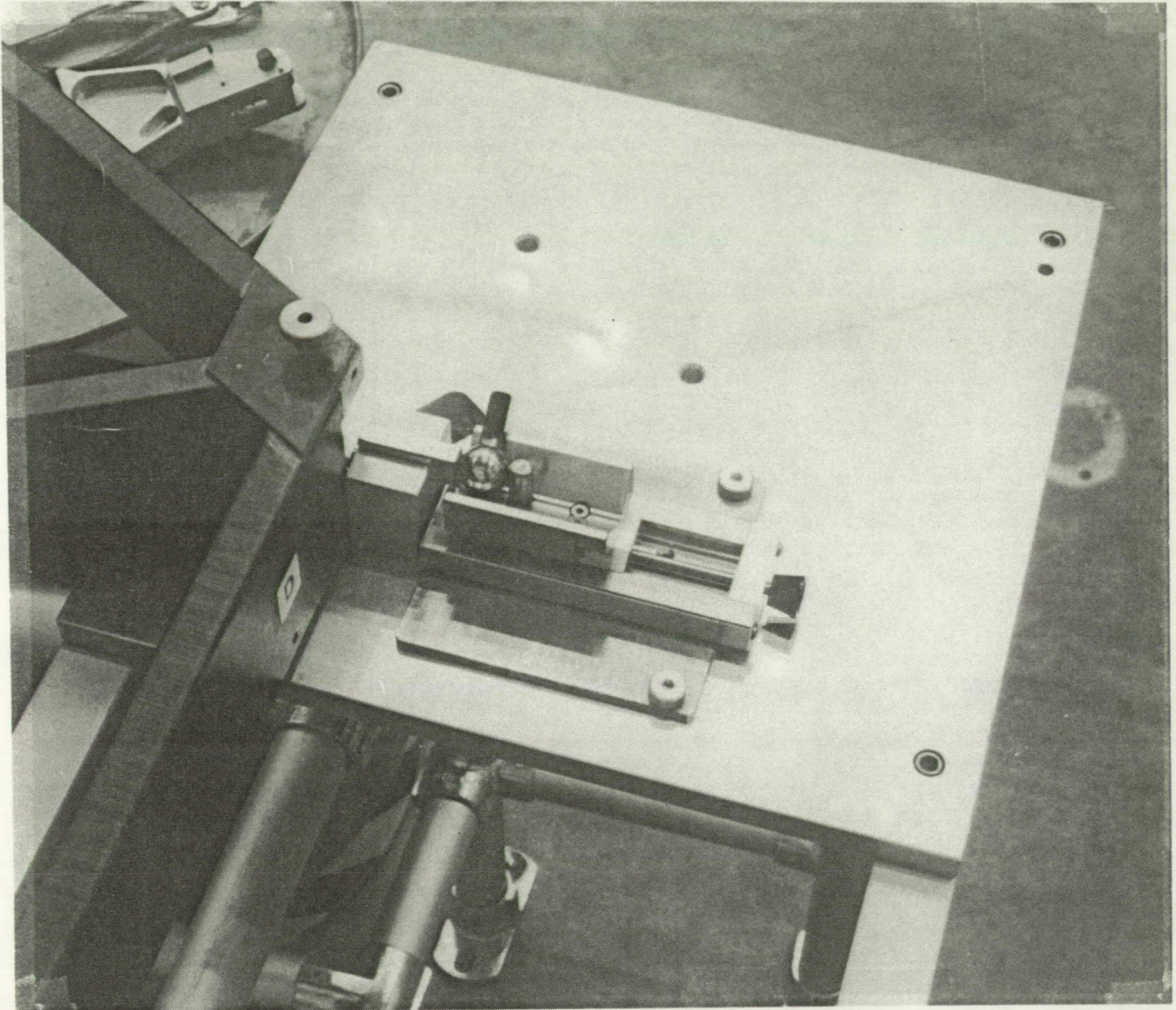


Figure 3.5-2. The Striker Alignment Tooling Captures The Sphere Using A V-Block And Vertical Pin. A Gauge Block With The Proper Length Insert Places The Sphere The Correct Distance From The Corner Fitting



ORIGINAL PAGE  
BLACK AND WHITE PHOTOGRAPH

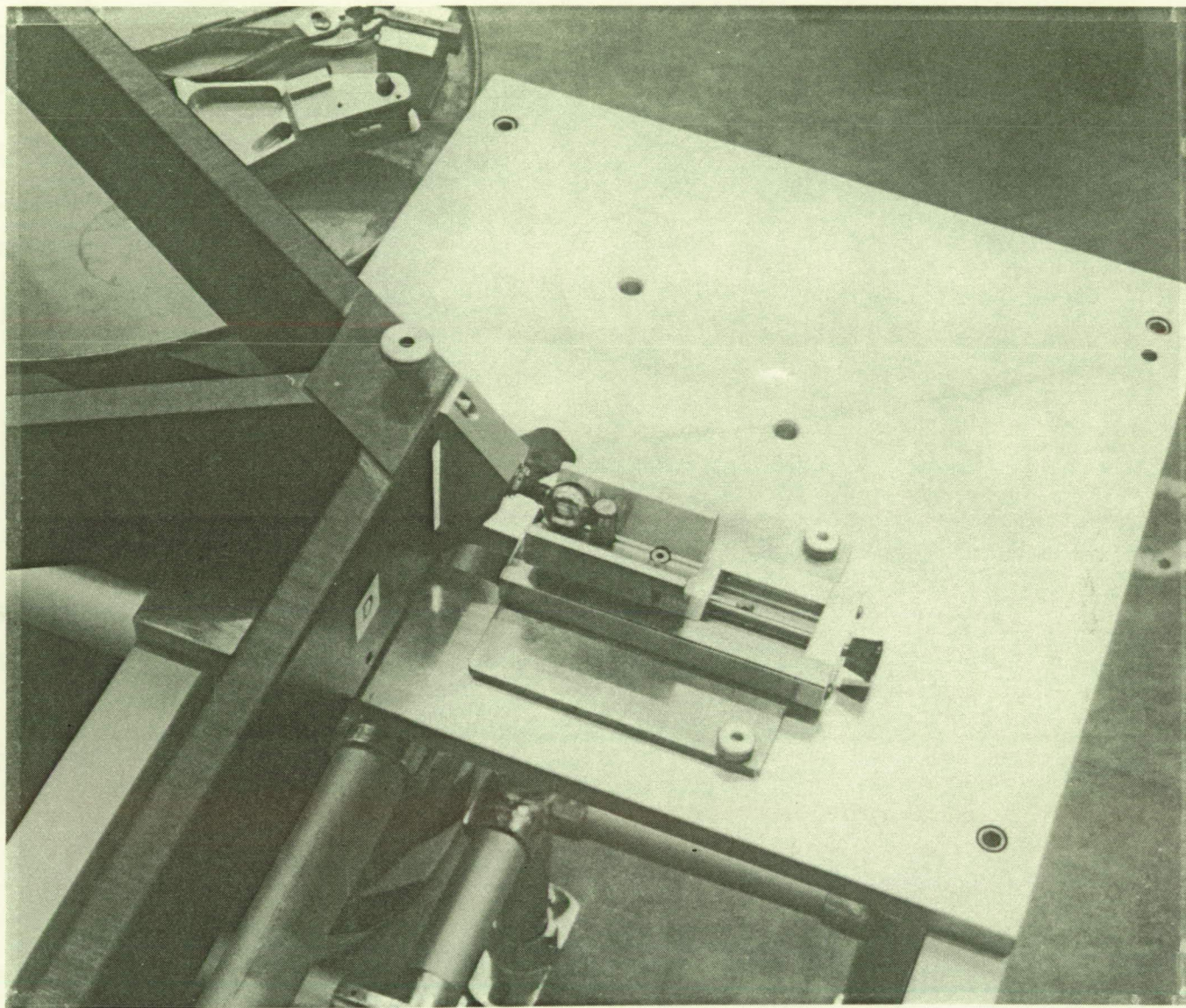


Figure 3.5-3. The Striker Assembly Is Placed In The V-Block and Mounted To the Hexagonal Panel And The Vernier Is Pushed Up Against The Sphere. The Difference Between The First Reading In Figure 3.5-2 and This Reading Determines The Shim Thickness.



ORIGINAL PAGE  
BLACK AND WHITE PHOTOGRAPH

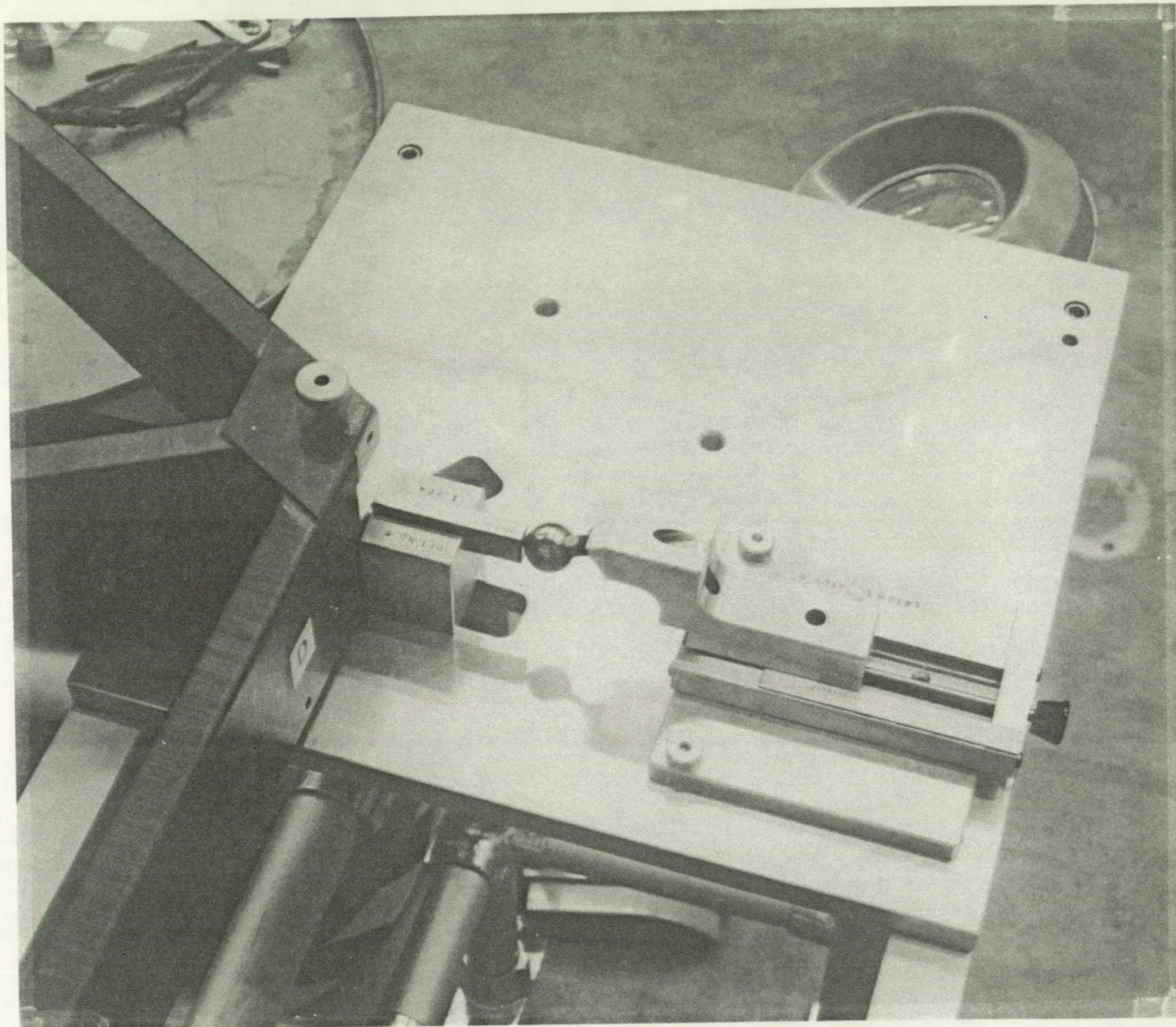


Figure 3.5-4. A Striker Sphere Is Mounted On The Vernier To Mount The Latches In Their Proper Location. The First Reading Is The Proper Location Of The Latch Sphere.

fitting (Figure 3.5-5). The vernier reading is taken and subtracted from the ideal reading. By subtracting the two readings a proper shim thickness can be determined. Shims of the proper thickness are placed behind the latch housing and it is loosely fastened to the panel. A vernier reading is taken to double check the latch position. If the reading is within tolerance, the latch is mounted to the panels and the bolts are liquid shimmed into place. This prevents the latches from slipping during the testing cycles. The hexagonal panel assembly is now completed and ready for testing.

### 3.6 Concentrator Weight Summary

At completion of the fabrication of the concentrator components, the weight of a panel, facet, and latch assemblies were measured. A single hexagonal panel without the facets or latch assemblies weighed 36 pounds. A single facet weighed 1.6 pounds. Each latch assembly was weighed with the following results: Type I - 1.6 pounds, Type II - 1.5 pounds, Type III - 1.4 pounds and Type IV - 1.7 pounds.



ORIGINAL PAGE  
BLACK AND WHITE PHOTOGRAPH

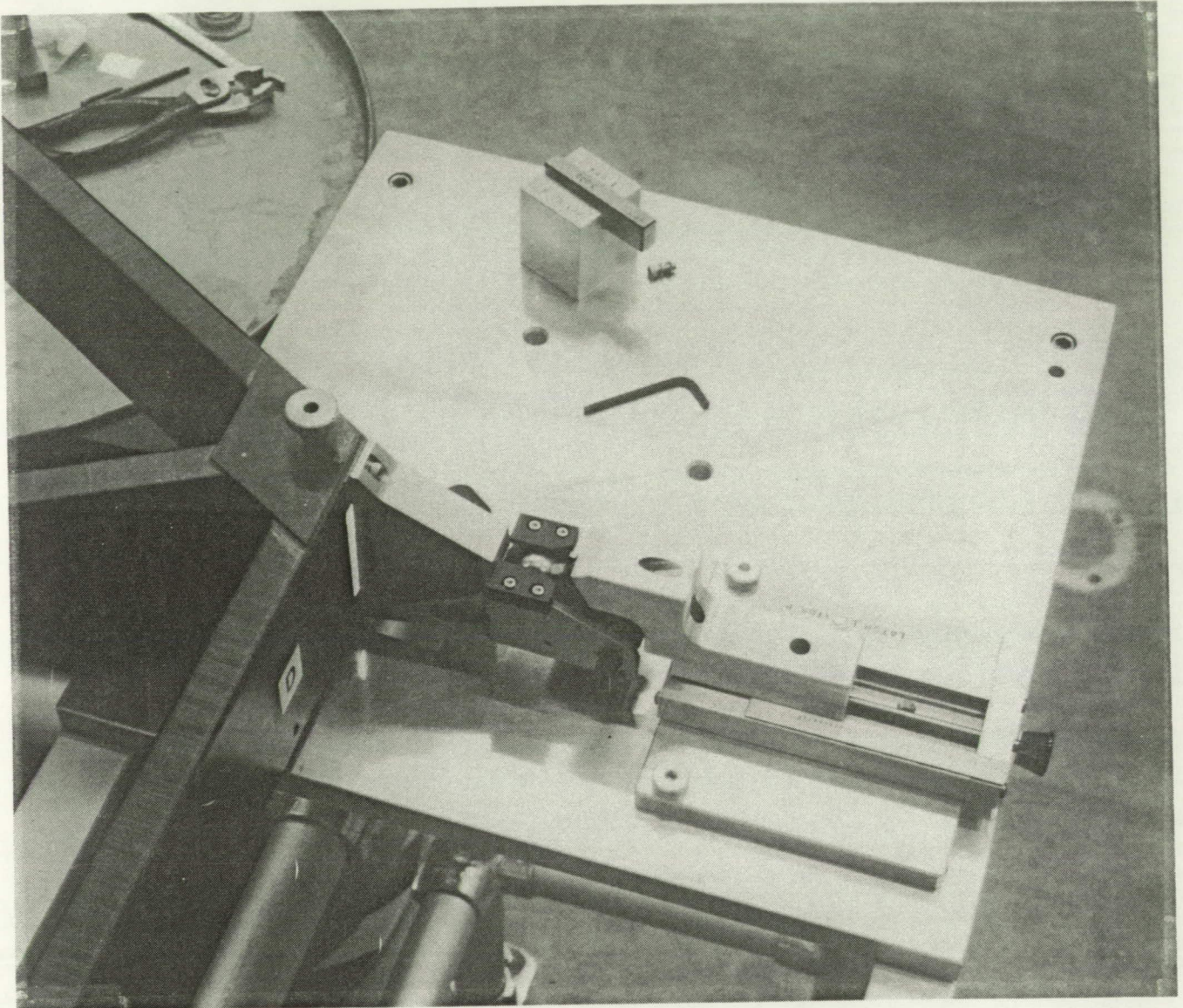


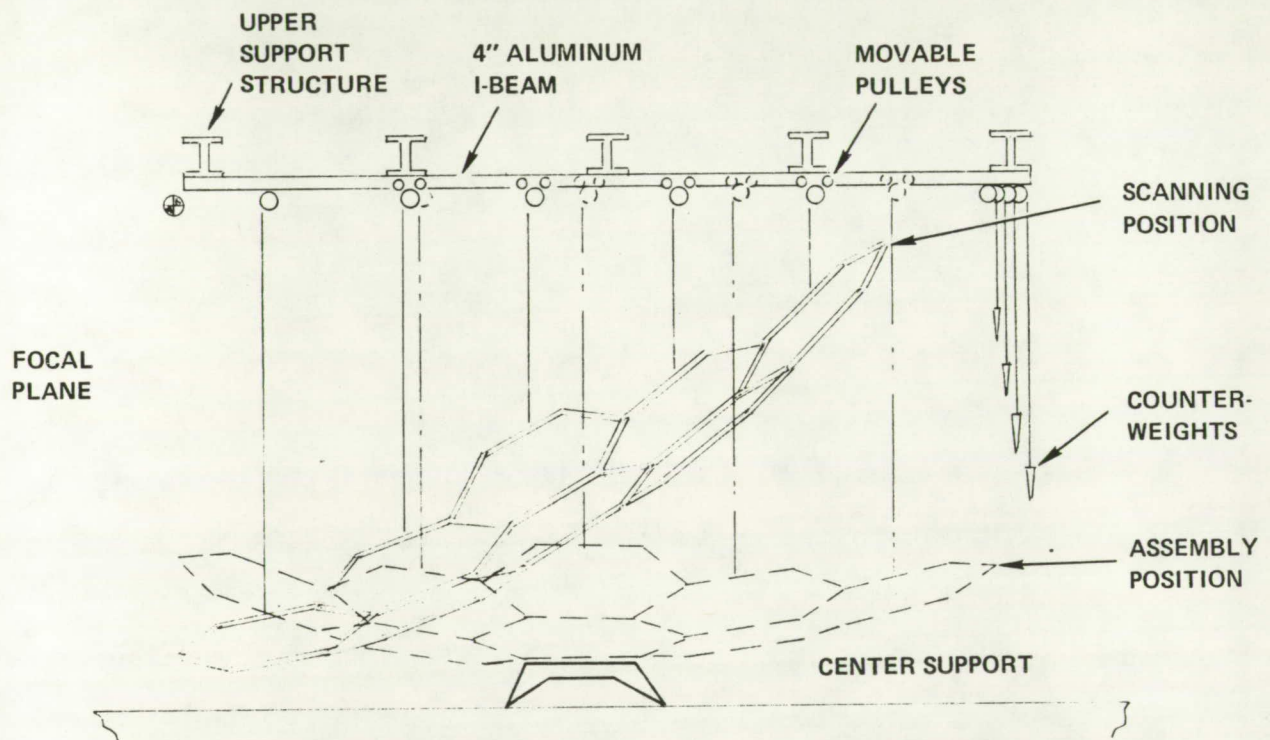
Figure 3.5-5. The Latch Is Attached To The Tooling Sphere Then It Is Mounted To The Hexagonal Panel. A Vernier Reading Is Taken To Establish the Proper Shim Thickness To Place Behind The Latch Housing.

#### 4.0 ASSEMBLY AND ALIGNMENT OF THE COUNTERBALANCE AND OPTICAL SCANNING EQUIPMENT

Section 4.0 provides a brief description of the counterbalance system and the optical scanning equipment that were used to perform the optical and structural repeatability tests described in Section 5.0. Section 4.1 will describe the counterbalance system shown in Figure 4.0-1. The counterbalance system provides a means for offloading the weight of the hexagonal panels, facets, latches and associated hardware. During the design phase of the program, it was determined that the structure must be counterbalanced. A concentrator with a one hertz deployed natural frequency and a diameter of 65 feet could not support its own weight without adding a significant amount of structure. If the structure was added, the concentrator would exceed the weight requirement for the Space Station Freedom flight reflector by a factor of two to three and therefore would not meet the objectives of the program. In order to have a more "flight like structure" a counterbalance system was needed. The counterbalance system was required to be capable of operating in two different positions. The first position is called the assembly position and is used to erect the concentrator and help establish EVA assembly scenarios. A second position in which the concentrator is in a canted position relative to the floor is required to perform the optical scanning of the composite mirror facets. In order to maintain the precise geometry involved in optical testing of the concentrator a collimated light source must be used to represent the suns rays. Through design trade studies it was determined that the collimated light source could be held vertical using two tilt sensors and a feed back



## COUNTERBALANCE



ORIGINAL PAGE IS  
OF POOR QUALITY

Figure 4.0-1. Schematic Of The Counterbalance System Showing The Concentrator In The Assembly and Optical Scanning Positions

loop to adjust small micrometers attached to the light source. A schematic of the desired system can be seen in Figure 4.0-2. The collimated light is reflected from a concentrator mirror onto a translucent screen located at the focal point of the concentrator. A video camera is mounted behind the screen to record the location of the reflected image on the focal plane. This required the canted second position which is called the optical scanning position. (Reference Figure 4.0-1.)

Section 4.2 will describe the laser scanner system, a brief description of the laser feedback and control system, and the motor driven gantry that moves the laser to the proper location above the concentrator.

Section 4.3 describes the first assembly of the concentrator that is needed to prepare for the final testing of the concentrator. The testing is then described in Section 5.0.

#### 4.1 Counterbalance Description and Assembly

The counterbalance system presented a significant design challenge during the course of the program. An ideal counterbalance system should provide a vertical load of equal value to the load induced by gravity. It should act through the center of gravity of the panel assembly and not induce sideloads or moments into the assembled panel that would distort the geometric shape of the concentrator. The pulley system used to support the nineteen cables and their associated counterweights must be low friction and not add significant hysteresis to the system. Harris produced a counterbalance capable of offloading the 19 hexagonal panels and allowed for manual slewing of the concentrator into the optical scanning position. The

## FACET ADJUSTMENT AND ALIGNMENT SCHEMATIC

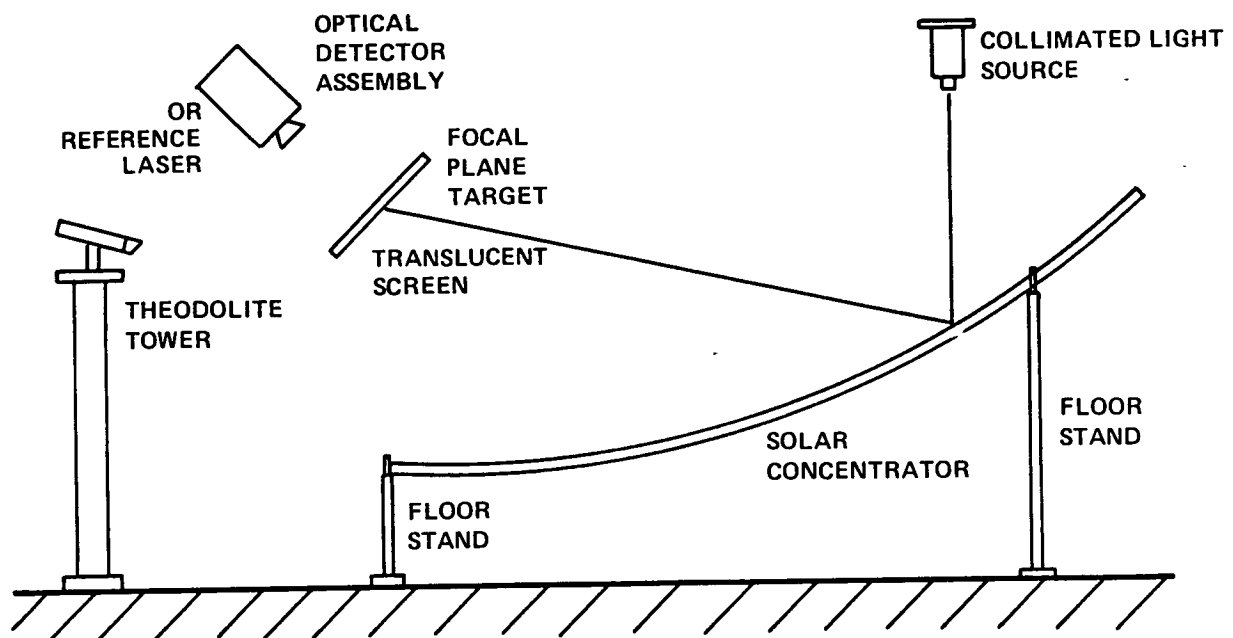


Figure 4.0-2. Schematic Of The Entire Laser Scanner System That Was Presented In The SCAD Critical Design Review

counterbalance also provides support for the laser scanner and optical test equipment with minimal blockage to the concentrator. A schematic of the counterbalance can be seen in Figure 4.1-1.

The main structural portion of the counterbalance is comprised of four standard roof trusses that are supported at the ends by eight, 10 inch diameter, columns. X-braces are placed between the columns to tie the structure together and complete the structural mainframe. The following is an abbreviated version of the procedure used to assemble the counterbalance mainframe structure:

- o Optically locate the position of the columns, panel centers and scanning support towers and mark the floor at these locations. The panel centers and scanning support tower locations will be used at a later time.
- o Erect columns C1 and C2 (Figure 4.1-2), a picture can be seen in Figure 4.1-3
- o Install truss T1 to columns C1 and C2, a picture can be seen in Figure 4.1-4
- o Erect columns C3 and C4
- o Install truss T2 to columns C3 and C4
- o Install structural cross members at location ties ST1 and ST2
- o Erect columns C5 and C6
- o Install truss T3 to columns C5 and C6
- o Install structural cross members at location ST3 and ST4
- o Erect columns C7 and C8

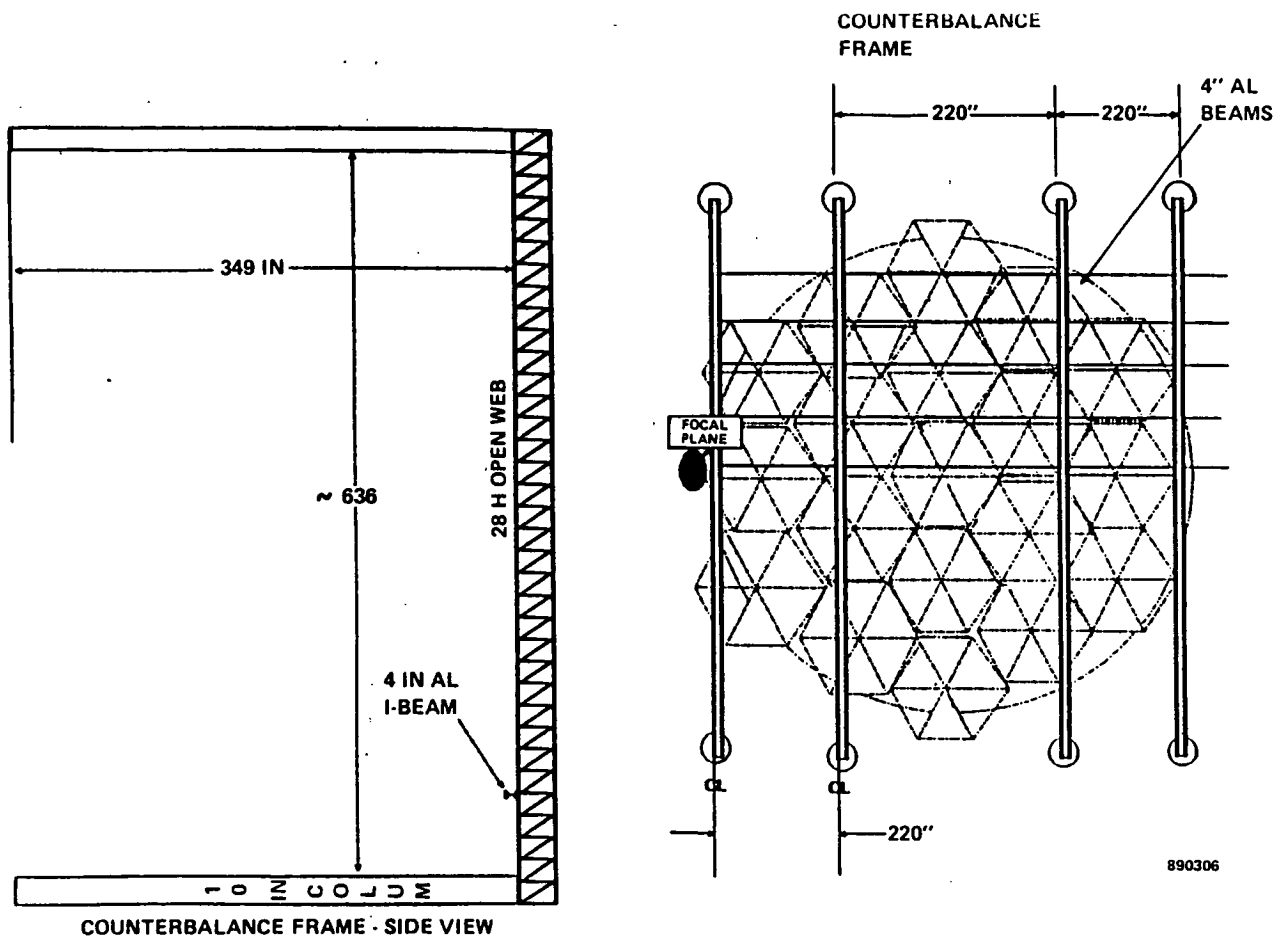


Figure 4.1-1. Schematic Of The Counterbalance Structure Comprised Of Four Standard Roof Trusses That Are Supported By Eight 10 Inch Diameter Columns



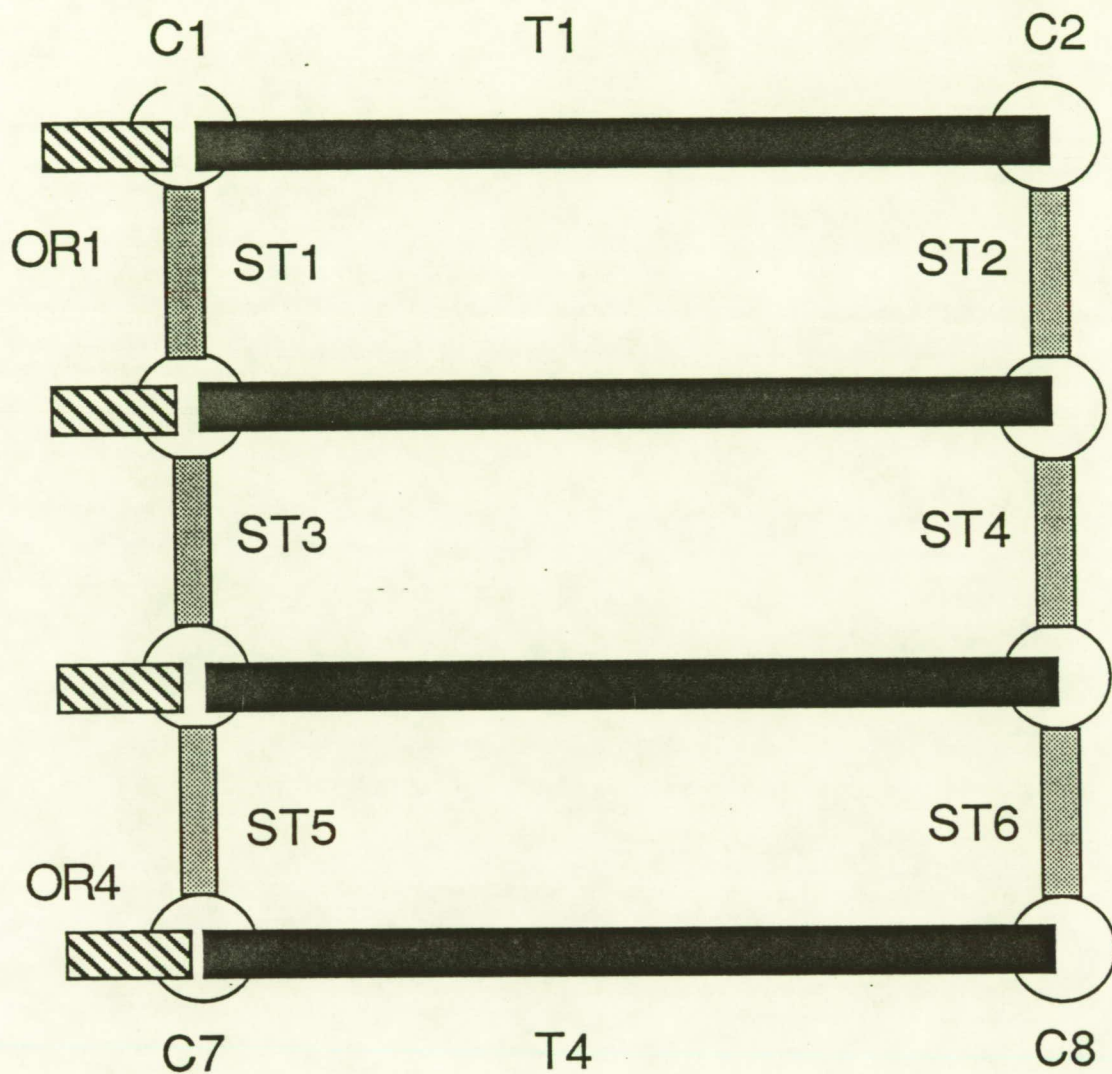


Figure 4.1-2. Nomenclature For The Columns C1 Through C8 and Trusses T1 Through T4. The Structural Stiffeners (Cross-Braces) Are Represented As ST1 Through ST6 and The Outriggers For The Optical Scanner Are OR1 Through OR4.



ORIGINAL PAGE  
BLACK AND WHITE PHOTOGRAPH

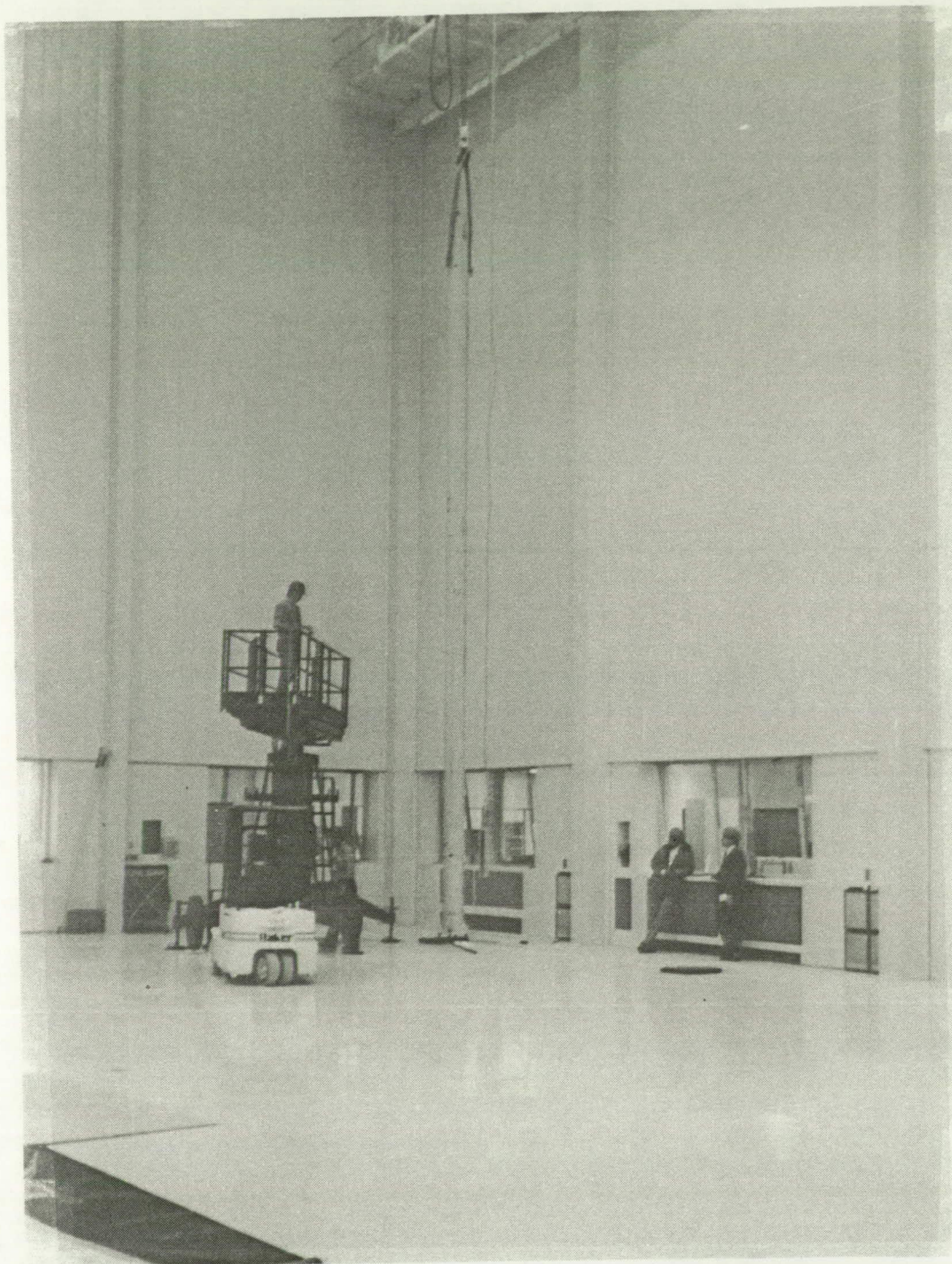


Figure 4.1-3. Erection Of The First Counterbalance Column At The Power System Facility (PSF) At NASA LeRC In Cleveland, Ohio



ORIGINAL PAGE  
BLACK AND WHITE PHOTOGRAPH

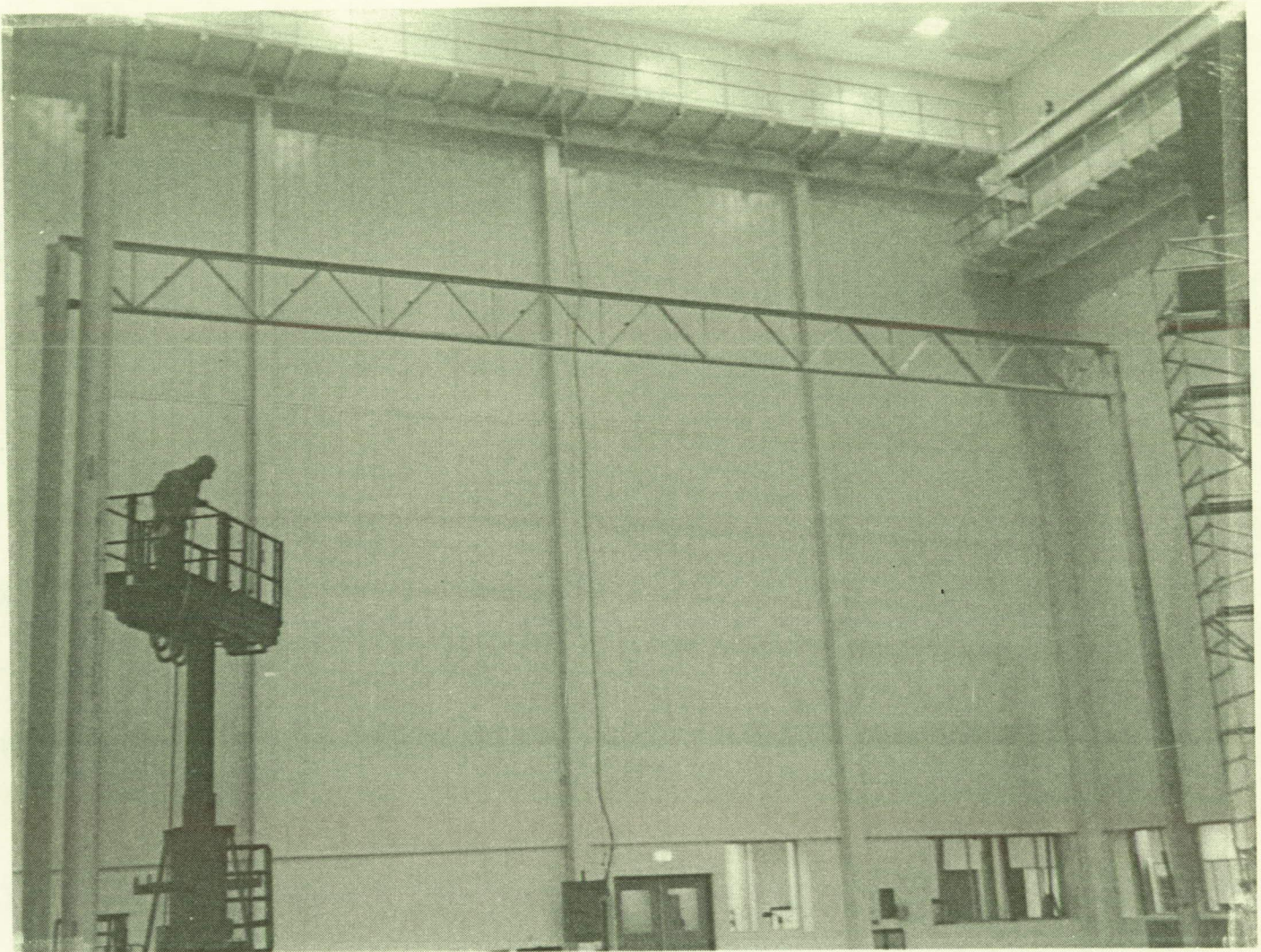


Figure 4.1-4. Completion Of The First Bay Of The Counterbalance System With Columns C1 and C2 and Truss T1

- o Install truss T4 to columns C7 and C8
- o Install structural cross members at location ST5 and ST6
- o Install outriggers OR1 to OR4. The outriggers provide a location for the scanner structure to move and scan facets on that portion of the concentrator that is used to stiffen the trusses at the center. The completed mainframe structure can be seen in Figure 4.1-5.
- o Install upper tie network that is used to stiffen the trusses at the center

The counterbalance mainframe components are made using proven structural steel design and will support many times the loads experienced during the testing of the concentrator. All components contain a factor of safety of five or higher and were analyzed using finite element models. The structure was also proofloaded following construction. The reduced profile trusses provide resistance to vertical loads with minimal deflection and, because they are trusses, they support sideloads much better than a simple joist. Another advantage to the truss network is their relatively high stiffness to weight ratio, for handling, and the minimal blockage created for the laser scanner.

The trusses on the counterbalance also support a linear shaft rail system on which the laser scanner rides during movement of the laser system. A rail is mounted at the top of each truss and covers the entire length of that truss. The rails must be parallel to each other to allow the scanner



ORIGINAL PAGE  
BLACK AND WHITE PHOTOGRAPH

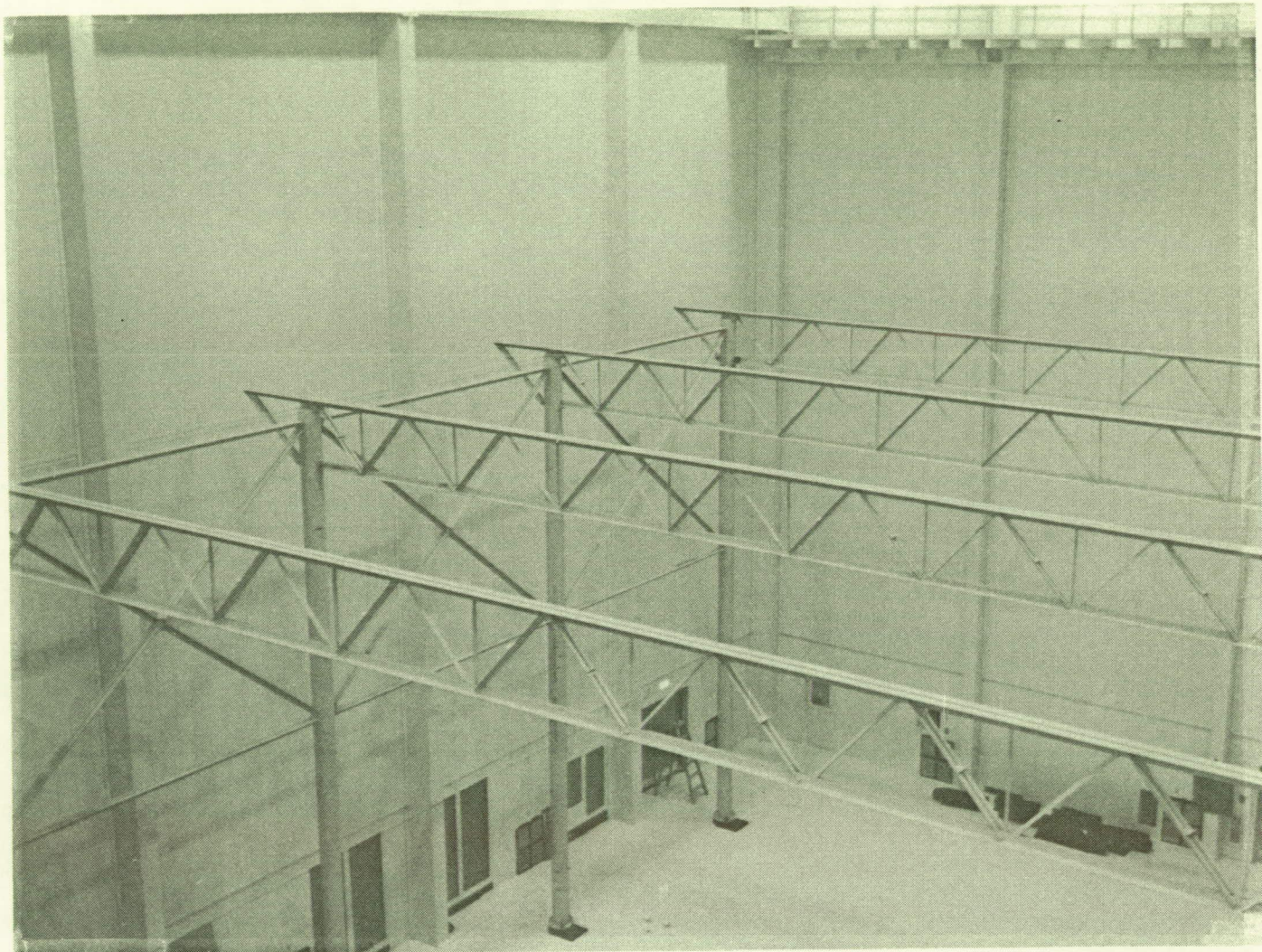


Figure 4.1-5. Completed Counterbalance Mainframe Structure.  
The Outriggers and Stiffening Cross Members Can Be Seen  
In The Upper Left Portion Of The Photograph



to slide across the top of the structure. The scanner contains four sets of linear bearings that ride on each of the four rails attached to the trusses. If the rails are not parallel, the scanner will either bind up or will induce considerable loads in the system. The scanner linear shaft rail can be adjusted to plus or minus .50 inches to compensate for a .50 inch truss misalignment. Thus, the trusses must be within .50 inches of the centerline between columns as shown in Figure 4.1-6.

The alignment of the truss is checked by marking a line from the center of each column to its corresponding column (Ex. C1 to C2, C3 to C4 etc.). A plumb bob is dropped every three feet from the center of the truss and the location compared to the line between columns. If the distance is greater than .50 inches then the truss is pushed or pulled to the proper location and the upper tie network is used to keep the truss in place.

The laser scanner linear shaft rail is now ready for installation to the truss network. The rail is loosely mounted to the trusses as shown in Figure 4.1-7. A theodolite was then mounted at the top of column C4. The theodolite contains two bubble levels and is placed level with respect to gravity. The theodolite and a unique rail alignment tool were used to align the rails as follows:

1. Use the theodolite (transit) with a height gauge to locate the highest point on each of the four trusses.
2. Mark this point and add a 1/4 inch shim under the linear shaft rail at this point. This establishes the highest point on the truss.

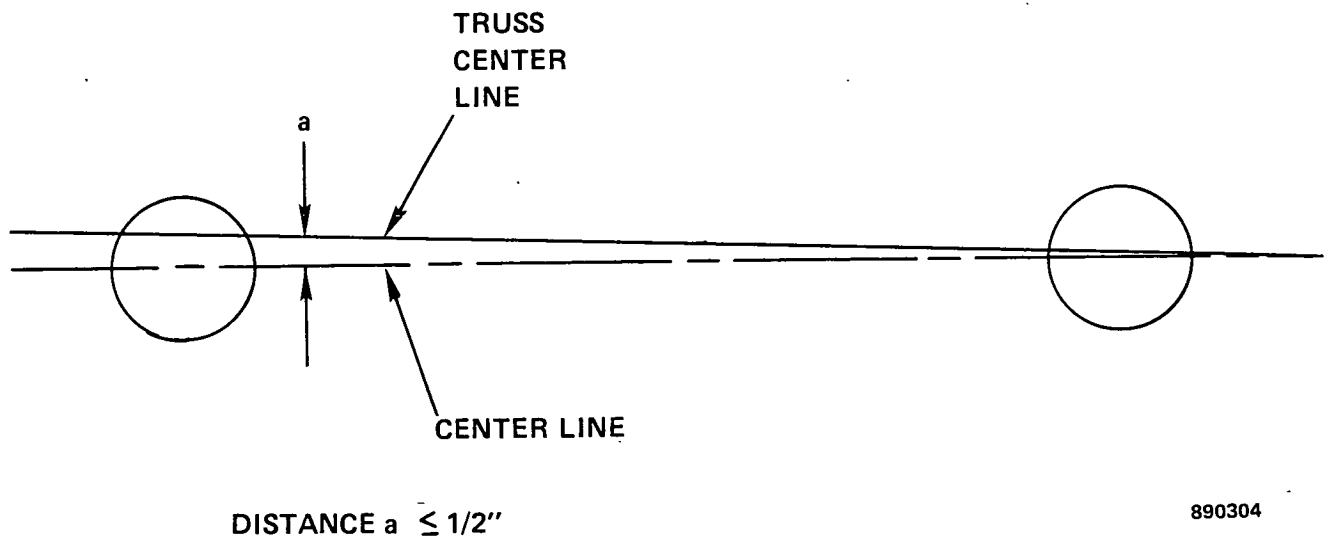


Figure 4.1-6. Centerline Of The Truss Must Be Located To Within 0.5 Inches Of The Column Centerline. The Scanner Rails Have Only Plus Or Minus 0.5 Inches Of Adjustment To Compensate For Truss Bow.

ORIGINAL PAGE  
BLACK AND WHITE PHOTOGRAPH

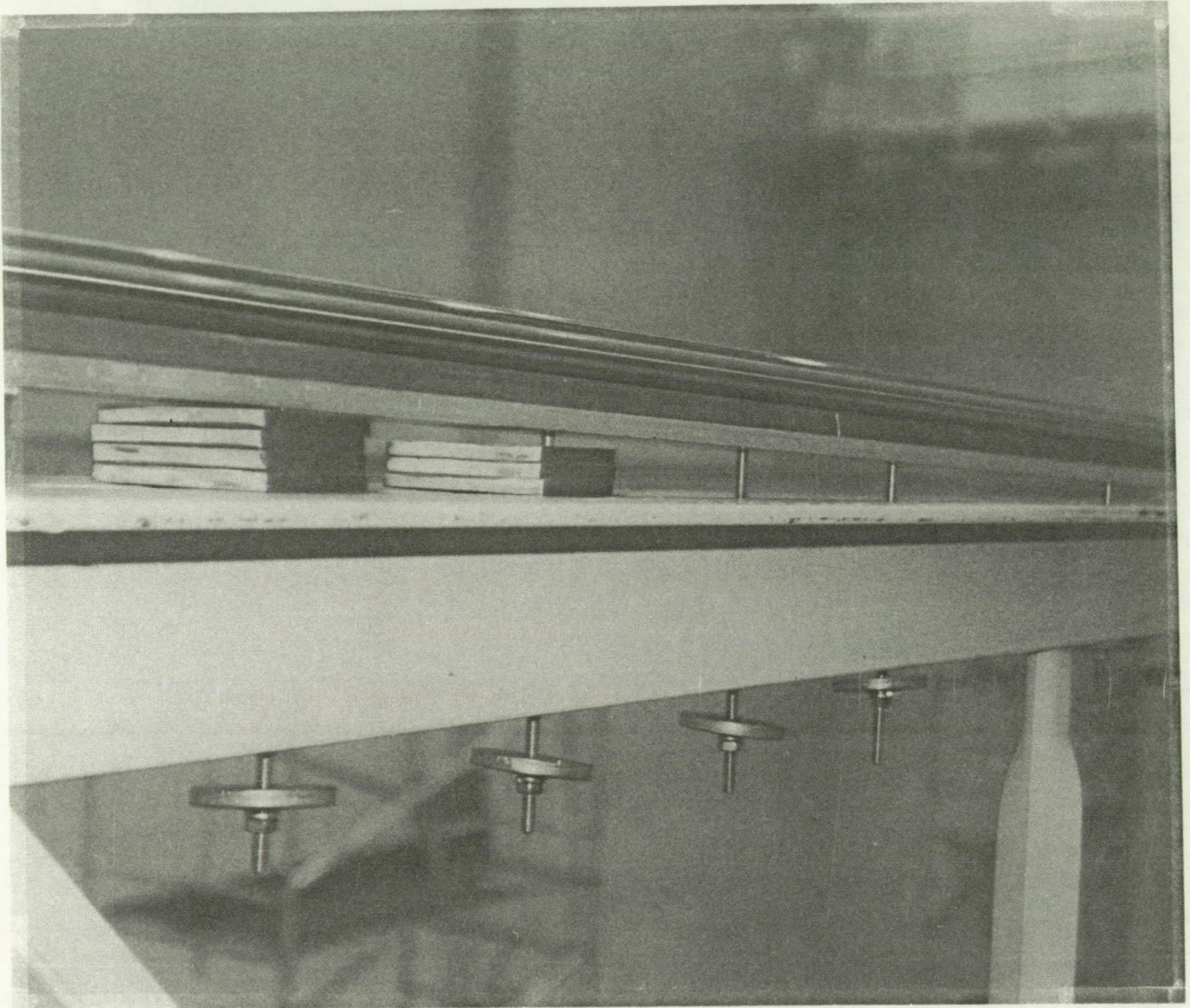


Figure 4.1-7. The Linear Bearing Shaft Is Mounted Loosely To The Top Of Truss 2 and The Shimming and Alignment Process Has Started

3. Mount the rail alignment tool, shown in Figure 4.1-8, and adjust the height of the tool until the target is on the theodolite (transit) cross hair.
4. The entire rail system will be set to this height by moving the alignment tool along the rails and shimming as required. A shimmed rail is shown in 4.1-9. (The rails are not securely fastened until they are set in plane and parallel.)
5. Establish linearity in the rail on truss 2.
6. Move the theodolite (transit) to column 6 to align the rail on top of truss three.
7. Locate the ends of the rail on truss 3 with a tape measure 220 inches away from the linear shaft rail previously mounted on truss 2.
8. Bring the theodolite (transit) in line with these two points and align the rest of the rail (this operation establishes parallelism between the rail on truss 2 and truss 3).
9. Repeat steps 6 through 8 on the rails mounted to trusses 1 and 4.
10. Mount the laser scanner stops, shown in Figure 4.1-10, at both ends of each truss (this prevents the laser scanner system from running off the end of the truss).
11. Mount laser scanner gear racks on truss 1 and 4.



ORIGINAL PAGE  
BLACK AND WHITE PHOTOGRAPH

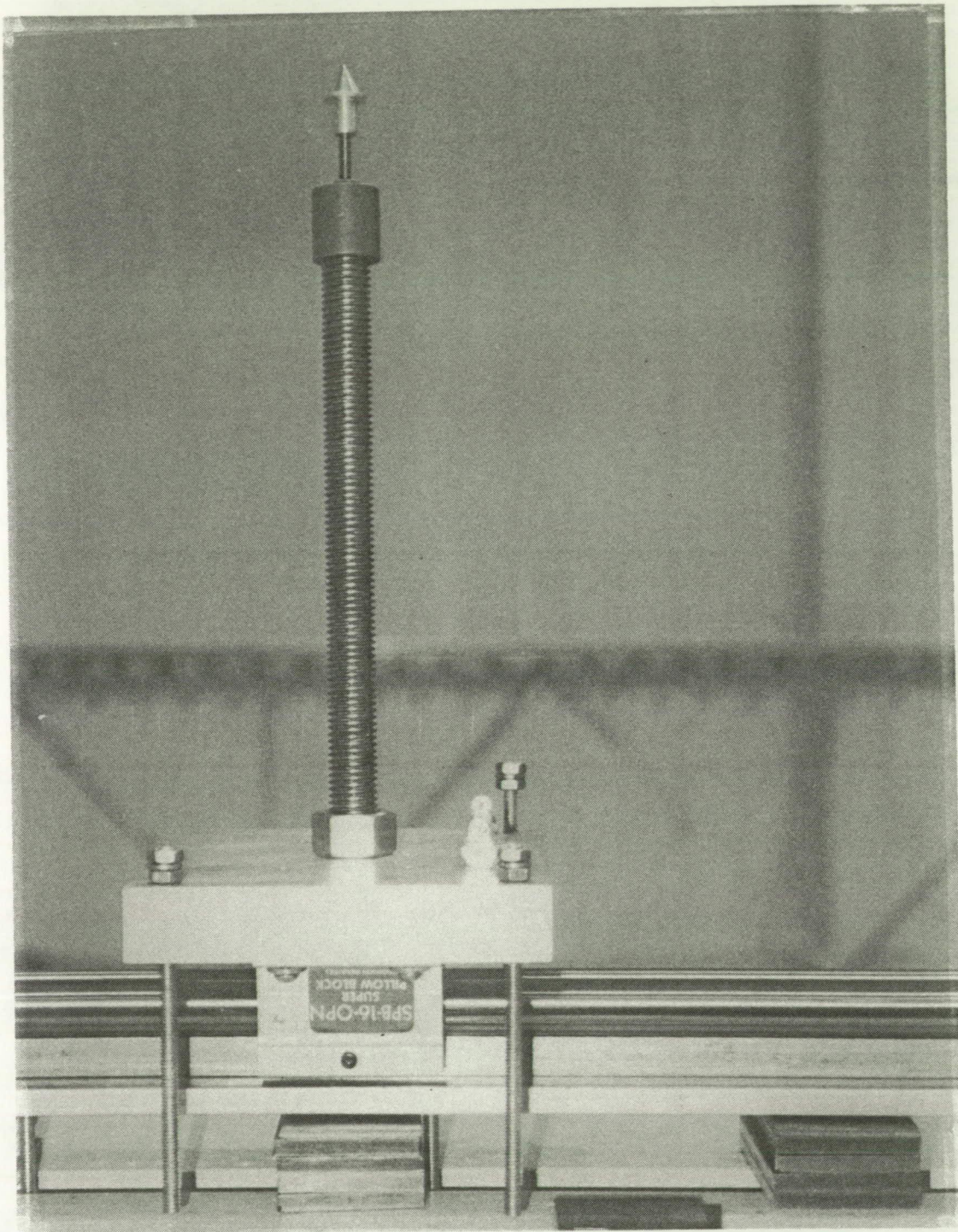


Figure 4.1-8. Linear Bearing Shaft Alignment Tool Was Combined With A Theodolite Mounted To The Columns To Set The Rails. The Pillow Block Holds The Tool Along The Rail Axis And The Bubble Level On The Front Is Used To Keep The Tooling Ball Vertical.



ORIGINAL PAGE  
BLACK AND WHITE PHOTOGRAPH

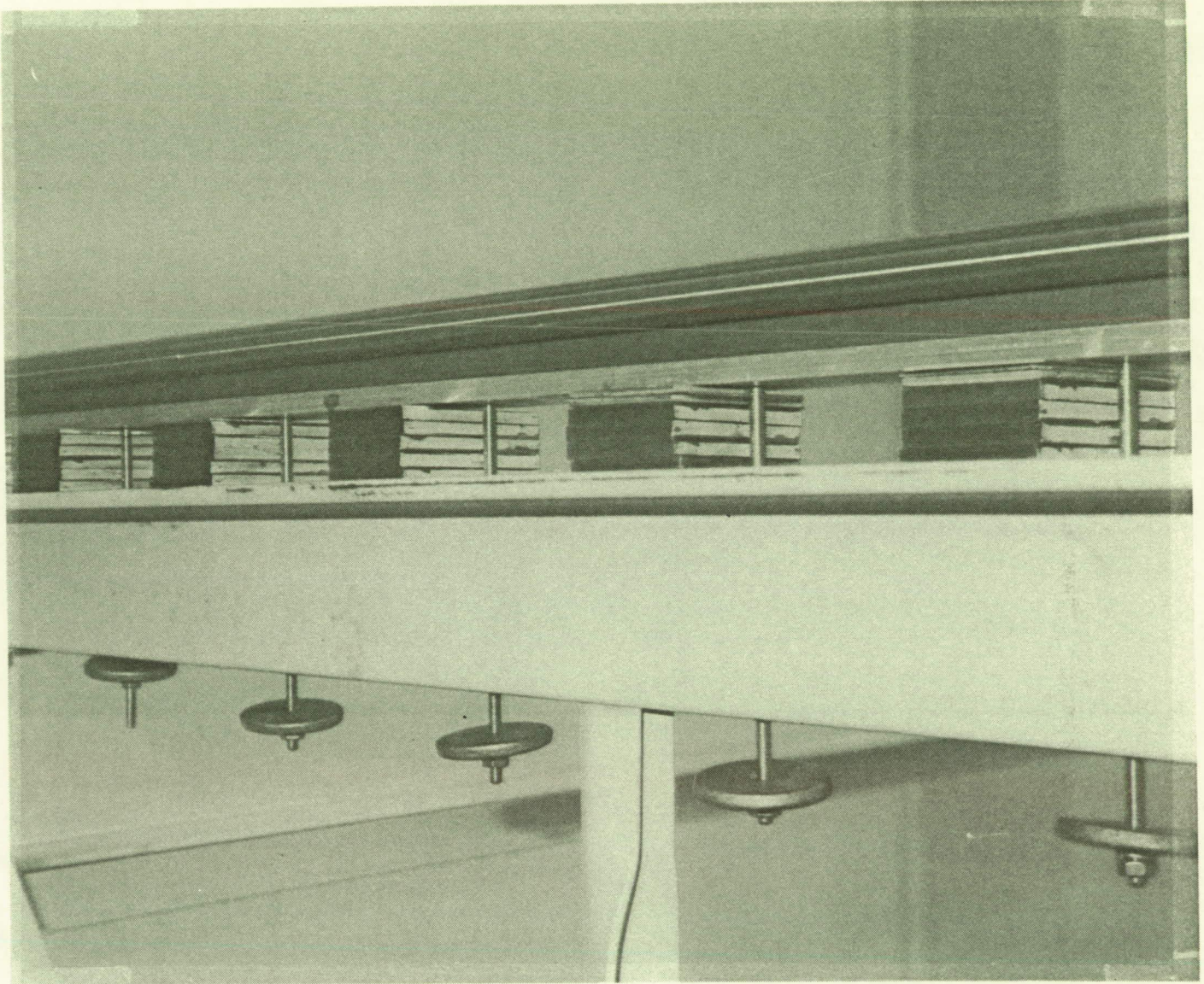
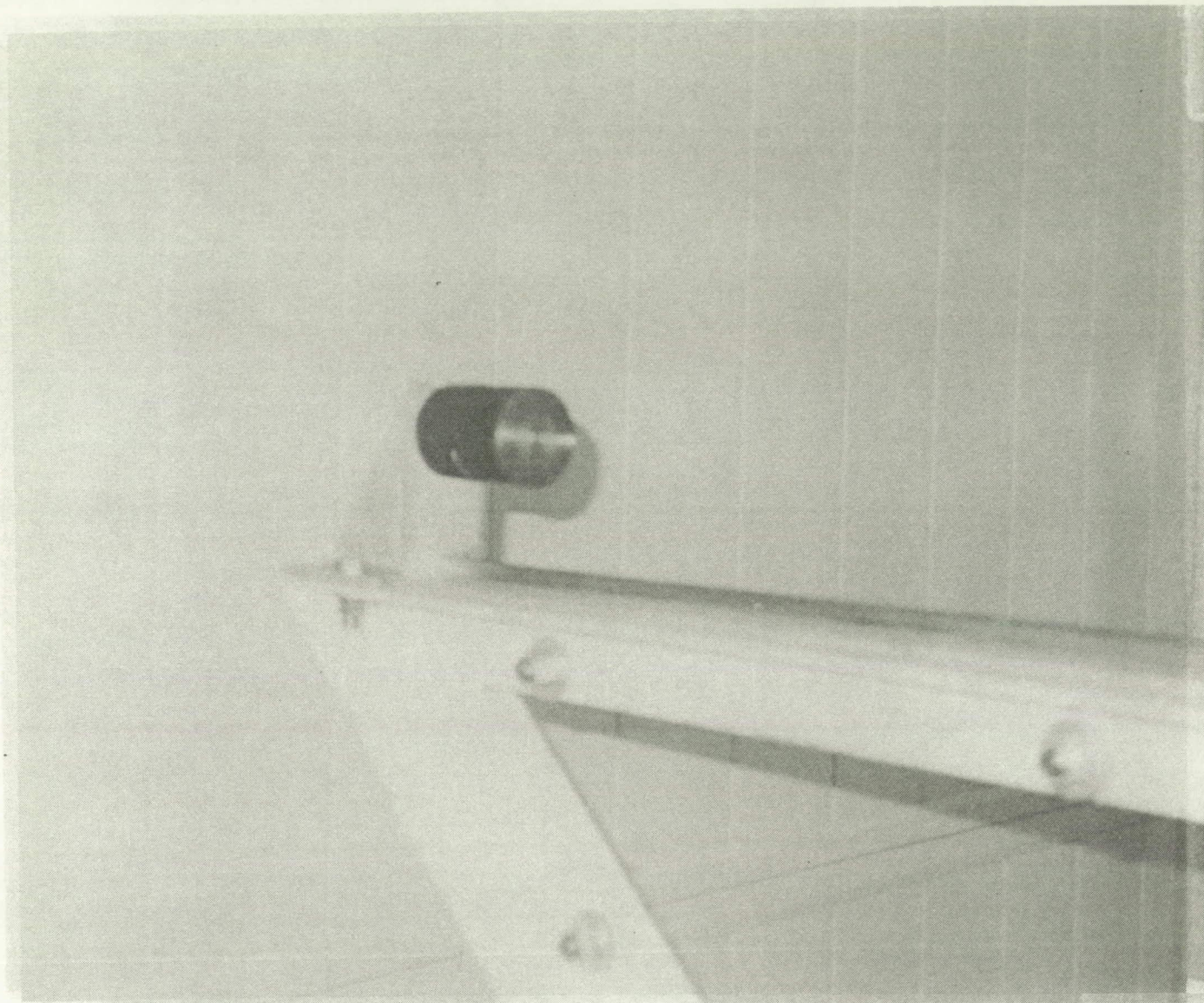


Figure 4.1-9. The Shimming Operation Is Completed For The First Rail  
On Truss 2 and Was Then Performed On The Remaining Three Trusses



ORIGINAL PAGE  
BLACK AND WHITE PHOTOGRAPH



ORIGINAL PAGE IS  
OF POOR QUALITY

Figure 4.1-10. Large Rubber Stops Are Mounted To The Ends Of The Trusses To Prevent The Scanner From Running Off The End Of The Rail. Motor Control Software Also Prevents The Scanner From Hitting The Stops.

After the linear shaft rail system is complete, the laser scanner is mounted on the rail system and brought into operation. The rails and laser scanner have been installed at this point because they are not accessible when the remainder of the counterbalance system (rails and pulleys) has been installed. Installation of the laser scanner will be discussed in more detail in Section 4.2.

The panel support system is a series of pulleys and counterbalance weights used to support the center of each of the 19 hexagonal panels. The pulleys directly above the hexagonal panel are mounted on a set of bearings which ride on the flange of a light weight aluminum I-Beam. A schematic of the system can be seen in Figure 4.1-11. A trolley type system used to support the pulleys allows the cable to move from the assembly position to the optical scanning position and maintain a line of action directly above the hexagonal panel. It was determined through analysis that the cables should be vertical within .15 degrees (.03 inches per foot of height) to prevent inducing a moment in the panel that would cause geometric distortion. Thus, the trolleys are needed to maintain that verticality. The theoretical panel center locations for the assembly and optical scan position were marked on the floor with a theodolite system prior to assembling the counterbalance. A plum bob is dropped from the center of the pulley trolley and the trolley is aligned with the mark on the floor at the assembly position. A hard mechanical stop is set at this point. The operation is repeated in the optical scanning position and the hard stop is

## COUNTER BALANCE PULLY SYSTEM

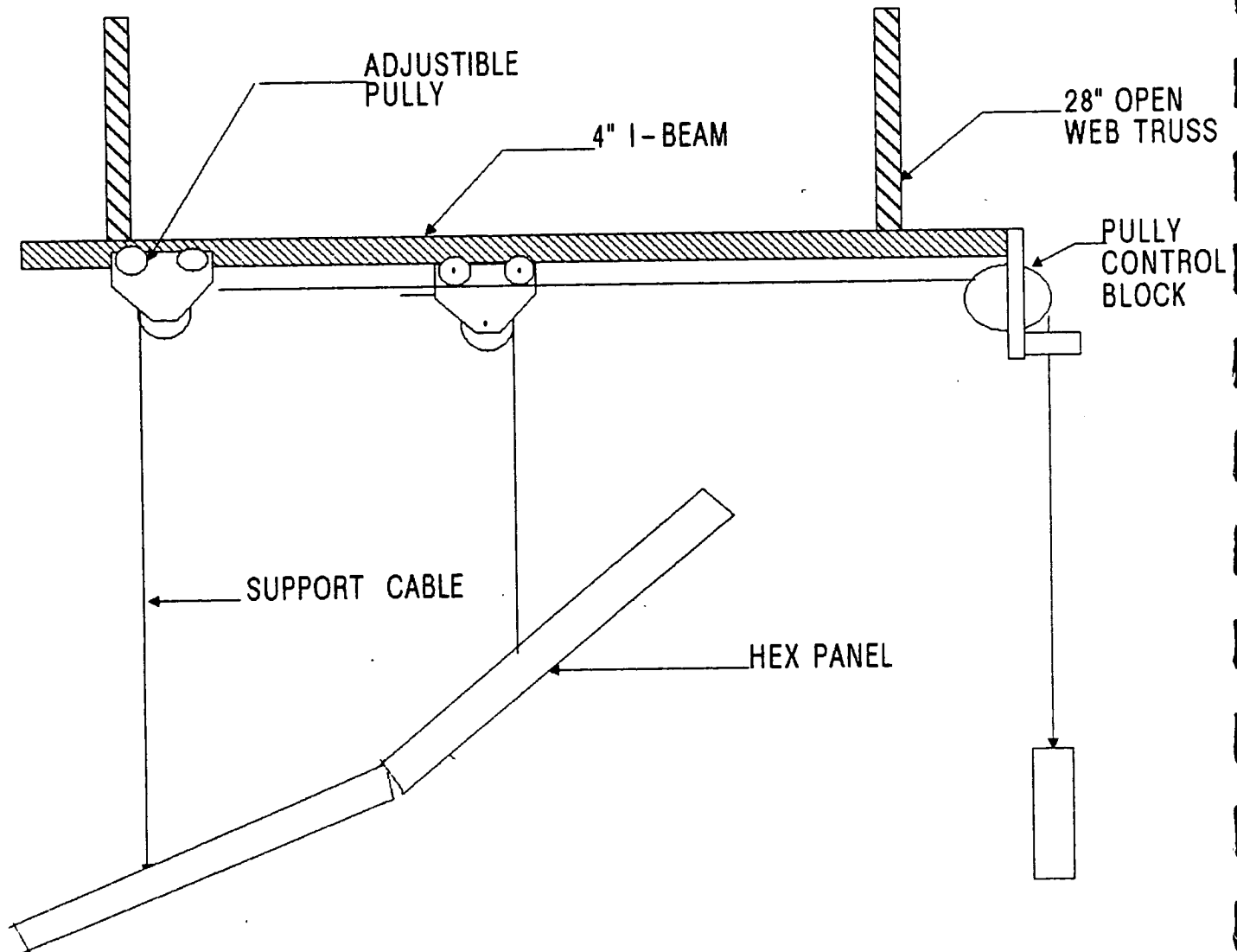


Figure 4.1-11. Panel Support System Used To Counterbalance Nineteen Individual Hexagonal Panels During Assembly and Test

located. Next, the pulley and trolley system are bottomed out against the hard stops to be aligned in the assembly and optical scanning position. A brief assembly scenario goes as follows:

1. The Aluminum I-beam trolley guides are attached to the bottom of the mainframe trusses. The trusses have been marked with the location of the I-beam centerlines to obtain a good starting point for the alignment process.
2. Install the trolleys and trolley stops in the proper location. Do not tighten the stops at this time. (The I-beams and trolleys are shown in Figure 4.1-12.)
3. Drop a plumb bob from each trolley and adjust the I-beam trolley guide and trolley stops until the trolley is aligned to the assembly and optical scanning panel center position.
4. Install the pulley control blocks shown in Figure 4.1-13.
5. Install the counterbalance cable assemblies for each trolley.
6. Proofload the cables to 100 lbs. (Cables are to be proofloaded to 2 times the maximum tension they will see. Since the block in the cable assembly provides a 2:1 mechanical advantage, the cable will see approximately 40 lbs. in a fully populated panel.)

The pulley control blocks are installed at the end of each I-beam section and keep the counterbalance weights hanging over the end of the mainframe structure. The area below the weights was off limits to personnel



ORIGINAL PAGE  
BLACK AND WHITE PHOTOGRAPH

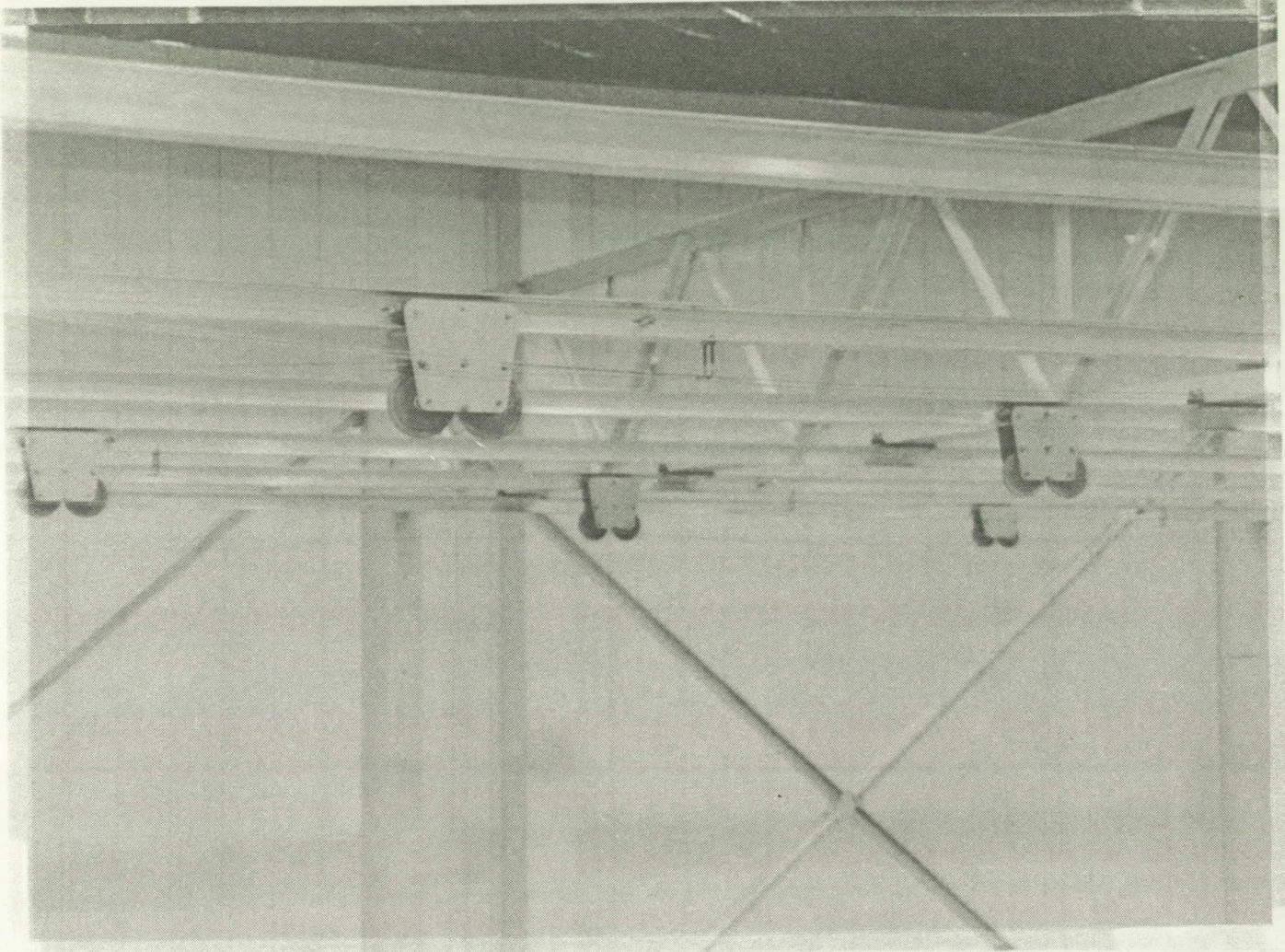
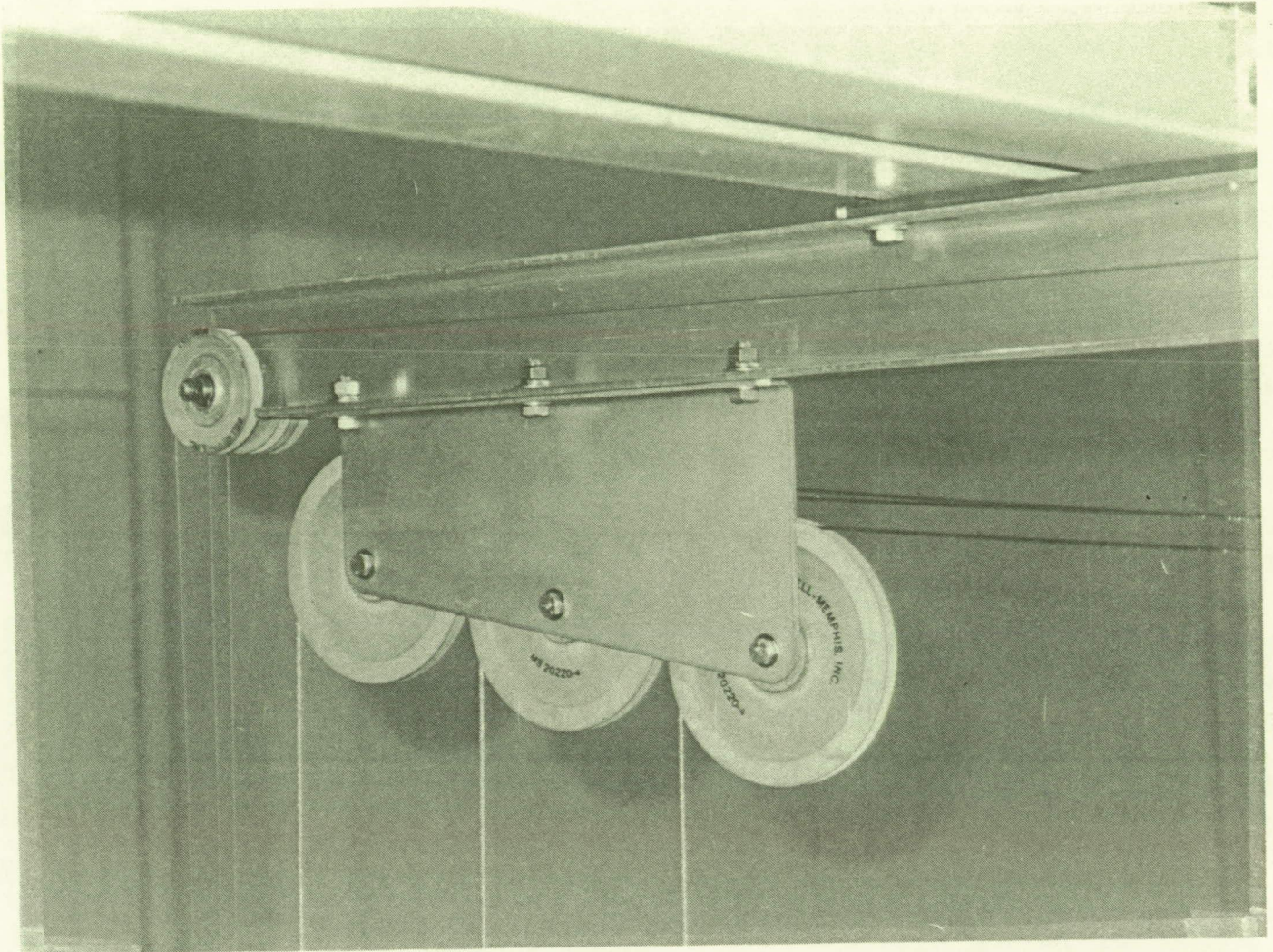


Figure 4.1-12. The Aluminum I-Beams Are Mounted To The Bottom Of The Counterbalance Trusses. They Support The Pulley Trolley System That Is Used To Offload The Panels In The Assembly and Scan Position.



ORIGINAL PAGE  
BLACK AND WHITE PHOTOGRAPH



ORIGINAL PAGE IS  
OF POOR QUALITY

Figure 4.1-13. Pulley Control Blocks Are Attached to The Ends Of The Aluminum I-Beams. The Small Pulley and Cable Are Used To Pull The Trolley Against The Stops From The Ground To Place The Concentrator In The Assembly and Scan Position.

to prevent accidents and for general safety. Having the weights away from the structure will also prevent damage to the hardware should a cable break.

The translucent target and camera shown previously in Figure 4.0-2 may now be installed on the counterbalance mainframe. The target support structure and camera mount are preassembled on the floor and are mounted to truss number four in a predetermined position (Figure 4.1-14). With a theodolite measurement system the translucent target is located at the focal point of the concentrator and hard mounted to that location.

Next the optical scanning support towers must be installed. The three support towers are used to represent the delta frame structure of the flight concentrator. Pictures of the scanning tower supports can be seen in Figure 4.1-15 and 4.1-16.

#### 4.2 Laser Scanner

The laser scanner provides a collimated light source parallel to the optical axis (vertical with respect to gravity) for testing the concentrators optical performance. The laser scanner, shown in Figure 4.2-1, is a 2 degree-of-freedom apparatus that operates similar to an x-y axis overhead crane. The laser and the automatic leveling system that maintains laser verticality are mounted on a small motor driven cart referred to as the carriage. The carriage is mounted on a motor driven beam (gantry) and travels perpendicular to the path of the beam. Since the gantry is 60 feet long, each end is equipped with a motor that is tied into a motor control



ORIGINAL PAGE  
BLACK AND WHITE PHOTOGRAPH

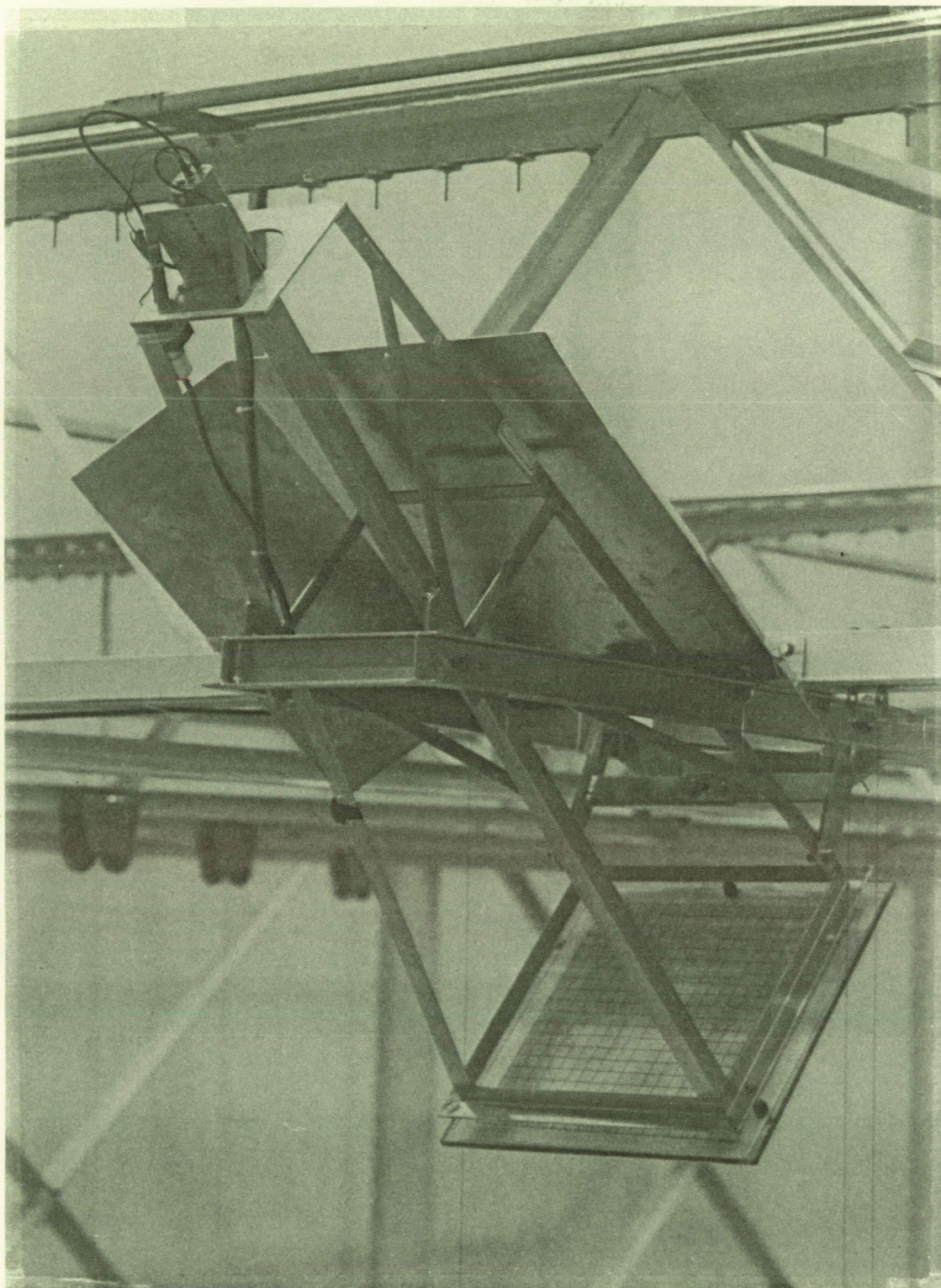


Figure 4.1-14. The Target Support Structure and Viewing Camera Are Mounted To The Counterbalance Structure At A Precise Location On Truss 4



ORIGINAL PAGE  
BLACK AND WHITE PHOTOGRAPH

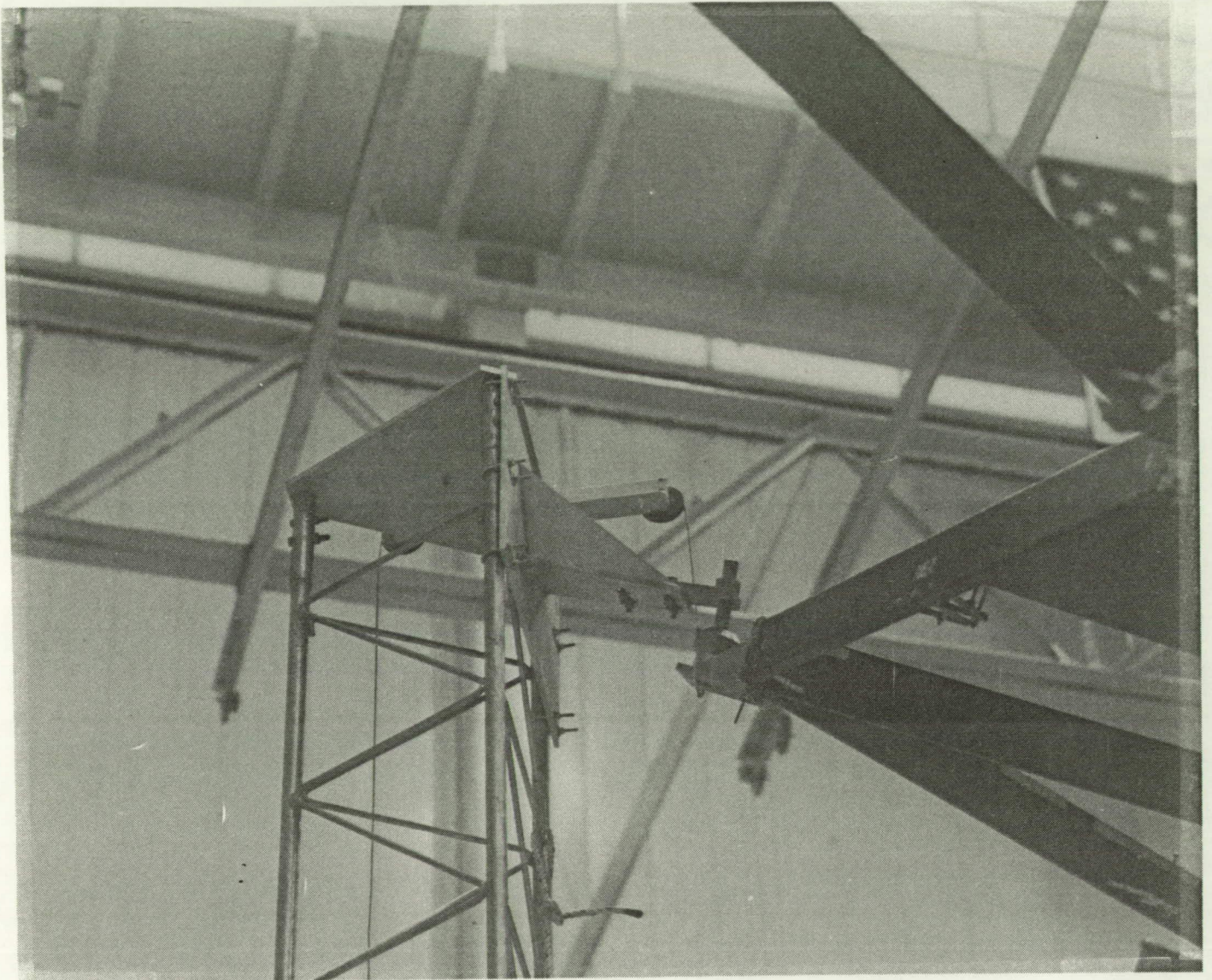


Figure 4.1-15. The Scanning Towers Are Used To Support The Concentrator  
In The Optical Scan Position and To Simulate The Three Point Mount  
Of The Delta Frame Structure On The Flight Design



ORIGINAL PAGE  
BLACK AND WHITE PHOTOGRAPH

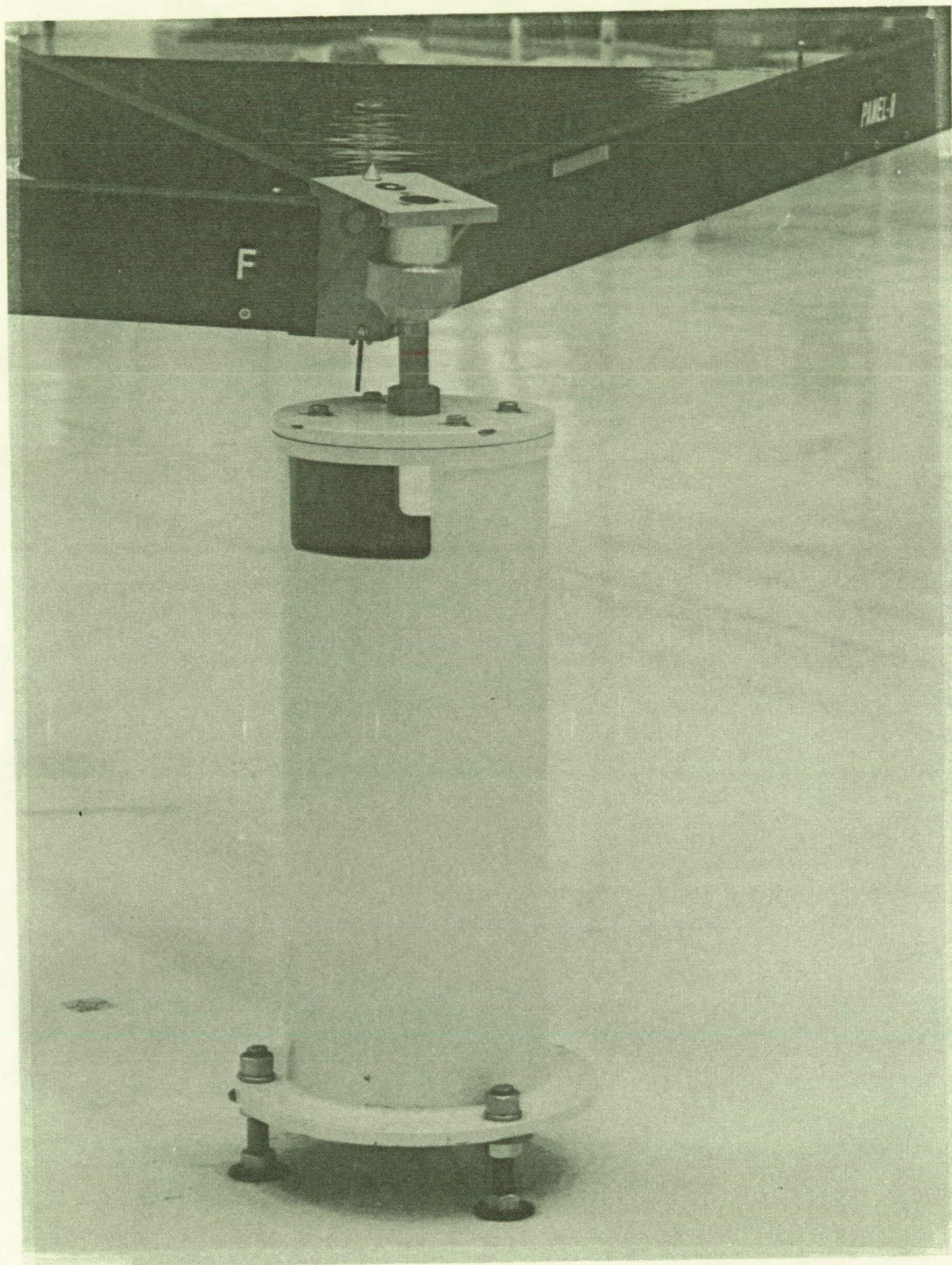


Figure 4.1-16. Short Support Stand Used At The Point Closest To The Floor. There Are Two Tall Towers, Figure 4.1-15 and One Short Support To Make Up The Three Point Mount.

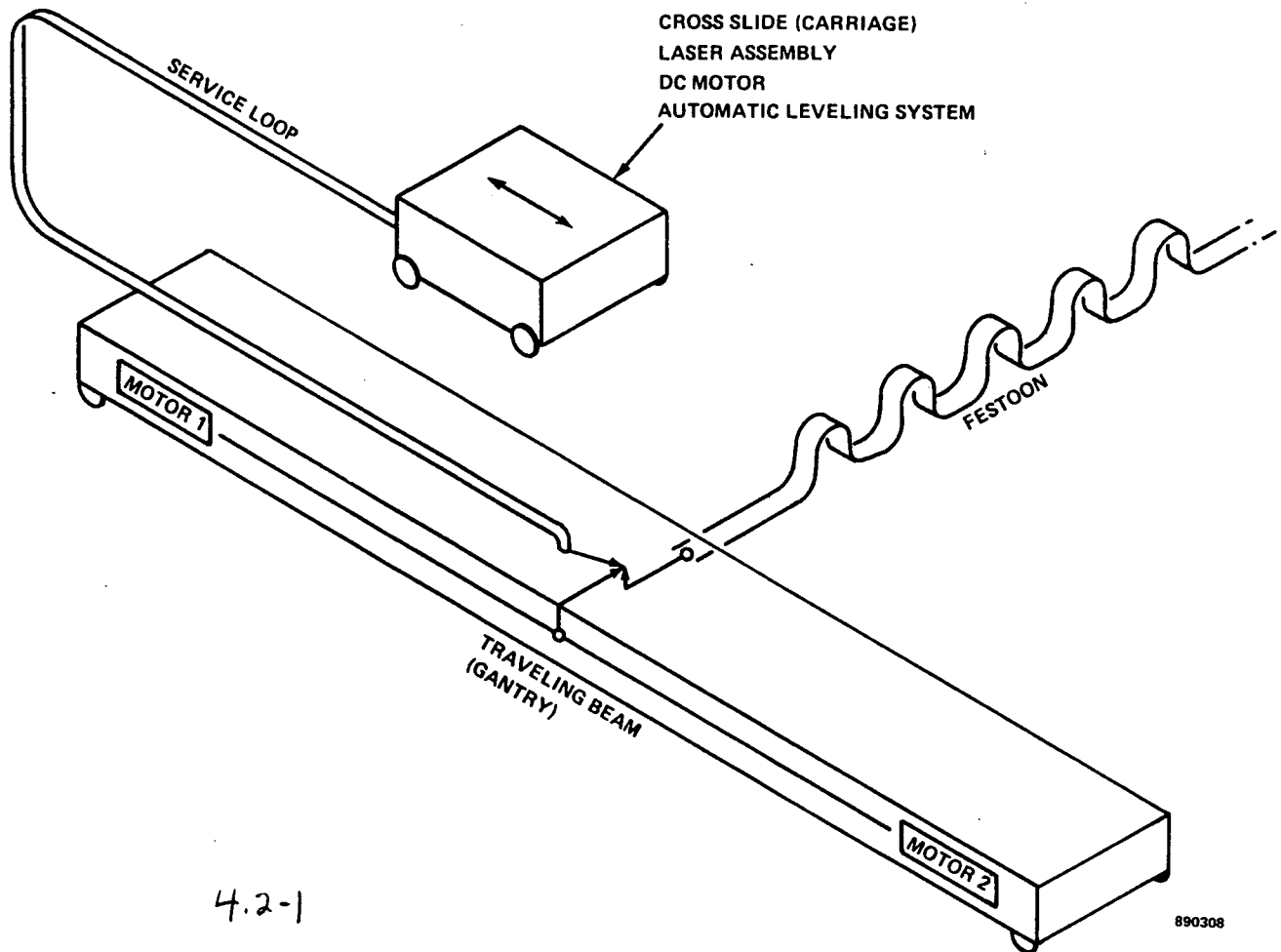


Figure 4.2-1. Lase Scanner Assembly Is Comprised Of The Main Beam With Two Synchronized Drive Motors That Travels In The Y Direction and The Carriage With A Single Motor That Travels Across The Beam In the X Direction

circuit that keeps the gantry tracking straight. This is done by providing inputs from the motor incoders to a feedback and control loop that keeps the two motors synchronized with respect to speed and revolutions. The carriage travels along the x axis and the gantry along the y axis as shown in Figure 4.2-2 and 4.2-3.

Mechanically, the scanner is a large beam structure (gantry) fitted with linear shaft rails that guide a moving platform (carriage) along its length. The gantry is fitted with roundway bearings and rollers that guide it along the linear shaft rails on the counter balance truss structure. A functional mechanical diagram is shown in Figure 4.2-4.

The motion of the laser scanner is produced by three DC motors that are part of a computer driven servo system. Two motors, located at each end of the scanner gantry, drive pinion gears which mate to a rack that runs the length of the trusses number one and four (Figure 4.2-3). The third motor drives a pinion gear which mates with a rack that runs the entire length of the gantry. As the motor is driven the carriage moves along the length of the gantry. A motion control card, mounted in the PC Bus is driven with interactive software, provides acceleration and velocity profiles to the servo amplifier which relays the signal to the motors. The servo amplifier receives velocity feedback from an integral tachometer in each motor and positional feedback from optical encoders that track the gear rack in series with each motor. A functional electrical diagram of the system is shown in Figure 4.2-5.



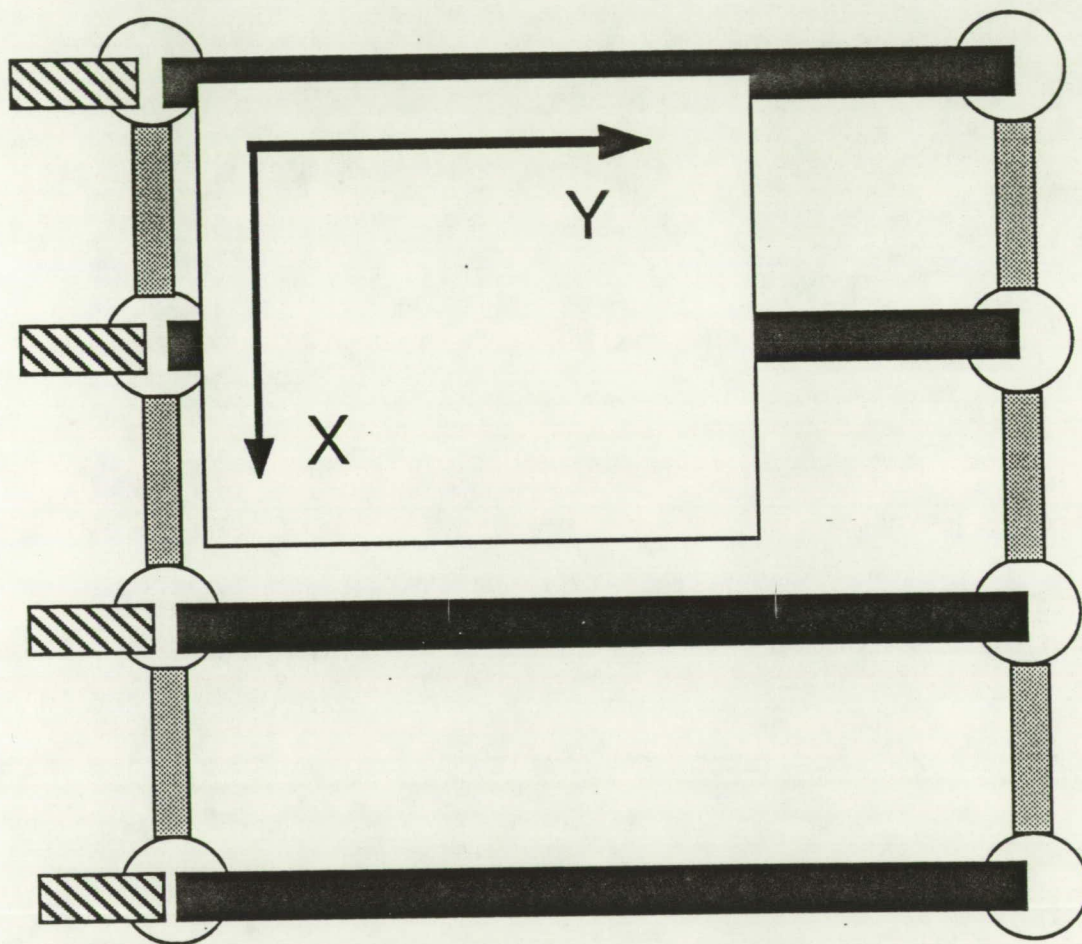


Figure 4.2-2. The Main Gantry (Beam) Travels Across The Counterbalance Structure In The Y Direction (Along The Trusses) and The Carriage Travels Perpendicular To The Trusses In The X Direction



ORIGINAL PAGE  
BLACK AND WHITE PHOTOGRAPH

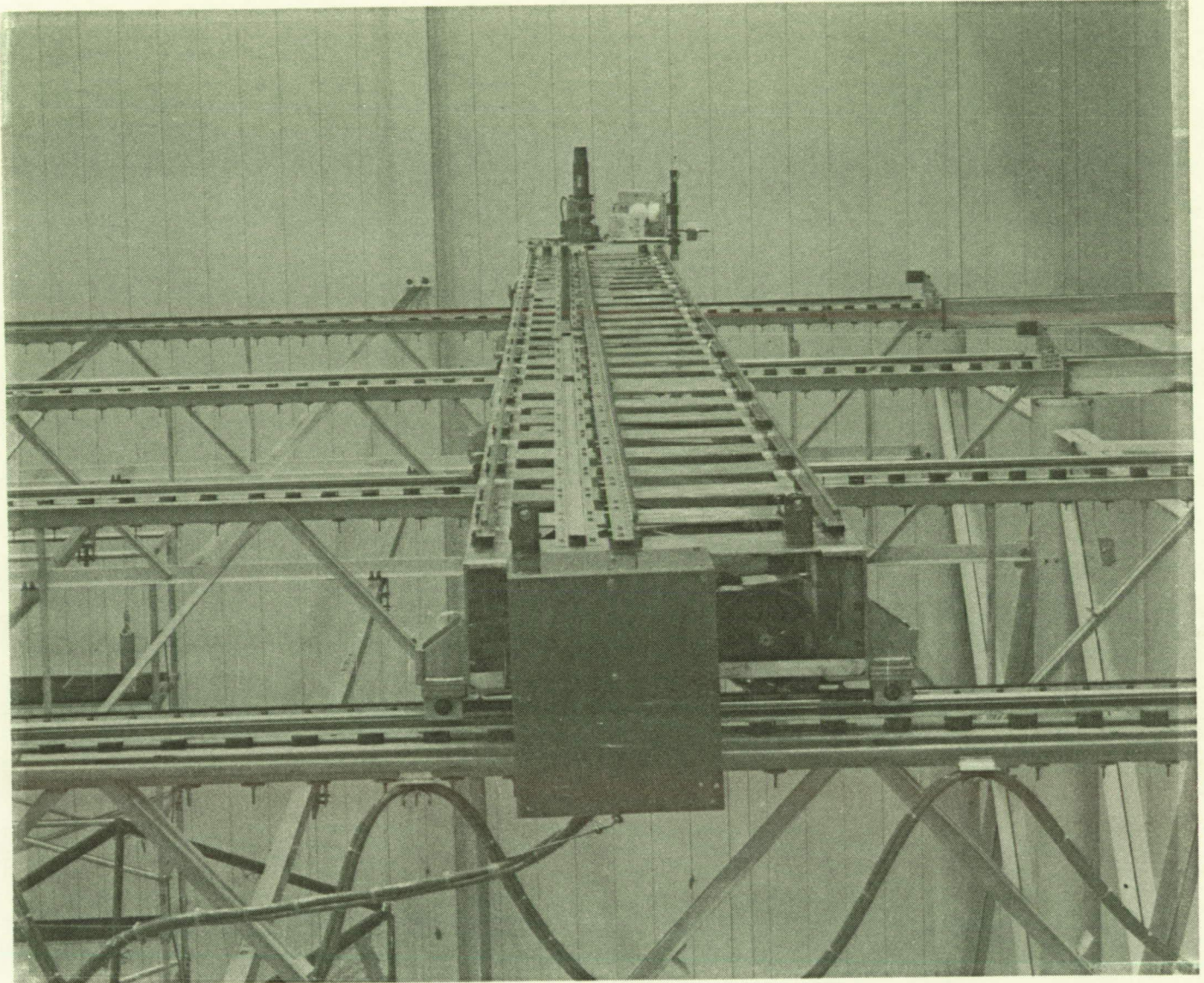
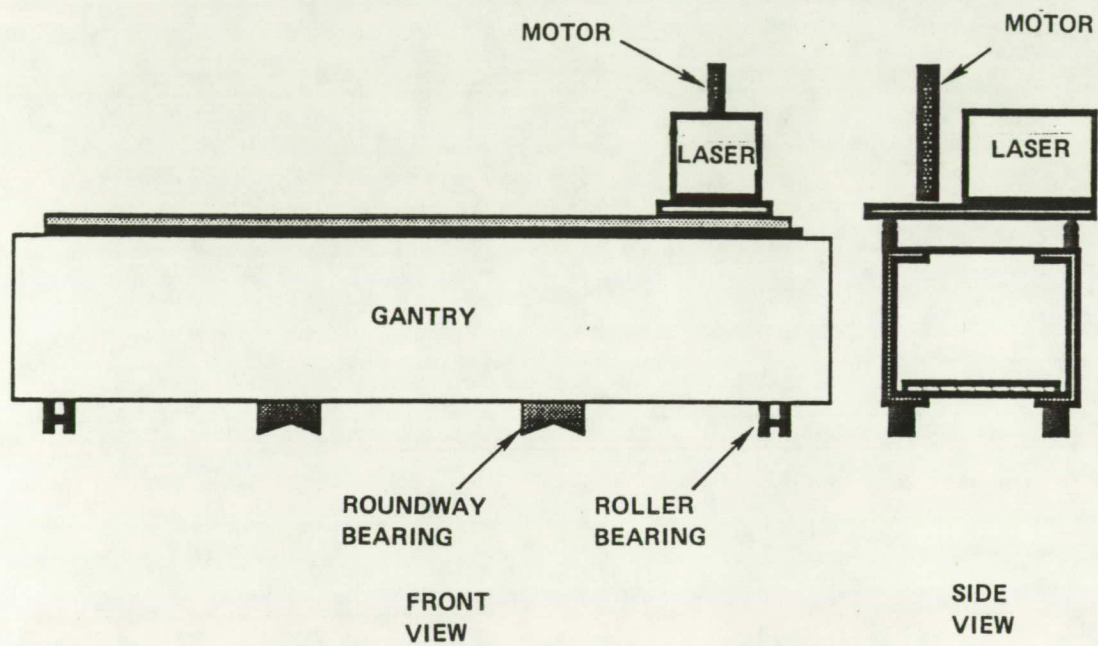


Figure 4.2-3. Shows The Actual Laser Scanner System In PSF At NASA LeRC  
In Cleveland. The Foreground Shows The Rack and Gear Drive System.  
The Laser Carriage Is Shown On the Far Side Of The Structure.





890295

Figure 4.2-4. Functional Mechanical Diagram Of The Laser Scanner System

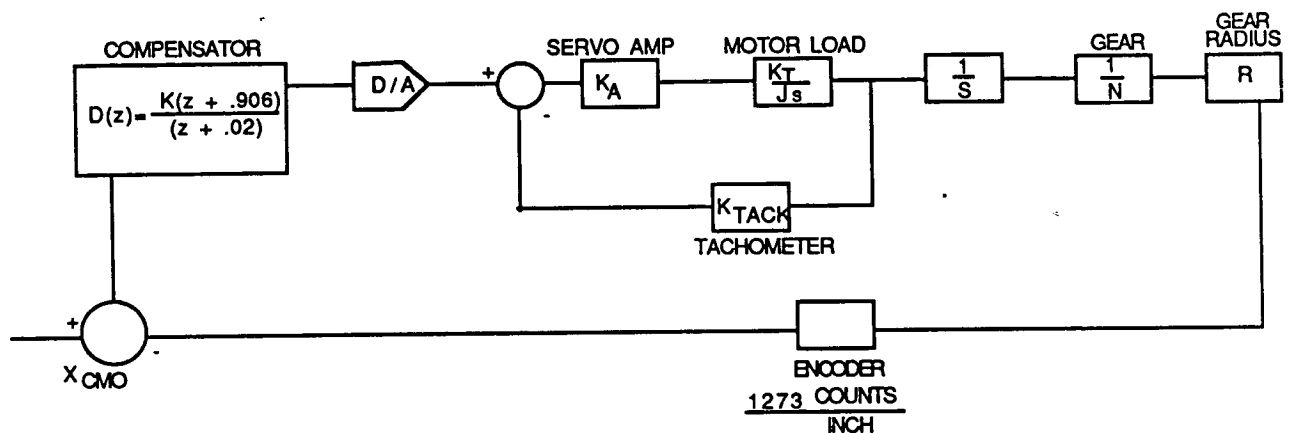


Figure 4.2-5. A Functional Electrical Diagram Of The Laser Scanner Motor Control Circuit. This Circuit Is Used To Keep The Two Motors On The Main Gantry Synchronized.

System safety is implemented with both hardware and software. Each motor has a brake which is activated when a manual system shutdown switch is tripped. Limit switches located at the periphery of the motion area send a signal that causes the motion controller to shut the system down when tripped. Motion is restricted in the direction of travel when the switch is tripped. The system cannot continue motion in the direct of travel toward the switch and must be instructed to move in the opposite direction to release the tripped switch. This eliminates the possibility of starting the system and breaking the switches or gantry hardware. In addition to the hardware implemented safety features, the software has subroutines that shut the system down if the scanner is commanded out of its range of motion or the gantry beam ends are not tracking each other (skewed with respect to the structure). The software also shuts the system down when an input signal is lost from a motor encoder. If all electrical safety systems fail, the counterbalance is equipped with mechanical stops to prevent the scanner from running off the top of the mainframe structure.

The laser is mounted on an automatic leveling platform that rides on the carriage. The automatic leveling system maintains the laser verticality by signaling two motor micrometers to manipulate the platform until the level condition is sensed.

The laser system consists of a Class IIb Helium Neon laser, a 10 to 1 beam expander, an electronic shutter, and a neutral density filter. A functional diagram is shown in Figure 4.2-6. The resulting laser system is



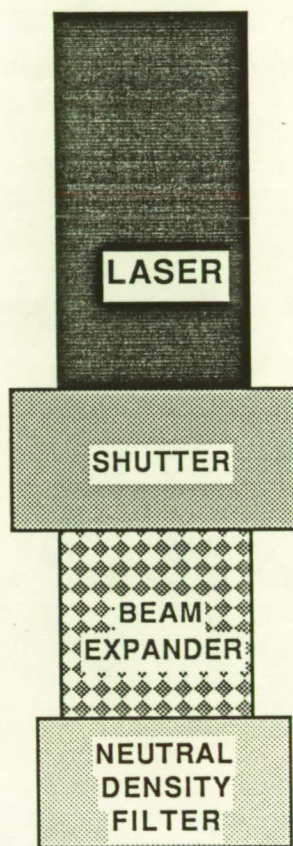


Figure 4.2-6. The Neutral Density Filter Was Placed On The Laser To Result In A Class I System That Is Safe For Operation In The PSF Building

classified as a Class I system. The Neutral Density Filter attenuates the power output of the system to 0.3mW. Although a low power laser can be purchased, the quality of the internal optics leads to greater beam divergence. The Neutral Density Filter results in a safe laser system with a high quality beam.

The automatic leveling system is composed of two highly accurate electrolytic gravity sensors (tilt sensors) commonly used for leveling aircraft, two motor micrometers with a resolution of 0.02 microns and a feedback loop. The tilt sensor sends a voltage signal to the feedback loop when the out of level condition is sensed. The tilt loop amplifies the signal and drives the corresponding motor micrometer until the level condition is sensed.

The tilt sensors and laser are mounted orthogonal to each other as shown in Figures 4.2-7 and 4.2-8. In addition, the laser is mounted in a stage (adjustable tooling) that is equipped with micrometers on the two orthogonal axes. Therefore, the tilt sensors do not need to be located with extreme accuracy on the platform because the micrometers are used to position the laser relative to the tilt sensors and eliminate manufacturing tolerances.

Laser verticality is achieved by activating the tilt loop then reflecting the laser beam off a pool of mercury which becomes level with respect to gravity. The stage micrometers are adjusted until the beam is reflected back onto itself. When the beam is reflected off the mercury pool

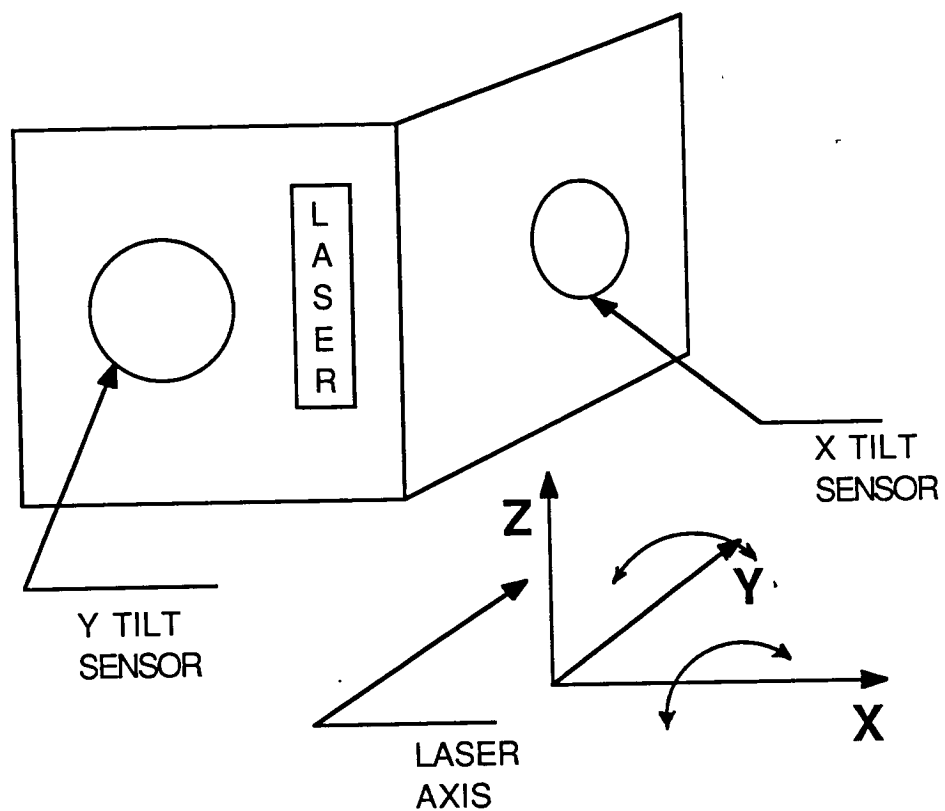
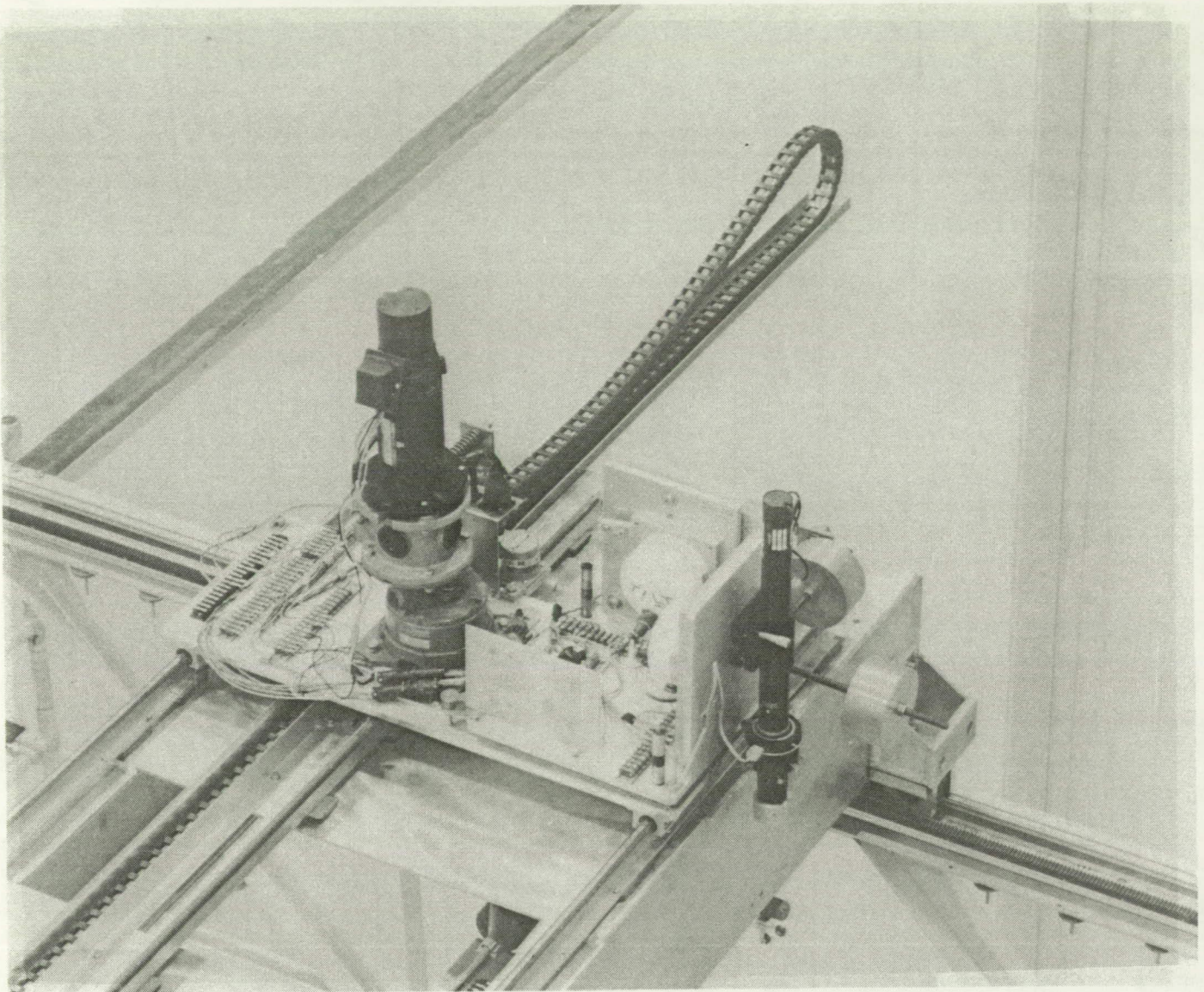


Figure 4.2-7. The Two Tilt Sensors Are Mounted Orthogonal To Each Other To Maintain Laser Verticality For the Optical Repeatability Testing



ORIGINAL PAGE  
BLACK AND WHITE PHOTOGRAPH



ORIGINAL PAGE IS  
OF POOR QUALITY

Figure 4.2-8. An Actual Photograph Of The Laser Scanner Carriage System. The Sperry Tilt Sensors Can Be Seen On The Two Vertical Faces and The Laser Is Pointed Over The Side Of The Gantry. The Vertical Card Is The Harris "Top Gun" Feed Back and Control Loop Between The Motor Micrometers and The Tilt Sensors.



and back to the aperture of the laser it is vertical to less than .25 milliradians. This is well within the measurement accuracy needed for concentrator testing. The power cable festoon for the gantry and carriage system can be seen in Figure 4.2-9. The cables are routed to the back of the control console as seen in Figure 4.2-10. Within the cables are the lines from the motor encoders, motor brakes, power to the carriage, motor power cables, laser power cable tilt sensor power cables, etc. The control console can be seen in Figure 4.2-11. It contains the PC that is used for gantry and carriage control, the laser power switch, the tilt sensor power switch, the system kill switch and the motor control circuit boards and power supply. A detailed description of the code and the automatic leveling system is given in Appendix F as well as a system calibration and operational procedure.

#### 4.3 Concentrator Assembly

This section describes the steps needed to attach the hexagonal panels to the counterbalance structure and assemble the concentrator for the first time prior to testing. This is an abbreviated sequence to help the reader understand the assembly process and the steps involved.

The first step involved is to attach panel 1 (central panel) to the counterbalance cable as shown in Figure 4.3-1. A pseudo three degree of freedom rational device was developed for the panel to cable interface. The circular pad that sets on the hexagonal panel contains a bearing that allows

ORIGINAL PAGE  
BLACK AND WHITE PHOTOGRAPH

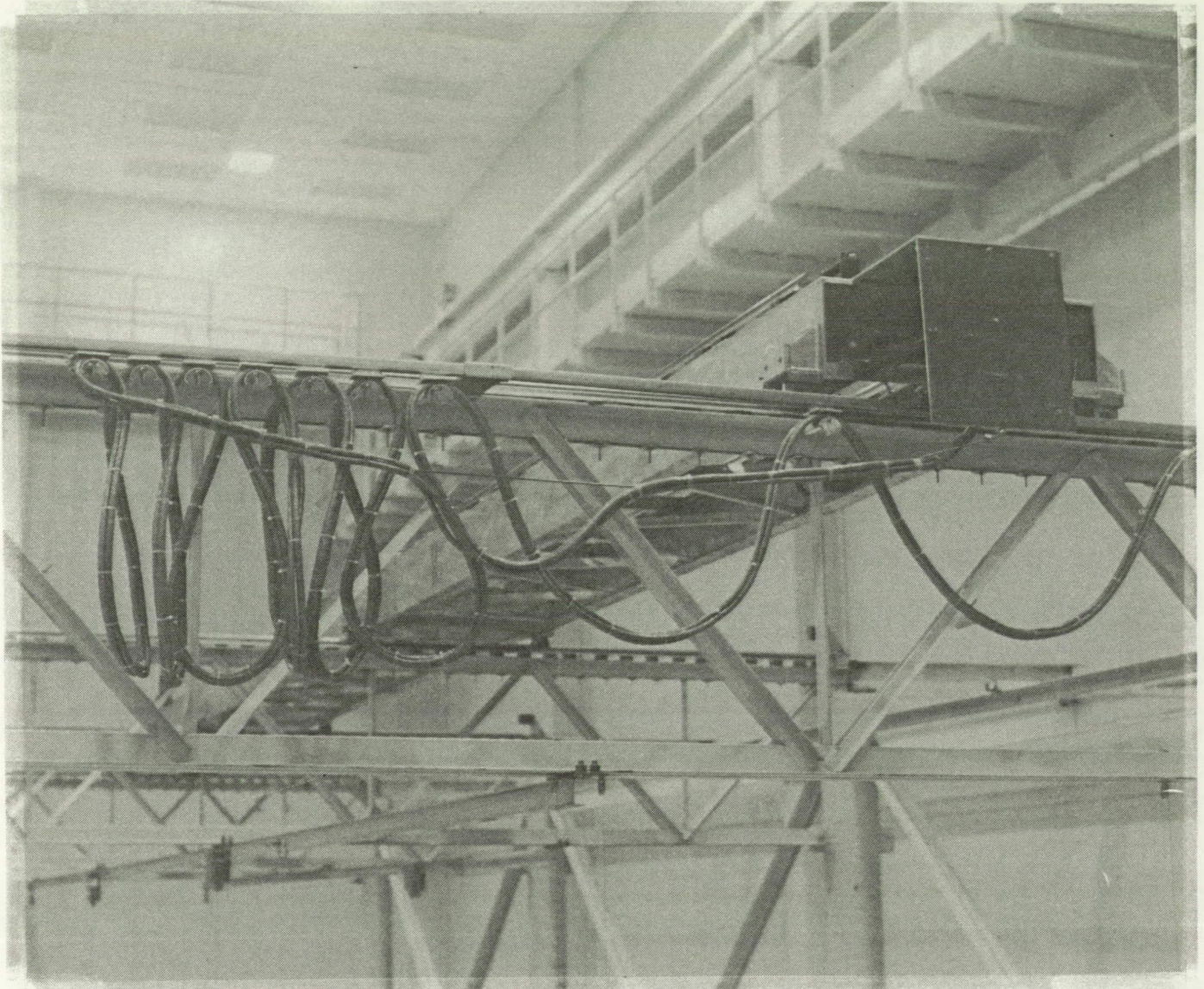


Figure 4.2-9. Cable Festoon That Allows The Electrical and Feedback Wiring To Follow The Gantry As It Travels In The Y Direction



ORIGINAL PAGE  
BLACK AND WHITE PHOTOGRAPH

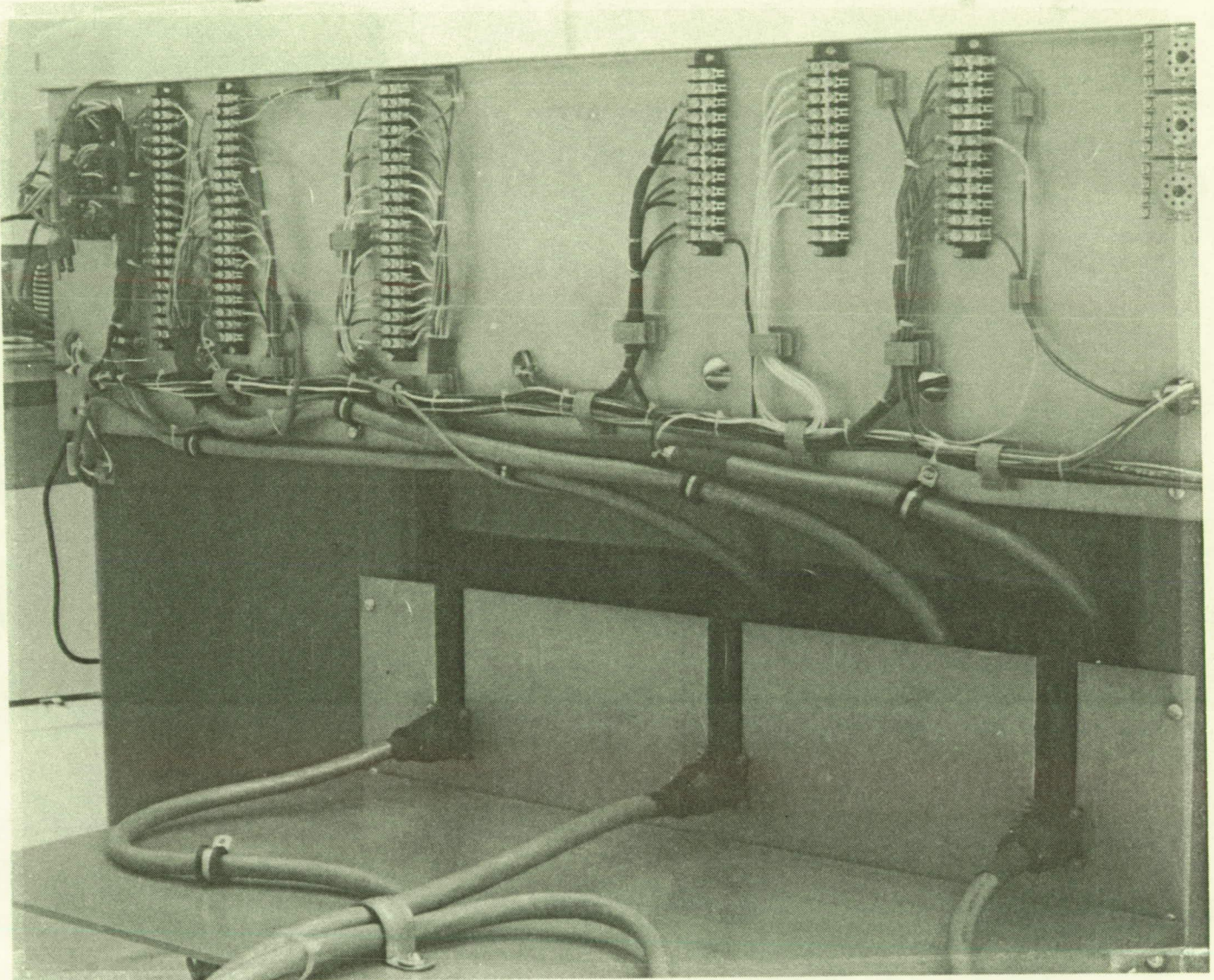


Figure 4.2-10. Wiring Is Routed From The Cable Festoon To The Back Of  
The Control Console In The PSF Highbay Area



ORIGINAL PAGE  
BLACK AND WHITE PHOTOGRAPH

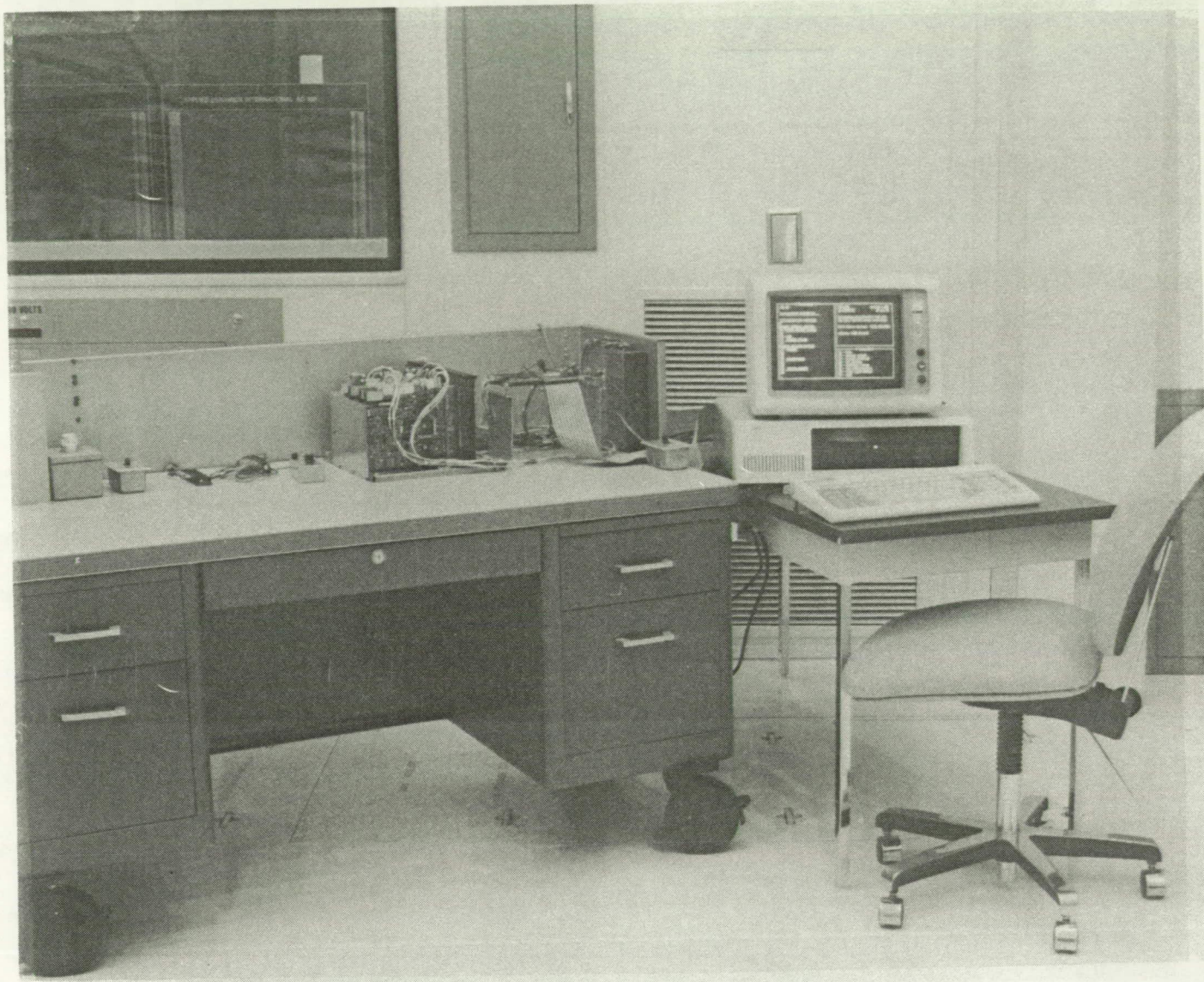


Figure 4.2-11. Laser Scanner Control Console Contains The PC Used To Control The Scanner Location. The System Kill Switch Is Seen On The Far Left Of The Console and The Motor Control Circuit Boards and Power Supply Appear In The Center Of The Photograph.



ORIGINAL PAGE  
BLACK AND WHITE PHOTOGRAPH

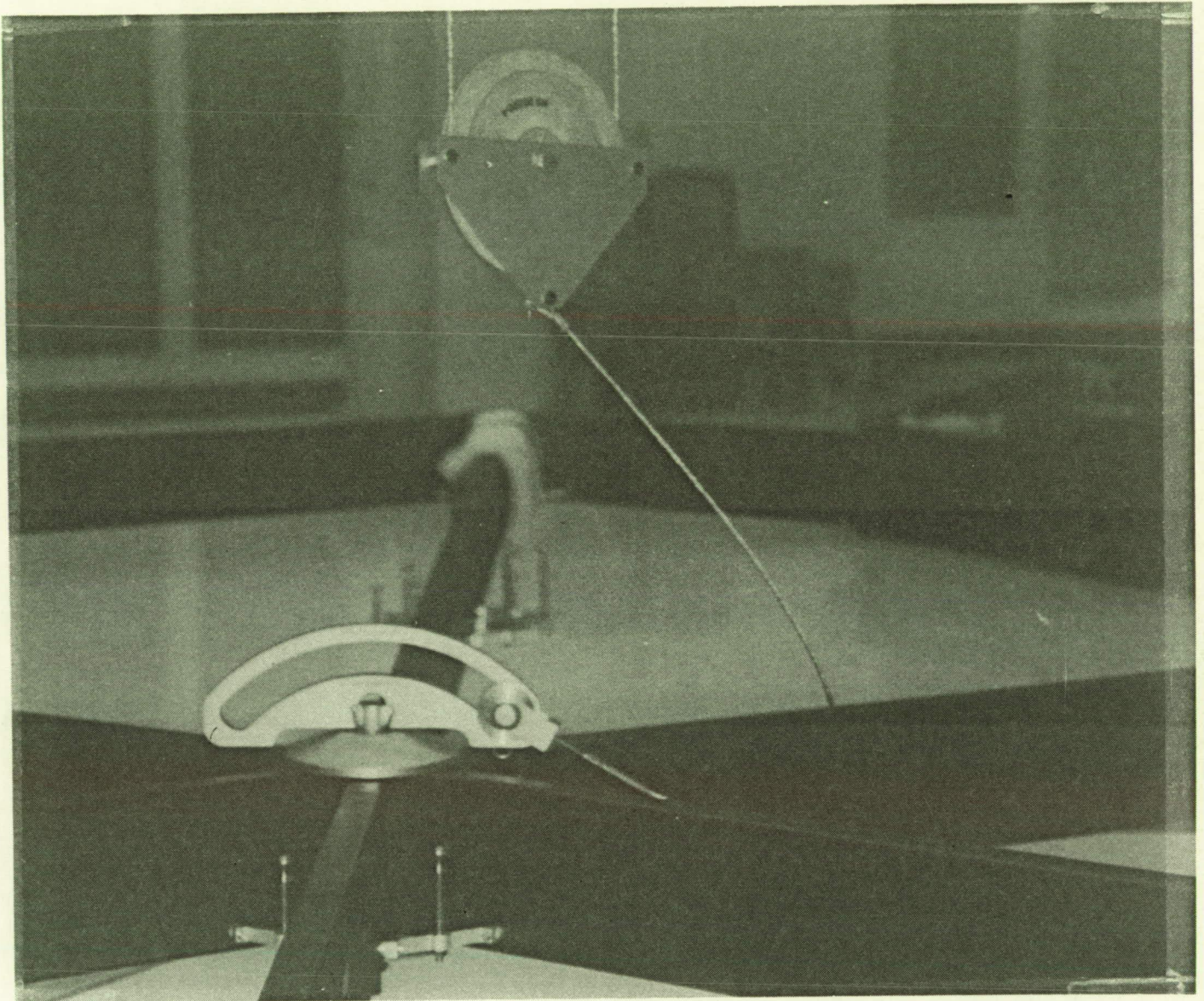


Figure 4.3-1. The Hexagonal Panel Interfaces With The Counterbalance Cable Through A Pseudo Three Degree Of Freedom Rotational Device

the cable interface to swivel. The swivel has a slot in the shape of an arch in which the cable end fitting is allowed to roll on a bearing. The arch is defined radially from the center of gravity of the panel. Thus, as the cable rotates and moves along the arch, the line of action of the counterbalance load is through the center of gravity of the panel. This can be seen in Figures 4.3-2 and 4.3-3.

With two people supporting the panel at floor level the weight canister is attached to the free end of the counterbalance cable. The canister contains enough lead shot equal to .5 times the panel weight. The pulleys on the cable trolley and the pulley above the panel provide a two to one mechanical advantage. Lead shot is then added or subtracted from the canister until the panel is free floating. Stick on weights are attached to the hexagonal panels to compensate for corners that do not contain latches or where facets are not being used. These weights are added until the panel is both free floating and parallel to the floor. This insures that the cable is supporting the load through the center of gravity of the panel.

The central panel support fixture is now assembled and placed in the center of the PSF facility. A plumb bob is dropped from the center of the panel and another plumb bob is dropped from the point of the hexagon that points toward panel number eight. Panel one is then mounted to the central panel support structure. With the panel on the fixture it is moved until the plumb bobs align with their appropriate mark on the floor and the central panel support fixture is mounted to the floor.



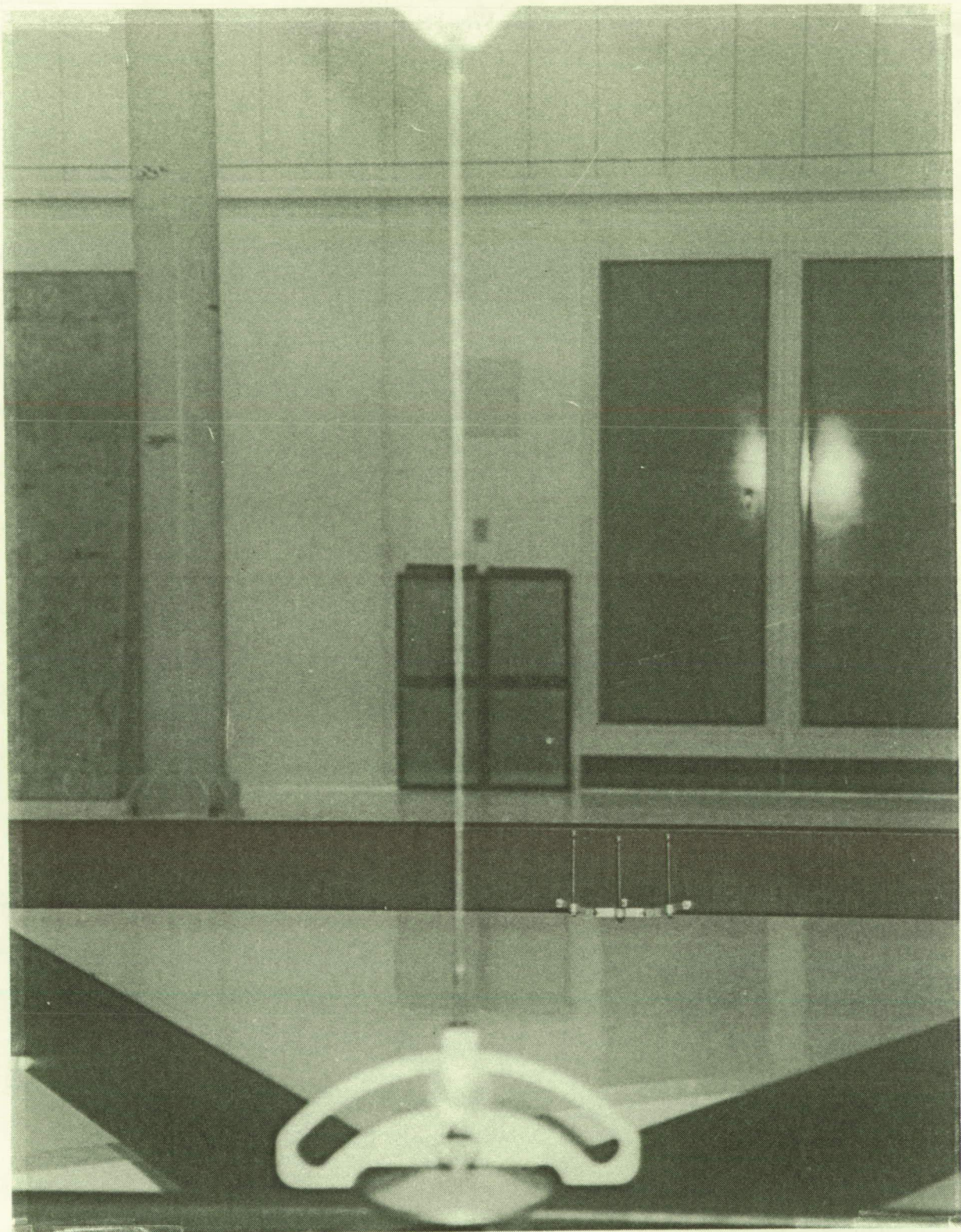


Figure 4.3-2. The Cable Is Tensioned After Being Attached To The Hexagonal Panel. The Arch Of The Slot Forces The Line Of Action Of The Cable through the Center Of Gravity Of The Panel.



ORIGINAL PAGE  
BLACK AND WHITE PHOTOGRAPH



Figure 4.3-3. The Slotted Metallic Part Shown In The Picture Is Mounted To A Bearing Which Allows The Part To Rotate For Compound Angles As Seen Above



Panel two is attached to its designated cable and counterbalanced in the same manner as panel one. Panel two is then latched into place to panel one. This process is repeated for panels three through nineteen until the completed concentrator is in the assembly position.

To place the concentrator in the optical scanning position, the corners of panel twelve and sixteen are attached to a pulley and winch system on the two tall tooling towers. The pulleys and cables at the top of the tower can be seen in Figure 4.1-15 in the previous section. With the concentrator restrained by safety ropes and four people, the central support stand is removed. The winches are used to slowly raise the concentrator into the optical scanning position. Once in the scanning position the concentrator is locked in place using the ball and socket fittings shown in Section 4.1. This completes the assembly of the concentrator and places it in a position to start the structural and optical repeatability testing. The tests will be described in detail in Section 5.0.

## 5.0 TESTING

A series of three repeatability tests were conducted to validate the Truss Hex Concentrator design. In essence, the objective of this testing was to verify that the concentrator can be assembled and aligned on earth and the structure can be reassembled on-orbit and maintain the as-built contour and optical characteristics.

### 5.1 Seven Panel 1-G Repeatability Test

A seven panel 1-G test was conducted to gather repeatability data and to evaluate the latches and assembly process before full unit testing. Although the spaceborne concentrator will never see this condition on-orbit, it was analyzed and the structure proofloaded to this load for testing purposes. In addition to the repeatability data gathered in the seven panel test, it provided a significant amount of insight into assembly techniques, additional tooling, and design improvements required to progress the design to maturity. The quick test provided valuable experience for subsequent Space Station Freedom activities and the SCAD full up test as well.

A finite element model of a panel verified that it will exhibit insignificant warpage under its own weight and can be assumed a rigid body. Therefore, each panel was equipped with only 3 targets that define the plane of the panel. The seven inner panels and their target locations are shown in Figure 5.1-1. A schematic of a target is shown in Figure 5.1-2.

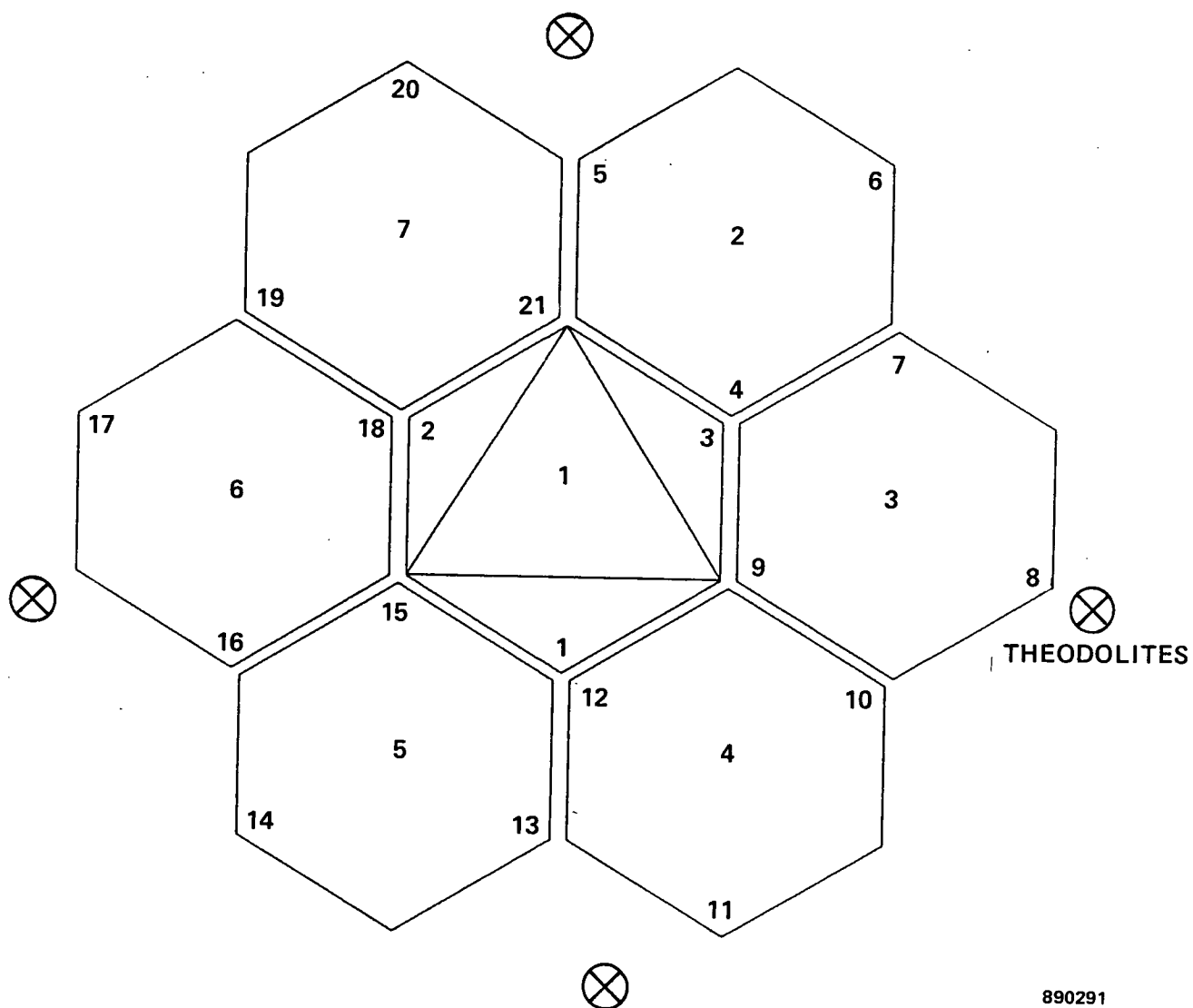


Figure 5.1-1. The Seven Panel Structural Repeatability Target Locations, Panel Numbers and Theodolite Locations Are Shown Above

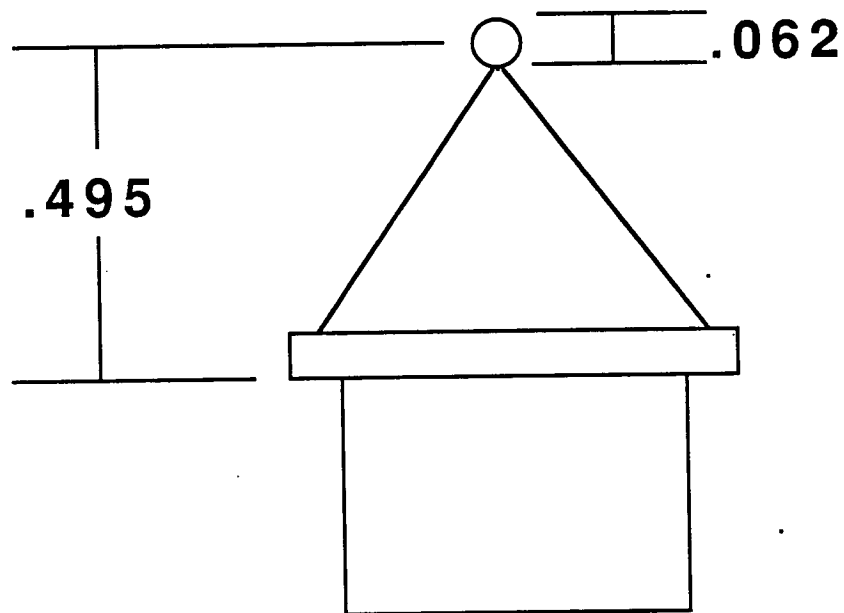


Figure 5.1-2. Tooling Target Used To Define The Location Of The Hexagonal Panel. Three Targets Were Placed On Each Panel To Define A Plane And Measure Rotational Variations.



The locations of the targets were determined with the Harris Theodolite measurement system. The raw data from the theodolites is fed into DAMS, an interactive Harris software tool, which performs a simultaneous coordinate transformation and regression. The data is transformed from the arbitrary theodolite coordinate system into a user defined coordinate system. A regression or "best fit" technique is used in which the error between data sets is minimized. The entire process consists of finding the set of translations and rotations required to convert the measured coordinates from the theodolite system to the user's system, such that the error between the regressed coordinate sets is minimized. This is called "best fit" of the two data sets. Refer to Appendix E for a more detailed explanation of the data manipulation process.

#### 7-Panel Test Procedure

- o Locate theodolites as shown in Figure 5.1-1
- o Calibrate theodolites
- o Shoot targets with theodolites
- o Disassemble concentrator
- o Reassemble concentrator
- o Reshoot targets with theodolites
- o Disassemble concentrator
- o Reassemble concentrator
- o Let concentrator set overnight
- o Reshoot targets with theodolites

### 7-Panel Results Analysis

The regressed theodolite data is shown in Figure 5.1-3. The theodolite data was regressed under the assumption that the targets on the central panel are fixed since it is attached to the support framework which is bolted to the concrete floor. Target 1 was chosen as the reference coordinate system origin. The X axis was directed through target 3 and target 2 was used to define the xy plane; thus, the Z axis is directed normal to panel 1 (vertical) and perpendicular to the gravitational field.

The theodolite data was transformed into rotational data for comparison to the SCAD repeatability requirements. The panel rotations were extracted by comparing the panel normal vector, that is normal to the plane defined by the three panel targets, with that of each successive iteration. The process is shown in Figure 5.1-4 and the resulting rotational data in Figure 5.1-5.

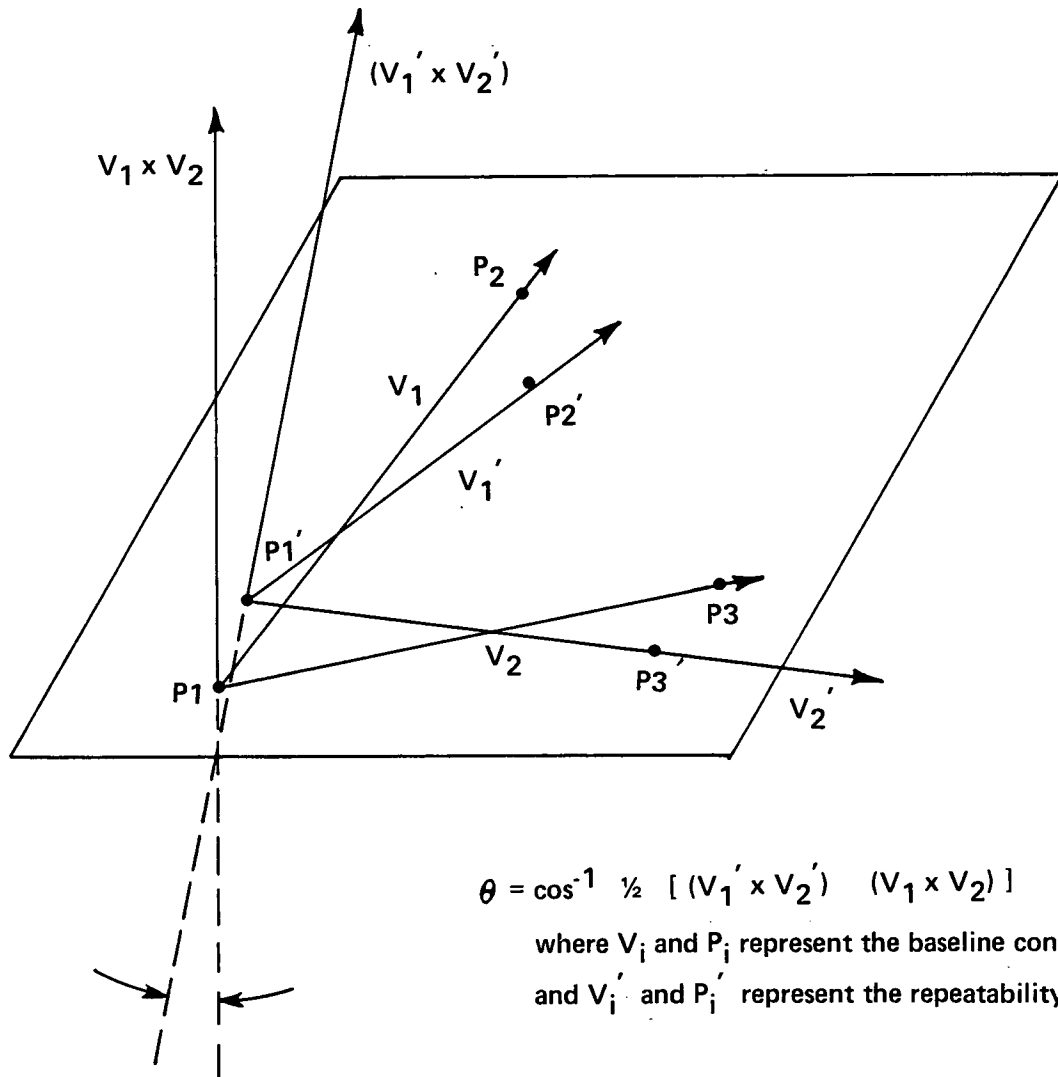
The three sets of rotational data in Figure 5.1-5 fall well below the hexagonal panel repeatability error budget of 1.25 milliradians. The rotational error between data sets 1 and 2 is greatest of the three cases generated. This error is attributed to settling in latch assemblies caused by 1-G loads. The striker plates on the latches were liquid shimmed with epoxy to help minimize motion; however, thread tolerances in the striker ball shafts were not reduced to zero before this test. After the test was completed, it was observed that the striker balls were rotating. This rotation was stopped by liquid shimming the striker ball stud with Loctite to provide the zero tolerance fit.

	X <sub>1</sub>	Y <sub>1</sub>	Z <sub>1</sub>	X <sub>2</sub>	Y <sub>2</sub>	Z <sub>2</sub>	R <sub>X12</sub>	R <sub>Y12</sub>	R <sub>Z12</sub>
1	0.0000	0.0000	0.0000	0.0000	0.0000	0.0000	0.0000	0.0000	0.0000
2	69.1020	119.6371	0.0000	69.1003	119.6307	0.0000	-0.0017	-0.0064	0.0000
3	138.1482	0.0000	0.0000	138.1412	0.0000	0.0000	-0.0070	0.0000	0.0000
4	148.5428	-0.0020	0.8522	148.5291	-0.0035	0.8554	-0.0137	-0.0015	0.0032
5	216.6569	119.6344	12.4956	216.6347	119.6251	12.5372	-0.0222	-0.0093	0.0416
6	284.7743	-0.0080	23.7328	284.7513	-0.0064	23.7921	-0.0230	0.0016	0.0593
7	211.9340	-48.0100	12.3502	211.9202	-48.0150	12.3633	-0.0138	-0.0050	0.0131
8	142.4089	-166.8176	24.0039	142.3927	-166.8172	23.9808	-0.0162	0.0004	-0.0231
9	74.2623	-48.8776	0.9896	74.2574	-48.8759	0.9806	-0.0049	0.0017	-0.0090
10	64.3481	-127.7600	12.6532	64.3409	-127.7636	12.6228	-0.0072	-0.0036	-0.0304
11	-73.3463	-126.9585	23.8680	-73.3494	-126.9614	23.8108	-0.0031	-0.0029	-0.0572
12	-5.1878	-8.9886	0.8590	-5.1864	-8.9884	0.8484	0.0014	0.0002	-0.0106
13	-78.4919	-39.8761	12.3497	-78.4895	-39.8824	12.3180	0.0024	-0.0063	-0.0317
14	-146.5878	79.7526	23.9026	-146.5937	79.7412	23.8553	-0.0059	-0.0114	-0.0473
15	-10.3512	79.7696	1.0060	-10.3558	79.7618	1.0018	-0.0046	-0.0078	-0.0042
16	-73.7393	127.8170	12.5872	-73.7417	127.8073	12.5685	-0.0024	-0.0097	-0.0187
17	-4.1412	246.6485	23.7418	-4.1535	246.6340	23.7518	-0.0123	-0.0145	0.0100
18	63.9160	128.6313	0.8701	63.9110	128.6245	0.8719	-0.0050	-0.0068	0.0018
19	73.8306	207.5628	12.2962	73.8176	207.5535	12.3224	-0.0130	-0.0093	0.0262
20	211.4907	206.7560	23.7959	211.4694	206.7394	23.8650	-0.0213	-0.0166	0.0691
21	143.3748	88.7430	0.9538	143.3638	88.7400	0.9751	-0.0110	-0.0030	0.0213

	X <sub>1</sub>	Y <sub>1</sub>	Z <sub>1</sub>	X <sub>3</sub>	Y <sub>3</sub>	Z <sub>3</sub>	R <sub>X13</sub>	R <sub>Y13</sub>	R <sub>Z13</sub>
1	0.0000	0.0000	0.0000	0.0000	0.0000	0.0000	0.0000	0.0000	0.0000
2	69.1020	119.6371	0.0000	69.0923	119.6396	0.0000	-0.0097	0.0025	0.0000
3	138.1482	0.0000	0.0000	138.1406	0.0000	0.0000	-0.0076	0.0000	0.0000
4	148.5428	-0.0020	0.8522	148.5289	0.0029	0.8615	-0.0139	0.0049	0.0093
5	216.6569	119.6344	12.4956	216.6337	119.6275	12.5165	-0.0232	-0.0069	0.0209
6	284.7743	-0.0080	23.7328	284.7570	0.0017	23.7768	-0.0173	0.0097	0.0440
7	211.9340	-48.0100	12.3502	211.9257	-48.0029	12.3670	-0.0083	0.0071	0.0168
8	142.4089	-166.8176	24.0039	142.3933	-166.8118	23.9981	-0.0156	0.0058	-0.0058
9	74.2623	-48.8776	0.9896	74.2535	-48.8761	0.9912	-0.0088	0.0015	0.0016
10	64.3481	-127.7600	12.6532	64.3413	-127.7651	12.6452	-0.0068	-0.0051	-0.0080
11	-73.3463	-126.9585	23.8680	-73.3545	-126.9598	23.8369	-0.0082	-0.0013	-0.0311
12	-5.1878	-8.9886	0.8590	-5.1849	-8.9892	0.8598	0.0029	-0.0006	0.0008
13	-78.4919	-39.8761	12.3497	-78.4906	-39.8779	12.3317	0.0013	-0.0018	-0.0180
14	-146.5878	79.7526	23.9026	-146.5953	79.7455	23.8581	-0.0075	-0.0071	-0.0445
15	-10.3512	79.7696	1.0060	-10.3595	79.7649	0.9924	-0.0083	-0.0047	-0.0136
16	-73.7393	127.8170	12.5872	-73.7442	127.8111	12.5545	-0.0049	-0.0059	-0.0327
17	-4.1412	246.6485	23.7418	-4.1484	246.6401	23.7397	-0.0072	-0.0084	-0.0021
18	63.9160	128.6313	0.8701	63.9071	128.6308	0.8684	-0.0089	-0.0005	-0.0017
19	73.8306	207.5628	12.2962	73.8159	207.5687	12.3141	-0.0147	0.0059	0.0179
20	211.4907	206.7560	23.7959	211.4698	206.7504	23.8435	-0.0209	-0.0056	0.0476
21	143.3748	88.7430	0.9538	143.3616	88.7430	0.9684	-0.0132	0.0000	0.0146

	X <sub>2</sub>	Y <sub>2</sub>	Z <sub>2</sub>	Y <sub>3</sub>	X <sub>3</sub>	Z <sub>3</sub>	R <sub>X23</sub>	R <sub>Y23</sub>	R <sub>Z23</sub>
1	0.0000	0.0000	0.0000	0.0000	0.0000	0.0000	0.0000	0.0000	0.0000
2	69.1003	119.6307	0.0000	69.0923	119.6396	0.0000	-0.0080	0.0089	0.0000
3	138.1412	0.0000	0.0000	138.1406	0.0000	0.0000	-0.0006	0.0000	0.0000
4	148.5291	-0.0035	0.8554	148.5289	0.0029	0.8615	-0.0002	0.0064	0.0061
5	216.6347	119.6251	12.5372	216.6337	119.6275	12.5165	-0.0010	0.0024	-0.0207
6	284.7513	-0.0064	23.7921	284.7570	0.0017	23.7768	0.0057	0.0081	-0.0153
7	211.9202	-48.0150	12.3633	211.9257	-48.0029	12.3670	0.0055	0.0121	0.0037
8	142.3927	-166.8172	23.9808	142.3933	-166.8118	23.9981	0.0006	0.0054	0.0173
9	74.2574	-48.8759	0.9806	74.2535	-48.8761	0.9912	-0.0039	-0.0002	0.0106
10	64.3409	-127.7636	12.6228	64.3413	-127.7651	12.6452	0.0004	-0.0015	0.0224
11	-73.3494	-126.9614	23.8108	-73.3545	-126.9598	23.8369	-0.0051	0.0016	0.0261
12	-5.1864	-8.9884	0.8484	-5.1849	-8.9892	0.8598	0.0015	-0.0008	0.0114
13	-78.4895	-39.8824	12.3180	-78.4906	-39.8779	12.3317	-0.0011	0.0045	0.0137
14	-146.5937	79.7412	23.8553	-146.5953	79.7455	23.8581	-0.0016	0.0043	0.0028
15	-10.3558	79.7618	1.0018	-10.3595	79.7649	0.9924	-0.0037	0.0031	-0.0094
16	-73.7417	127.8073	12.5685	-73.7442	127.8111	12.5545	-0.0025	0.0038	-0.0140
17	-4.1535	246.6340	23.7518	-4.1484	246.6401	23.7397	0.0051	0.0061	-0.0121
18	63.9110	128.6245	0.8719	63.9071	128.6308	0.8684	-0.0039	0.0063	-0.0035
19	73.8176	207.5535	12.3224	73.8159	207.5687	12.3141	-0.0017	0.0152	-0.0083
20	211.4694	206.7394	23.8650	211.4698	206.7504	23.8435	0.0004	0.0110	-0.0215
21	143.3638	88.7400	0.9751	143.3616	88.7430	0.9684	-0.0022	0.0030	-0.0067

Figure 5.1-3. Regressed Theodolite Data From 7-Panel Test



890311

Figure 5.1-4. Comparison Of The Original Data Set For A Panel (P)  
 To The Second Data Set (P Prime) To Obtain The Rotational  
 Change Of The Hexagonal Panel



Deviation Of Hex Panel  
Normal Vector (Milliradians)  
From Measurement X To Measurement Y

Panel	X=1	X=1	X=2
<u>Number</u>	<u>Y=2</u>	<u>Y=3</u>	<u>Y=3</u>
1	0.000	0.000	0.000
2	0.421	0.254	0.204
3	0.254	0.163	0.093
4	0.339	0.240	0.108
5	0.312	0.243	0.168
6	0.209	0.250	0.075
7	0.395	0.274	0.122
Average	0.322	0.237	0.128

Assume worst case for error budget

Margin = Error Budget - Observed Error

= 1.250 - 0.421

= 0.829

Figure 5.1-5. Hexagonal Panel Error For The Three Measurement Sets Taken In the Seven Panel Structural Repeatability Test

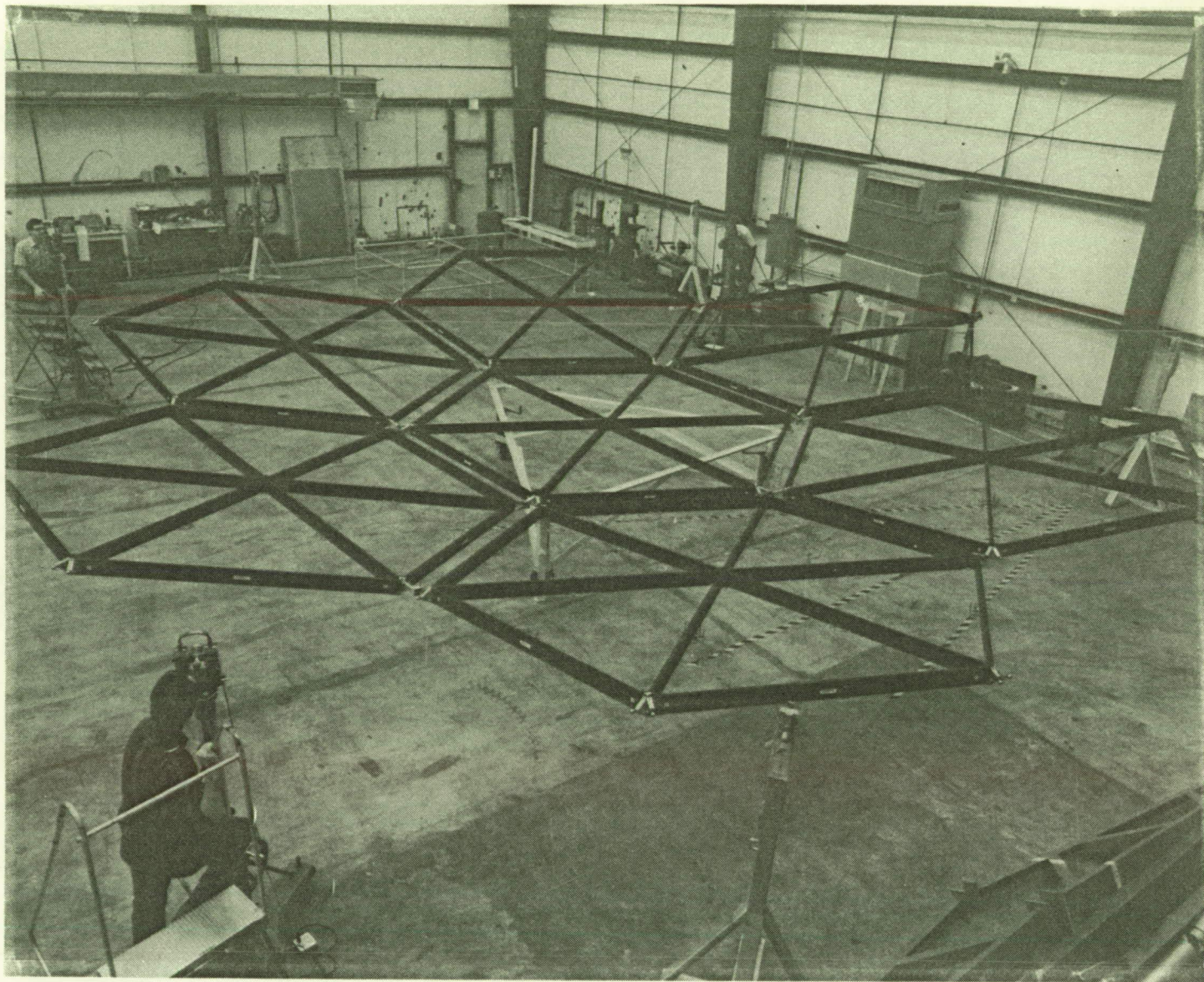
The reduced error exhibited between data sets 2 and 3 and 1 and 3 is attributed to this settling action. The 24 hour pseudo creep test shown between data sets 2 and 3 eliminates short term setting effect caused by the loose strikers. The seven panel test setup is shown in Figure 5.1-6.

## 5.2 Nineteen Panel (Counterbalanced) Structural and Optical Repeatability Testing

The simulated 0-G testing was performed on the counterbalanced nineteen panel concentrator. The testing consisted of two phases: a structural repeatability test and an optical repeatability test. The structural repeatability phase was performed on the 19 panel counterbalanced model in the same manner as the seven panel 1-G test. The optical repeatability phase was performed using the laser scanner described in the previous section.

The laser provided a light source parallel to the optical axis of the concentrator that was reflected off the facets and back to the focal point. In the initial optical test, the reflected ray was centered on an opaque grid located at the focal plane by adjusting the facets with the standoffs as previously described. The optical repeatability was quantified by comparing the movement of the spot before and after the concentrator was disassembled and reassembled. The reflected ray is monitored with a video camera located behind the opaque grid which is located at the focal plane. An optical testing schematic is shown in Figure 5.2-1.

ORIGINAL PAGE  
BLACK AND WHITE PHOTOGRAPH



ORIGINAL PAGE IS  
OF POOR QUALITY

Figure 5.1-6. Seven Panel Structural Repeatability Test Performed  
At Harris Corporation In Palm Bay, Florida

## FACET ADJUSTMENT AND ALIGNMENT SCHEMATIC

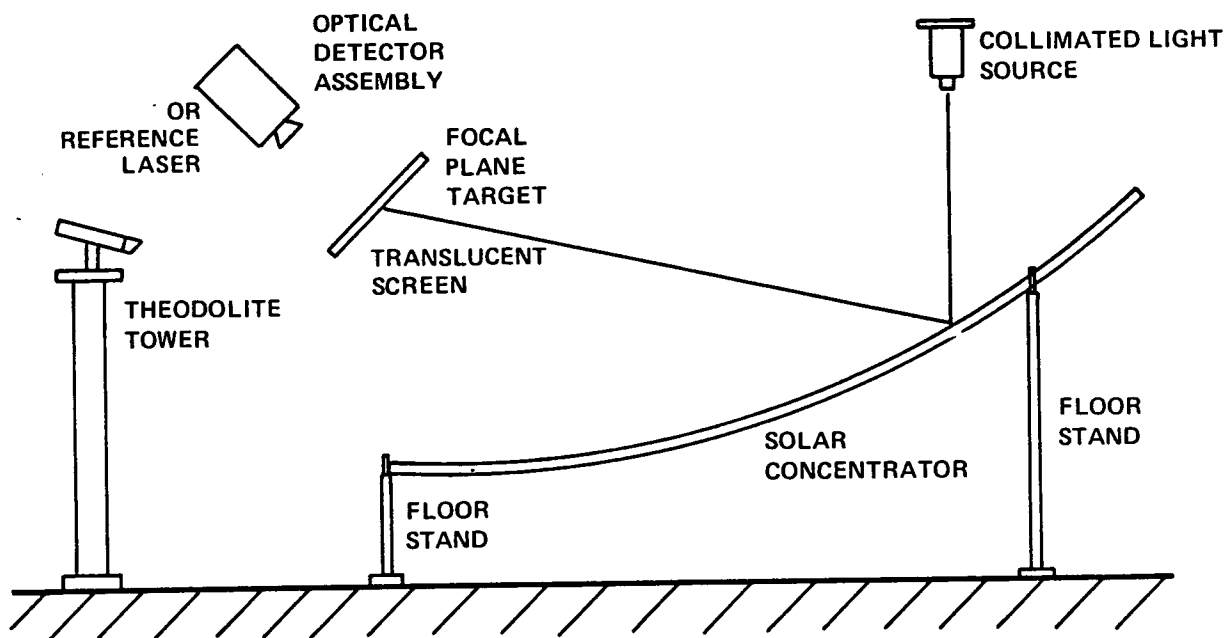


Figure 5.2-1. Optical Test Schematic For The Nineteen Panel Optical Repeatability Test



#### Nineteen Panel (Counterbalanced) Test Procedure

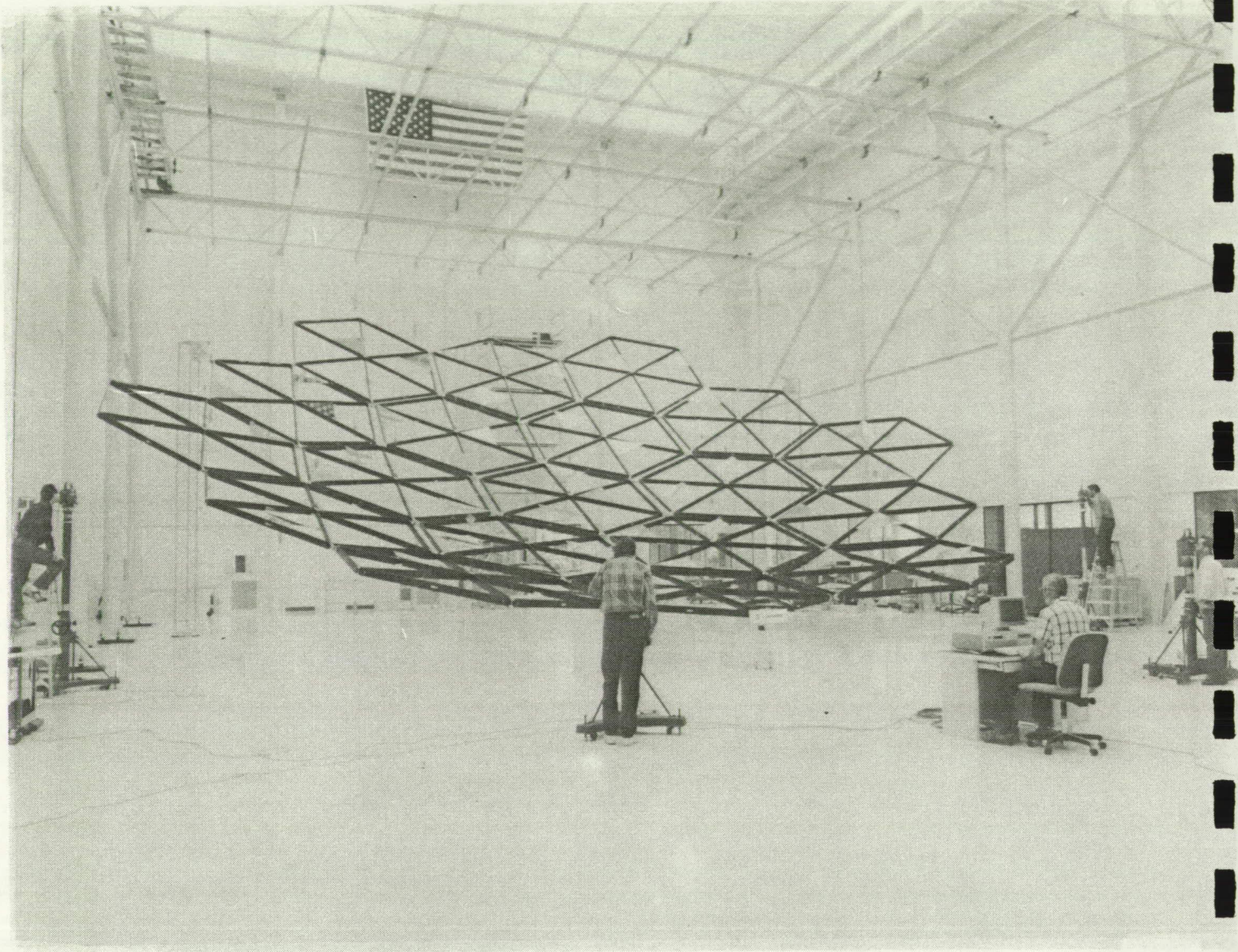
The 19 hex panels were counterbalanced and assembled in the assembly position. (In the assembly position the central panel is attached to the central support fixture which holds it parallel to the floor and the outer two rings are placed around it. This is the same position that the seven panel 1-G testing was conducted.)

Then, the concentrator is rotated into the scan position, shown in Figure 5.2-2. The scan position locates the concentrator such that the optical boresight is vertical or directrix of the parent paraboloid is parallel to the floor. The concentrator is attached at three tower points. These points not only keep the concentrator in the desired testing orientation, they provide stiffness to simulate the delta frame on the flight concentrator. All testing was performed in the scan position.

With the concentrator in the scan position, testing is conducted as follows:

- o Move laser beam to facet center.
- o Adjust facet with standoffs using the laser scanner, until the reflected beam strikes the focal plane grid at the center as shown in 5.2-3.
- o Take a picture of the video monitor to record data. (Shown in Figure 5.2-4)
- o Locate theodolites as shown in Figure 5.2-5

ORIGINAL PAGE  
BLACK AND WHITE PHOTOGRAPH

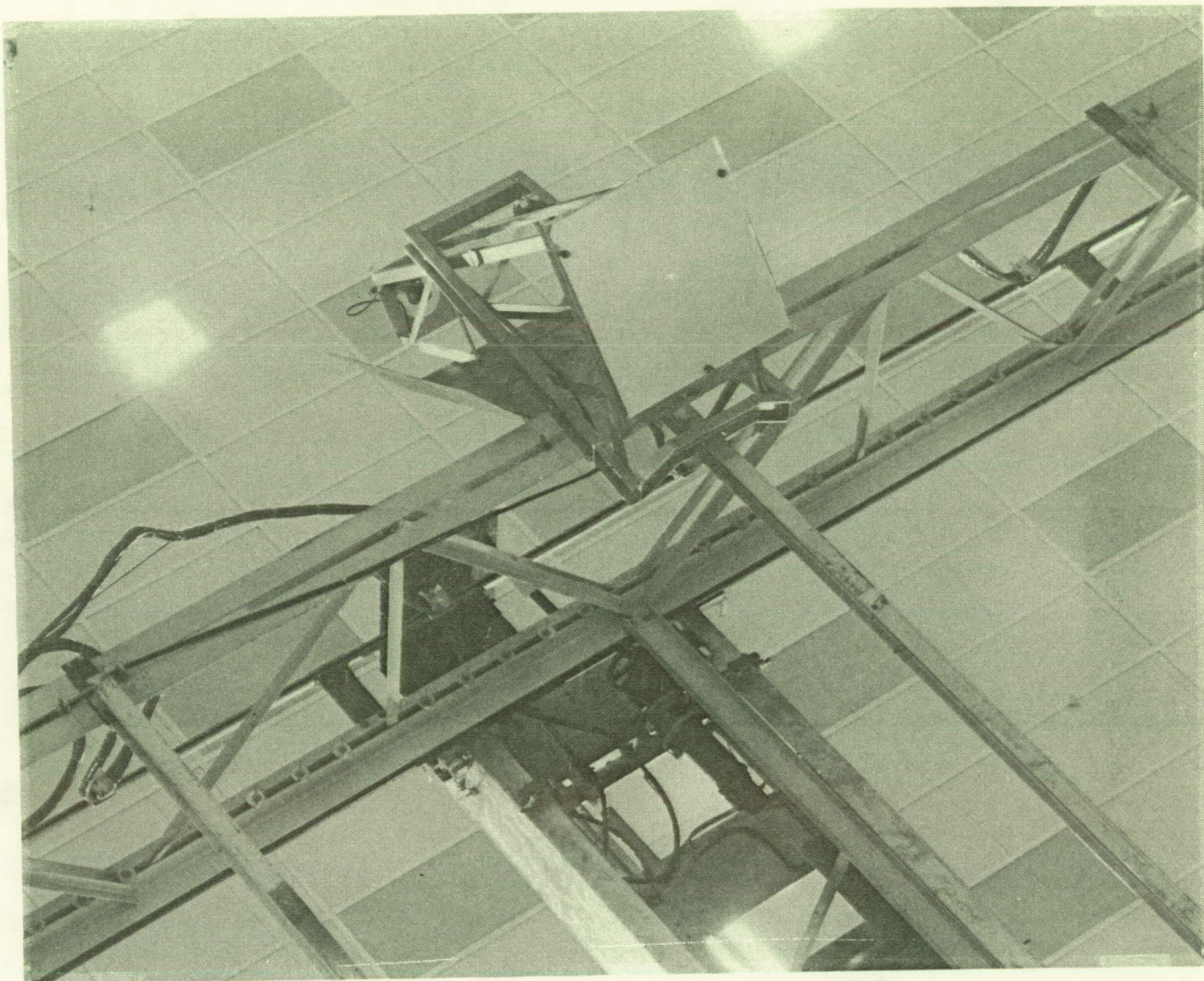


ORIGINAL PAGE IS  
OF POOR QUALITY

Figure 5.2-2. Solar Concentrator Advanced Development Concentrator Rotated Up To The Optical Scan Position. Harris Engineers and Technicians Are Measuring The Concentrator Using The Theodolite System As Part Of The Structural Repeatability Test.



ORIGINAL PAGE  
BLACK AND WHITE PHOTOGRAPH



ORIGINAL PAGE IS  
OF POOR QUALITY

Figure 5.2-3. The Facet Is Adjusted Until The Reflected Image Of The  
Laser Beam Intersects The Center Of The Receiver Aperture Target  
Located At The Focal Point Of The Concentrator



ORIGINAL PAGE  
BLACK AND WHITE PHOTOGRAPH

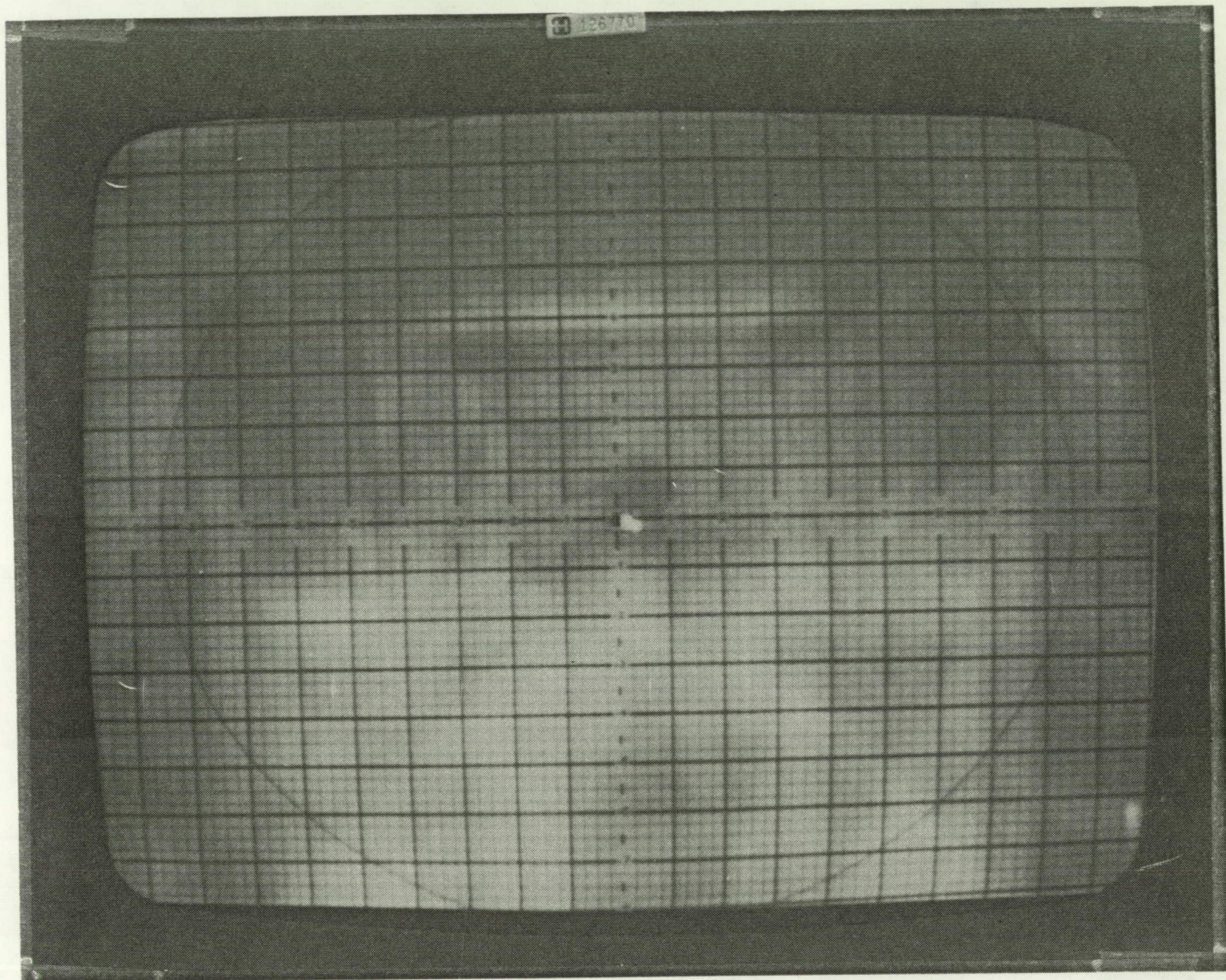


Figure 5.2-4. Picture Of The Television Monitor Which Receives The Signal From The Camera Behind The Aperture Target. This Is The Image Seen On The Ground From Figure 5.2-3.



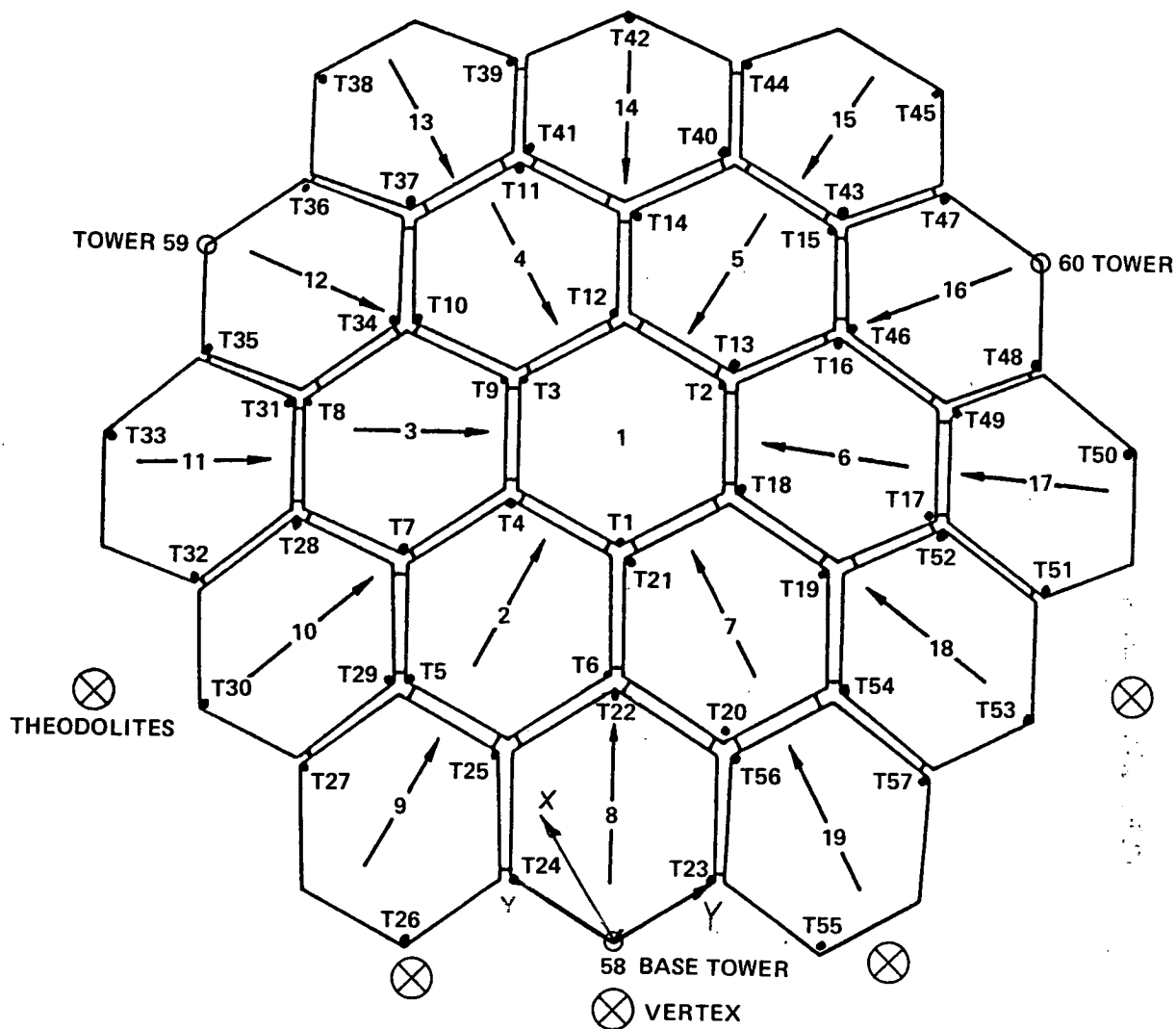


Figure 5.2-5. Shows The Theodolite Placement For The Measurement Of The Concentrator During The Optical/Structural Repeatability Test. The T-Numbers Correspond To The Three Targets Per Hexagonal Panel Used To Define The Plane and Location Of That Panel.

- o Calibrate theodolites.
- o Shoot targets with theodolites.
- o Slew concentrator to assemble position.
- o Disassemble concentrator.
- o Reassemble concentrator.
- o Rotate back to scan position.
- o Reshoot targets with theodolites.
- o Rescan mirrors with laser and record data with photo.

#### 0-G Results Analysis

The structural repeatability analysis for the 19 panel (counter-balanced) testing was identical to the seven panel 1-G testing. The target locations, theodolite locations, and reference coordinate system are shown in Figure 5.2-5 and the regressed theodolite data is shown in Figure 5.2-6. The resulting rotational data is shown in Figure 5.2-7. The reference coordinate system is generated by assuming the three tower attachment points fixed. The origin is located at the base tower (target 58), the x axis runs through target 59; and target 60 determines the xy plane.

The optical repeatability test is, in essence, a structural repeatability test. In addition to quantifying the repeatability of the panels and latching system, the optical repeatability test establishes the alignment stability of the facet and the facet mounting hardware. In this test, the facet alignment error was measured using a small optical quality mirror at the facet center. This allowed the laser to be more accurately measured by removing beam spreading due to facet surface specularities.

(INCHES)

	X <sub>1</sub>	Y <sub>1</sub>	Z <sub>1</sub>	X <sub>2</sub>	Y <sub>2</sub>	Z <sub>2</sub>	R <sub>X12</sub>	R <sub>Y12</sub>	R <sub>Z12</sub>
1	215.1408	124.3286	60.4084	215.1280	124.3332	60.3964	-0.0128	0.0046	-0.0120
2	284.2318	243.9691	60.2542	284.1774	243.9601	60.2469	-0.0544	-0.0090	-0.0073
3	353.3228	124.3368	60.2418	353.3010	124.3338	60.2373	-0.0218	-0.0030	-0.0045
4	279.0451	75.4552	59.5328	279.0372	75.4662	59.5371	-0.0079	0.0110	0.0043
5	210.9321	-42.5128	36.5115	210.9595	-42.5121	36.5149	0.0274	0.0007	0.0034
6	141.3542	76.2823	48.0319	141.3604	76.2825	48.0362	0.0062	0.0002	0.0043
7	288.9211	-3.4595	47.9985	288.9282	-3.4660	48.0054	0.0071	-0.0065	0.0069
8	426.5730	-2.6164	36.1067	426.6024	-2.6081	36.1149	0.0294	0.0083	0.0082
9	358.5228	115.3514	59.3838	358.5282	115.3439	59.3912	0.0054	-0.0075	0.0074
10	431.7904	84.4638	47.6533	431.7947	84.4647	47.6605	0.0043	0.0009	0.0072
11	499.8828	204.1194	35.8182	499.8800	204.1106	35.8266	-0.0028	-0.0088	0.0084
12	363.7047	204.1153	59.3236	363.6865	204.1061	59.3263	-0.0182	-0.0092	0.0027
13	289.3978	252.9639	59.3943	289.4004	252.9753	59.3993	0.0026	0.0114	0.0050
14	427.0766	252.1161	47.5275	427.0899	252.1266	47.5469	0.0133	0.0105	0.0194
15	357.4637	370.8936	35.8507	357.4518	370.8875	35.8688	-0.0119	-0.0061	0.0181
16	279.4938	331.8830	47.7040	279.4788	331.8777	47.7180	-0.0150	-0.0053	0.0140
17	141.7804	330.9807	36.2717	141.7765	330.9836	36.2997	-0.0039	0.0029	0.0280
18	209.9380	213.0698	59.4744	209.9478	213.0700	59.4736	0.0098	0.0002	-0.0008
19	136.6254	243.9406	47.8866	136.6444	243.9431	47.9049	0.0190	0.0025	0.0183
20	68.5601	124.2765	36.2855	68.5605	124.2758	36.2960	0.0004	-0.0007	0.0105
21	204.7721	124.3164	59.5408	204.7800	124.3137	59.5419	0.0079	-0.0027	0.0011
22	132.1775	76.4068	46.4448	132.1746	76.4068	46.4486	-0.0029	0.0000	0.0038
23	-1.6285	78.8822	11.9864	-1.6365	78.8733	11.9901	-0.0080	-0.0089	0.0037
24	67.4742	-40.7694	12.1949	67.4699	-40.7790	12.1970	-0.0043	-0.0096	0.0021
25	137.8306	-9.5949	34.4555	137.8354	-9.5909	34.4646	0.0048	0.0040	0.0091
26	72.6056	-122.6325	-11.0490	72.6088	-122.6327	-11.0490	0.0032	-0.0002	0.0000
27	208.8428	-125.9346	11.7410	208.8710	-125.9356	11.7552	0.0282	-0.0010	0.0142
28	353.3055	-49.5809	34.8010	353.3346	-49.5880	34.8232	0.0291	-0.0071	0.0222
29	215.1270	-49.5785	35.0951	215.1486	-49.5834	35.1106	0.0216	-0.0049	0.0155
30	284.1893	-164.2512	0.7981	284.2267	-164.2636	0.8124	0.0374	-0.0124	0.0143
31	430.6193	-9.5723	34.0319	430.6434	-9.5699	34.0255	0.0241	0.0024	-0.0064
32	359.5823	-125.9182	11.4871	359.6082	-125.9325	11.5109	0.0259	-0.0143	0.0238
33	495.7986	-122.5944	-11.4701	495.8247	-122.5988	-11.4699	0.0261	-0.0044	0.0002
34	436.2730	76.4366	46.1104	436.2964	76.4385	46.1202	0.0234	0.0019	0.0098
35	500.9433	-40.7289	11.7015	500.9753	-40.7318	11.6973	0.0320	-0.0029	-0.0042
36	570.0330	78.9511	11.3712	570.0504	78.9593	11.3825	0.0174	0.0082	0.0113
37	507.9103	124.3251	33.7635	507.9216	124.3259	33.7678	0.0113	0.0008	0.0043
38	638.2488	124.2791	-12.1004	638.2680	124.3041	-12.0957	0.0192	0.0250	0.0047
39	573.0922	243.9889	10.7379	573.1202	243.9973	10.7519	0.0280	0.0084	0.0140
40	434.7516	330.9039	34.3487	434.7751	330.9175	34.3644	0.0235	0.0136	0.0157
41	503.9048	211.2745	34.4033	503.8929	211.2688	34.4051	-0.0119	-0.0057	0.0018
42	568.5385	328.3917	-0.3170	568.5375	328.3848	-0.3121	-0.0010	-0.0069	0.0049
43	361.4662	377.8386	33.7497	361.4772	377.8395	33.7569	0.0110	0.0009	0.0072
44	497.6956	374.5190	10.7346	497.6772	374.4966	10.7434	-0.0184	-0.0224	0.0088
45	426.6049	490.7715	-12.0789	426.5920	490.7748	-12.0593	-0.0129	0.0033	0.0196
46	284.1848	339.7581	46.0943	284.1897	339.7575	46.1248	0.0049	-0.0006	0.0305
47	353.2056	454.3333	11.3983	353.2018	454.3171	11.4089	-0.0038	-0.0162	0.0106
48	215.0124	454.3113	11.6941	215.0045	454.2948	11.7108	-0.0079	-0.0165	0.0167
49	206.8460	377.8186	34.0999	206.8605	377.8166	34.1264	0.0145	-0.0020	0.0265
50	141.5475	490.7446	-11.5769	141.5090	490.6850	-11.5679	-0.0385	-0.0596	0.0090
51	70.5707	374.4438	11.4345	70.5796	374.4415	11.4458	0.0089	-0.0023	0.0113
52	133.5702	330.8705	34.8750	133.5615	330.8707	34.9008	-0.0087	0.0002	0.0258
53	-0.2657	328.2657	0.4912	-0.2522	328.2602	0.5024	0.0135	-0.0055	0.0112
54	64.5144	211.2089	34.8804	64.5224	211.2008	34.8934	0.0080	-0.0081	0.0130
55	-69.9462	124.2145	-11.2979	-69.9393	124.2045	-11.3051	0.0069	-0.0100	-0.0072
56	60.5293	124.2670	34.1877	60.5261	124.2639	34.2013	-0.0032	-0.0031	0.0136
57	-4.7555	243.8977	11.4786	-4.7553	243.8851	11.4787	0.0002	-0.0126	0.0001

RMS VALUES

X = 0.015      Y = 0.011      Z = 0.009

ORIGINAL PAGE IS  
OF POOR QUALITY

Figure 5.2-6.. Regressed Theodolite Data From The 19 Panel Test

Deviation Of Hex Panel  
Normal Vector (Milliradians)  
After Disassembly and Reassembly

<u>Panel</u>	<u>Slope Error (mR)</u>
1	0.055
2	0.021
3	0.008
4	0.069
5	0.109
6	0.217
7	0.112
8	0.020
9	0.072
10	0.055
11	0.253
12	0.084
13	0.112
14	0.190
15	0.134
16	0.178
17	0.177
18	0.160
19	0.167

Average                      0.115

Margin = 1.25 - 0.253

= .997

Figure 5.2-7. Rotational Change Of The Hexagonal Panels Following Disassembly and Re-assembly As Measured With The Theodolite System



The concept of surface specularity is shown in Figure 5.2-8. When using the Silverlux facets, the laser image spreads due to poor surface specularity as shown in Figure 5.2-9. It is difficult to determine the exact center location of the reflected laser image; therefore, the reliability of the data generated decreases. The optical quality mirrors placed in the center of the facet allows for an accurate assessment of the facet alignment repeatability error without including the local error introduced by poor surface specularity.

The rotational repeatability is determined by using the distance that the image moves on the focal plane and the distance the facet lies away from the focal point. The method used is shown in Figure 5.2-10 and the resulting repeatability data is shown in Figures 5.2-11 and 5.2-12. Since only 48 facets were produced, they were randomly scattered throughout the concentrator with two or three facets placed in each panel. A map of the facet locations is shown in Figure 5.2-13.

Ultimately, the performance of the concentrator will be judged on its delivery of the solar flux to the receiver. A plot of the intensity on the side wall of the receiver showing the theoretical pattern and the error induced pattern is shown in Figure 5.2-14. As Figure 5.2-14 shows the 0-G error is barely discernable in the flux intensity profile delivered to the receiver.

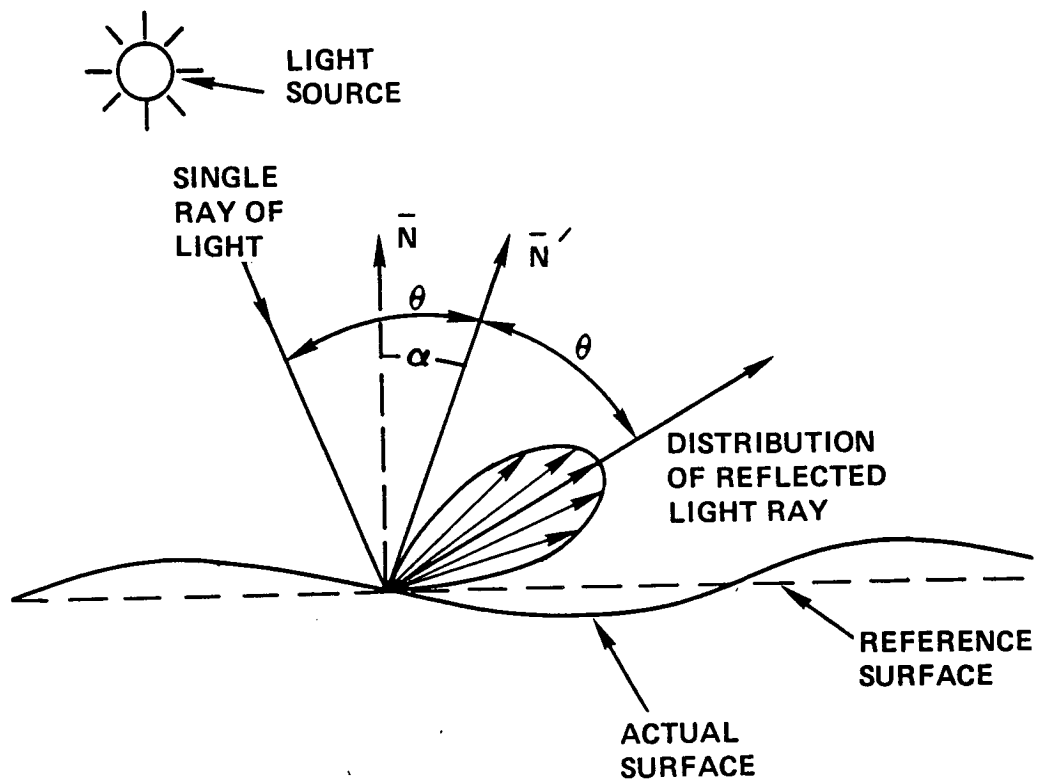
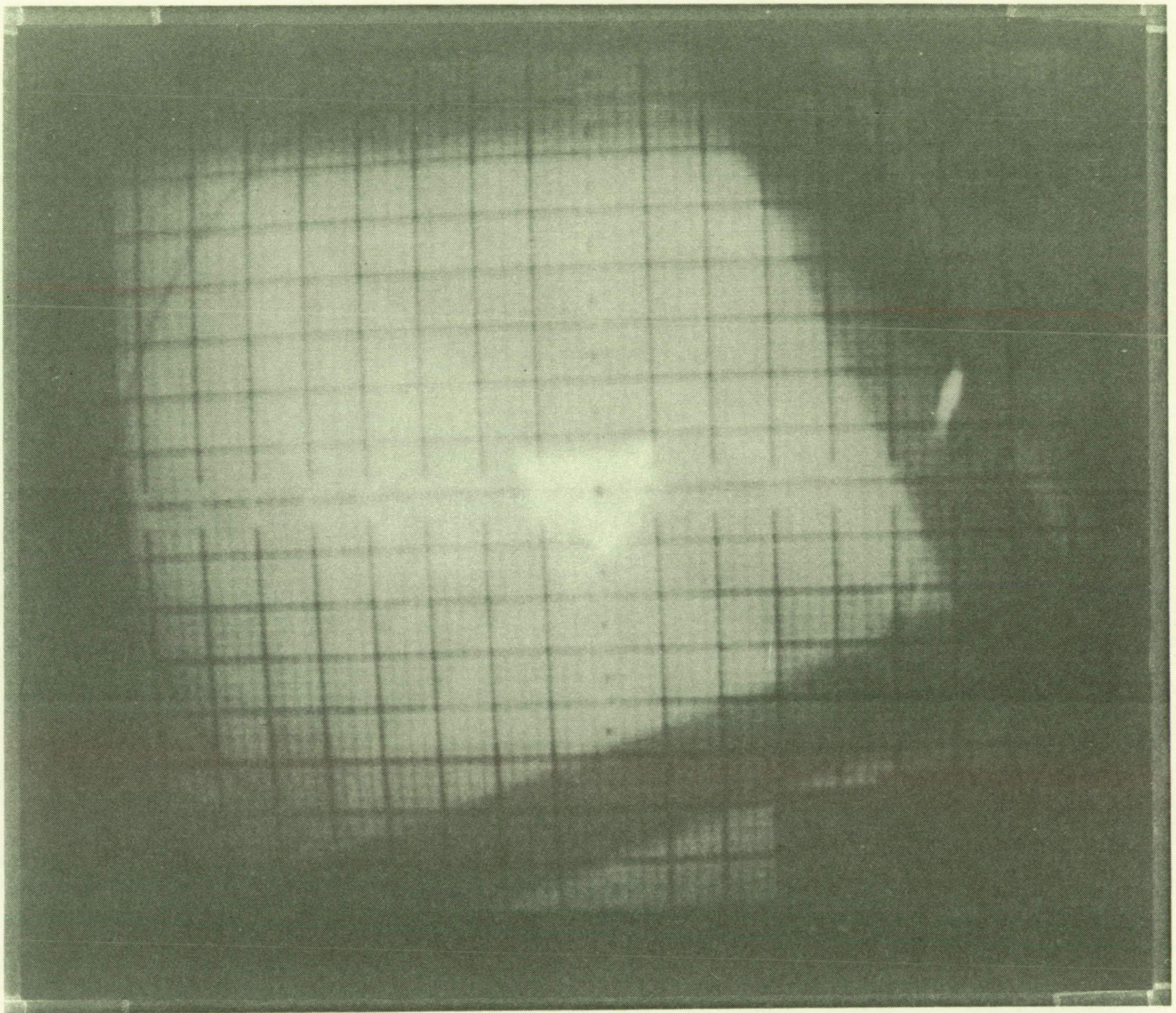


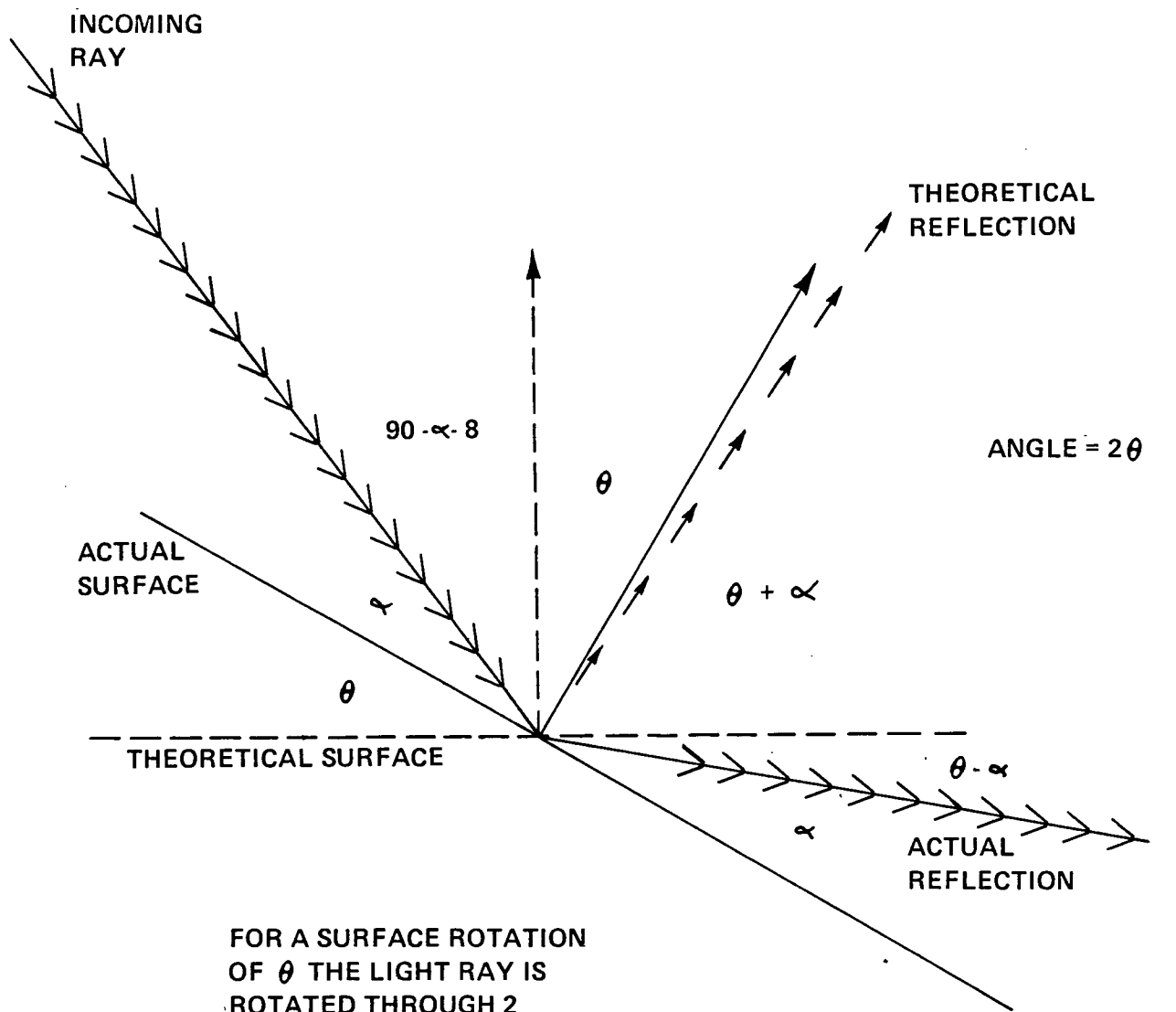
Figure 5.2-8. The Concept Of Specularity Is Shown Above. An Ideal Ray Would Reflect At  $N'$  If The Surface Was Flat And Specular. The Reflected Ray Has A Distribution Of Light That Is Not Perfect and Causes A Spreading Of The Image.

ORIGINAL PAGE  
BLACK AND WHITE PHOTOGRAPH



ORIGINAL PAGE IS  
OF POOR QUALITY

Figure 5.2-9. In Order To Obtain More Accurate Data For The Optical Repeatability Test Optical Mirrors Were Placed On The Facets To Reduce The Beam Spreading Seen Above. Figure 5.2-4 Shows The Image With The Mirrors.



890290

Figure 5.2-10. The Angular Change Of The Image On The Focal Plane Is Calculated By Knowing The Distance From The Facet To The Focal Plane and The Distance The Image Moves In The Focal Plane



## SCAD FACET ALIGNMENT DATA

PANEL	FACET	SCANNER X (COUNTS)	SCANNER Y (COUNTS)	CAMERA ERROR X	CAMERA ERROR Y	CAMERA TOTAL ERROR (INCHES)	DISTANCE FROM FOCAL POINT (INCHES)	SLOPE ERROR (MILLIRADIANS)
1	5	362434	448176	0	-.25	.250	442.89	.28
1	8	409384	388647	-.25	-.125	.280	425.43	.33
1	16	293422	432765	.125	0	.125	473.78	.13
2	7	590546	309847	0	0	0	378.65	0
2	11	518906	265520	.125	0	.125	401.78	.16
2	20	515319	382927	0	0	0	391.34	0
3	10	397965	157551	-.125	0	.125	461.56	.14
3	14	325607	200793	0	-.125	.125	480.44	.13
3	22	411976	287452	.250	0	.250	432.90	.29
4	5	221046	353665	-.125	0	.125	509.03	.13
4	7	286026	308308	0	-.250	.250	482.32	.26
4	12	204303	250748	0	.125	.125	529.03	.12
5	6	244565	527283	0	0	0	500.60	0
5	14	178017	482146	0	-.250	.250	532.18	.23
6	11	365112	548093	.125	-.125	.177	449.92	.19
6	17	324825	635392	.375	-.250	.451	480.44	.46
7	9	564412	454165	0	0	0	379.45	0
7	13	466506	454445	0	0	0	406.82	0
7	17	468646	541882	0	-.125	.125	412.78	.15
8	2	674413	388363	.250	.125	.279	357.00	.39
8	24	749383	433703	1.00	-1.00	1.414	352.20	2.01
9	14	629576	203824	0	-.125	.125	388.66	.16
9	21	699862	307265	.125	.125	.177	361.95	.24
10	4	502387	154112	.125	.250	.280	427.34	.32
10	8	580074	112459	.125	.125	.177	420.52	.21
11	18	335205	104444	-.50	-.375	.625	499.03	1.63
11	24	456415	63748	0	0	0	467.83	0
12	5	233916	168726	0	-.125	.125	527.94	.12
12	10	266854	67844	0	0	0	539.49	0
12	16	172383	155523	-.250	-.250	.354	563.27	.31
13	3	82168	218761	0	0	0	602.78	0
13	19	74257	305665	-.250	-.250	.354	596.77	.29
14	8	128882	387803	0	.250	.250	558.77	.23
14	13	52446	359136	.625	.350	3.555	606.02	2.93
14	19	72474	490430	0	0	0	594.78	0

Figure 5.2-11. Resulting Optical Repeatability Data From The SCAD Testing

SCAD FACET ALIGNMENT DATA  
(CONTINUED)

PANEL	FACET	SCANNER X (COUNTS)	SCANNER Y (COUNTS)	CAMERA ERROR X	CAMERA ERROR Y	CAMERA TOTAL ERROR (INCHES)	DISTANCE FROM FOCAL POINT (INCHES)	SLOPE ERROR (MILLIRADIANS)
15	3	79226	585793	0	0	0	599.62	0
15	19	87219	673095	-.250	-.625	.673	611.06	1.55 *
16	11	229350	639176	0	-.125	.125	524.84	.12
16	15	171809	679605	0	-.125	.125	563.27	.11
16	23	282501	725930	0	0	0	519.62	0
17	7	455213	772503	0	-.125	.125	467.83	.13
17	11	380672	730791	0	0	0	480.19	0
17	17	346485	814151	0	-.375	.375	519.23	.36
18	1	551972	681245	0	0	0	413.55	0
18	13	474066	640813	0	0	0	427.30	0
19	10	699746	529923	.250	.250	.354	361.95	.48
19	15	602446	589909	.125	.250	.280	385.99	.36
19	20	681003	661040	.250	.250	.354	387.82	.45

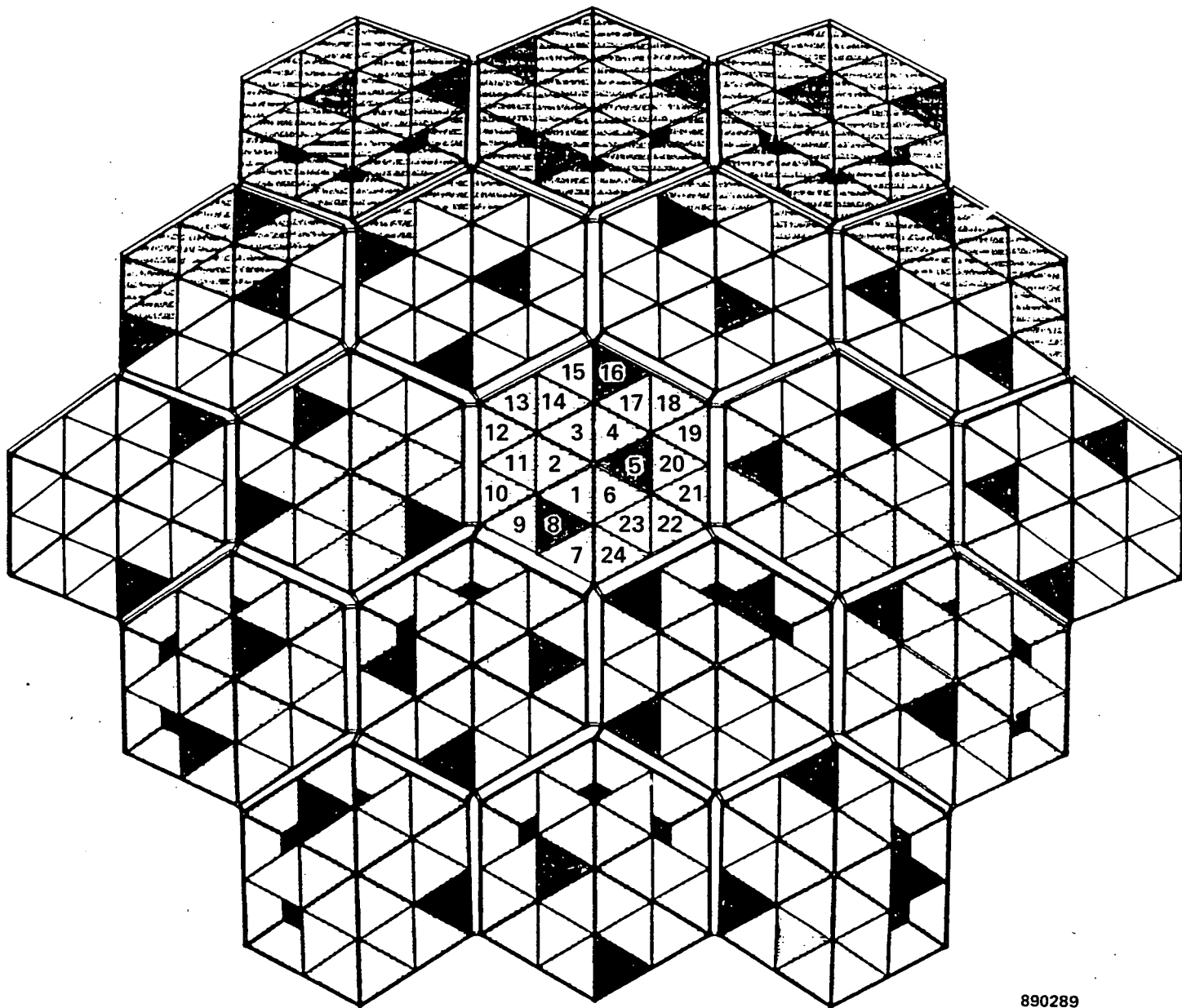
$$\text{SLOPE ERROR} = \frac{1}{2} \frac{\text{CAMERA TOTAL ERROR}}{\text{DISTANCE FROM FOCAL POINT}}$$

\* DATA POINT THROWN OUT

AVERAGE SLOPE ERROR = 0.159 MILLIRADIANS

1 INCH = 1273 COUNTS

Figure 5.2-12. Results Of Optical Repeatability Data From The SCAD Prototype Testing



890289

• VERTEX

Figure 5.2-13. Map Showing The Location Of The 48 Facets In The Concentrator. The Central Panel Denotes The Facet Numbers and Are The Same For The Remaining 18 Hexagonal Panels.

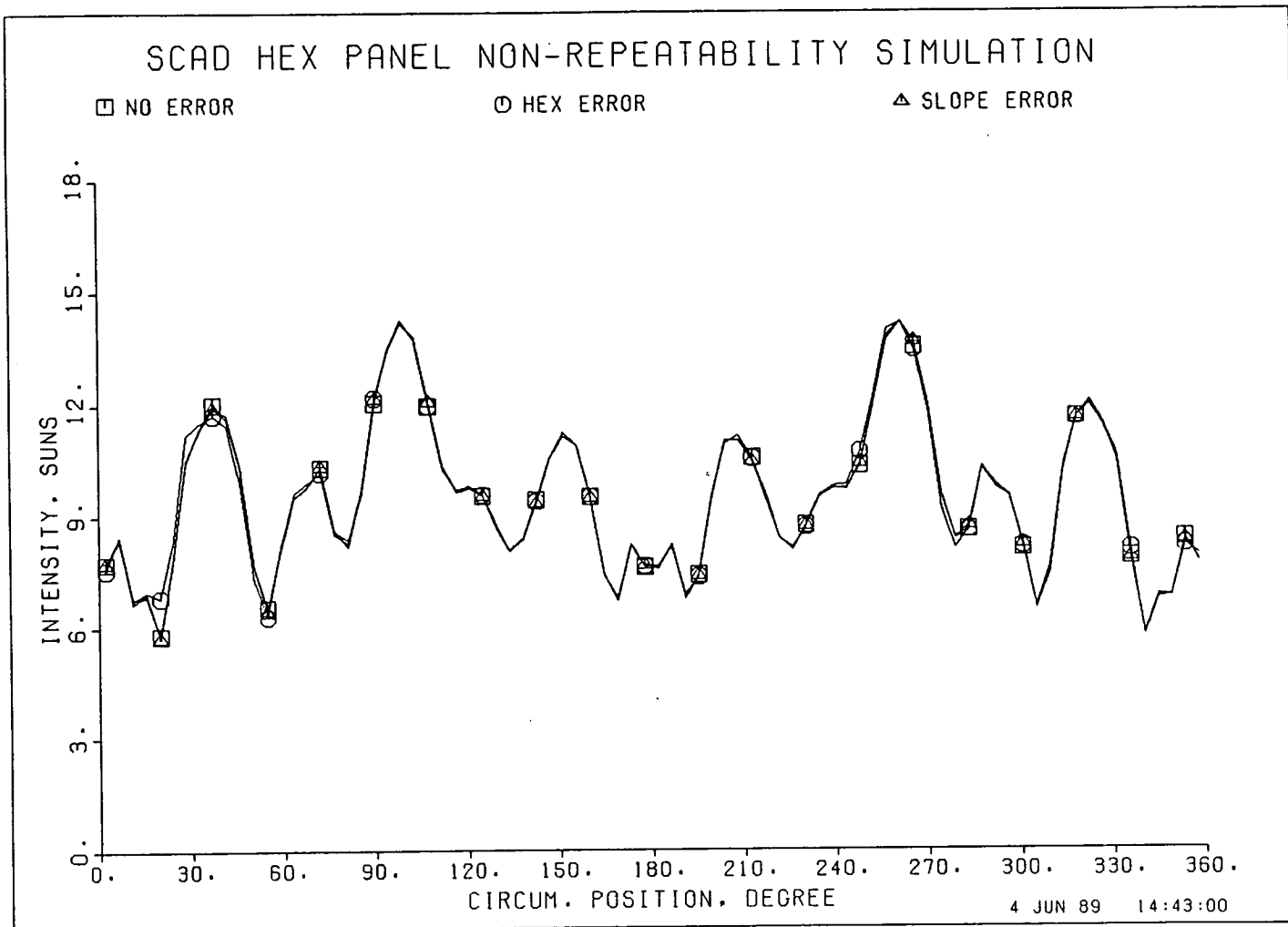


Figure 5.2-14. The Small Squares Are The Theoretical Circumferential Flux Distribution If All Facets Are Pointed Toward The Focal Point. The Small Circles Are The Comparison With The Hex Error Measured During The Optical Repeatability Test Applied To the Model. The Difference Is Negligible.



#### Nineteen Panel (Counterbalanced) Error Analysis

The optical repeatability data gathered on five of the facets fell outside the error range measured of the remaining facets. The five facets were investigated and the following anomalies were found.

##### Facet 24, Panel 8

This point showed a significant error that fell well out of the allowed error budget. This data point was particularly suspect due to the facet being located at the highest traffic point in the testing area. Further exploration showed the facet was wedged against the balancing weights attached to the panel beam. The weight was altered to free the facet. When this was done, the resulting image was centered with negligible error.

##### Facet 17, Panel 6 - Facet 19, Panel 15 - Facet 18, Panel 11

These three data points had relatively high errors. Although they were within the acceptable range, they were investigated for irregularities. All three facets had standoffs that were not seated properly in the facet. The inadequate pressure from the spring retaining clips to seat the facet was caused by the ball of the standoff being recessed too far into the facet. This can be corrected by controlling the thickness of the facet and the bond joints in the facet attachment hardware. A design improvement that would alleviate the need to tightly control the

facet is making the ball larger and allowing it to protrude further below the surface.

Facet 13, Panel 14

This data point exhibited an extremely large error. When the laser was moved back to the point to explore, the error appeared to be minimal; however, the tilt sensors had not been activated. When the tilt loop was activated, the scanner had to be moved an inch to get the beam into the center of the small mirror. The resulting image was that of the second testing sequence. As a result of this scenario, we concluded the tilt loop was not activated when this facet was initially adjusted.

THIS PAGE INTENTIONALLY BLANK

6.0 REFERENCES

1. "Space Station Work Package 4 Power System Final Draft, Conceptual Design Final Study Report", Harris Government Aerospace Systems Division, 19 December 1985, Rockwell International Contract No. R50PAB85560973, NASA Contract No. NAS3-24666.
2. O'Neill, Mark J., E-Systems Inc., "A Unique New Fresnel Lens Solar Concentrator", Silver Jubilee Congress of the International Solar Energy Society, Atlanta, GA, May 1979.
3. "Remotely-Controlled Docking System", NASA JSC Houston, NASA MSC-18969, 1984.
4. Solar Concentrator Advanced Development Technical/Management Proposal, Volume 1, Harris Government Aerospace systems Division, 2 May 1985, Response to NASA LeRC RFP2-171017, pp. 5-97 to 5-113.
5. O'Neill, M. J., "Solar Concentrator and Energy Collection System", U. S. Patent No. 4,069,812, 24 January 1978.
6. JSC 30000 Space Station Program Definition and Requirements, Section 3, Space Station System Requirements, Appendix 3.1, Natural Environment Design Requirements, January 1986.
7. L. J. Leger, "Oxygen Atom Reaction with Shuttle Materials at Orbital Altitudes", "NASA TM-58246, May 1982.
8. L. J. Leger, J. T. Visentine, and J. F. Kuminecz, "Low Earth Orbit Atomic Oxygen Effects on Surfaces", AIAA 22nd Aerospace Sciences Meeting, 1984, Paper No. 84-0548.
9. L. J. Leger, I. K. Spiker, J. F. Kuminecz, T. J. Ballantine, and J. T. Visentine, "STS Flight LEO Effects Experiment-Background Description and thin Film Experiments", AIAA Shuttle Environment and Operations Meeting, October 1983.
10. W. S. Slomp, B. Santos-Mason, G. F. Sykes, Jr., and W. G. Witte, Jr., "Effects of STS-8 Atomic Oxygen Exposure on Composites, Polymeric Films, and Coatings", AIAA 23rd Aerospace Sciences Meeting, 1985, Paper 85-0415.
11. J. T. Visentine, L. J. Leger, J. F. Kuminecz, and I. K. Spiker, "STS-8 Atomic Oxygen Effects Experiment", AIAA 23rd Aerospace Sciences Meeting, 1985, Paper 85-0415.
12. A. F. Whitaker, S. A. Little, R. J. Harwell, D. B. Griner, and R. F. DeHaye, "Orbital Atomic Oxygen Effects on Thermal Control and Optical Coatings", AIAA 23rd Aerospace Sciences Meeting, 1985, Paper No. 85-0416.



13. H. S. Rauschenbach, "Solar Cell Array Design Handbook", van Nostrand Reinhold, New York, NY, 1980, p. 411.
14. W. R. Hudson, et. al., NASA TM X-73598, 1977.
15. M. J. Mirtich and H. Mark, NASA TN D-3187, 1966.
16. F. Grum and G. W. Luckey, Applied Optics, 7, 2289 (1968).
17. Solar Concentrator Advanced Development Task 1 Final Report, Harris Government Aerospace Systems Division Contract NAS-3-24670, June 1986.
18. Solar Concentrator Advanced Development Preliminary Design Review Document, Harris Government Aerospace Systems Division Contract NAS-3-24670, 16 September 1986.
19. Solar Concentrator Advanced Development Critical Design Review Document, Harris Government Aerospace Systems Division, Contract NAS-3-24670, 27 January 1987.

APPENDIX A  
SCAD MIRROR FACET FINAL REPORT  
HERCULES CORPORATION

Document No. H241-12-20-006  
Date 22 December 1988

# **SOLAR CONCENTRATOR ADVANCED DEVELOPMENT (SCAD) COMPOSITE MIRROR FACET ASSEMBLIES**

Final Report

Prepared for

**HARRIS CORPORATION**  
Government Aerospace Systems Division  
Melbourne, Florida



Missiles, Ordnance and Space Group  
Bacchus Works • Magna, Utah 84044

## CONTENTS

<b>1</b>	<b>INTRODUCTION</b>	<b>1-1</b>
<b>2</b>	<b>SILVERLUX FACET DESIGN AND FABRICATION PROCESS DEVELOPMENT</b>	<b>2-1</b>
<b>3</b>	<b>SILVERLUX FACET PRODUCTION</b>	<b>3-1</b>
3.1	Objective	3-1
3.2	Facet Description	3-1
3.3	Manufacturing Processes	3-1
3.3.1	Back Skin Fabrication	3-1
3.3.2	Face Skin Fabrication	3-1
3.3.3	Honeycomb Core and Aluminum Insert Preparation	3-4
3.3.4	Facet Assembly	3-4
3.3.5	Manufacturing Process Discussion	3-4
3.4	Inspection Data	3-5
<b>4</b>	<b>IMPROVED SURFACE CLEANLINESS DEVELOPMENT PROGRAM</b>	<b>4-1</b>
4.1	Objectives/Background	4-1
4.1.1	Task I--Release Agent Transfer	4-1
4.1.2	Task II--Machining Contamination Control	4-2
4.1.3	Task III--Protective Coatings	4-3
4.1.4	Task IV--Handling and Shipping Criteria	4-4
4.2	Manufacturing Process Discussion	4-4
<b>5</b>	<b>OPTICAL TESTING</b>	<b>5-1</b>
5.1	Optical Requirements	5-1
5.2	Selection of Measurement Techniques	5-1
5.2.1	Total Hemispherical Reflectance	5-1
5.2.2	Specular Reflectance	5-1
5.2.3	Slope Error	5-1



## CONTENTS (Cont)

5.3	Specific Test Equipment	5-2
5.3.1	Devices and Services (D&S) SSR Total Hemispherical Reflectometer	5-2
5.3.2	D&S Portable Specular Reflectometer	5-2
5.3.3	Slope Error Equipment	5-2
5.4	Test Results	5-4
5.4.1	Total and Specular Reflectance	5-4
5.4.2	Slope Error Results	5-5
5.5	Conclusions	5-9
5.6	Data	5-9
6	CONCLUSIONS AND RECOMMENDATIONS	6-1
	Appendix A--Photos of Facet Assembly Process	A-1
	Appendix B--Slope Errors Measurement Photos	B-1

## FIGURES

1-1	Space station solar concentrator	1-2
1-2	Solar concentrator model showing 19 hex panel design	1-3
1-3	Typical facet	1-4
1-4	Single hex panel after assembly at Harris Corporation	1-5
3-1	Facet construction	3-2
3-2	SCAD facets manufacturing flow	3-3
4-1	Current bonding process for VDA facets	4-5
4-2	Schematic showing bonding setup used for assembly of VD type facets	4-7
5-1	Schematic of instrumentation used to determine slope error on a parabolic or spherical reflector	5-3
5-2	Change in reflection recorded at the viewplane when the ring target is displaced from the center of curvature	5-8

## TABLES

2-1	Aluminum Vapor Deposition	2-1
3-1	Facet Inspection Data	3-6
4-1	Specular Reflectance Achieved with Various Release Agents	4-1
4-2	Protective Coatings Summary	4-3
4-3	Reflectance Measurements Using Various Protective Coatings	4-4
5-1	Specular Reflectance and Total Hemispherical (Air Mass Zero Corrected) Reflectance Data for Composite Mirror Facets Tested under the SCAD Program	5-4
5-2	Sample Slope Error Distribution Calculation as Performed on Facet VDA-003; Measurements are Fractions of Total Facet Area Shadowed by the Indicated Ring Size; Average $\sigma$ Value for a Gaussian Distribution of Slope Error is Determined from the Data in the Second Table	5-5
5-3	Compilation of FL Measurements and Calculated $\sigma$ Values for Gaussian Distributions of Slope Error in SCAD Program Facets; Error Columns, FL ERR and $\sigma$ ERR, Have the Same Units as Preceding Columns; Analysis and Interpretation of Data is Given in the Text	5-6
5-4	Facet Slope Error Measurements	5-9

## 1. INTRODUCTION

Electric power on the Space Station will be used to operate life support systems, communication and information processing systems, laboratories and eventually manufacturing and processing facilities. The overall power requirement for the Space Station can easily exceed 200 kW. Photovoltaic power is planned for the first phase of the Space Station, providing 37.5 kW of power. The planned expansion of the Space Station in the second phase will add 50 kW of solar dynamic (SD) electrical power.

Solar dynamic power systems have the advantage of higher system efficiencies than photovoltaic systems and, as a result, allow a reduction of 75% surface area for a comparable amount of net power generated. This aspect of solar dynamics is particularly advantageous in low earth orbit where atmospheric drag is significant for large structures. A reduction of drag results in significant operational savings through a reduction in reboost fuel costs.

Spaceborne and terrestrial solar dynamic power systems are similar in that they operate under the same basic physics laws. As a result, they have common thermal and optical performance requirements. The objectives of the Solar Concentrator Advanced Development (SCAD) program are to develop critical technologies for spaceborne solar concentrators through the design, fabrication, assembly and optical evaluation of a full-scale prototype solar concentrator that will be characterized in a terrestrial environment.

The environmental, launch, and deployment requirements of a spaceborne solar concentrator are vastly different from terrestrial requirements. Additional work beyond the SCAD program will be needed to provide concentrator designs to simultaneously meet weight, stowed volume, and spaceborne environmental durability requirements.

The basic design of the solar concentrator is an offset truss hexagonal panel design. Curved hexagonal panels are used to form an approximately parabolic mirror that concentrates the sun's energy into a thermal receiver. Figures 1-1 and 1-2 show a model of a basic Truss Hex solar concentrator with parabolic mirror and support struts, thermal receiver, radiator, and a section of the Space Station transverse boom.

The Truss Hex solar concentrator for the SCAD program is comprised of 19 hexagonal panels latched together at the corners. Each panel houses 24 triangular mirror facets that form the reflective surface. Each facet is a spherically contoured equilateral triangle, 1 meter on a side. Figure 1-3 shows a typical facet. A total of 456 mirror facets are needed to fully populate the SCAD concentrator.

Figure 1-2 shows the layout of the 19 hexagonal panels and Figure 1-4 shows a single hex after assembly at Harris Corporation.

The hexagonal panels are fabricated from 12 Gr/Ep rectangular shaped beams with a cross section of 1 in. x 4.266 in. and a length of 2 meters.

Hercules involvement in the SCAD program consisted of two contracts, one to supply beams and one to supply mirror facets. The SCAD beam program was completed in September, 1987. The program consisted of design, fabrication, and delivery of 228 Gr/Ep UHM/3501-6 beams. Those beams have since been used by Harris Corporation to successfully assemble the framework for the SCAD concentrator (19 hex panels using 12 beams each).

The requirements of the second contract were originally to design, fabricate and deliver 456 mirror facets to fully populate the SCAD concentrator. These facets were baselined using Silverlux



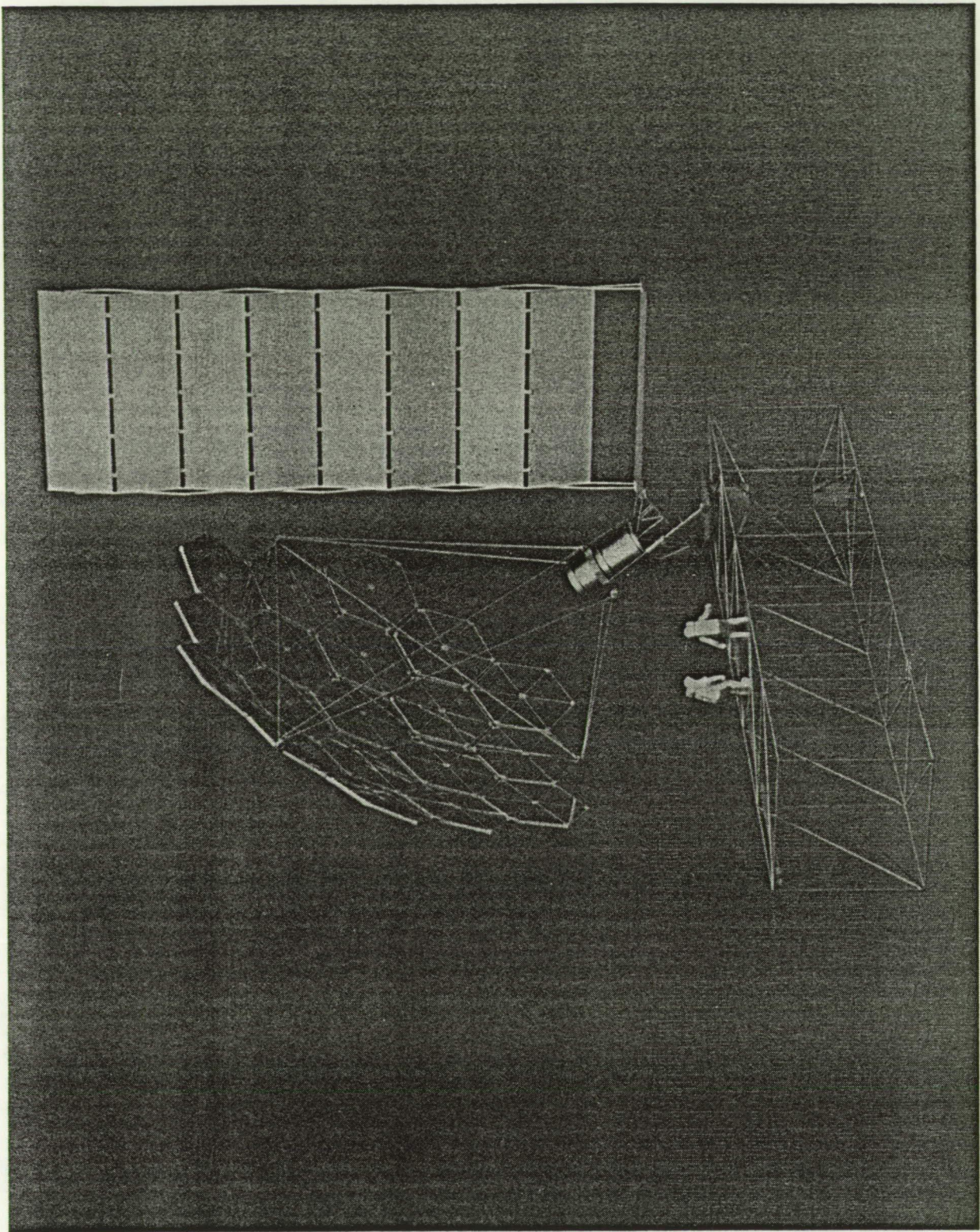


Figure 1-1. Space station solar concentrator



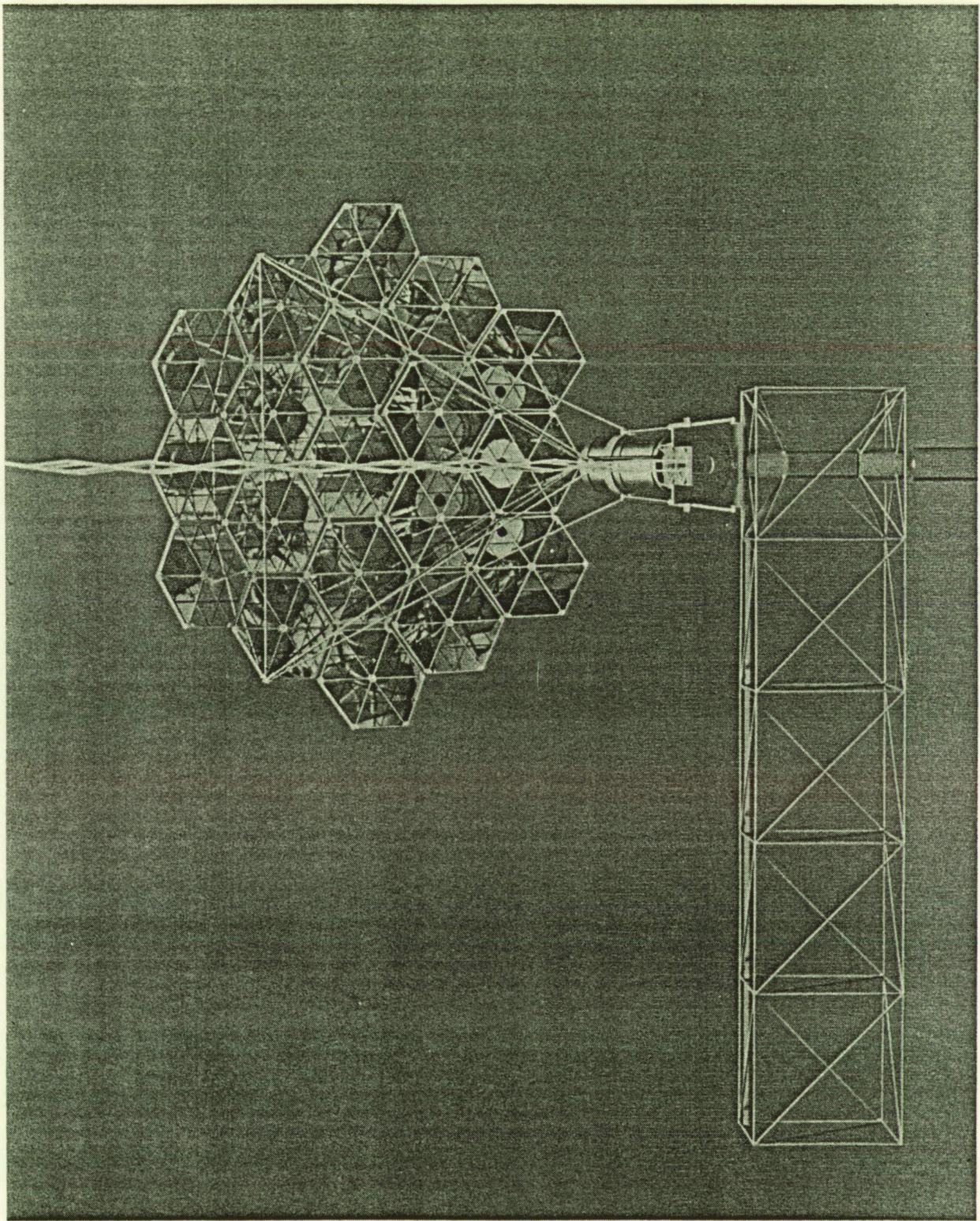


Figure 1-2. Solar concentrator model showing 19 hex panel design



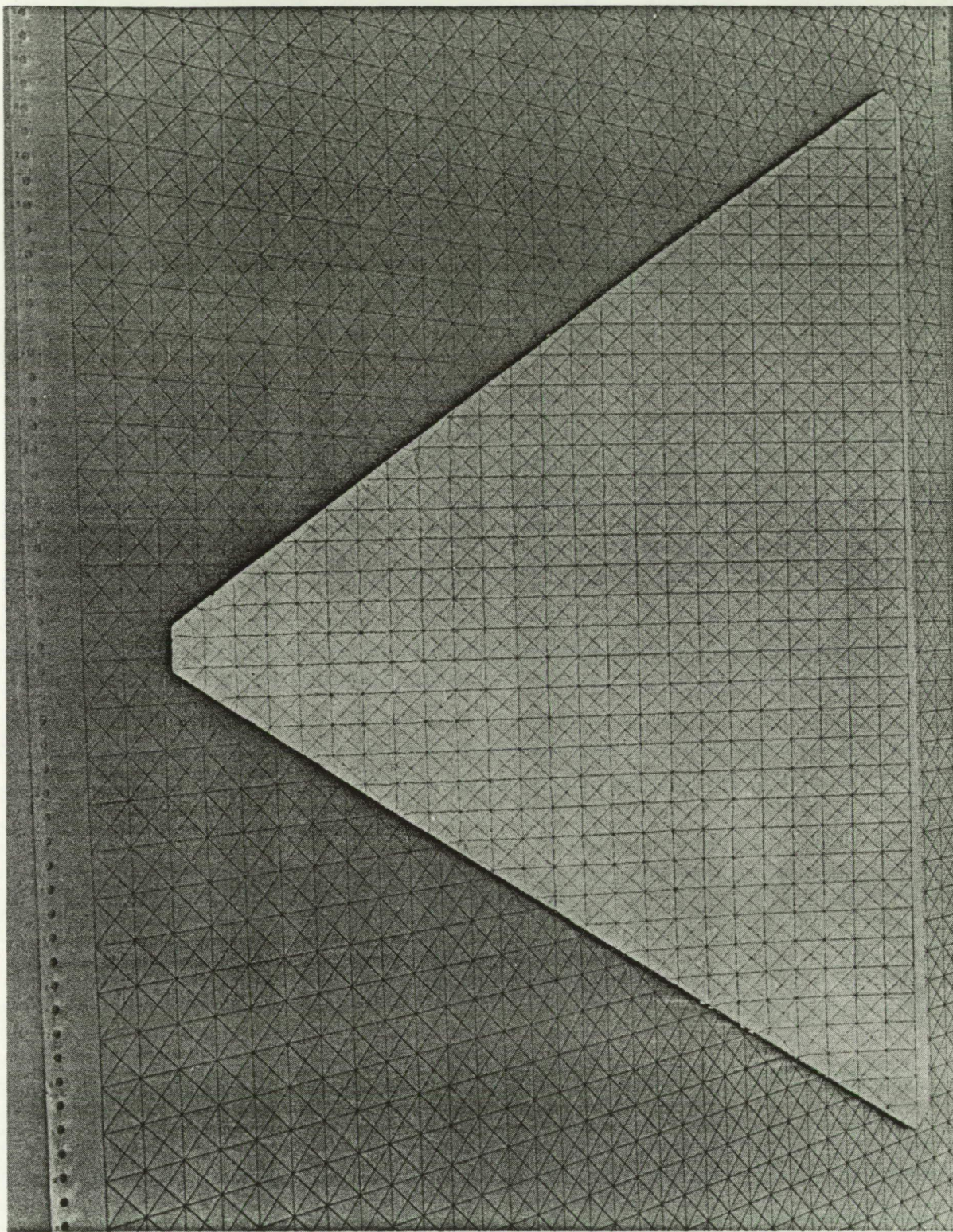


Figure 1-3. Typical facet



ORIGINAL PAGE  
BLACK AND WHITE PHOTOGRAPH

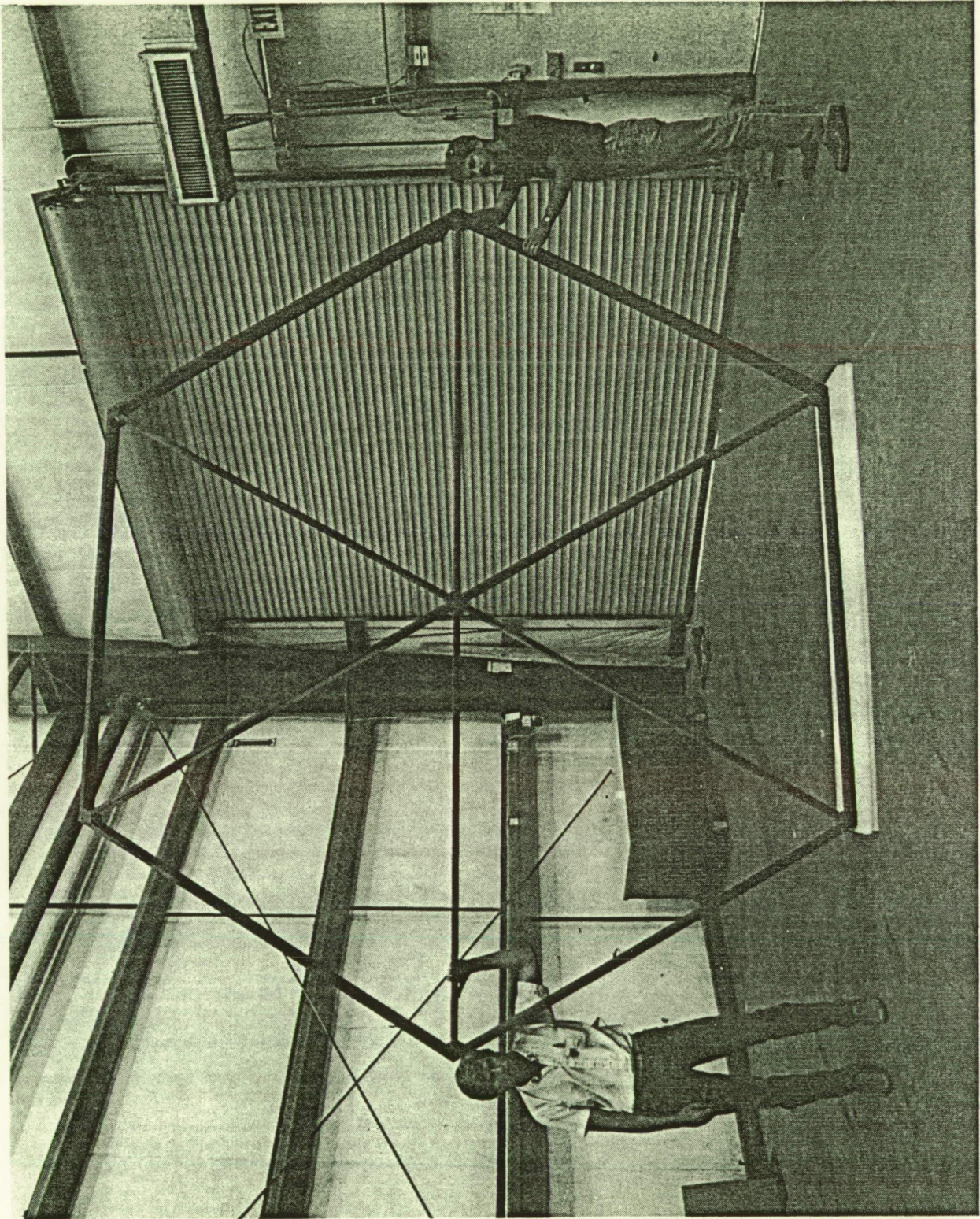


Figure 1-4. Single hex panel after assembly at Harris Corporation

ORIGINAL PAGE IS  
OF POOR QUALITY



reflective film (a product of 3M) as the reflective coating because a vapor deposited reflective surface type facet, that could meet SCAD optical requirements, had not yet been developed.

In late 1987, a meeting was held at NASA Lewis Research Center with Harris and Hercules where the scope of the SCAD program was changed. Although facets using Silverlux film met SCAD optical requirements, they were not candidates for the Spaceborne solar concentrator because the adhesive backing used to bond the Silverlux film to the Gr/Ep facet was not space qualified. Thus, it was decided that the SCAD funding would be better used by fabricating a limited number of Silverlux facets and using part of the SCAD funding to further develop a more space like vapor deposited type facet that would have a graphite face sheet surface finish smooth enough and clean enough to accept a vapor deposited coating of aluminum or silver and meet the SCAD optical requirements.

The rescoped SCAD program then consisted of (a) production of 48 Silverlux mirror facets (determined to be the minimum number of facets needed to selectively populate the prototype solar concentrator and still be able to optically characterize it), and (b) a development program aimed at improving surface cleanliness, improving the reflective surface of the facets. To meet these two objectives, it was also necessary to define and further understand mirror facet reflectance requirements and then to identify, perform, and interpret tests and test results to confirm facet optical properties.

The main purpose of this report is to describe the SCAD facet program. Section 2 gives a brief overview of the development that lead to the Silverlux facet design and fabrication process. Section 3 gives the details of that design and the details of the fabrication process used to fabricate the 48 deliverable Silverlux facets. Section 4 describes the improved surface cleanliness development program. Section 5 gives the details of the optical testing used to characterize the facets and presents the measured optical data for the deliverable facets. Section 6 presents program conclusions and recommendations for future work. Appendix A presents a series of photos showing the detailed facet assembly and bonding process. Appendix B presents a series of photos taken to measure facet slope error.

## 2. SILVERLUX FACET DESIGN AND FABRICATION PROCESS DEVELOPMENT

At the start of the SCAD program, optical reflective requirements were not clearly understood. Therefore, the goal was to produce samples based on visual goodness until test methods were identified and samples qualitatively compared.

The first samples were fabricated using elevated cure resin systems. Many metallic base plates (base tool) with varying degrees of surface finish were evaluated. In conjunction with the base plates, many release agents were tried. Release agents included liquids, aerosols, waxes, and films applied to the base plates before skin layup.

Releases other than films were eliminated because removal of resin flashing left on the base plates degraded the tools surface finish. The surface finish was very critical because the epoxy resin masks the tool during cure. Release films only provided a surface finish as good as the film itself. Glass base plates with liquid and aerosol release agents used earlier were evaluated because films were not acceptable. Glass provided an excellent surface finish that resisted abrasion during cleaning. Using the glass plate and a Frekote 700 liquid release agent, many samples of fabric and unidirectional graphite epoxy prepreg were evaluated using a 350°F cure. In all cases, the surface profile did not equal the profile of glass plate. Thickness variation of the epoxy resin under the graphite fibers and between the fibers over the glass plate surface created the profile problem. During cool down of the 350°F cure, the thickness differential of the epoxy resin and CTE differential between graphite and epoxy created the profile change. Many different layup and elevated cure variations were processed to minimize the profile changes with only minimal success.

Room temperature cure epoxy resin systems were evaluated to eliminate surface profile variation. Epoxy was mixed, degassed and applied to dry graphite fabric on a released glass base plate. Variations of resin volume were tried until an acceptable surface finish was fabricated.

Throughout this early development, work samples were sent to 3M for VDA coatings. Goodness was based on optically measured diffuse light given by each sample. As the surface quality improved, other optical measurements were required to distinguish the reflective surface quality. (Section 5 describes selected measurement techniques for verification of optical requirements.) Table 2-1 shows hemispherical and specular reflectance for a few samples fabricated using room temperature and elevated temperature epoxy resin cure systems. "A" and "GG" series samples were cured at 350°F. "RMT" series samples were cured at room temperature. Through the early development work, a fabrication process was defined that produced high quality reflective epoxy surfaces.

TABLE 2-1. ALUMINUM VAPOR DEPOSITION

Sample No.	Total Hemispherical (Solar Avg, Air Mass 2)	Specular Reflectance (660 nm)	
		26 mrad	15 mrad
A-4	86.9	NA	52.8
GG1-C	90.5	NA	51.8
GG2-C	90	NA	58
GG6	90.7	NA	84.9
RMT-01A	86.7	87.1	87.6
RMT-02A	85.2	84.6	82.6
RMT-02C	86.2	86	85.1
RMT-01D	85.6	86.9	86.0

This fabrication process was used to produce prototype facets using Silverlux film as the final reflective surface. These Silverlux facets met the SCAD optical requirements and the process was baselined as the process to produce the 456 SCAD facets needed to fully populate the SCAD concentrator.

As mentioned in the introduction, the SCAD program was rescope and only 48 facets were fabricated using Silverlux film. Details of the Silverlux facet design and production process are given in Section 3.

### 3. SILVERLUX FACET PRODUCTION

#### 3.1 OBJECTIVE

One of the main objectives of the SCAD program was to produce 48 composite mirror facet assemblies with a Silverlux reflective surface. These facets were for use in the full size solar concentrator frame constructed from composite box beams produced by Hercules for Harris Corporation.

The design approach for the Silverlux type facets was to fabricate a low risk facet assembly using previously developed processes. These processes had produced facets that would meet functional requirements in a terrestrial based concentrator, but would require improvement to meet space based mirror facet solar concentrator requirements. The Silverlux facets were fabricated to Harris Specification No. 100005 and Drawing No. 5000041 and 5000048.

#### 3.2 FACET DESCRIPTION

An exploded view of a composite mirror facet assembly is shown in Figure 3-1. The facet is a sandwich structure with a spherical contour where the radius of curvature is 1063.75 in.  $\pm$  24 in. The face skin consists of graphite cloth (Hercules Magnamite A193P) impregnated with an epoxy resin. The back skin is Magnamite A193P/3501-6 prepreg cloth. Both skins are one ply each, approximately 0.014-in.-thick. The core of the sandwich is vented aluminum honeycomb, 0.270-in.-thick. The skins are bonded to the core with a room temperature curing adhesive, and separated by a fiberglass cloth to prevent galvanic interaction. Aluminum inserts are bonded into the corners of the honeycomb with a foaming adhesive. The facets are mounted to the supporting structure at the aluminum inserts. The reflective coating, Silverlux film, is applied to the concave surface. The weight goal for the entire assembly was set at 1.0 lb. Optical requirements are described in Section 4.

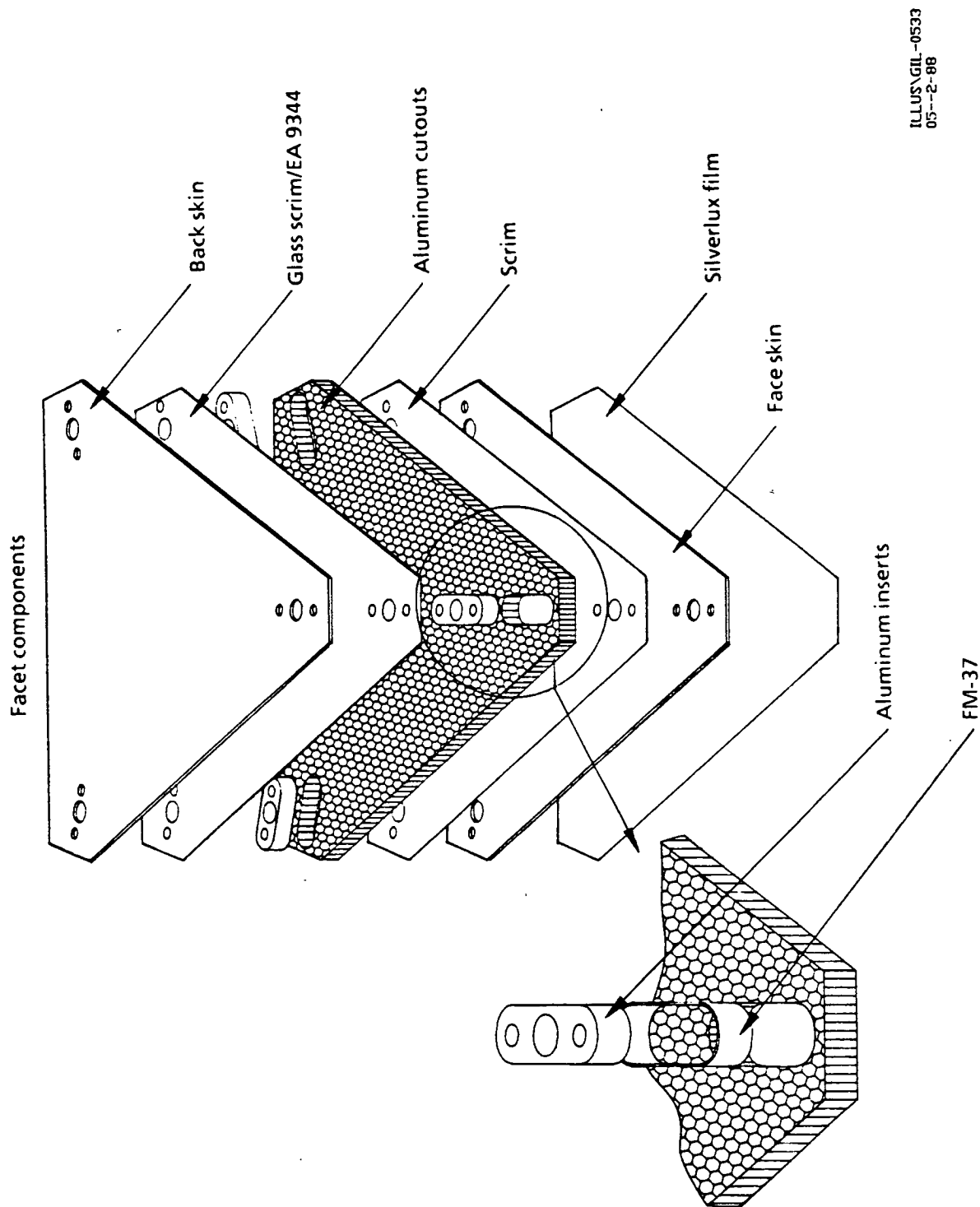
#### 3.3 MANUFACTURING PROCESSES

Figure 3-2 shows the manufacturing flow for a Silverlux type facet. The details of each part of process is given below.

**3.3.1 Back Skin Fabrication (Steps 1 to 4, Figure 3-2)** The facet back skins are fabricated from AS4/3501-6 graphite prepreg material. Step No. 1 (Figure 3-2) consists of cleaning and applying release agent to the working surface of the aluminum base plate used for the material layup. In Step No. 2, the prepreg material is laid up on the flat base plate and consolidated under vacuum. The back skins are made using a large one-ply sheet approximately 3 ft wide by 12 ft long. In Step No. 3, the vacuum bagged prepreg is cured in an autoclave. The large cured sheet is cut by hand into several back skins in Step No. 4. The back skins are then machined to final net size and the nine mounting holes are drilled. There is a 0.011 in. difference in the hole pattern diameter between the front and back skins because they are cured flat and then bonded into the final facet assembly on a curved surface tool.

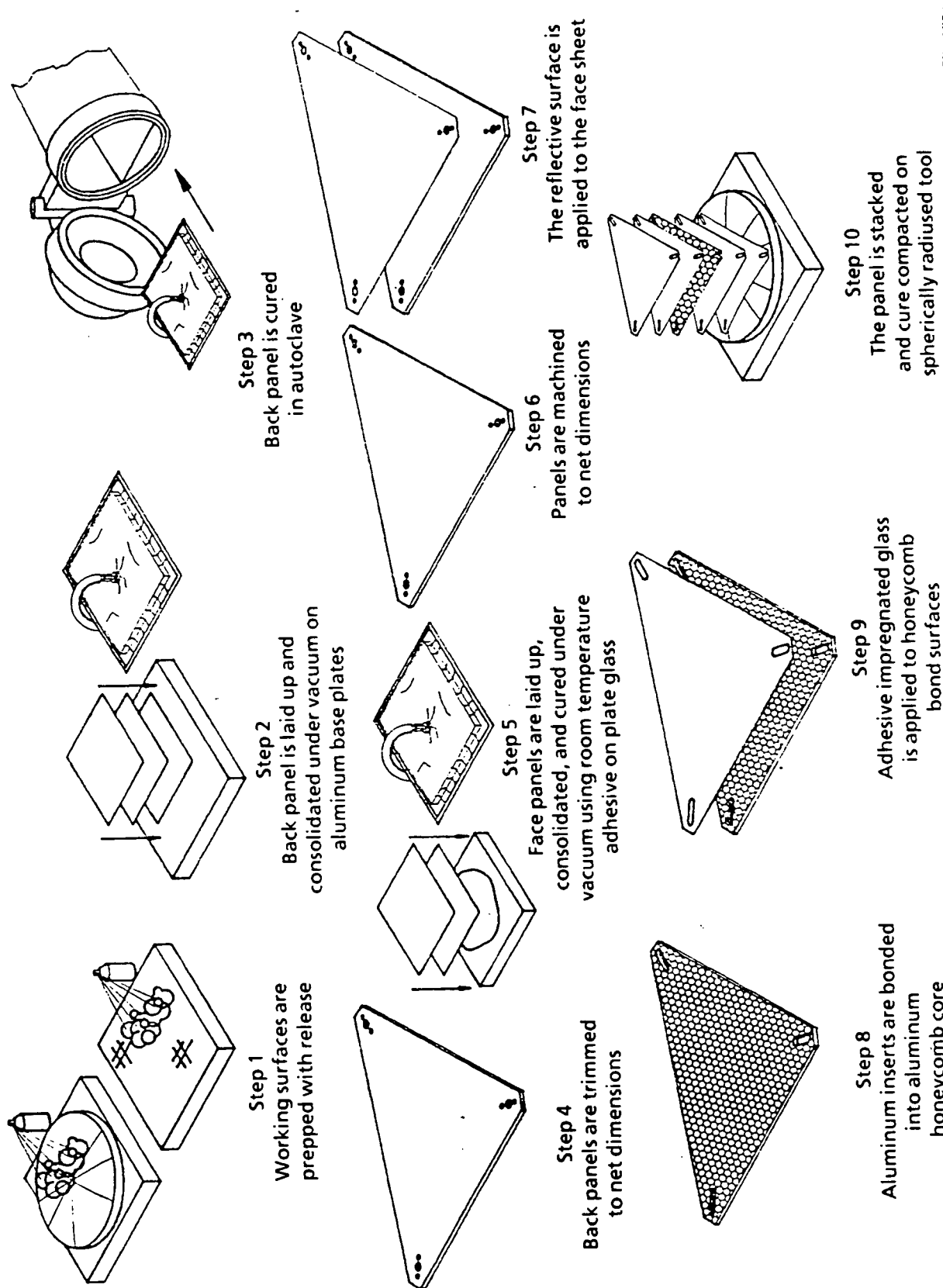
**3.3.2 Face Skin Fabrication (Step 1 and Steps 5 to 7, Figure 3-2)** It was necessary to use float glass as the base plate lay up tool to get the optical quality surfaces needed for the face sheets. In Step No. 1 (Figure 3-2) the glass plate is prepared with a release agent. The surface is cleaned, sprayed with a release agent and polished to ensure an even release coat. In Step No. 5 the face skins are laid up on the glass plate. The face skins are made from a room temperature curing epoxy adhesive resin (EA 956) and graphite cloth, magnamite A193P. The resin is screeded evenly onto the glass plate and then the triangular precut cloth is layed onto it. The cloth and resin are vacuum bagged and under vacuum pressure, the resin soaks into the graphite cloth and cures at room temperature. The face sheets are laid up and cured flat.





ILLUS\GIL-0533  
05--2-88

Figure 3-1. Facet construction



ILLUS\NGIL--0524  
04-20-88

Figure 3-2. SCAD facets manufacturing flow

After curing is complete, the face skin is removed from the glass plate. In Step No. 6 nine holes are drilled in the three corners of the triangular face skin and then it is machined to net size.

The face skins were sent to solar kinetics in Dallas, Texas, for application of the Silverlux film in Step No. 7. The Silverlux laminated film consists of a peelable protective film, a thin facing silver foil, a backing film, and a pressure-sensitive adhesive and its peelable backing. The Silverlux film is applied by running the graphite epoxy face skins and the Silverlux film through a set of squeeze rollers. The Silverlux film bonds to the face skins with the pressure-sensitive adhesive. The face skins were then shipped back to Hercules for final assembly into mirror facets.

**3.3.3 Honeycomb Core and Aluminum Insert Preparation (Step 8, Figure 3-2)** The honeycomb core material is 0.270 in. thick vented aluminum with a cell size of 0.25 in. It was purchased from the vendor premachined to net size with insert cutouts also premachined. The inserts were machined in house from aluminum.

In Step No. 8 the aluminum inserts are prepared for bonding into the precut honeycomb. The outside edges of the inserts are covered with FM-37 foaming adhesive and inserted into the precut holes in the honeycomb at each corner of the triangle. The honeycomb/insert assembly is fixed in place using a template and gage pins to hold everything in place while the foaming adhesive is cured at 250°F. The cured honeycomb/insert assembly is now ready for bonding into the final curved facet assembly.

**3.3.4 Facet Assembly (Steps 9 and 10, Figure 3-2)** The final facet assembly process consists of bonding the face skins and back skins onto the aluminum honeycomb core on a spherical radiused tool to produce the curved facet sandwich assemblies. The sandwich bonding operation is fairly detailed. A detailed description is given in this section.

All of the components, face skins, back skins and honeycomb core are manufactured flat. However, the final bonded sandwich structure conforms to the spherically radiused tool, resulting in the curved facet assembly.

The bonding begins by removing the peel plys from the face and back skins and dry-fitting them, with the honeycomb core, on the mold. Gage pins are inserted through all six 0.250 in. diameter holes to align the skins, inserts, and core. If any mismatch of hole diameters or honeycomb location exists, they are reworked to ensure the assembly lies smoothly on the tool. The skins and core are removed, taped to a clean working surface, and degreased. The two-part epoxy adhesive is then mixed and applied to all the bonding surfaces, using paint rollers to obtain even coverage and a billet on the honeycomb. A lightweight fiberglass cloth is then applied to the skin and trimmed to size. The tool is covered with one layer of porous, Teflon coated fiberglass cloth that acts as a leak path to eliminate air underneath the smooth face skin, and acts as a release to prevent any stray adhesive from bonding to the tool. The sandwich is assembled on the tool and pinned together through the holes at the corners. Several fabrication aids are placed on top of the sandwich to ensure uniform pressure over the surface, and the whole assembly is compacted under vacuum during the 15 hour room temperature cure. After cure, the facet is removed, unpinned, and placed into a protective bag to await inspection and shipping.

**3.3.5 Manufacturing Process Discussion** Production of the SCAD reflective facets presented several problems, even though they were intended to be low risk, using previously developed processes. Although there were no major problems with the materials or processes, several operations needed additional fine tuning to repeatably achieve the required quality.

The most difficult requirement, from a manufacturability standpoint, was the slope error goal of 1.5 rms (Section 5 gives a definition for slope error). The first step in obtaining a good reflector surface is in making a smooth, pit-free face skin. The pits are caused by air bubbles trapped by the

carbon fiber cloth against the glass base plate. The resin is degassed under a vacuum as long as possible before pouring it on the glass, but some bubbles are still introduced unless much time and care are taken when screeding the resin and applying the carbon fiber cloth. Air bubbles are removed from the top side of the cloth when the whole layup is placed under a vacuum bag. Three different peel ply and breather combinations were tried to optimize the evacuation of air from the layup. The breather combinations were evaluated on the visual quality of the face skin cure (for example absence of dry fiber, fiber print through, air bubbles, or other imperfections). Tiny pits, of less than 0.001 in. diameter were judged acceptable for these skins because they would be covered by the Silverlux film. We also noted the temperatures of the resin and plate had an effect on the surface, because of the relationship between temperature and viscosity.

The second problem in obtaining a facet with low slope error is to minimize honeycomb print-through. Initially, a curved, weighted caul (approx 80 lb) was planned to provide the necessary bond pressure through the sandwich. However, during the Silverlux application process, the graphite epoxy face skin was deformed, probably by the high pressure from the vendor press roller. (They also show more fiber print-through than face skins without the Silverlux.) The deformation appeared as waviness causing the skins to not lie flat, requiring more bonding pressure than planned to force the skin to conform to the tool. At this point, we replaced the weighted caul system with a partial vacuum bag, and then tried several vacuum pressures. The lowest slope error was achieved with approximately 9-in. Hg of vacuum. The partial vacuum was obtained by sealing the bag using full vacuum to help spot leaks easily, and then closing the vacuum connection and reducing vacuum until the gage read 10 in. Hg. The gage was then checked hourly up to 8 hours, and vacuum refreshed whenever it dropped below 8 in. Hg. The integrity and reliability of the vacuum was greatly increased by switching to a clear Capram nylon bagging film that routinely yielded leaks less than 1 in. Hg after 16 hours.

Further contributions to slope error come from the honeycomb and the hard aluminum inserts at the corners. If the honeycomb has any dings, dog-eared foil, or unexpended foil, deviations appear on the face skin surface. The inserts, 1.5-in. long by 0.5-in. wide, tend to flatten the corners. While we did not measure each feature's contribution to slope error with the optical test setup, the surface deviation is easily visible to the eye and can be observed in the photos used in the inspection illustrated in Appendix B (Figures B-1 through B-3).

Most dimensions were within nominal per the facet drawing. Per Harris direction, facets were judged acceptable, without additional rework.

### 3.4 INSPECTION DATA

The first nine deliverable facets were inspected for dimensional and optical requirements. (Section 5 describes optical test methods and results). The features inspected were straightness, length from middle of each side to the opposite point, angularity of the sides, widths of the corners, hole pattern diameter, and weight. No formal quality assurance was used on this program but rather quality was "built in." The inspections were performed by engineering aides, and directed by the project engineer. The data recorded is summarized in Table 3-1.



**TABLE 3-1. FACET INSPECTION DATA**

Serial No.	Weight with Film	Straightness Max Deviation (in.)			Overall Length (From Top to Side:)			Angle (From Datum to Side:)		Corner:		Hole Pattern Gage Test
		Datum B	Left	Right	Datum B	Left	Right	Left	Right	Width (in.)	Center (in.)	
(Nominal = )	(484)	(0.020)			(32.833)			(60°)		(1.00)	(0.50)	
(Requirement = )	Goal	Maximum			(± 0.020)			(± 33°)		(± 0.01)	(± 0.01)	(Pass/fail)
SCAD-001	691.7	0.020	0.012	0.014	32.862	32.861	32.856	60.33	60.16	0.995	0.501	Pass
SCAD-002	624.0	0.030	0.032	0.022	32.844	32.839	32.841	61.50	62.08	0.998	0.478	Pass
SCAD-003	638.2	0.018	0.024	0.020	32.843	32.845	32.844	60.08	59.83	0.997	0.505	Pass
SCAD-004	706.9	0.019	0.016	0.019	32.839	32.841	32.833	60.58	61.16	0.982	0.485	Pass
SCAD-005	684.8	0.030	0.028	0.014	32.850	32.846	32.850	60.58	60.41	0.991	0.499	Pass
SCAD-006	669.0	0.028	0.017	0.018	32.844	32.840	32.858	60.16	60.33	1.005	0.502	Pass
SCAD-007	725.6	0.025	0.029	0.032	32.845	32.833	32.850	60.16	60.08	1.090	0.493	Pass
SCAD-008	726.9	0.024	0.022	0.015	32.853	32.854	32.795	60.08	60.42	0.995	0.511	Pass
SCAD-009	719.4	0.020	0.019	0.035	32.838	32.853	32.863	60.66	60.00	0.970	0.497	Pass
SCAD-010	724.0	0.007	0.019	0.030	32.846	32.850	32.844	61.50	60.00	0.997	0.467	Pass
SCAD-011	727.6	0.029	0.010	0.034	32.850	32.846	32.846	61.42	61.50	1.000	0.501	Pass
Average	691.0	0.022	0.022	0.034	32.850	32.846	32.846	61.42	61.50	1.000	0.501	Pass

A total of 13 facets were inspected to ensure repeatability. The hole pattern was inspected by pinning the sandwich into the drill fixture and was accurate to less 0.001 in. as verified by tool and gage. The weights of the facets were taken with and without the peelable outer protective film for the Silverlux surface. The film was removed only from facets that had to be optically inspected, and weighed about 15 grams. An increase in the weights can be seen after serial number -007. This was caused by an increase in the amount of adhesive to prevent debonds that appeared in early development facets.

## 4. IMPROVED SURFACE CLEANLINESS DEVELOPMENT PROGRAM

### 4.1 OBJECTIVES/BACKGROUND

The second portion of the rescoped SCAD program was to develop significantly improved surfaces for composite mirrors. This commitment was made based on NASA-Lewis preference for a more spaceborne like metalized mirror surface as opposed to the nonspace qualified Silverlux film baselined for the 48 production facets, and on the realization that existing technology could not produce the high quality surfaces required for vapor deposition. Although not a requirement, the ultimate goal for the development program was to meet the reflectance requirements of the original SCAD scope (specular reflectance of 0.926, hemispherical reflectance of 0.90, and slope error of 1.5 mrad), and to deliver three full-size facets that would demonstrate these improved processes.

Early program work, Phase I development, centered on surface finish quality. Many process tools and materials were evaluated as to their effect on surface profile, pitting and cleanliness. In parallel to this study, work was being done to identify the real optical performance requirements and available test methods for surface finish measurements.

The general direction for all the development was to improve the cleanliness of the epoxy resin surface. Based on work done early in the program, the four tasks chosen were: (a) release agent transfer, (b) machining contamination, (c) protective coatings, and (d) shipping and handling protection.

Progress on all tasks were evaluated by vapor depositing a metal coating on the surface of the sample and then measuring reflectance values. The metal chosen for all samples was aluminum. Therefore, in comparing reflectance measurements of development samples to Silverlux film or silver coatings, the values must be adjusted to account for the different theoretical reflectances of silver and aluminum (Section 5.4 describes test results and gives further discussion). Also, all measurements mentioned in the development section are raw data, not adjusted for air mass or other factors.

**4.1.1 Task I--Release Agent Transfer** The progress made from early efforts indicated the best material for a base plate was float glass. However, the release agent used to coat the glass transferred to the epoxy surface and caused cloudiness in the metallized surface, reducing its reflectance. Our approach was to survey and test available release agents and to briefly investigate new directions such as release films, sputter coating and permanent release coatings. All candidates were evaluated by laying up a 12 in. x 12 in. face skin using the release agent, and then sending the sample to 3M for vapor deposition of an aluminum coating. The quality of the coating is very sensitive to any contamination, and can be quantified as specular and hemispherical reflectance. These data are summarized in Table 4-1. Some samples appeared so cloudy that we decided they were not worth testing.

TABLE 4-1. SPECULAR REFLECTANCE ACHIEVED WITH VARIOUS RELEASE AGENTS

Manufacture	Release Agent Designation	Typical Specular Reflectance
Chem-Trend	Monocoat E147	87.0
Dexter-Hysol	Freekote 700	87.3
Releasomers	XK22	83.7
Maclube	1700	82.1
Dexter-Hysol	Freekote 44	83.7
Miller-Stephenson	MS-122	70.0

Six of the major manufactures of release agents were contacted and asked to recommend their best low transfer product and to send samples. The companies and their products were: (a) Dexter Hysol with Freekote 700 and Freekote 44, (b) Miller Stephanson's MS-122, (c) Releasomers with XK-22, (d) McLube with MAC 358-88, (e) McLube 1700, and (f) Chend-Trend with Monocoat E157. We eliminated waxes, silicone based formulas, and tried mostly fluorocarbon dispersions, or proprietary formulations. After the first lot of samples was coated and measured, the best two candidates, Freekote 700 and Monocoat E157, were chosen for further optimization of the application process. The three process variables chosen for optimization were amount of buffing, temperature of the plate and/or baking of the release agent, and amount of the initial coating applied. After the second round of samples, Monocoat E157 was chosen as the least transferring release agent for glass plates.

The final process evolved for Monocoat E157 was to degrease the glass, apply 5 cc to a clean cloth and wipe it on the plate, let it dry for 10 to 15 minutes, and hand buff until nothing was visible on the glass surface. The plate was then heated to 200°F for 15 minutes and was ready for layup when the surface temperature dropped to less than 100°F. Using this process, specular reflectance values of greater than 88% were consistently achieved.

Further study into the durability of the coating had been planned, to determine how many samples could be fabricated without recoating. However, this was canceled because the face skins tend to leave residue that needed to be cleaned off, thereby removing any release coating. Also, from a cost-benefit view, the risk of damaging the glass plate, if resin sticks to it, or of producing a rough surface, is not worth the expense of applying a new coat after each use.

The investigation into alternative methods producing clean face skins did not yield any positive results. A small glass plate was spatter coated with Teflon, but did not form a good enough barrier to release the epoxy resin. Another avenue analyzed was a base of nonstick film, such as Teflon, in tension. Drawbacks of this are imperfections in the film, and the cost of tooling to stretch the film. This might still be an area for future consideration.

**4.1.2 Task II--Machining Contamination Control** The second area targeted to help improve the facet surface contamination, was to eliminate surface contamination. In the current manufacturing flow, the parts are all trimmed to their net size before bonding. However, because the surface to be metalized is so much more sensitive to contamination, the same conventional machining methods used for the Silverlux sandwiches (routing and drilling) is unacceptable because of the lubrication used. This task was studied on three fronts, (a) alternative machining methods (waterjet, ultrasonic knife, routing/milling, and die-cutting), (b) cleaning methods after machining, or (c) protective coatings during machining. The results in this area were evaluated more on the basis of feasibility, cleanliness, and visual inspection of the surface rather than reflectivity data. This was felt to be adequate, because the differences between methods were very easy to see, and because optical degradation only occurred near the edges, or at contaminated spots. The protective coatings were also a separate task, but were considered for protection during machining. None of the coatings were successful, as discussed in Section 4.1.3.

Of the three methods, the die-cutter was determined to be the best. Its biggest advantage over the other methods is that lubrication is not needed during cutting and that no dust is produced. It also produces a good edge when only one ply is cut at a time. Die cutting would also be feasible for higher volume production rates, requires simple tooling (a die board), is repeatable, and can meet tolerances of 0.002 in.

Ultrasonic cutting was tested using a hand held Branson cutter. The operation produces an acceptable edge, and some dust. At high feed rates through cured resin, the knife heats up and burns the resin and the blade quickly wears out. The waterjet produces a better edge, but yields more dust as well as some moisture on the surface under the film. The operation could be improved

by using a fixture that clamps over the Teflon film to prevent contamination from water. The waterjet has the capability of cutting many plies at once, up to several inches. Both the waterjet and the ultrasonic cutting are suitable for high volume rates, and can be mounted on a gantry type robot, and automated.

Any of these methods could be feasible if the face skin were adequately protected by a strippable coating, and/or cleaned after machining. Regardless of added processing and expense to producing a facet, the increase in reliability and confidence would be well worth the cost. All of the coatings evaluated, however, caused significant reductions in reflectance.

A survey of cleaning methods was also fruitless. Past experience from Hercules, 3M and Sandia has shown that any solvent cleaning will leave a residue that appears as cloudiness in the metallized surface. The only contaminants that can be successfully removed are dry particulates such as dust, or machining debris to a limited extent. These types of particles are removed simply by blowing with dust-off or other clean compressed gas. Any kind of physical contact has the potential to transfer residue to the surface, including some polymeric films used for bagging the parts during storage and shipping. Several types of films were tried before choosing Teflon film to wrap all samples and parts.

**4.1.3 Task III--Protective Coatings** The objective of Task III was to find a removable coating to protect the surface finish of the face skin without leaving a residue. It's primary function would be to provide protection from face skin layup through machining, bonding, and shipment to 3M for a VD coating. If feasible, it could also protect the VD coating until the concentrator is assembled in space. Our approach was to establish processing limits for the samples, and then search for off-the-shelf coating products to test on 9-in. x 9-in. face skin samples. The samples, along with control samples, were then sent to 3M where the coating was stripped, and VDA applied. Upon receipt, we measured reflectance of the samples and compared the coated samples with the control samples.

Most of the coatings sought were polymers in a solvent solution, or adhesive backed solid films. The ideal coating would be easily sprayed, cure at room temperature (or less than 200°F), and be stripped off easily in one piece. Although many conformal coatings are available, few are formulated to be removed by hand, or cured at low temperatures. Conformal coatings are usually applied permanently to metal or electronic parts, allowing them to be removed if desired, with solvents or acids. The products tested are summarized in Table 4-2. Each product required a slightly

**TABLE 4-2. PROTECTIVE COATINGS SUMMARY**

Manufacturer	Product Designation	Base	Solvent	Flash Point	Color
3M	2253	Synthetic resin	Tolvene, MIBK	45°F	Red-orange
D Aircraft	Dapcoat 10220	Rubber	Water	None	Green-blue
Tech Spray	Fine-L-Kote AR	Acrylic	(Aerosol)		Clear
McGhan NuSil	D-1002	Silicone	Naptha	48°F	Translucent
Spray-on	00322	Vinyl lacquer	MEK, MIBK, MeCl, Acetone	20°F	Gray

different application process that had to be optimized to obtain a thick, peelable coating. The results of the reflectance measurements are shown in Table 4-3. The effect of the residue is most noticeable in the hemispherical reflectance redesign, indicating the amount of light being blocked. The unpeelable coatings bonded very well to the surface, as the result of either the microporosity of the sample or the chemical affinity to epoxy resin. None of the coatings are acceptable because of cloudiness on the surface, or application difficulty.



**TABLE 4-3. REFLECTANCE MEASUREMENTS USING VARIOUS PROTECTIVE COATINGS**

Manufacturer	Coating Designation	Specular Reflectance	Hemispherical Reflectance
NA	Uncoated control	87.0	85.0
3M	2253	85.5	64.0
Sprayon	00322	84.5	69.6
D Aircraft	Dapcoat 10220	(a)	(a)
Tech spray	Fin-L-Kote AR	(a)	(a)
McGhan NuSil	R-1009	(a)	(a)
a. Not measured because of an unpeelable coating.			

**4.1.4 Task IV--Handling and Shipping Criteria** The objective of this task was to establish methods and containers that would protect the facets, when fabricated with an improved surface, from being damaged during handling and shipping. The major opportunities for damage can be eliminated by shipping container design, packaging for shipping, storage and handling during manufacturing process, and fixtures for testing. Our approach was to build on existing Hercules experience in manufacturing composite, plan additional protection of the sensitive surface as much as possible, minimize handling steps in the manufacturing process, and then incorporate any additional knowledge learned.

The major damage modes a facet can suffer are (a) surface chemical contamination (such as fingerprints, grease), (b) scratches on the face skin from dust and/or abrasion, (c) delamination of the sandwich structure. To prevent contamination, clean room procedures are followed, including use of gloves to handle the sensitive surface. As a barrier, a piece of Teflon film is cut to the size of the face skin and tightly taped to it as soon as the skin is removed from the glass plate and trimmed. The film remains on the skin when it goes to 3M where it is removed for the vapor deposition process and then replaced until bonding. As soon as the sandwich is cured, a new piece of film is taped on the sandwich. The sandwich is also sealed in a bag for storage and shipping. By using the Teflon barrier, we eliminate the tiny scratches caused when the reflective surface slides against the relatively loose bag.

The shipping containers are designed to support the facets on 3 in. of the corners with foam cutouts. They are in a vertical position, minimizing contact against the surface by the bag, and allowing any trapped particulates to fall to the bottom of the bag instead of lying on the surface. The container could be further improved by supporting the facets using the mounting hardware on the corners, eliminating any contact with the reflective surface. Also, in process protective shells, or some similar device, should be used for all in process storage. This would eliminate many of the handling steps and shuffling of skins necessary in the current manufacturing plan.

## **4.2 MANUFACTURING PROCESS DISCUSSION**

The culmination of the development task was to fabricate three full-scale facets incorporating the results of the four surface improvement tasks (Figure 4-1). Appendix B shows a series of photos of the assembly process. The face skins were metallized before bonding so that if any defects appeared we could scrap just a face skin instead of a whole sandwich. The results of Tasks I, III and IV were completely incorporated into the NDA facets. Task II, Machining Contamination, could not be incorporated because the cost of a die cutter board was beyond the scope of the development budget. Instead, they were trimmed with hand shears.

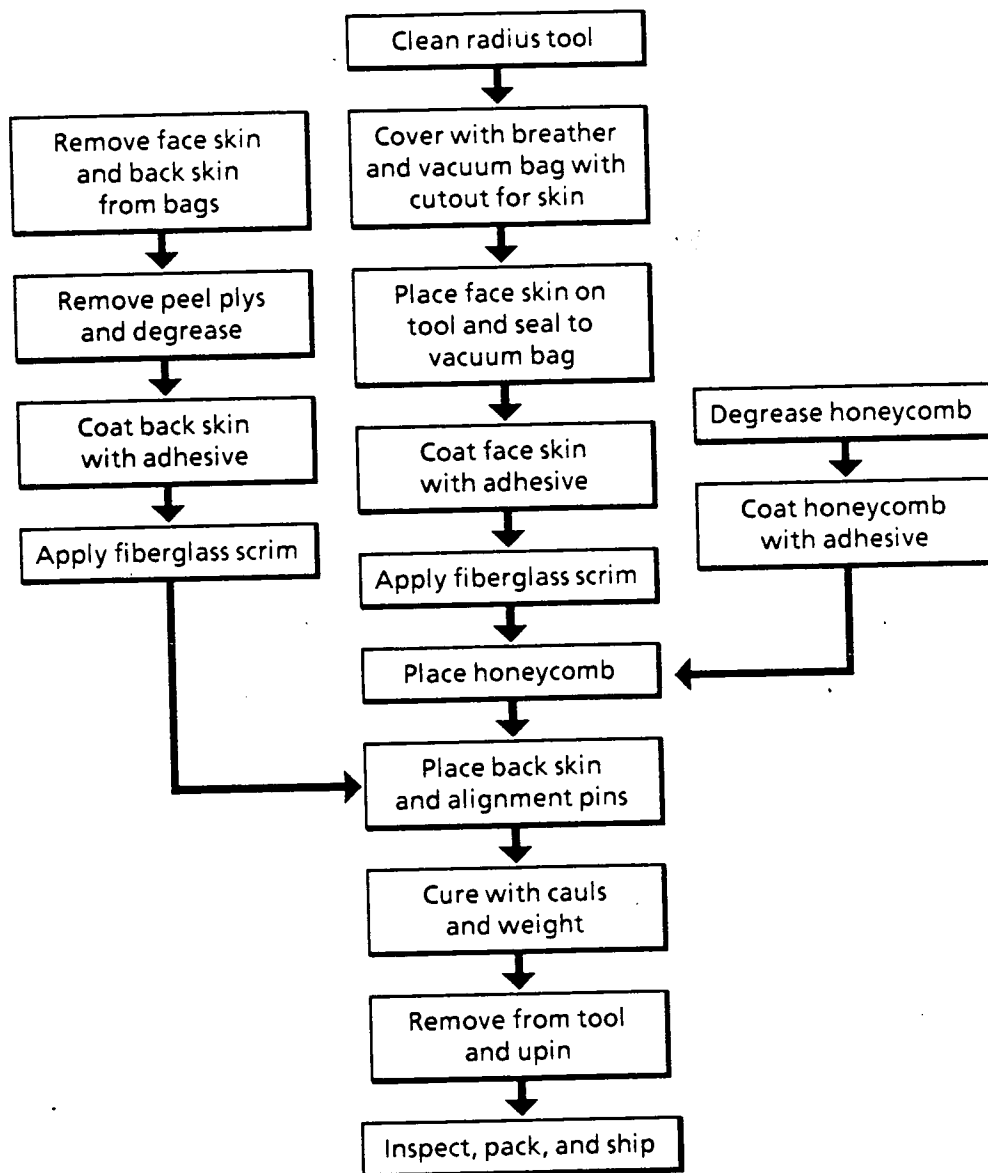


Figure 4-1. Current bonding process for VDA facets

A major innovation in the bonding process decreased the slope error to a sigma of 1.5 mrad. In the Silverlux facet bonding process, the whole sandwich was under a vacuum bag with 8 to 10 in. Hg pressure. The VDA facets were bonded by sealing the vacuum bag to the edge of the face skin (Figure 4-2). Even considering the poor seal obtained on a composite surface, a vacuum pressure of 20 to 24 in Hg was easily obtainable. Pressure on the honeycomb and back skin was supplied by some rubber and metal sheets. This method produced three facets with an average slope error of 1.5 mrad, and specularity of 89.5%.

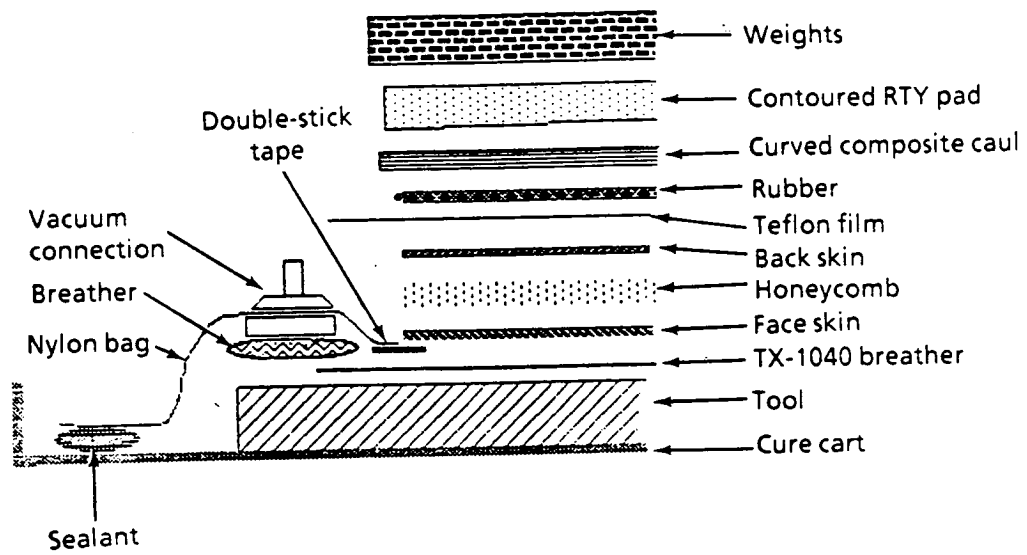


Figure 4-2. Schematic showing bonding setup used for assembly of VD type facets



## 5. OPTICAL TESTING

The SCAD program was designed to produce lightweight mirror facets for a terrestrial concentrator similar to that planned for use on the Space Station. A major goal of this program was to determine if composite mirrors meet or have the potential to meet the optical requirements for such systems. This necessitated first understanding and defining reflectance requirements, and then identifying, performing and interpreting tests to confirm facet properties. This report will discuss the techniques and equipment used for evaluation, and the results of such evaluation for the delivered facets.

### 5.1 OPTICAL REQUIREMENTS

The following optical properties were specified for the SCAD facets:

- Total hemispherical reflectance, corrected to a solar spectrum at air mass zero, equals 0.90.
- Specular reflectance at 660 nm through a 15 mrad full cone aperture equals 0.926.
- Assuming a Gaussian distribution of the facet's slope error,  $\sigma$  (the first standard deviation of the error's spread) equals 1.5 mrad.

These values were defined for facets coated with 3M Silverlux reflective film. Samples were also produced with electron-beam deposited aluminum coatings. A correction factor for the different reflectivities of aluminum and silver was implied but not specified. (This will be discussed later.)

### 5.2 SELECTION OF MEASUREMENT TECHNIQUES

**5.2.1 Total Hemispherical Reflectance** The standard technique for measuring total reflectance employs a uniformly, highly reflective integrating sphere with a characterized light source and a detector. Often the light source does not exactly replicate the solar spectrum, so corrections are made to obtain appropriate solar readings. Less error is introduced if the sphere's sample, detector and light ports are small in relation to the total area of the sphere. Comparison with standard references assures accuracy; replicate readings across the sample improve the precision of measurements.

**5.2.2 Specular Reflectance** Specular reflectance describes the divergence of a collimated beam caused by microscopic irregularities on the sample's surface. Standard portable instrumentation is available for such measurements.<sup>1,2</sup> These portable reflectometers can accommodate samples of various sizes, but usually operate at only one wavelength and with selected, set apertures. Standard references are again used for accuracy, and replicate readings distributed across the sample increase the precision. Measurements are made at right angles to each other to average out any directionality caused by composite fiber orientation.

**5.2.3 Slope Error** A standard technique has not been defined for slope error measurements. Several of the techniques employed, such as laser ray tracing and the imaging methods of Sandia National

1. Freese, J. M., "The Development of a Portable Specular Reflectometer for Field Measurements of Solar Mirror Materials," Sandia Report, SAND78-1918, Sandia National Laboratories, Albuquerque, NM, 1978; Pettit, R. B., Freese, J. M. and Mahoney, A. R., "The Development of a Portable Specular Reflectometer for Monitoring Solar Mirror Materials," SPIE-Vol 428 (Optical Materials and Process Technology for Energy Efficiency and Solar Application), (1983) 125-134.
2. Pettit, R. B., "Characterizing Solar Mirror Materials Using Portable Reflectometers," Sandia Report, SAND82-1714, Sandia National Laboratories, Albuquerque, NM, 1982.

Labs and SERI, require intensive computer analysis to determine errors. Time and cost limitations on this program made these techniques impractical. A simpler, more rapid, and more easily implemented method was sought.

Such a method has been established with IR&D funding for our continuing research on composite mirrors. This technique<sup>3</sup> is illustrated in Figure 5-1. The method involves placing a ring target around a camera located at the mirror's radius of curvature. The camera records the reflection of the ring target off the mirror. The size of the ring used for reflection can be directly related to the magnitude of the slope error on the mirror's surface. Theoretically it is possible to calculate the Gaussian distribution of the mirror's error from a single reading. However, a series of different sized rings was used to corroborate measurements and improve precision to  $\pm 0.5$  mrad (minimum error). The accuracy of the technique is more difficult to determine because we lack a standard of known error.

This measurement technique also required an accurate determination of the focal length or radius of curvature. Optical techniques to find focal lengths were preferred because contact measurement methods could damage the mirror surface. Sunlight reflected off the mirror was suitable for defining the surface focal region, but errors in alignment and sun tracking may increase the error envelope of the final values. Similarly, the combined microscopic and macroscopic errors of the surface distort the reflected beam to form a beam waist rather than a focal point. The inner and outer limits of this focal region were recorded. Several (6 to 12) replicate sets of readings were taken to improve precision.

### 5.3 SPECIFIC TEST EQUIPMENT

**5.3.1 Devices and Services (D&S) SSR Total Hemispherical Reflectometer** A Devices and Services (D&S) SSR total hemispherical reflectometer was used for total reflectance readings. A standard light trap and a secondary standard cross-calibrated at Sandia confirmed instrumental accuracy during the series of readings. Three readings were recorded at each of 15 separate locations on the facet. This instrument was borrowed from Sandia, and had to be returned before the electron-beam deposited facets could be evaluated. The precision of this instrument is about 1%. A report by R. B. Pettit indicates this instrument may underestimate the solar spectral reflectance by as much as 5%.<sup>2</sup>

This instrument approximates an air mass two spectrum, rather than the air mass zero spectrum desired. Graphite/epoxy samples similar to the face sheets used for SCAD were previously measured on Sandia's Beckman spectrophotometer, which reports accurate (error  $< 1.0\%$ ) values for air mass zero and air mass two. The air mass zero correction factors determined from the study of Silverlux coated and aluminum deposited composites ( $0.9601 \pm 0.0008$  and  $1.002 \pm 0.0008$ , respectively) were used on the present data. However, because of the possible underestimation of the solar spectrum by the D&S instrument, the air mass zero values reported herein may be low by  $\leq 6\%$ .

**5.3.2 D&S Portable Specular Reflectometer** A D&S Portable Specular Reflectometer was borrowed from Sandia for specular reflectance evaluation. The wavelength of this instrument is 660 nm, and the aperture was set to 15 mrad (full cone). Fifteen distributed measurement locations were defined for each facet. At these locations four readings were taken at right angles to each other. The reading from this instrument's NBS traceable standard was checked after each location was interrogated, and a second standard measured at Sandia ensured additional accuracy; precision is 0.5%.

**5.3.3 Slope Error Equipment** The slope error equipment was shown schematically in Figure 5-1. Mounts to hold the facets, ring targets, and camera were designed and produced in-house. A CCD with a telephoto lens was used to record each ring's reflection. This image was viewed on a video

3. Christ, G. R., "Determining the Slope Error of a Parabolic Reflector," NASA Tech Brief 8 (1984), Item 50, from JPL Invention Report NPO-15713/SC-1283, pp i, 1-4.

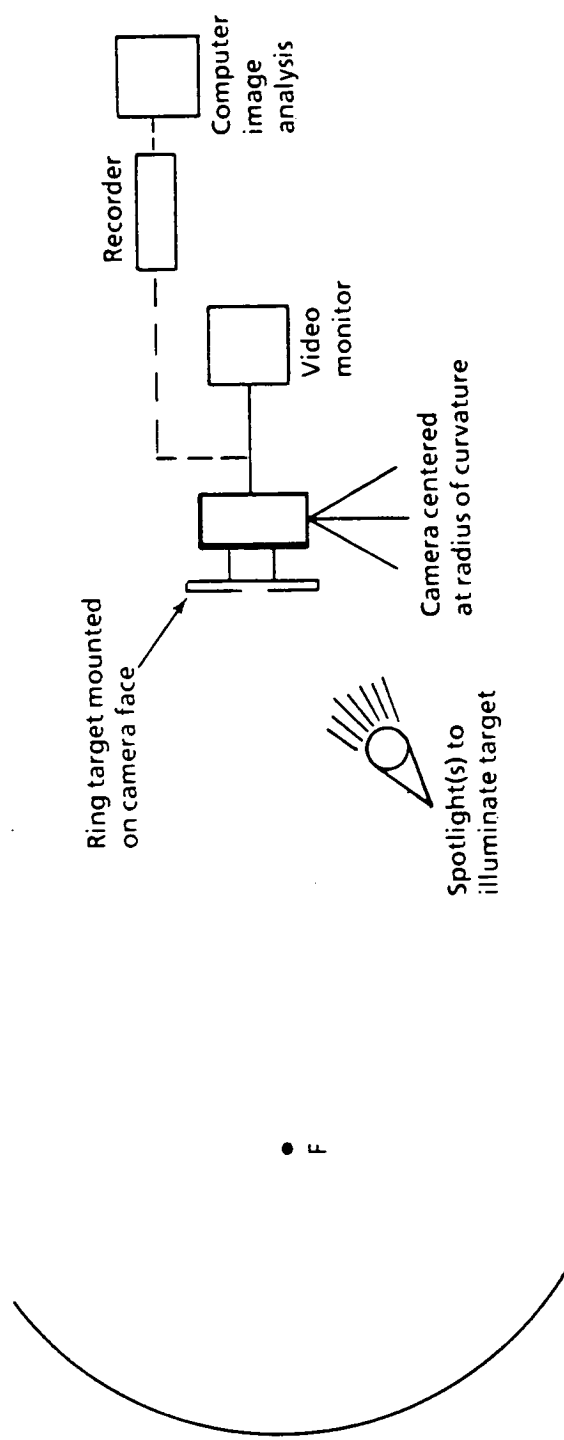


Figure 5-1. Schematic of instrumentation used to determine slope error on a parabolic or spherical reflector

monitor, and recorded on high quality film for later enlargement. The enlarged photographs were then evaluated using a PC-compatible image analyzer. Regions darkened by the rings and the total facet area were recorded for the Gaussian analysis. Triplicate readings were reported for each photograph.

## 5.4 TEST RESULTS

**5.4.1 Total and Specular Reflectance** The specular and total reflectance data for tested SCAD facets are compiled in Table 5-1. The facets identified as SCAD-xxx were reflectively coated with 3M Silverlux adhesive film; those designated VDA-xxx were coated with electron-beam deposition of aluminum at 3M. Specular and total reflectance values averaged over the number of readings taken (60 and 45, respectively) are reported. The standard deviation (Std Dev) of these readings are given in the adjacent column. All standard deviations were calculated using the limited data equation for  $\sigma_{n-1}$ . Note that this error is not the accuracy of the instrument, but the spread or precision of the measurements recorded. Avg and dev identifies the average and standard deviation of the averaged reflectance readings for all the facets in each group. VDA-001 has been excluded from the aluminized facet average because it was made by a different, unimproved process. The measurement equipment had to be returned to Sandia before the total reflectance readings could be made on the improved VDA facets.

**TABLE 5-1. SPECULAR REFLECTANCE AND TOTAL HEMISPHERICAL (AIR MASS ZERO CORRECTED) REFLECTANCE DATA FOR COMPOSITE MIRROR FACETS TESTED UNDER THE SCAD PROGRAM**

Facet	Spec Refl (15 mrad)	Std Dev	Total Refl (AM0)	Std Dev (Silverlux Polymer Film [not vapor deposited])
SCAD-001	90.6	1.7	86.3	0.4
SCAD-002	94.6	1.2	86.0	0.4
SCAD-003	93.9	3.5	85.9	0.4
SCAD-004	94.4	0.9	85.8	0.4
SCAD-005	95.3	0.5	86.1	0.4
SCAD-006	94.5	0.4	86.4	0.4
SCAD-007	94.2	2.4	85.9	0.3
SCAD-008	94.2	1.3	85.8	0.3
SCAD-009	94.1	2.2	86.1	0.5
SCAD-010	94.0	1.1	86.3	0.3
Avg and dev	94.0	1.3	86.1	0.2
VDA-001	71.6	5.4	83.5	
VDA-002	89.5	0.4	NA	
VDA-003	89.8	0.3	NA	
VDA-004	89.5	0.4	NA	
VDA-005	90.0	0.3	NA	
Avg and dev (VDA 2-5)	89.7	0.3		

The specular reflectance data for Silverlux coated facets shows that the specified 92.6% value has been met or exceeded. The air mass zero total reflectance values appear lower than the specified 90%, but this may be the result of the measurement technique. The D&S SSR can underestimate even the air mass two spectrum. This problem is even more pronounced for second surface reflective coatings,<sup>2</sup> such as the 3M Silverlux film. When the original SSR readings are then multiplied by the 0.9601 correction factor, it is not surprising that less than 90% reflectance is achieved; uncorrected values of  $\geq 94\%$  (approaches values reported for first surface, unoxidized silver)<sup>4</sup> are required to obtain the specified corrected value. Given the possible underestimation by the instrument, this is not likely to occur. In addition, the correction factor was determined from a

- Drummeter, L. F. and Hass, G., "Solar Absorbance and Thermal Emittance of Evaporated Coatings," *Physics of Thin Films*, 2 (1964), 305-361; "Coefficient of Absorption of Solar Radiation," *Handbook of Chemistry and Physics*, 58th Ed (CRC Press Inc., Cleveland, OH, 1977); Pettit, R. B. and Roth, E. P., "Solar Mirror Materials: Their Properties and Uses in Solar Concentrating Collectors," *Sandia Report*, SAND79-2190, Sandia National Laboratories, Albuquerque, NM, 1979.





trigonometry and reported in the adjacent column. Measurements 1 through 3 are replicate measurements of the percent of the facet darkened by the rings. The average of these three readings is reported along with the standard deviation ( $\sigma_{n-1}$ ). This is a measure of the precision of the replicate measurements, not the total standard deviation associated with the values. The total error on the final calculation will be discussed below.

Once an average area was determined for each ring, Gaussian distribution calculations were performed. A standard erf z table<sup>6</sup> was used. One  $\sigma$  for a Gaussian distribution includes 68% of the total area. By comparing the fractional areas with the table, a fraction of the  $\sigma$  value was obtained. Sigma is then equal to the slope error (defined by the ring used) divided by the fractional  $\sigma$  value obtained from the table. The data used in these calculations and the resulting  $\sigma$  values for individual rings on each facet are recorded in the Appendix.

Readings at several different ring sizes verified whether or not the error distribution was truly Gaussian, and also allowed correction for faulty photographs. Individual readings were only excluded from the final averaging if a given  $\sigma$  calculation was significantly different ( $> 2$  standard deviations) from the rest of the values and/or an obvious problem with the photograph (such as overexposure) was evident.

Errors affecting the final  $\sigma$  calculation include uncertainty in the radius of curvature ( $\pm 2$  ft), and up to 2% variation in area determination caused by contrast changes within a series of photographs. These changes may alter the final result by up to 0.5 mrad and this value was set as the lower error limit. Occasionally, additional error increased this limit.

Table 5-3 is a compilation of the focal length (FL) and  $\sigma$  values associated with each of the tested SCAD program facets. SCAD-xxx identifies facets coated with Silverlux film, while VDA-xxx

**TABLE 5-3. COMPILATION OF FL MEASUREMENTS AND CALCULATED  $\sigma$  VALUES FOR GAUSSIAN DISTRIBUTIONS OF SLOPE ERROR IN SCAD PROGRAM FACETS; ERROR COLUMNS, FL ERR AND  $\sigma$  ERR, HAVE THE SAME UNITS AS PRECEDING COLUMNS; ANALYSIS AND INTERPRETATION OF DATA IS GIVEN IN THE TEXT**

Facet	FL (ft)	FL ERR	$\sigma$ (mrad)	$\sigma$ ERR
SCAD-001	43.0	0.3	2.5	0.5
SCAD-002	44.1	0.8	2.7	0.5
SCAD-003	44.5	0.5	2.2	0.5
SCAD-004	47.2	1.5	2.0	0.5
SCAD-005	45.9	1.6	3.2	0.5
SCAD-006	46.2	2.0	2.7	0.5
SCAD-007	51.1	1.2	3.4	0.8
SCAD-008	41.9	4.6	6.7	0.5
SCAD-009	49.6	2.0	5.8	1.2
SCAD-010	48.8	2.0	2.9	0.5
SCAD-011	45.0	1.9	1.4	0.5
SCAD-045	40.3	0.8	3.7	0.9
Avg and dev	45.6	3.2	3.3	1.5
Avg and dev-1	45.1	2.8	3.0	1.1
VDA-SQ	26.0	1.2	1.7	0.5
VDA-2S08	32.5	1.7	5.1	0.5
VDA210/24	38.4	0.8	3.7	0.9
VDA210/26	42.1	0.6	1.7	0.5
VDA-003	40.8	0.5	1.5	0.5
VDA-004	40.9	1.5	1.4	0.5
VDA-005	40.8	0.5	1.0	0.5
Avg and dev (VDA2-5)	40.6	1.3	1.9	1.1

6. Young, H. D., Statistical Treatment of Experimental Data, (McGraw-Hill, NY, 1962), p. 161.

facets were directly coated with aluminum. The focal length (FL) ERR column lists the error ( $\sigma_{n-1}$ ) associated with the replicate measurements of the focal length. For SCAD-008, this value is very high, and may be caused by wind loading and misalignment with the sun during measurement. measurements were repeated on other days, but the variance is still large. Such an uncertain FL may displace the radius of curvature as well. If this is displaced by greater than the allowed 2 ft, the reflection of the rings may also be distorted, and incorrect  $\sigma$  values accrue. Therefore avg and dev (average and standard deviation) for all the SCAD-xxx facets are reported, as well as avg and dev-1, which are the same calculations with the SCAD-008 data excluded. With this exclusion, an average focal length of 45.1 ft is obtained, compared to a specified value of 44.3 in.  $\pm$  1 in.

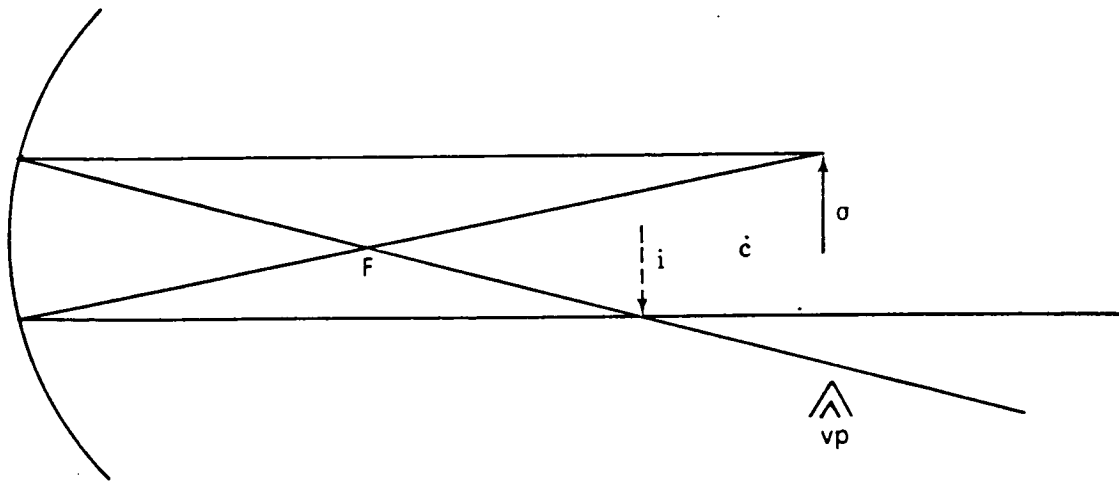
A slightly improved  $\sigma$  value for the slope error distribution is also obtained when SCAD-008 data are not used. However, the value is still larger than the specified 1.5 mrad. A combination of manufacturing details may account for this error. Reflective films may exhibit 1-2 mrad slope error caused by their adhesive backing; such errors are visible on Silverlux as "orange peel." The nonoptimized, pressurized application of the film, and the additional pressure formation of the curved surface is likely to introduce even more slope error. Visually, this can be seen as honeycomb print through and a ring pattern from the forming tool. There was insufficient time to correct these problems on the Silverlux coated samples, but were addressed on the development program for the aluminized facets.

Data for the facets coated with electron-beam deposited aluminum are shown in the lower half of Table 5-3. The first two entries were subscale, developmental samples prepared on a shorter radius tool, therefore, they are not included in the final avg and dev data compilation.

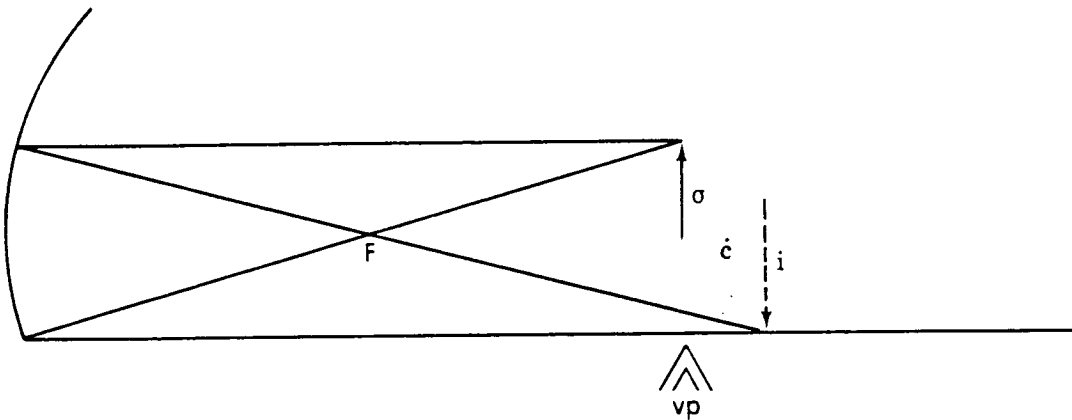
VDA-002 was measured for focal length on two different days, 24 October and 26 October. Different focal lengths were obtained, probably caused by different alignments with the sun or different wind conditions. Values taken on another day were intermediate between these sets, and an average focal length of 40.64 ft  $\pm$  1.88 ft obtained from all 24 sets of readings. However, slope error ring measurements were taken at the radii defined by the 10/24 and 10/26 data sets. Later correction of these errors was not possible, because the test area was required for another contract. This did offer an interesting test of the slope error technique, however, what effect would locating the camera 4.5 ft in front of the radius of curvature or 3 ft behind it have on the calculated slope error distribution? The results from VDA21024 and VDA21026 show that the  $\sigma$  value changes by 2.0 mrad. Location beyond the radius of curvature intercepts a diverging reflection, so more area appears dark (Figure 5-2). This results in a smaller apparent  $\sigma$  value. The reflection in front of the radius of curvature is more difficult to define but at least some of the reflected light is compressed to a smaller region (Figure 5-2). The  $\sigma$  calculation yields a larger value, since less of the surface appears dark. From these data, it is concluded that the true  $\sigma$  value lies somewhere between 3.7 and 1.7 mrad. A detailed analysis was not performed to exactly determine the value.

VDA-005 presents a similar problem. In this case, the focal length was precisely measured, but a mathematical error caused the slope error measurements to be recorded at 85.6 ft rather than the indicated 81.6 ft. Again, remeasurement was not possible because of time constraints on the test area. I suspect the reported  $\sigma$  value for this facet is low. The data from VDA21024 and VDA21026 suggests that it may be as much as 1.0 mrad larger than reported. However, even if the worst case ( $\sigma$  = 2.0 mrad) is assumed, the average for all three facets only increases to 2.06  $\pm$  0.94 mrad.

It would be most helpful to produce and measure additional facets so a realistic average value could be reported. In lieu of this, it can be noted that there appears to be an improvement in the slope error distribution as the result of processing changes incorporated in the later aluminum coated facets. This improvement was accompanied by a visual improvement in the appearance of the mirror surface, and in a more tightly focused reflected beam.



a. Ring target ( $\sigma$ ) placed beyond center of curvature places  $vp$  beyond  $i$



b. Ring target ( $\sigma$ ) placed in front of center of curvature causes  $vp$  to intercept reflections before they are fully focused at  $i$

Figure 5-2. Change in reflection recorded at the viewplane ( $vp$ ) when the ring target ( $\sigma$ ) is displaced from the center of curvature ( $c$ )



## 5.5 CONCLUSIONS

Optical data indicate that composite mirrors that closely approach requirements expected for a solar concentrator system can be produced. Over the course of this contract, numerous changes have been implemented to improve the mirrors. Our experience and increased understanding of this area, will allow us to include additional improvements in future programs.

## 5.6 DATA

Table 5-4 compiles the individual area measurements and  $\sigma$  calculations for each measured facet. The first entry under a facet designation is the average percent area darkened by a given ring size. The second entry is the  $\sigma$  value in mrad for a Gaussian distribution defined by that area measurement. Other comments are included where appropriate.

**TABLE 5-4. FACET SLOPE ERROR MEASUREMENTS**

Facet	Ring Size (in.)				
	2.265	3.5	4.5	5.5	6.75
SCAD-001					
% area	27.0	58.0	66.0	79.0	79.0
$\sigma$	3.2	2.1	2.3	2.1	2.6
SCAD-002					
% area	14.0	24.5	51.0	66.0	83.0
$\sigma$	6.1	5.4	3.0	2.7	2.3
SCAD-003					
% area	22.5	59.5	69.0	80.0	78.0
$\sigma$	3.7	2.0	2.1	2.0	2.5
SCAD-004					
% area	29.0	64.0	84.0	83.0	78.0
$\sigma$	2.7	1.7	1.4	1.8	2.4
SCAD-005					
% area	28.5	33.0	42.0	58.0	76.0
$\sigma$	2.8	3.7	3.7	3.1	2.6
SCAD-006					
% area	31.0	48.0	60.0	58.0	68.0
$\sigma$	2.6	2.5	2.4	3.1	3.1
SCAD-007					
% area	8.5	27.0	35.0	65.0	66.0
$\sigma$	8.4	4.1	4.0	2.4	2.9
SCAD-008					
% area	Photos inconsistent	Photos inconsistent	25.9	32.7	38.5
$\sigma$	--	--	6.8	6.5	6.7
SCAD-009					
% area	18.0	22.0	23.0	25.0	37.0
$\sigma$	4.1	5.3	6.5	7.2	5.9
SCAD-010					
% area	28.0	49.0	57.0	62.0	63.5
$\sigma$	3.0	2.5	2.7	3.0	3.5
SCAD-011					
% area	11.1	80.7	87.6	89.8	96.2
$\sigma$	7.5	1.3	1.4	1.6	1.5
SCAD-045					
% area	22.3	49.3	45.5	47.3	Photo too light
$\sigma$	7.4	2.7	3.8	4.5	
VDA-SQ					
% area	81.2	94.1	96.0	97.1	98.6
$\sigma$	1.4	1.5	1.8	2.0	2.1

TABLE 5-4. (Cont)

Facet	Ring Size (in.)				
	2.265	3.5	4.5	5.5	6.75
VDA-SUB % area $\sigma$	23.0 5.0	34.0 5.1	43.0 5.1	52.0 5.0	59.5 5.2
VDA-2 (10/24) <sup>a</sup> % area $\sigma$	15.8 6.2	31.9 4.6	42.6 4.4	64.6 3.2	83.4 2.6
VDA-2 (10/26) <sup>b</sup> % area $\sigma$	51.2 1.6	68.0 1.7	86.1 1.5	92.5 1.5	97.6 1.5
VDA-003 % area $\sigma$	60.2 1.4	80.4 1.4	87.0 1.5	93.4 1.5	95.1 1.8
VDA-004 % area $\sigma$	53.0 1.6	81.1 1.4	92.9 1.3	97.5 1.3	98.9 1.4
VDA-005 <sup>a</sup> % area $\sigma$	81.3 0.9	92.1 1.0	98.6 0.9	99.6 1.0	99.8 1.0
a. Measured in front of curvature radius. b. Measured beyond curvature radius.					

## 6. CONCLUSIONS AND RECOMMENDATIONS

The main objective of the SCAD program was to develop critical technologies for spaceborne solar concentrators through the design, assembly, and optical evaluation of a full-scale prototype solar concentrator that would be characterized in a terrestrial environment.

In support of the SCAD program, 228 composite beams have been fabricated and delivered for the main concentrator framework. Mirror facets (48) have also been fabricated and delivered to partially populate the SCAD concentrator to facilitate optical characterization and alignment tests. In addition, a development program has been completed resulting in facets with higher quality and cleaner composite surfaces necessary for vapor deposited metal reflective coatings. Although the SCAD program advanced the state of the art in composite mirror technology, many areas need to be addressed before deploying a solar concentrator for Spaceborne service. A post-SCAD meeting was held to consolidate information from both Harris and Hercules to identify materials and processes that would improve mirror facet optical and environmental performance while meeting other critical design requirements (e.g., weight, stiffness). Representatives from Hercules and Harris drew on lessons learned over the past two years to identify issues and potential solutions needed to successfully produce highly specular mirrors using graphite reinforced epoxies.

Major issues discussed, along with potential causes and solutions, are:

- **Specularity** - Reduction in specularity is primarily caused by roughness in the substrate surface; solutions are primarily based on methods to minimize surface roughness.
  - **Causes**
    - Resin shrinkage during cure cycle
    - Large CTE difference between resin and fiber causes print through
    - Pressure loading of fibers/resin during cure
    - Nonuniformity of fiber distribution
    - Large tow diameters
    - Fabric crossovers
    - Surface pitting
    - High resin content
    - Moisture absorption in the resin
    - Contamination before and after coating
    - Microcracking
    - Temperature changes may affect specularity
  - **Solutions**
    - Low shrinkage resin systems

- Room temperature cure resins
- Cure at operating temperature
- Postcure strain relief
- Room temperature secondary cure
- Higher CTE fibers
- Glass microballoons in resin (syntactic foam) to reduce CTE
- Graphite microballoons
- Add graphite whiskers to epoxy (near homogeneous composite)
- Thinner plies (smoother distribution of fibers)
- Graphite veil and 1 mil plies
- Spray epoxy gel coat
- Sol gel coating to planarize
- Replicate mirror surface
- Thermoplastics, polycarbonates
- **Slope Error** - Slope error is the deviation of the actual geometry from the theoretical geometry or perfect facet shape
  - Causes
    - Honeycomb print through
    - Excessive bonding pressure
    - Shrinkage of adhesive fillets
    - Excessive adhesive
    - Nonuniformity of bondline between honeycomb and face sheet
    - Springback caused by internal stresses and thermal distortions
    - Tool inaccuracies
    - Face sheet not held down on tool during cure
    - Contaminants between face sheet and tool
    - Disbonds, voids
    - Nonsymmetric face sheets



- Resin buildup on one face sheet side
- Uneven tension in face sheet
- Residual stress in face sheet from forming on flat surface
- Nonisotropic layup, fabric versus unidirectional
- Face sheet and honeycomb edge effects
- Flat inserts distort corners
- Mounting constraints
- Handling loads
- Solutions
  - Reduce bonding pressure
  - Vacuum chuck techniques
  - Control vacuum pressure
  - Gel bags
  - Room temperature adhesives to minimize internal stresses
  - Fine weave unidirectional
  - Beam backup structure
  - Edge closeout or C-channel
  - Lamina/laminate orientation, construction
  - Smooth tool, lapping, diamond machining
  - Accurate measurement of tool
  - Remove breather
  - Tooling bridge
  - Clean/degrease components
  - Clean room manufacturing
  - Optimize insert design
  - Optimize flexure design
  - Minimize handling, optimize procedures

- Aluminize backside to minimize thermal gradient
- **Weight**
  - Causes
    - Excessive face sheet thickness
    - Excessive adhesive
    - Inefficient hardpoint design
    - Unnecessary scrim
    - Dense adhesive
  - Solutions
    - Identify thinner prepreg materials
    - 1 mil prepreg
    - Eliminate glass scrim
    - Squeegee adhesive from face sheets
    - Control adhesive thickness
    - Less dense adhesives
  - Reticulating film adhesive
  - Perforated film adhesive
  - Adhesive filler
  - Slotted honeycomb
  - Graphite or titanium honeycomb (coated)
  - Reduce honeycomb wall thickness
  - J-beam stiffening structure
  - Ribbed aluminum sheet
  - Optimize insert design
- **Surface Protection** - Protection is required for not only the environments but also against contamination during the manufacturing process
  - Causes--Environments

- Thermal cycling--could cause microcracking and other thermoelastic distortions
- Humidity--Moisture absorption by the resin causes hygroscopic distortion and reduces specularly
- Atomic oxygen--causes erosive degradation of soft substrate surfaces that reduces specularly
- UV radiation--cleaves chemical bonds in epoxy resins
- Solutions--Environments
  - Coat backside to minimize thermal gradient
  - Seal face sheets on both sides
  - Aluminum reflective coating to block UV
  - Copper undercoat to block UV with silver
  - Protect edges
- Causes--Handling
  - Soiling during fabrication will degrade coatings
  - Abrasion, soiling will reduce optical performance
  - Cleaning methods have not been identified
  - Solvents contaminate surface
- Solutions--Handling
  - Soiling during fabrication will degrade coatings
  - Abrasion, soiling will reduce optical performance
  - Cleaning methods have not been identified
  - Solvents contaminate surface
  - Identify strippable films and application methods
  - Identify methods to clean protective coatings
  - Electrostatic cleaning methods
  - Strip film sheet
  - Saran wrap
  - Inflatable balloon

- Material cleaned by atomic oxygen
- Replication
- Thick SiO<sub>x</sub>
- Eliminate shipping between process steps
- Design better containers
- Manufacturing in a clean room environment

The SCAD program has advanced solar concentrator technology for space use. Further research and development is needed to support the solar concentrator power generation system scheduled for the Phase 2 expansion of the Space Station. Continued development will lead to operational capability by the early 1990s.



**APPENDIX A**  
**PHOTOS OF FACET**  
**ASSEMBLY PROCESS**

The facet assembly process was described in Section 3.3.4. These photos of the assembly process will aid in understanding the complete procedure.



ORIGINAL PAGE  
BLACK AND WHITE PHOTOGRAPH

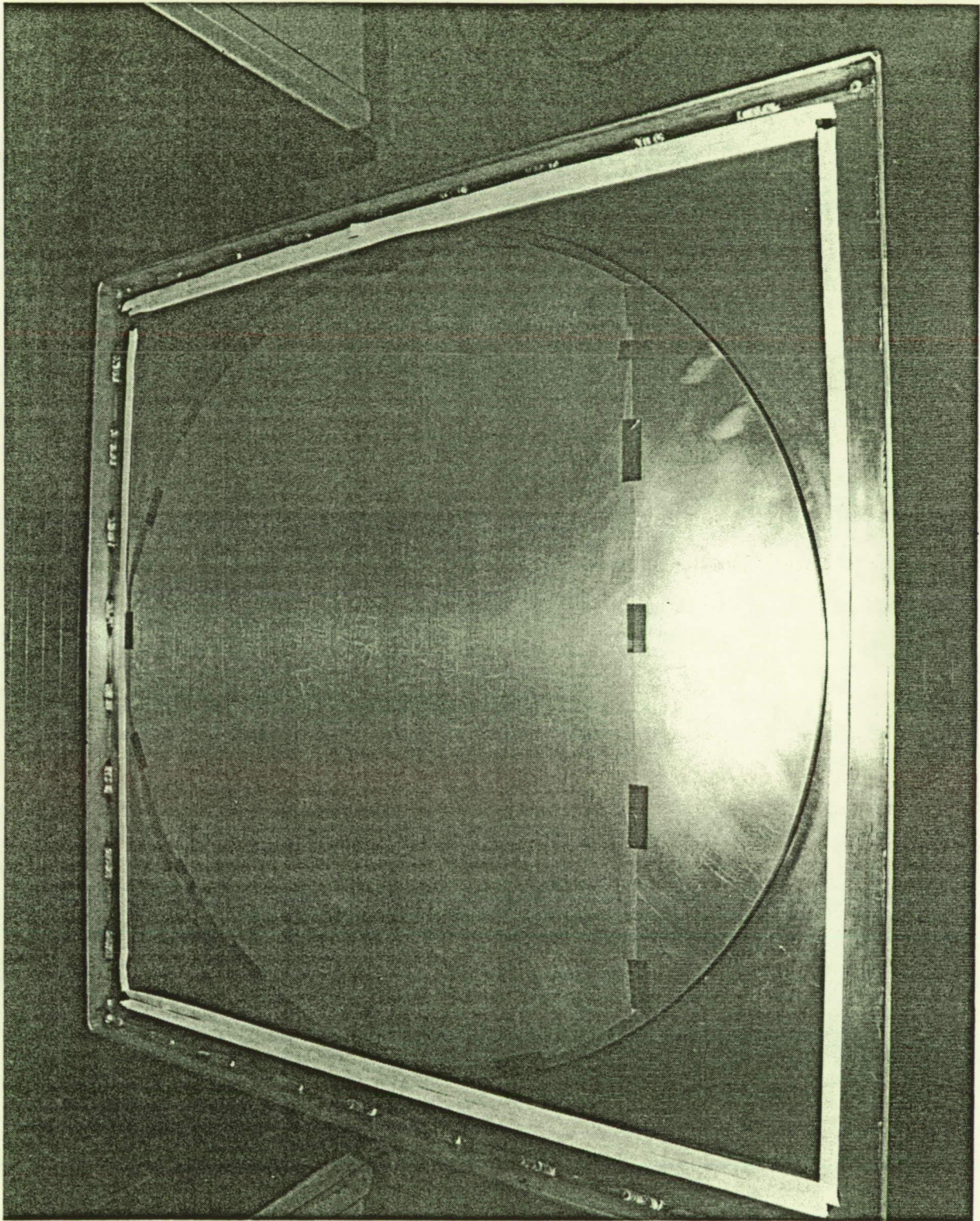


Figure A-1. The first step in the bonding process is to prepare the spherically contoured tool; surface is degreased, and then covered with one ply of Teflon coated fiberglass breather



ORIGINAL PAGE  
BLACK AND WHITE PHOTOGRAPH



Figure A-2. The face skin, back skin, and honeycomb core are laid out on a clean working surface where the peel plies are removed, and the parts degreased.



ORIGINAL PAGE  
BLACK AND WHITE PHOTOGRAPH

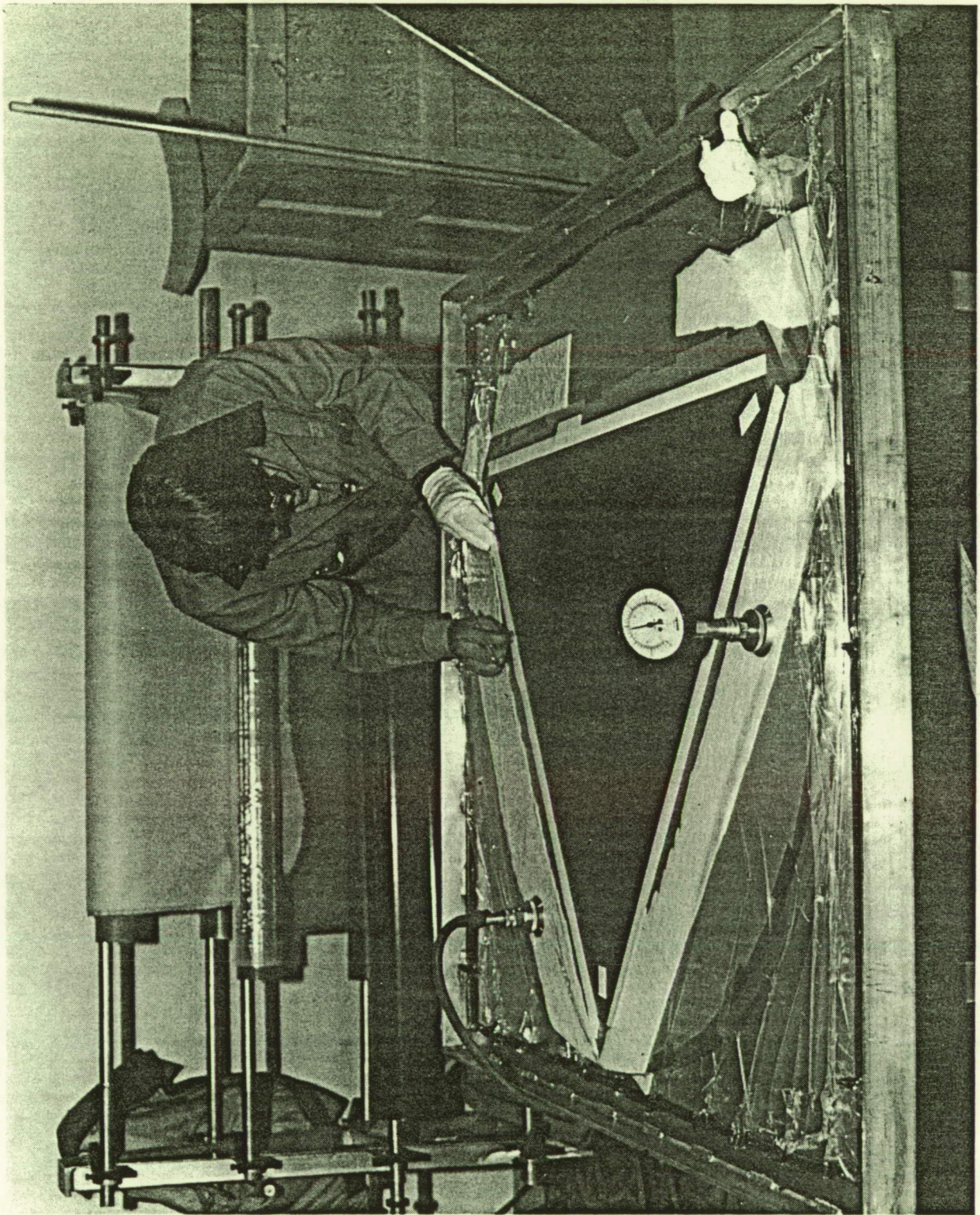


Figure A-3. The reflective face skin is placed on the bond tool, vacuum bag is sealed to the tool and to the edge of the face skin when vacuum pressure is applied, gage reading of about 20 in Hg is obtained. This process was only used for the vapor deposited metal facets



ORIGINAL PAGE  
BLACK AND WHITE PHOTOGRAPH

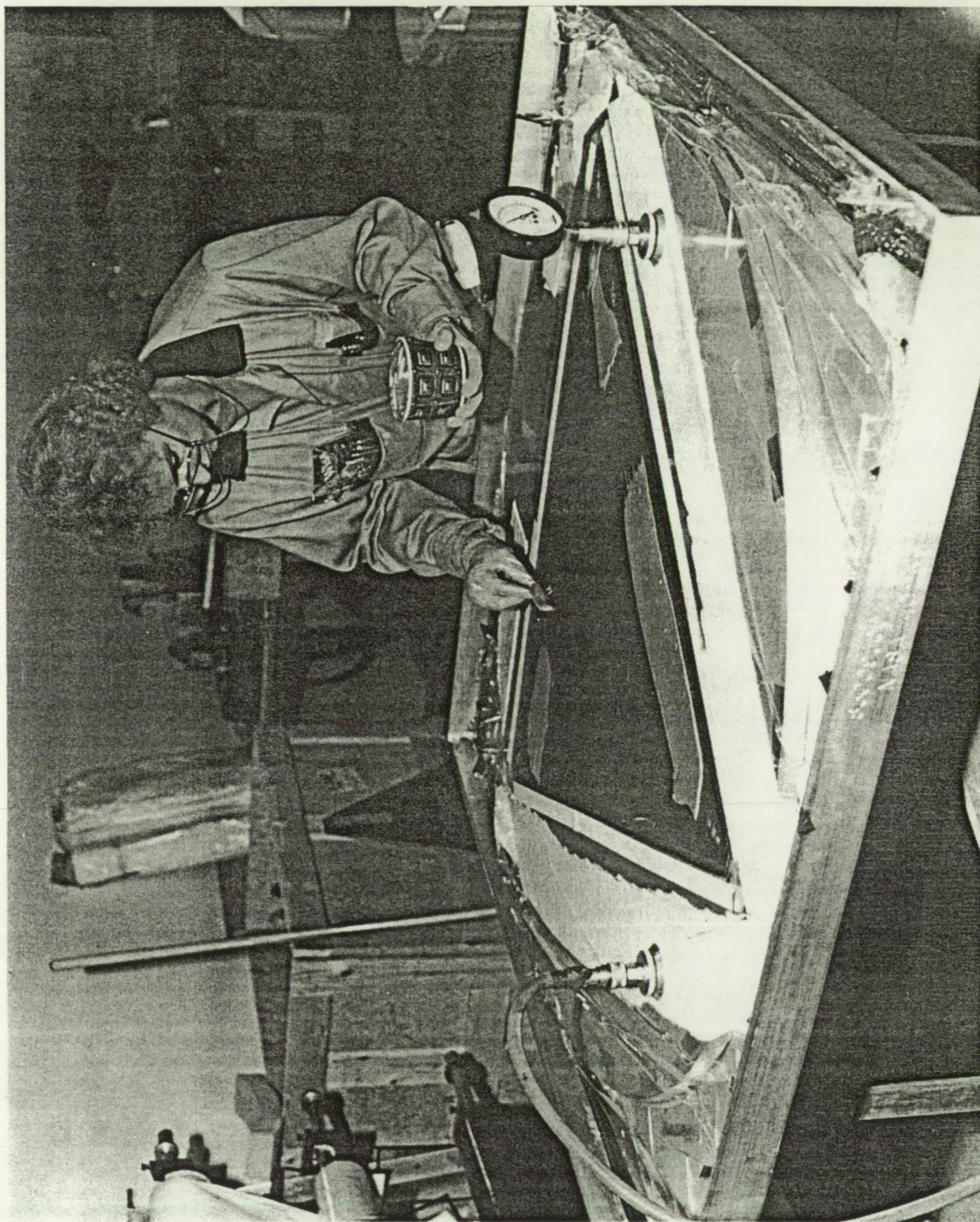


Figure A-4. With the face skin held firmly in place by vacuum pressure, the room temperature curing epoxy adhesive is screeded onto its back side



ORIGINAL PAGE  
BLACK AND WHITE PHOTOGRAPH



Figure A-5. Adhesive is spread to a uniform coating with short-bristled paint rollers; bondline is approximately 0.020 in. thick



ORIGINAL PAGE  
BLACK AND WHITE PHOTOGRAPH



Figure A-6. A 104 oz fiberglass scrim is applied to the wet surface; scrim acts as insulator between aluminum core and graphite skins to prevent galvanic corrosion



ORIGINAL PAGE  
BLACK AND WHITE PHOTOGRAPH

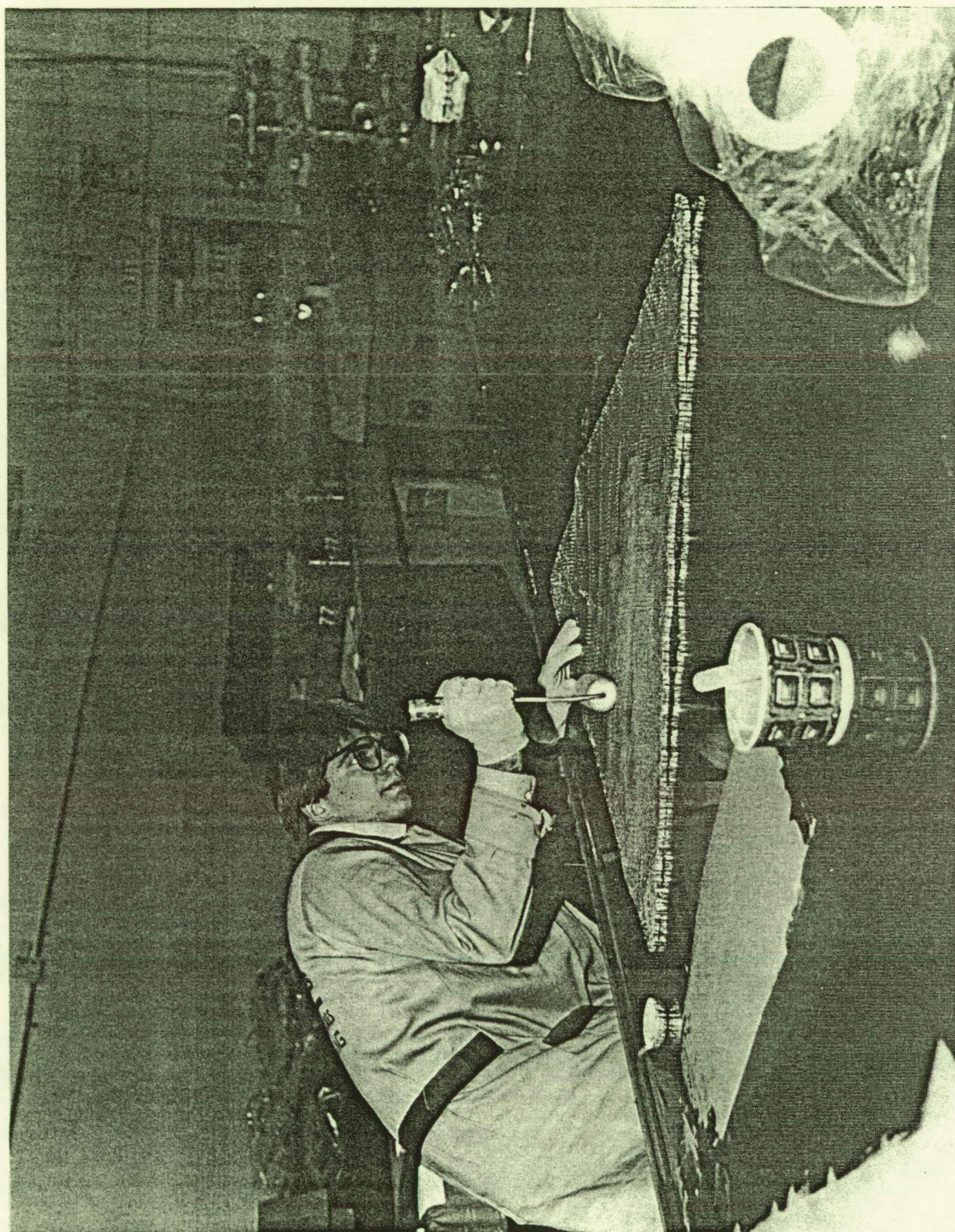


Figure A-7. Honeycomb is coated with adhesive; use of the paint roller enables adhesive to cover 0.020 in. down cell walls; aluminum inserts have previously been bonded into corners with foaming adhesive



ORIGINAL PAGE  
BLACK AND WHITE PHOTOGRAPH



Figure A-8. Honeycomb is placed onto face skin; holes in inserts are aligned to those in the face skin, and two gage pins are inserted at each corner

ORIGINAL PAGE IS  
OF POOR QUALITY





Figure A-9. Top side of honeycomb is also coated with adhesive



ORIGINAL PAGE  
BLACK AND WHITE PHOTOGRAPH



Figure A-10. Back skin is coated with adhesive

ORIGINAL PAGE IS  
OF POOR QUALITY



ORIGINAL PAGE  
BLACK AND WHITE PHOTOGRAPH

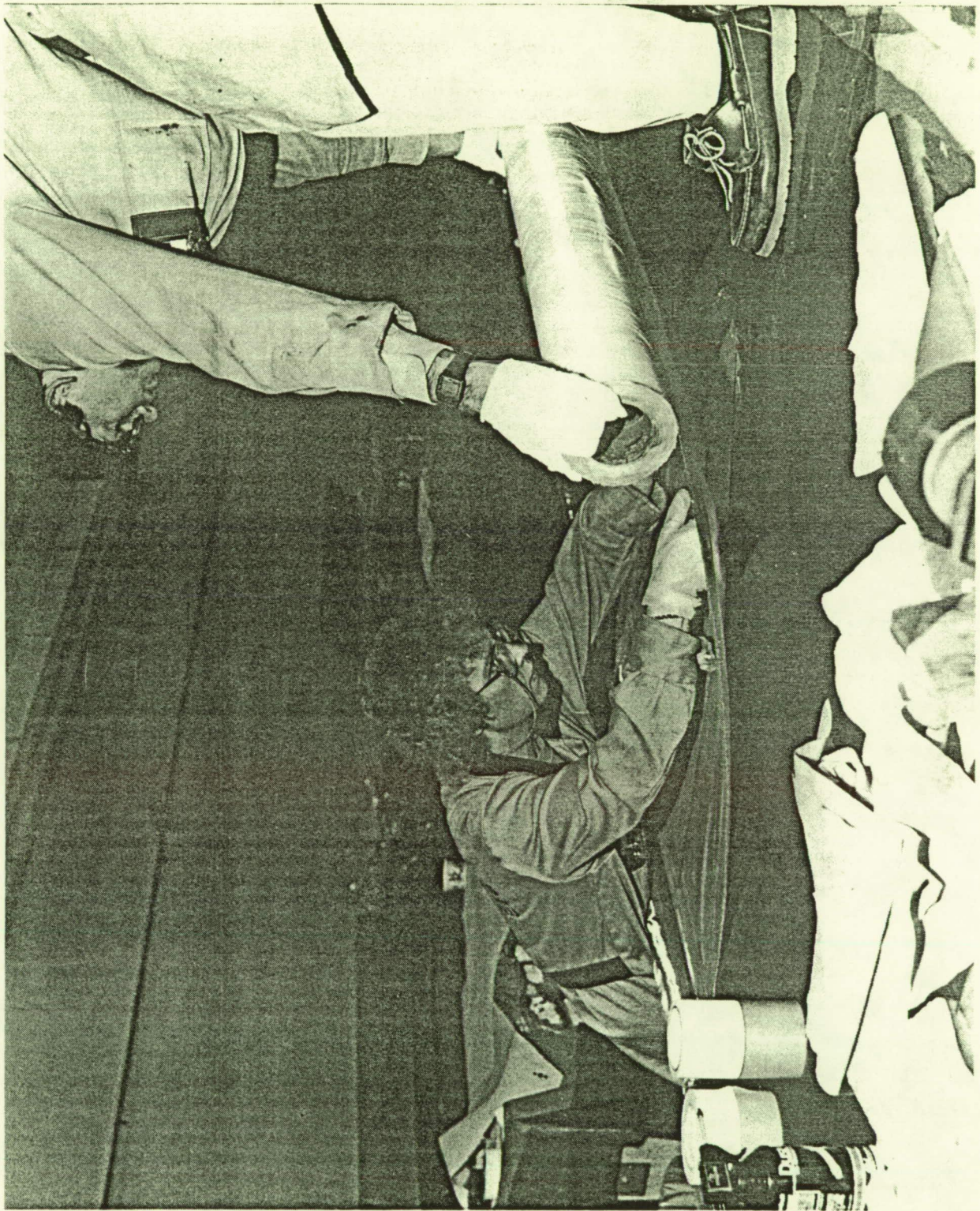


Figure A-11. Fiberglass scrim is applied to back skin

ORIGINAL PAGE  
BLACK AND WHITE PHOTOGRAPH

A-13

ORIGINAL PAGE IS  
OF POOR QUALITY

C-4



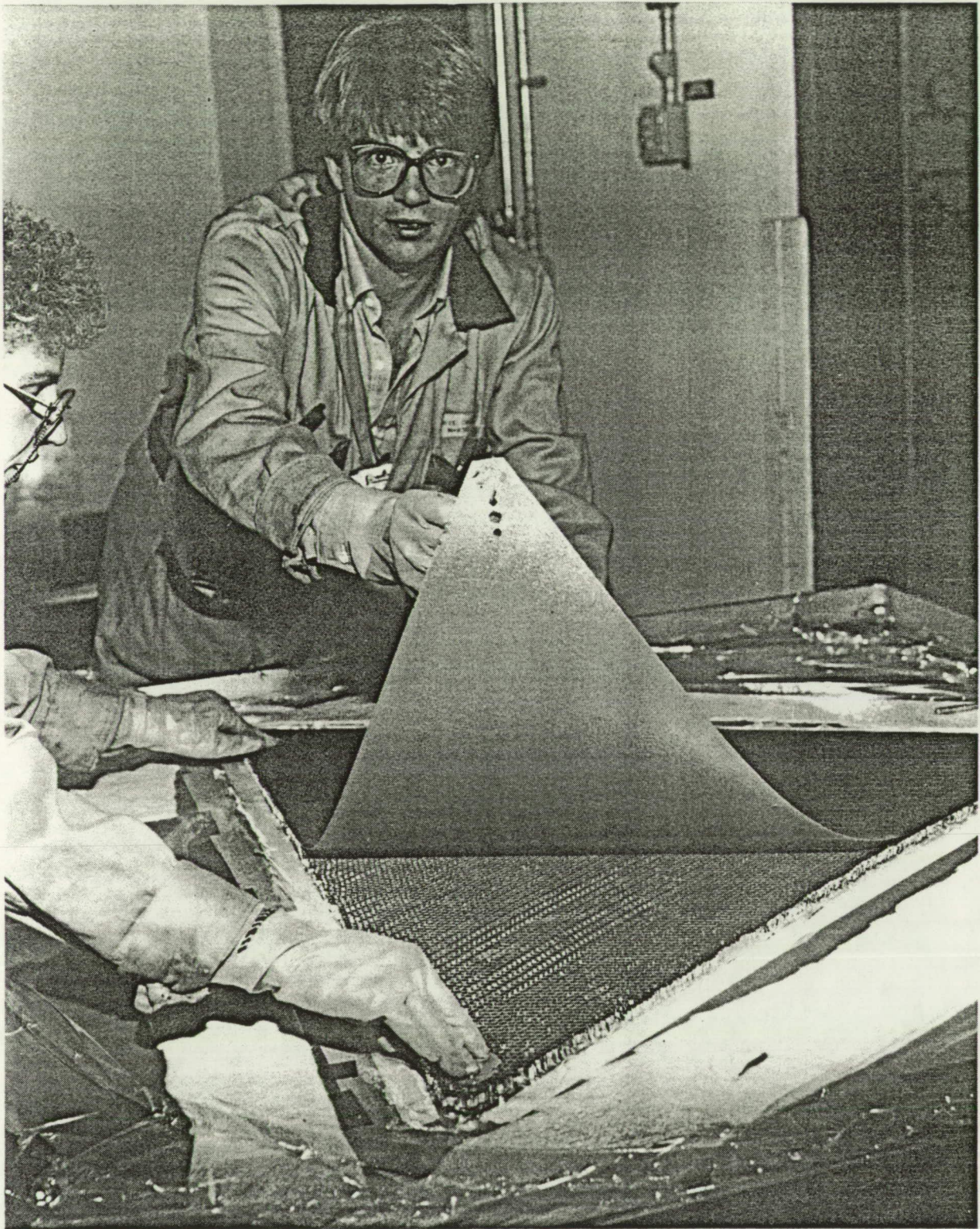


Figure A-12. Back skin is placed onto honeycomb, aligning holes to pins at each corner



ORIGINAL PAGE  
BLACK AND WHITE PHOTOGRAPH

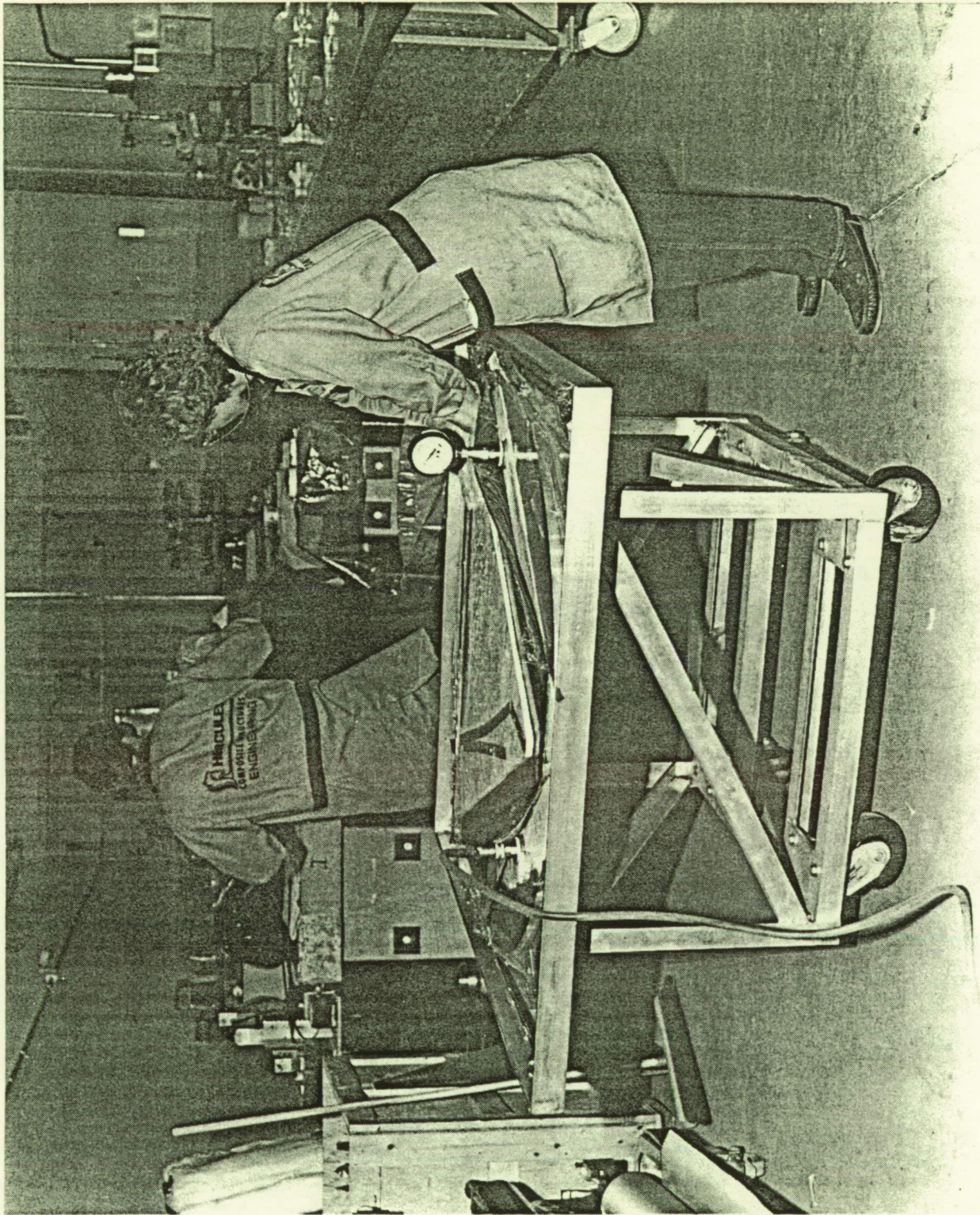


Figure A-13. Pressure on top of sandwich is required to maintain uniform contact at bondline; molded RTV rubber sheet is used to match spherical contour



ORIGINAL PAGE  
BLACK AND WHITE PHOTOGRAPH

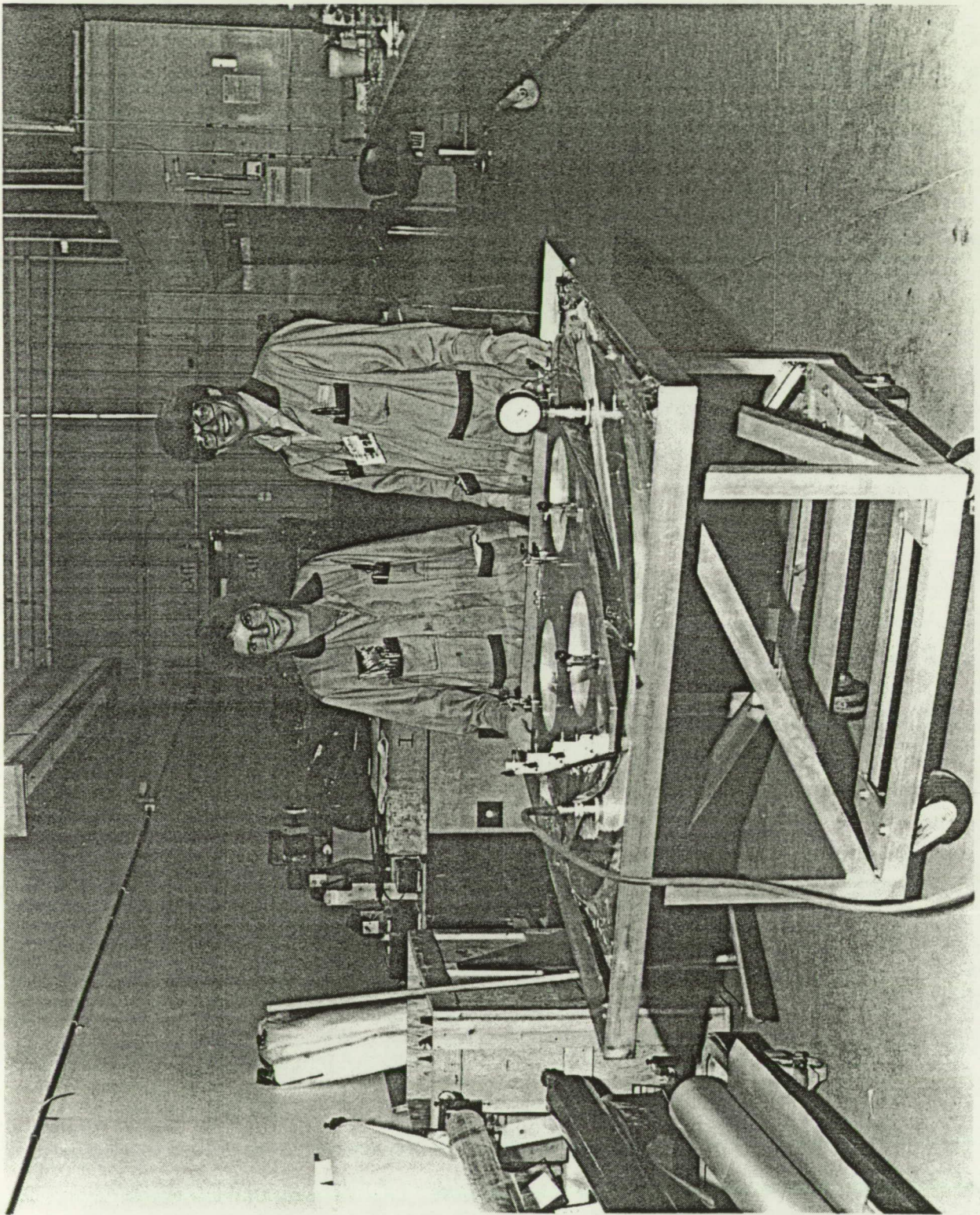


Figure A-14. Face skin drill fixture is placed on top of assembly to supply approx 50 lb of force to sandwich structure; adhesive cures at room temperature in 15 hours



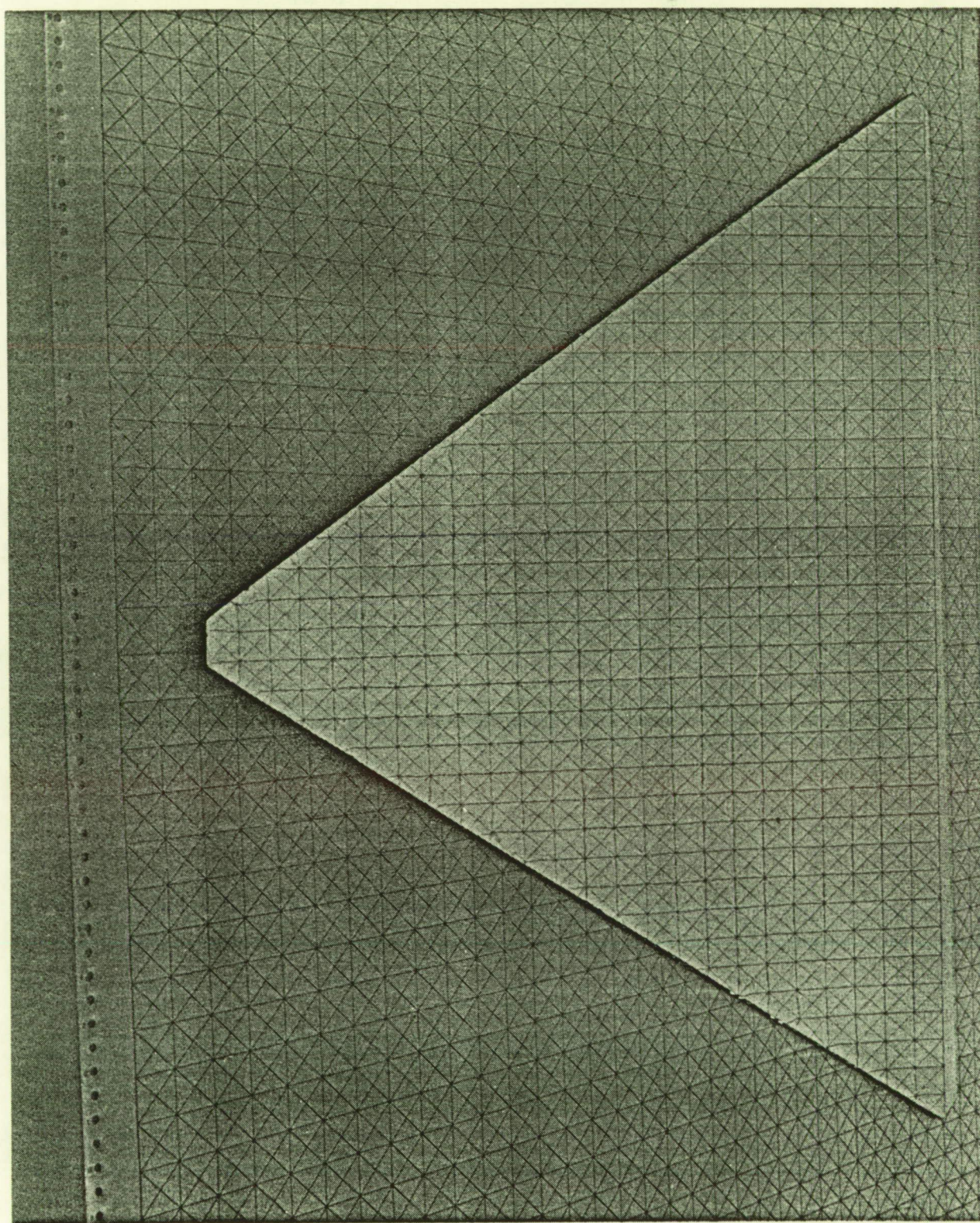


Figure A-15. Typical facet reflecting a 1-in. grid



**APPENDIX B**  
**SLOPE ERROR MEASUREMENT PHOTOS**

Details of slope error measurement was given in Section 5.2. These photos are typical of the type of photos obtained during facet slope error measurement.

Representative photographs from a series of slope error measurements are shown in Figures B-1 through B-3. Decreasing ring sizes were used for these photographs. The size of the ring can be directly related to the magnitude of the slope error. The largest ring (Figure B-1) darkens almost all the facet, indicating that most of VDA-003 has a slope error  $\leq 3.44$  mrad. Only areas with smaller slope errors will be darkened by smaller rings, as witnessed by the reduction in dark areas in Figures B-2 and B-3.

The calculation of  $\sigma$  values from dark area measurements was explained in the main text. For reference, these photographs were used to generate the first, third and fifth rows of VDA-003 data presented in Figure B-3.

ORIGINAL PAGE  
BLACK AND WHITE PHOTOGRAPH

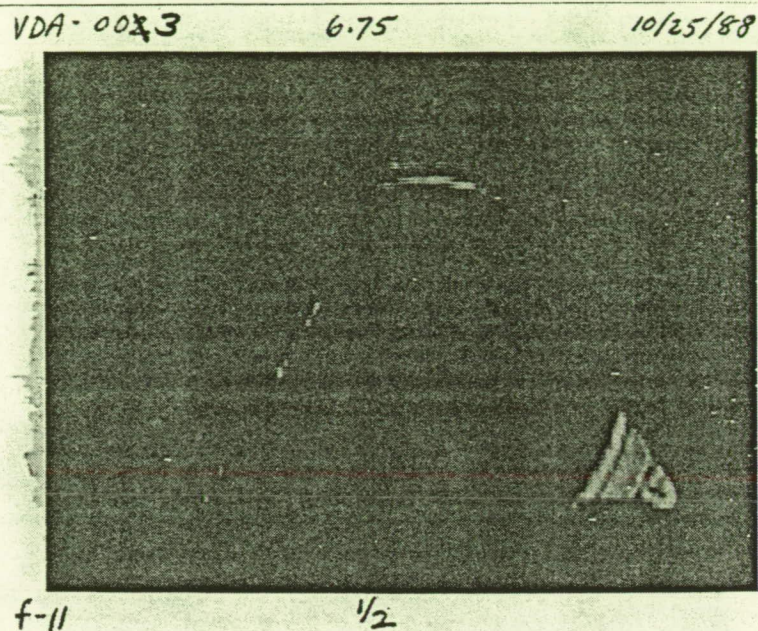


Figure B-1. Facet VDA-003 reflecting a ring target with  $r = 6.75$  in.; area darkened by ring has slope error of less than or equal to  $3.44$  mrad

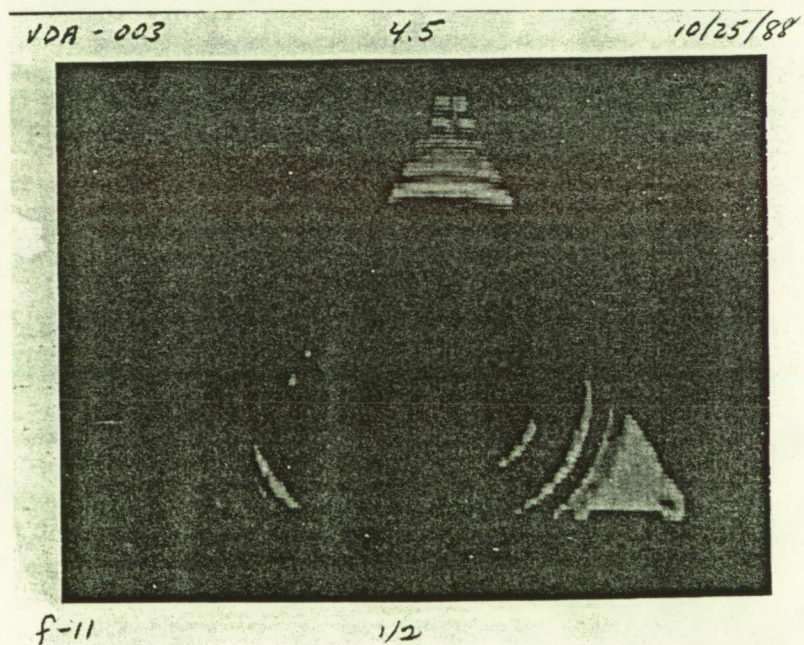


Figure B-2. Facet VDA-003 reflecting a ring target with  $r = 4.5$  in.; area darkened by ring has slope error of less than or equal to  $2.30$  mrad

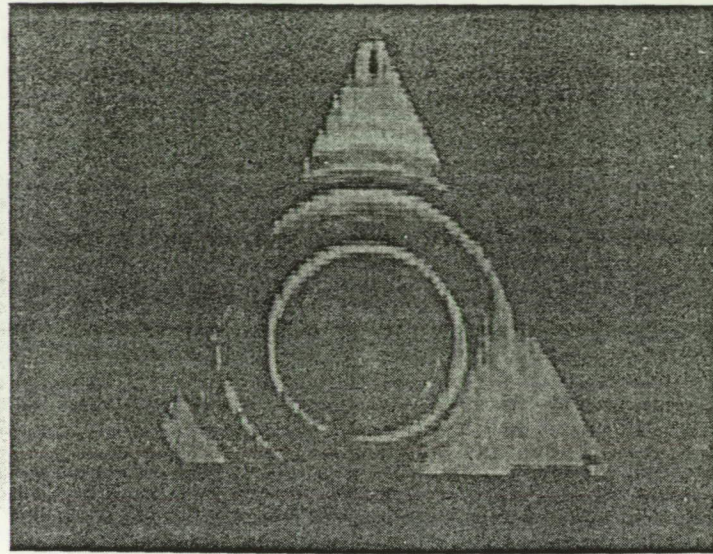


ORIGINAL PAGE  
BLACK AND WHITE PHOTOGRAPH

VDA-003

2.265

10/25/88



ORIGINAL PAGE IS  
OF POOR QUALITY

f-11

$\frac{1}{2}$

Figure B-3. Facet VDA-003 reflecting a ring target with  $r = 2.265$  in.; area darkened by the ring has slope error of less than or equal to  $1.16$  mrad

APPENDIX B

HEX PANEL REPAIR OUTLINE

## Appendix B

### Panel Repair

If a graphite box beam or bond joint fails during proofload, it can be repaired without compromising the structural integrity of the panel.

### Radial Beam Failure

The failure of a radial beam requires that the beam, two corner shear plates, and the hub shear plates be replaced.

First, the shear plates are removed by applying heat with a large soldering iron and breaking the bonds. Then the beam is removed by applying heat to the beam and removing the corner fitting from the beam. After the graphite parts are removed, the epoxy at the bond joints is removed with a Dremel tool and sand paper. When this operation is complete the panel is placed into the bonding fixture and .100 inch shims are placed under the locations without shear plates so warpage is not induced. The beam and top shear scheme plates are then bonded in accordance with the bonding procedure outlined in Section 3. After curing at least 12 hours the panel is flipped and the remaining shear plates are installed.

### Circumferential Beam Failure

A circumferential beam failure requires that the failed beam and the beam opposite it in the panel and all affected shear plates be replaced. The affected items are removed and surface preparation is completed in the same manner as the radial beam repair. After the panel has been prepared,



the panel is bonded with the same sequence of events as the panel bonding procedure Day 2 in Section 3.0, however, the .100 inch shims must be added under the locations without shear plates.

The repaired panel must be cured for 7 days and can then be proofloaded.

APPENDIX C

PANEL PROOFLOAD PROCEDURE

### 3.0 Requirements

#### 3.1 Test Levels

Applied loads for each of the three types of proofloading are:

1. Circumferential - 88 lbs, 6 locations; 6 tests
2. Radial - 100 lbs, 3 locations; 6 tests
3. Latch - 780 lbs, 2 locations; 3 tests

All loads shall be applied incrementally and as symmetrically as possible. The following loading sequence shall be used:

STEP	%MAX LOAD
1	0
2	25
3	0
4	25
5	50
6	75
7	100
8	75
9	50
10	25
11	0

#### 3.2 Test Durations

Full loads shall be applied for the minimum duration sufficient to demonstrate that the structure was able to support the load. The complete loading sequence shall be applied as expeditiously as possible to minimize the possibility of structural creep.

#### 3.3 Pass/Fail Criteria

The successfulness of the proofload tests is determined by the ability of the structure and bond joints to support the proofloads without cracking, splintering or delamination and without catastrophic failure.

If catastrophic failure of a bond joint, structural beam or shear plate occurs, the Test Director shall immediately stop the test, remove the load from the structure and follow the procedures outlined in the paragraph entitled Test Failures.



Non-catastrophic failures may be indicated by acoustic events (popping, cracking) which may be caused by a weakening of the structure. Some noise from deflections of the tooling and structure can be expected. At the discretion of the Test Director, suspicious acoustic events shall be investigated by unloading the structure and measuring the repeatability of the deflection measurements on the dial indicators to determine whether or not the structure has weakened. After successful application of the proofload, the structure and structural bonds shall be inspected for any visible signs of cracking, splintering or delamination.

#### Test Failures

In the event of a failure, testing shall be suspended for all structures until the cause of the failure is determined and an appropriate course of action is defined by the Failure Review Board.

Testing may be resumed without customer approval if the failure mode does not interfere with or affect the performance of the concentrator. If the failure necessitates a design or manufacturing procedure change, verbal approval from the customer must be obtained before proceeding to retrofit and/or refurbish the structure.

### 3.4 Safety Precautions

The following safety precautions shall be followed:

1. At no times shall a single individual attempt to lift more than 65 lbs at one time. Two people may lift weights between 65 and 130 lbs. A crane should be used to lift weights in excess of 130 lbs.
2. Weights shall be applied incrementally and as evenly distributed as possible.
3. Accumulated dust, grease and grime shall be removed from the hex support rods and cups just prior to the application of any loads.
4. Safety glasses shall be worn while loads are applied to the structure.
5. Steel toe shoes are recommended for all test personnel that are responsible for handling weights.

### 3.5 Handling Requirements

1. A minimum of two people are required to lift, turn or carry a hex structure assembly. Special care should be taken to prevent any inadvertent damage to the structure caused by dropping, bumping or general mishandling.

#### 4.0 Test Procedure

##### 4.1 Test Preparations

1. Thoroughly clean the proofloading structure support rods and cones prior to assembly.
2. Adjust and level the seven proofload fixture support cones to place them in their nominal positions. Tighten fingertight only.
3. Assembly six support rods on the hex structure and tighten to 60 in-lbs. Mount latch interface tools to hex corners and tighten to  $40.35 \pm 4.5$  in-lbs.
4. Remove structure from storage frame and place on proofload fixture. Allow support rods to center themselves in the cones.
5. Loosen all six circumferential cones and adjust their positions until all seven support rods are fully seated. Tighten cone screws to 75 in-lbs.
6. Mark the approximate locations for load application with masking tape at the locations shown in Figure 1. Mark the exact locations on the tape with a pen.
7. Verify that the total amount of weight needed for the proofload tests are on hand and are of the proper weights for incremental loading.
8. Check for proper calibration of the load cells.

##### 4.2 Sequential Operation and Verification Steps

###### Radial Beam Proofload

1. Place twelve, 25 lb weights beneath radial beam to be proofloaded.
2. Center ( $\pm .25"$ ) 3 slings over the marks made on the radial beam from paragraph 4.1, step 6 as shown in Figure 1.
3. Record structure and beam serial numbers on the data sheet.
4. Place a dial caliper on the top side of the beam near the center at the location marked "Z" in Figure 1. Zero the caliper.
5. Place 25lb weights on each sling, starting from position A and then positions B and C as shown in Figure 1.

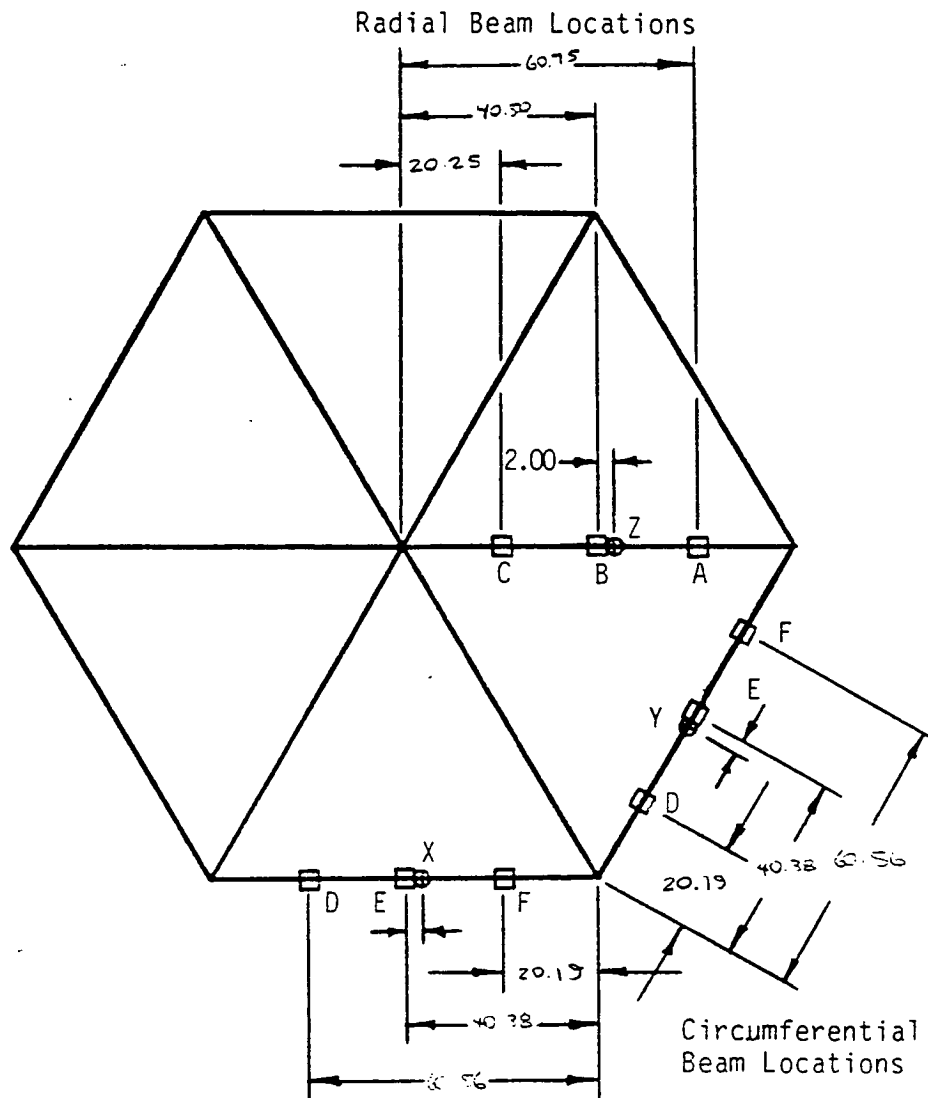


Figure 1. Radial and Circumferential Beam Proofload

6. Listen for any acoustic events which may indicate a weakening of the structure. If an abnormal acoustic event is heard, the Test Director (at his/her discretion) should determine if the structure has incurred damage by inspecting bond joints and structural members or by incrementally unloading the structure and comparing the dial caliber readings. If it is determined by the Test Director that the structure has incurred damage, then the procedures outlined in Paragraph 3.3, Test Failures shall be followed.
7. After the successful application of each load step record the total amount of applied weight, the deflection on the dial caliber and any significant comments or events.
8. Repeat steps 4 through 7 following the loading sequence in paragraph 3.1 until 100 lbs is applied at each location (300 lbs total).

9. Remove the weights in the reverse order from which they were applied. Record the readings on the dial calipers and compare with the readings in step 7 to determine if structural damage has occurred.
10. Repeat steps 1 through 9 for each of the other 5 radial beams.

#### Circumferential Beam Proofload

1. Place twelve, 22 lb weights beneath the two adjacent circumferential beams to be proofloaded.
2. Center ( $\pm .25"$ ) 6 slings over the marks made on the circumferential beams from paragraph 4.1, step 6 as shown in Figure 1.
3. Record structure and beam serial numbers on the data sheet.
4. Place a dial caliper on the top side of both circumferential beams near the center at the locations marked "x" and "y" in Figure 1. Zero the calipers.
5. Place 22 lb weights on each sling, starting from positions D and then positions E and F as shown in Figure 1. Two people should be available to load each beam.
6. Listen for any acoustic events which may indicate a weakening of the structure. If an abnormal acoustic event is heard, the Test Director (at his/her discretion) should determine if the structure has incurred damage by inspecting bond joints and structural members or by incrementally unloading the structure and comparing the dial caliber readings. If it is determined by the Test Director that the structure has incurred damage, then the procedures outlined in Paragraph 3.3, Test Failures shall be followed.
7. After the successful application of each load step record the total amount of applied weight, the deflection on the dial caliper and any significant comments or events.
8. Repeat steps 5 through 7 following the loading sequence in paragraph 3.1 until 88 lbs is applied at each location (528 lbs total).
9. Remove all weights in the reverse order in which they were applied. Record the readings on the dial calipers and compare with the readings in step 7 to determine if structural damage has occurred.
10. Repeat steps 1 through 9 five times, exercising the other five corners. Do not rotate or reposition the structure for each test.



### Latch Loads Proofloading

1. Remove the two support rods from the opposite corners of the structure, near the load application points as shown in Figure 2.
2. Loosen the four remaining support cones and readjust their positions to allow the support rods to fully seat, if necessary. Tighten the cone screws to 75 in-lbs.
3. Attach the corner attachment brackets and proofload cables to the corners which will be loaded as shown in Figure 2.
4. Adjust the location of the tiedowns on both ends of the structure such that the cables will pull on the corners at the angles prescribed in Figure 2.

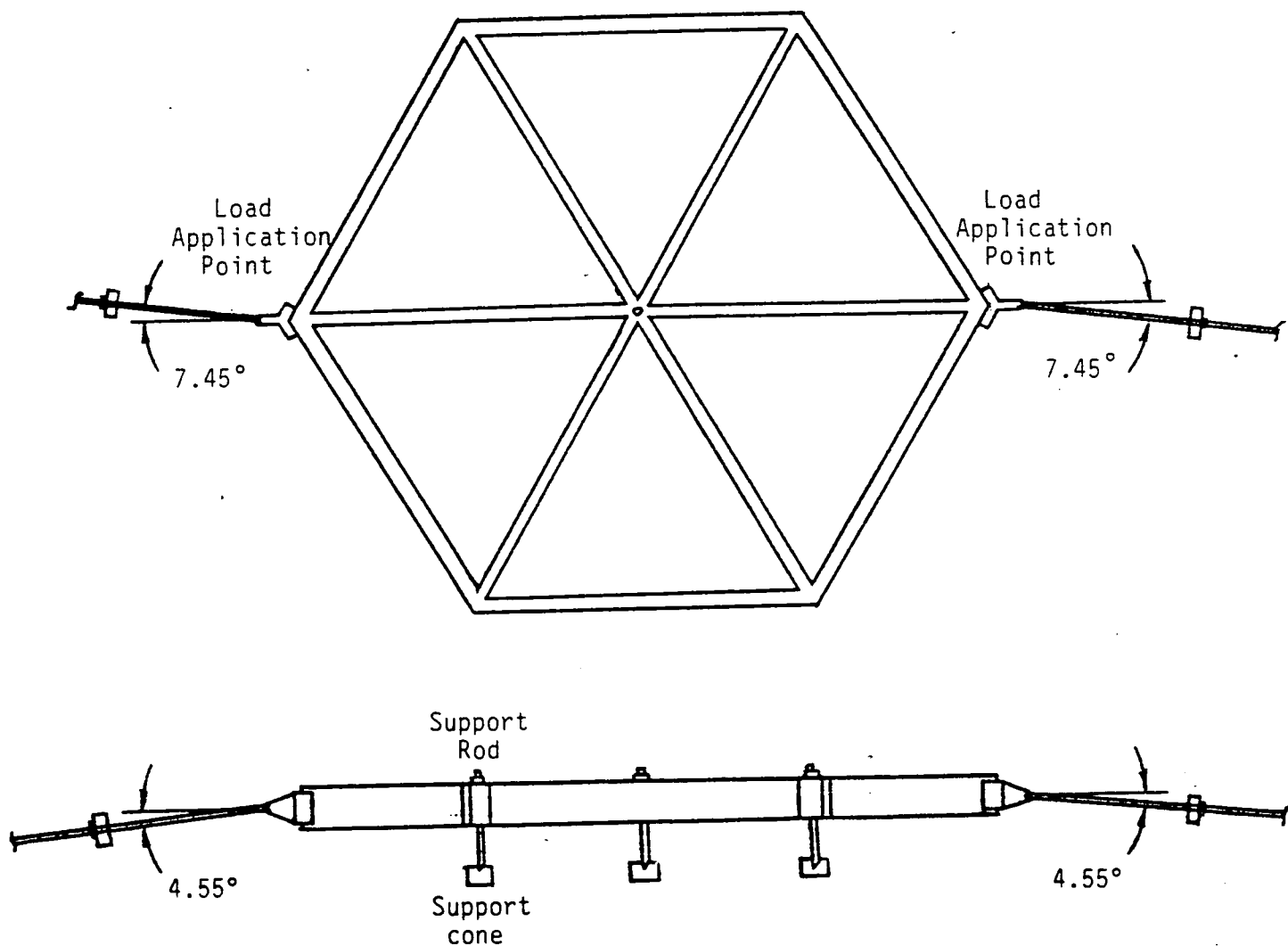


Figure 2. Latch Load Proofload

5. Remove the slack from the cables by tightening the turnbuckles.
6. Record the structure and radial beam (loaded) serial numbers on the data sheet.
7. Set dial calipers on both corners to measure longitudinal deflections of the corners. Apply the load to both corners simultaneously by turning both turnbuckles. Monitor the load with the load cells. At no time should the tension in each cable differ by more than 5 lbs.
8. Increase the load in 195 lb increments by following the loading sequence in paragraph 3.1 until 780 lbs is attained. Record the readings on the dial calipers and any significant comments or events after each load step has been successfully applied.
9. Listen for any acoustic events which may indicate a weakening of the structure. If an abnormal acoustic event is heard, the Test Director (at his/her discretion) should determine if the structure has incurred damage by inspecting bond joints and structural members or by incrementally unloading the structure and comparing the dial caliber readings. If it is determined by the Test Director that the structure has incurred damage, then the procedures outlined in Paragraph 3.3, Test Failures shall be followed.
10. After the successful application of each load step record the total amount of applied weight, the deflection on the dial caliper and any significant comments or events.
11. Remove the load by loosening the turnbuckles. Maintain an even tension within 5 lbs between both cables.
12. Record the deflections on the dial calipers at each load step.
13. Remove the corner attachments and reinstall the corner rod supports.
14. Repeat steps 1 through 13 twice by rotating the structure 60° to exercise all six corners.

#### 4.3 Recorded Data

Record all data described in section 4.2 in the table provided.

[illegible][illegible]

APPENDIX D

LATCH AND STRIKER INSTALLATION PROCEDURE



## 1.0 SCOPE

This specification establishes the procedure for the installation and alignment of strikers and latches onto the SCAD Hex Panel Structure.

## 2.0 TOOLS AND EQUIPMENT

<u>Special Equipment</u>	<u>Qty.</u>
a) Latch and Striker Positioner 1232-A-0200	1
b) Allen Wrenches	2
c) Torque Wrench	1

### Parts

a) Hex Structure Assembly	500020	19
b) Latch Assembly	500050	60
c) Striker Assembly	500065	60
d) Shim, Latch/Striker Housing	500064	A.R.
e) Screw, Cap HD Skt, 10-32 x 1/2 LG	NAS1351C3-8	240
f) Washer, Split Lock No. 10	NAS35338-138	240
g) Washer, Flat No. 10	NAS620C102	240

## 3.0 INSTALLATION AND ALIGNMENT

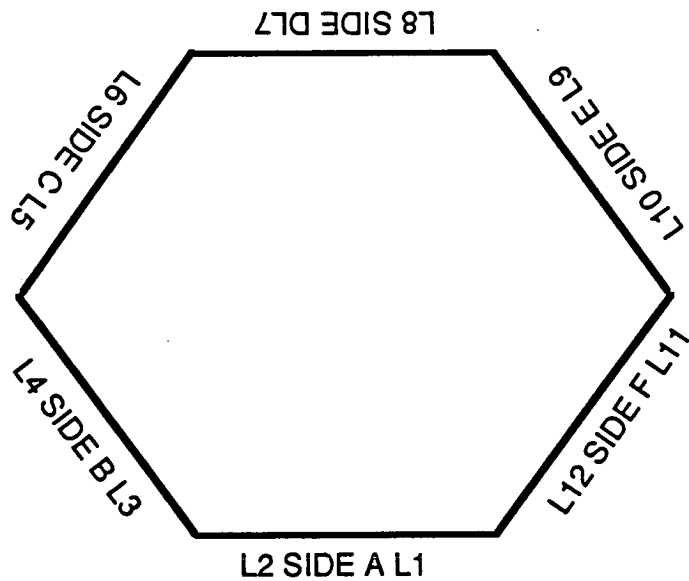
- 1) Mount the Hex Structure Assembly (500020) onto the alignment table (1232-A-0200).
- 2) Refer to Table 3.1, given the panel number and the panel side to determine which latch/striker to mount onto the hex structure.

- 3) Refer to Table 3.2 to determine the corresponding "locator" and "standard" detail number to be used to position the latch/striker.
- 4) Establish the proper "locator" position using the "standard". Lock the "locator" into place and record its position. Use the "standard locator" to aid in positioning the "standard".
- 5) Release the "locator" and slide it back to allow for the installation of the latch/striker.
- 6) Install the latch/striker loosely without shims.

NOTE: When installing a latch it may be necessary to attach the latch to the "locator" prior to attaching it to the panel.

- 7) Engage the latch/striker with the "locator" and slide them until the latch/striker is pressed firmly against the panel, then lock the "locator" and record its position.
- 8) To determine the proper shim (500064) thickness subtract the reading recorded above from the reading recorded in step 4.
- 9) Release the "locator" and re-install the latch/striker using a shim peeled to the thickness determined above.
- 10) Engage the latch/striker with the "locator" and slide them until the latch/striker is pressed firmly against the panel, then lock the "locator" and record its position.

- 11) Compare the position recorded in step 4 with the present position of the "locator". If the readings differ by more than  $\pm .001$  in., add or peel shim(s) as necessary and repeat the process until the readings differ by less than  $\pm .001$  in.



## LATCH LOCATION

Panel

No.	L1	L2	L3	L4	L5	L6	L7	L8	L9	L10	L11	L12
1	SIA	SIA	SIA	SIA	SIA	SIA	SIA	SIA	SIA	SIA	SI	SI
2	SIII	SIIIA	SII	-	LI	LI	-	SII	-	SIII	SIB	SIB
3	SIB	SIB	SIII	SIIIA	SII	-	LI	LI	-	LII	-	SIII
4	-	SIII	SIB	SIB	SIII	SIIIA	SII	-	LI	LI	-	LII
5	-	LII	-	SIII	SIB	SIB	SIII	SIIIA	SII	-	LI	LI
6	LI	LI	-	LII	-	SIII	SIB	SIB	SIII	SIIIA	SII	-
7	LII	-	LI	LI	-	LII	-	SIII	SIB	SIB	SIII	SIIIA
8	SIIA	-	LIII	-	LIIIA	LIII	-	SIIA	-	-	-	-
9	-	-	SIV	-	LIA	LIA	-	LIIA	-	-	-	-
10	-	-	SIIA	-	LIII	-	LIIIA	LIII	-	LIV	-	-
11	-	-	-	-	SIV	-	LIA	LIA	-	LIIA	-	-
12	-	-	-	-	SIIA	-	LIII	-	LIIIA	LIII	-	LIV
13	-	-	-	-	-	-	SIV	-	LIA	LIA	-	LIIA
14	-	LIV	-	-	-	-	SIIA	-	LIII	-	-	LIII
15	-	LIIA	-	-	-	-	-	-	SIV	-	-	LIA
16	LIIIA	LIII	-	LIV	-	-	-	-	SIIA	-	-	-
17	LIA	LIA	-	LIIA	-	-	-	-	-	-	-	-
18	LIII	-	LIIIA	LIII	-	LIV	-	-	-	-	-	-
19	LIIA	-	LIA	LIA	-	LIIA	-	-	-	-	-	-



LATCH/ STRIKER TYPE	STANDARD BLOCK DETAIL	LATCH LOCATOR "A"	LATCH LOCATOR "B"	BALL LOCATOR
LATCH I	6		X	
LATCH IA	2		X	
LATCH II	5	X		
LATCH IIA	1	X		
LATCH III	3	X		
LATCH IIIA	4	X		
LATCH IV	1	X		
STRIKER I	6			X
STRIKER IA	6			X
STRIKER IB	2			X
STRIKER II	5			X
STRIKER IIA	1			X
STRIKER III	3			X
STRIKER IIIA	4			X
STRIKER IV	1			X

TABLE 3.2

APPENDIX E

THEODOLITE MEASUREMENT SYSTEM DESCRIPTION

## APPENDIX E

### Harris Theodolite Measurement System

#### Introduction

The Harris theodolite measurement system consists of 4 Kern electronic theodolites driven with an IBM PC-AT or a Harris mainframe. The hardware is controlled by DAMS, an interactive Harris software tool.

#### System Calibration

The theodolite system is calibrated using a series of fixed targets and a length standard. The elevation and azimuth are recorded for each theodolite by the DAMS software. The calibration procedure is run on this data to determine the locations of the theodolites in an arbitrary measurement coordinate system. The arbitrary coordinate system typically has its origin at one of the theodolites.

#### Hardware Measurement

After the arbitrary measurement coordinate system has been established, the targets on the test structure are located in the measurement coordinate system. After all targets have been measured, DAMS performs a coordinate transformation on the data set from the measurement coordinate system to a reference system meaningful to the structure. This transformation takes place as follows:

$$R_{RP} = T_{RM} R_{MP} + R_{RM}$$

where

$R_{RP}$  defines the position vector of the position vector of the point P in the reference system.

$R_{MP}$  defines the position vector of the point P in the measurement system.

$R_{RM}$  defines the position vector of the measurement system origin in the reference system.

$T_{RM}$  is the rotation matrix defined by angles A, B, and C which aligns the respective axis of the measurement system with the reference system.

#### Data Regression and Repeatability

The data set that corresponds to each repeatability test sequence is then regressed (or best-fit) with respect to the other set(s). This regression technique uses a standard statistical algorithm that reports the RMS (root mean square) of the data sets. The RMS is a weighted average of the error between data sets the residual data shown is the raw error between each point.



APPENDIX F  
LASER SCANNER

SCANNER COMPUTER CODE

MOTION 2D

```

#A
MG
MG SPECIFY ABSOLUTE POSITION..
IN ENTER X POSITION (IN) =>,V1
IN ENTER Y POSITION (IN) =>,V2
MG
MG X = ;V1=;MG Y = ;V2=
MG
VO=1
IN OK ? 1)*YES 2) NO =>,VO
JP #a, VO=2
V4=V1*V54;V5=V2*V55
AC V56,V57,V57
SP V58,V59,V59
PA V4,V5,V5
CB1;CB2
MG
MG TILT/LASER OFF...
MG BEGINNING MOTION...
BG;AM
JS #T
WT 2000
MG
MG INITIATE LASER/TILT LOOP ?
VO=2
IN 1) YES 2)*NO =>,VO
JP #a,VO=2
MG
MG TILT LOOP ACTIVE...
SB1;WT 5000
MG LASER SHUTTER OPEN...
SB2
#a
MG
MG ANOTHER POINT ?
VO=1
IN 1)*YES 2) NO =>,VO
JP #A,VO=1
CB1;CB2
MG
MG LSER/TILT OFF...
MG
MG EXITING ABSOLUTE MOTION...
EN
#R
MG
MG SPECIFY MOTION INCREMENT...
IN ENTER X INCREMENT (IN)=>,V1
IN ENTER Y INCREMENT (IN)=>,V2
MG
MG X INCREMENT = ;V1=
MG Y INCREMENT = ;V2=
MG
VO=1
IN OK ? 1)*YES 2) NO =>,VO
JP #b,VO=2
V4=V1*V54;V5=V2*V55
AC V56,V57,V57
SP V58,V59,V59
PR V4,V5,V5

```

```

MG
MG BEGINNING  MOTION...
BG;AM
JS #T
WT 2000
MG
#b
MG INCREMENT AGAIN ?
VO=1
IN 1) *YES  2) NO =>,VO
JP #R,VO=1
MG
MG INITIATE LASER/TILT LOOP?
VO=2
IN 1) YES    2) *NO    =>,VO
JP #c,VO=2
MG
MG TILT LOOP ACTIVE...
SB1;WT 5000
MG LASER SHUTTER OPEN...
SB2
#c
MG
MG EXITING INCREMENTAL MOTION.
EN
#I
MG
MG INITIALIZING PARAMETERS...
GN 16,16,16
KI 0,0,0
V54=1273.2395
V55=1273.2395
V56=5000;V57=5000
V58=15000;V59=15000
AC V56,V57,V57
SP V58,V59,V59
DB 20,20,20
ER 1000,1000,1000
OE 1,1,1
MG
MG INITIALIZATION COMPLETE.
EN
#T
MG
MG CURRENT POSITION.
V4=PX/V54
V5=PY/V55
V6=PZ/V55
MG
MG X  (IN) = ;V4=
MG Y1 (IN) = ;V5=
MG Y2 (IN) = ;V6=
EN
#M
MG
MG          MENU
MG #I - Initialize Parameters
MG #C - Calibrate System
MG #A - Absolute Motion
MG #R - Relative Motion

```



MG #T - Tell Position (IN)  
MG #M - Display Menu  
EN  
#]  
MG  
MG LIMIT SWITCH TRIPPED...  
MG  
EN  
#[  
MO  
MG  
MG PROGRAM ABORT: POSITION  
MG ERROR LIMIT EXCEEDED...  
MG  
MG ERROR:  
TE;MG  
SH  
MG EXITING PROGRAM...  
MG  
EN  
#^  
MG  
MG INTERRUPT ENCOUNTERED...  
MG  
EN

BB7

SYSTEM STARTUP  
AND CALIBRATION

#### START UP:

- 1) Plug 110 supply cord into outlet
- 2) Power computer up
- 3) Pull red button up to power ground station
- 4) Turn laser on
- 5) At computer enter RUN <RTN>

This loads the motion control software.

- 6) Strike F3 to load program  
Type C:\SCAD\MOTION.2D <RTN>
- 7) Enter XQ #I

This initializes the system parameters

- 8) Enable the tilt loop
- 9) Check laser for verticality
- 10) Disable tilt loop
- 11) Move to desired position
- 12) Enable tilt loop

#### SHUT DOWN:

- 1) Disable tilt loop
- 2) Move to position (0,0,0)
- 3) Turn laser off
- 4) Push red button in
- 5) Turn computer off
- 6) Unplug 110 supply

## MOVEMENT:

Executing a move in the Motion X.2D program can be accomplished several ways:

- 1) PA x,y,z <RTN> (Position Absolute)  
BG <RTN> (Begin)

This command sequence moves the scanner to a specific point

- 2) IP x,y,z <RTN> (Increment Position)

This command moves the scanner a distance from the starting point. The advantage of using method 1 results from a lower error build up. Both methods require input in counts. There are approximately 1273 counts/inch.

- 3) XQ #A <RTN>

This command executes a subroutine that allows input in inches.

## OTHER USEFUL COMMANDS:

- 1) TP <RTN> (Tell Position)

The response from this command is the current location x,y,z in counts.

- 2) MO (Motors Off)

Turns the motors off.

- 3) SH (Servo Hear)

Reinstates the motors.

- 4) DP x,y,z (Define Position)

Defines position.

## INITIALIZATION PARAMETERS:

SPEED: 15000

ACCELERATION: 4096

GAIN: 16



## SYSTEM CALIBRATION:

### Initial Calibration:

The first step in calibrating the system is ensuring laser verticality. This is accomplished by reflecting the beam off a pool of mercury and adjusting the positioning micrometers on the laser mount until the beam is reflected back onto itself.

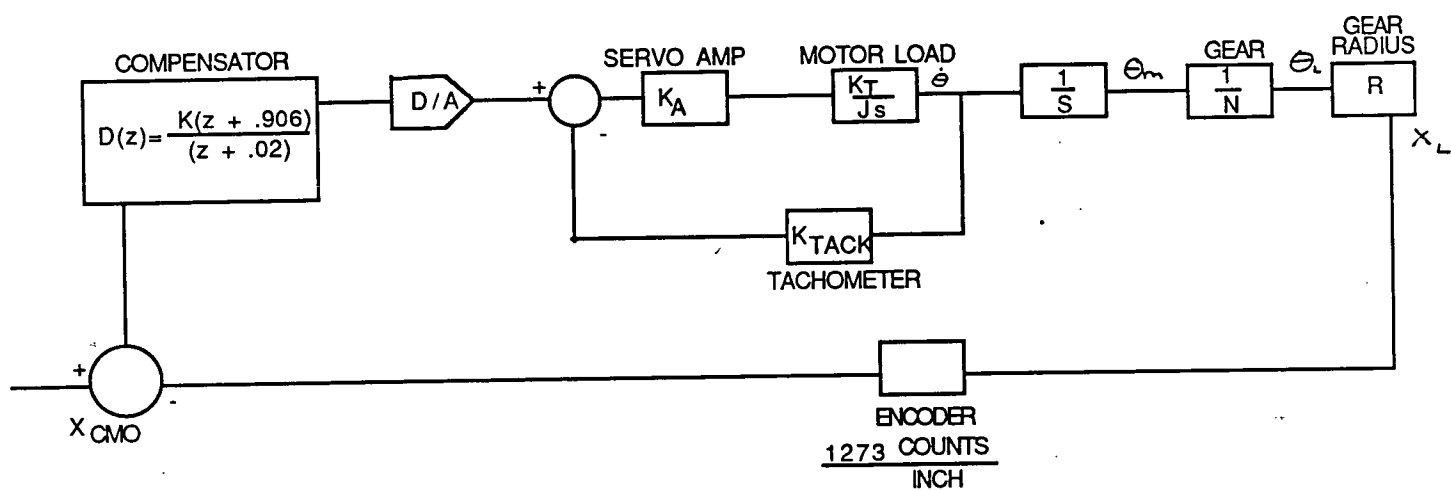
The second step is choosing the system zero. The scanner is moved to the desired location. The tilt sensor loop is turned on and a target is placed on the floor. The position is defined as 0,0,0 with the command Define Position.

The final step is to move the carriage along the X axis from 0 to the other end. Turn the tilt loop on and place a target at the location. (The position 700000,0,0 was used in the SCAD testing.) This final step assures the gantry is tracking straight.

### Calibration Maintenance:

The scanner should be checked a minimum of twice daily for calibration. To calibrate the scanner at 0,0,0, increment the scanner using the Increment Position (IP) command. When the laser is on the target, use Define Position.

Next, move the carriage to (700000,0,0). If the gantry is out of alignment, use the Increment Position command on the Z motor only. Then move the carriage back to zero and use the Define Position Command. Repeat the calibration maintenance procedure.



A Functional Electrical Diagram Of The Laser Scanner Motor Control Circuit.  
This Circuit Is Used To Keep The Two Motors On The Main Gantry Synchronized.



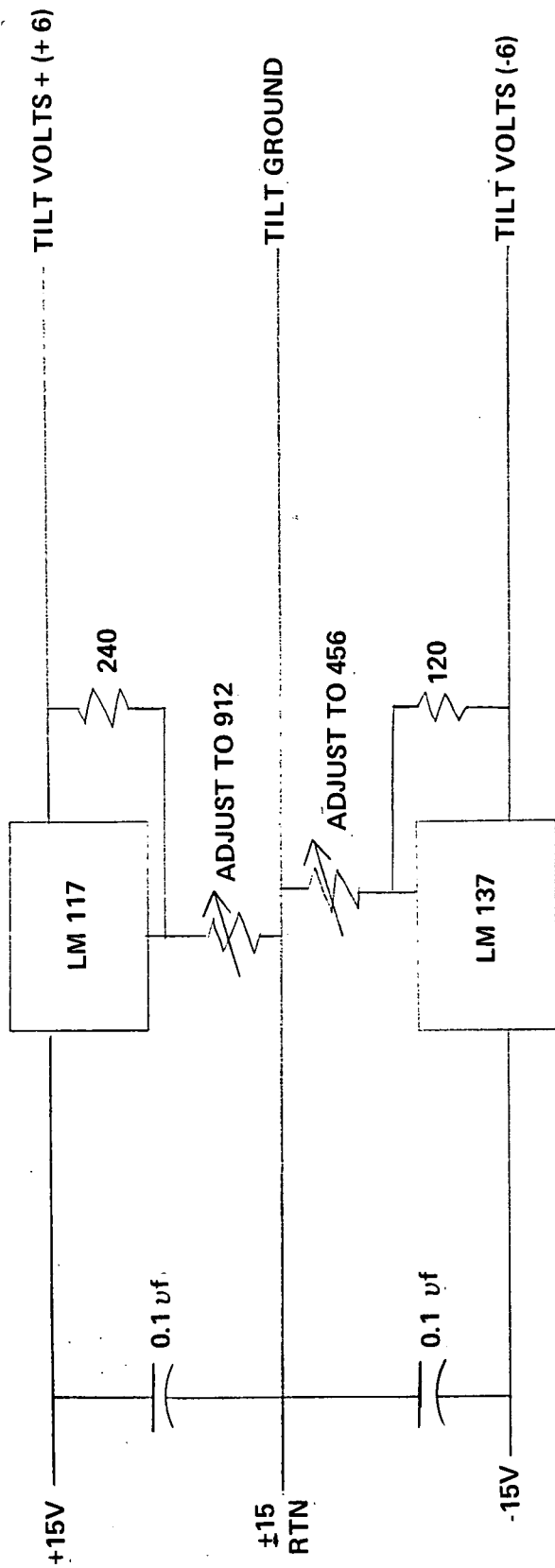
**FEEDBACK TILT LOOP**  
**1 REQUIRED FOR EACH AXIS**

U1 - HARRIS HA4741 QUAD OP AMP  
U2 - HARRIS HI201HS ANALOG SWITCH  
U3 - APEX PA01 POWER OP AMP

TITLE

ORIGINATOR

CHECKED BY



TILT SENSOR POWER SUPPLY

890307

PROJECT

DATE

PAGE

OF





## Report Documentation Page

1. Report No. CR-185173		2. Government Accession No.		3. Recipient's Catalog No.	
4. Title and Subtitle Solar Concentrator Advanced Development Program Final Report				5. Report Date October 1989	
				6. Performing Organization Code	
7. Author(s) Harris Corporation				8. Performing Organization Report No. None	
				10. Work Unit No.	
9. Performing Organization Name and Address Harris Corporation Government Aerospace Systems Division P. O. Box 94000 Melbourne, Florida 32902				11. Contract or Grant No. NAS 3-24670	
				13. Type of Report and Period Covered Contractor Report	
12. Sponsoring Agency Name and Address National Aeronautics and Space Administration Lewis Research Center 21000 Brookpark Road Cleveland, Ohio 44135				14. Sponsoring Agency Code	
15. Supplementary Notes Project Manager, Robert D. Corrigan, NASA Lewis Research Center, Cleveland, Ohio					
16. Abstract Solar Concentrator Advanced Development Program - Tasks 2 and 3 Final Report  The Solar Concentrator Advanced Development (SCAD) Program (NAS3-24670) was awarded to the Harris Corporation to develop a solar dynamic power system concentrator for space station applications, in particular the NASA Space Station Freedom. Solar dynamic systems have been developed for terrestrial applications, but have not been developed for space applications. The SCAD contract, for the development of a prototype solar collector for space applications, consisted of three tasks:  Task 1 Conceptual Design and Trade Studies, Materials, Special Tooling and Testing Task 2 Mechanical Design of Prototype Concentrator and Associated Tooling Task 3 Fabrication and Testing of the Prototype Concentrator and Tooling  Task 1 was reported in detail in NASA Contractor Report CR-179489. This report focuses on Tasks 2 and 3, and marks the completion of the Solar Concentrator Advanced Development Program. These tasks resulted in the successful design, fabrication and testing of a 60 foot diameter concentrator prototype that addressed several critical technology requirements for a space borne concentrator structure. The contents of this report includes design and fabrication details as well as test results.					
17. Key Words (Suggested by Author(s))				18. Distribution Statement	
19. Security Classif. (of this report)		20. Security Classif. (of this page)		21. No of pages	22. Price*